

DISSERTATION

MODELING AND IMPROVING URBAN HUMAN MOBILITY IN DISASTER SCENARIOS

Submitted by

Qiling Zou

Department of Civil and Environmental Engineering

In partial fulfillment of the requirements

For the Degree of Doctor of Philosophy

Colorado State University

Fort Collins, Colorado

Fall 2020

Doctoral Committee:

Advisor: Suren Chen

Paul Heyliger

John W. van de Lindt

Edwin K. P. Chong

Copyright by Qiling Zou 2020

All Rights Reserved

ABSTRACT

MODELING AND IMPROVING URBAN HUMAN MOBILITY IN DISASTER SCENARIOS

Natural and human-made disasters, such as earthquake, tsunami, fire, and terrorist attack, can disrupt the normal daily mobility patterns, posing severe risks to human lives and resulting in tremendous economic losses. Recent disaster events show that insufficient consideration of human mobility behavior may lead to erroneous, ineffective, and costly disaster mitigation and recovery decisions for critical infrastructure, and then the same tragedies may reoccur when facing future disasters. The objective of this dissertation is to develop advanced modeling and decision-making methodologies to investigate the urban human mobility in disaster scenarios. It is expected that the proposed methodologies in this dissertation will help stakeholders and researchers gain a better understanding of emergency human behavior, evaluate the performance of disrupted infrastructure, and devise effective safety management and resilience enhancement strategies. Focusing on the two important mobility modes (i.e., walking and driving) in urban environment, this dissertation (1) develops agent-based crowd simulation models to evaluate the crowd dynamics in complex subway station environment and investigate the interplay among emotion contagion, information diffusion, decision-making process, and egress behavior under a toxic gas incident; (2) develops functionality modeling, interdependency characterization, and decision models to assess and enhance the resilience of transportation networks subject to hazards.

ACKNOWLEDGEMENTS

I would first like to express my deep appreciation to my advisor Dr. Suren Chen, for his unwavering support and encouragement over the past five years. I am grateful to the opportunity he gave to work on my dissertation research topics. He has been a great mentor and a good friend. His guidance has made this a thoughtful and rewarding journey. Without his excellent supervision, the completion of my dissertation would not have been possible.

I am also thankful to the distinguished committee members, Dr. Paul Heyliger, Dr. John W. van de Lindt, and Dr. Edwin K. P. Chong. Their invaluable suggestions and comments have greatly improved the quality of this dissertation.

I would also like to thank my former and current fellow graduate students at Colorado State University, Dr. Yufen Zhou, Dr. Guangyang Hou, Yangyang Wu, Jingze Ren, et al. It was my great pleasure and honor to study and work with them at CSU. I value their friendship and support as well.

I also like to acknowledge the financial support for my research provided by the Center for Risk-based Community Resilience Center sponsored by National Institute of Standards and Technology (NIST), and the Mountain-Plains Consortium, a University Transportation Center funded by the U.S. Department of Transportation.

Last but not the least, I would like to thank my parents and my girlfriend Min Li for their wise counsel and sympathetic ears. They put up with me being distracted and missing many events. I am forever grateful for their patience and understanding.

DEDICATION

To my parents

TABLE OF CONTENTS

ABSTRACT.....	ii
ACKNOWLEDGEMENTS.....	iii
DEDICATION	iv
LIST OF TABLES	viii
LIST OF FIGURES	ix
CHAPTER 1 INTRODUCTION	1
1.1 Background	1
1.2 Literature review	4
1.2.1 Crowd simulation models.....	4
1.2.2 Modeling emotion contagion and information spread in crowd dynamics	7
1.2.3 System resilience of TN	9
1.2.4 Interdependencies between TN and other CISs.....	11
1.2.5 Resource prioritization strategies for TN.....	14
1.2.6 Resilience-based recovery scheduling of TN.....	16
1.3 Research gaps and motivations	20
1.3.1 Simulation of crowd dynamics in the subway station.....	20
1.3.2 Incorporation of human factors into crowd evacuation model under toxic gas incident	21
1.3.3 Resilience modeling of interdependent traffic-electric power system subject to hurricanes.....	24
1.3.4 Resource prioritization to enhance the resilience of interdependent traffic-electric power system	26
1.3.5 Resilience-based recovery scheduling of TN.....	28
1.4 Objectives.....	29
1.5 Outline of the dissertation	31
CHAPTER 2 AGENT-BASED EVACUATION SIMULATION FROM SUBWAY TRAIN AND PLATFORM.....	35
2.1 Introduction.....	35
2.2 Model development for subway evacuation.....	36
2.2.1 Subway system modeling.....	36
2.2.2 Pedestrian modeling	39
2.3 Simulation	45
2.3.1 Normal scenarios	48
2.3.2 Emergency scenarios	49
2.3.3 Discussion about factors influencing exit time	52
2.4 Conclusions	57
CHAPTER 3 SIMULATION OF CROWD EVACUATION UNDER TOXIC GAS INCIDENT CONSIDERING EMOTION CONTAGION AND INFORMATION TRANSMISSION	59
3.1 Introduction.....	59
3.2 Model descriptions	59

3.2.1 Hazardous environment: gas dispersion model	60
3.2.2 Agent design.....	61
3.2.3 Interactions among the agents: information transmission and emotion contagion	64
3.2.4 Crowd dynamics: modified social force model	71
3.3 Simulations.....	74
3.3.1 Room with one exit.....	76
3.3.2 Room with two exits	83
3.4 Conclusions.....	87
CHAPTER 4 RESILIENCE MODELING OF INTERDEPENDENT TRAFFIC-ELECTRIC POWER	
SYSTEM SUBJECT TO HURRICANES	90
4.1 Introduction.....	90
4.2 Framework description.....	91
4.2.1 Transportation network.....	92
4.2.2 Electric power network	96
4.2.3 Interdependencies between TN and EPN	100
4.2.4 Resilience assessment	105
4.3 Illustrative example.....	108
4.3.1 Resilience assessment of the original systems.....	113
4.3.2 Effects of resilience improvement strategies	116
4.3.3 Computational cost	123
4.4 Conclusions.....	124
CHAPTER 5 ENHANCING RESILIENCE OF INTERDEPENDENT TRAFFIC-ELECTRIC POWER	
SYSTEM BY PRIORITIZING MITIGATION AND REPAIR RESOURCES	125
5.1 Introduction.....	125
5.2 Network representation and functionality	126
5.2.1 Transportation network.....	126
5.2.2 Electric power network	131
5.2.3 Interdependencies between TN and EPN	134
5.3 Problem formulation and solution procedure.....	136
5.4 Illustrative example.....	143
5.4.1 Solutions of the decision model.....	150
5.4.2 Component priority indices for mitigation and repair actions.....	158
5.5 Conclusions.....	162
CHAPTER 6 RESILIENCE-BASED RECOVERY SCHEDULING OF TRANSPORTATION	
NETWORK IN MIXED TRAFFIC ENVIRONMENT: A DEEP-ENSEMBLE-ASSISTED ACTIVE	
LEARNING APPROACH	164
6.1 Introduction.....	164
6.2 Problem formulation	165
6.2.1 Functionality quantification of TN in mixed traffic environment.....	167
6.2.2 Problem formulation of resilience-based recovery scheduling of TN	174
6.3 Solution procedure	178

6.3.1 <i>Deep ensemble</i>	179
6.3.2 <i>Deep-ensemble-assisted efficient global optimization</i>	182
6.3.3 <i>Recovery priority ranking for stochastic case</i>	187
6.4 Illustrative example	188
6.4.1 <i>Deterministic case</i>	193
6.4.2 <i>Stochastic case</i>	202
6.4.3 <i>Computational cost</i>	205
6.5 Conclusions	206
CHAPTER 7 SUMMARY OF THE DISSERTATION AND FUTURE STUDIES	208
7.1 Summary and conclusions.....	208
7.2 Directions for future research.....	211
7.2.1 <i>Walking mobility</i>	211
7.2.2 <i>Driving mobility</i>	215
REFERENCES	219
CURRICULUM VITAE	247

LIST OF TABLES

Table 2.1 Simulation results of all cases	47
Table 3.1 Damage states of pedestrians caused by chlorine concentration.....	61
Table 3.2 Pedestrian’s attributes related with information transmission and emotion contagion	62
Table 3.3 Values of parameters related with the social force model	75
Table 4.1 Descriptions of TN and EPN of Centerville.....	109
Table 4.2 Values of parameters instantiating the resilience assessment of illustrative example.....	110
Table 4.3 Probabilistic information for attributes of tower and pole (Unnikrishnan and van de Lindt 2016)	110
Table 4.4 Probabilities of three blocking effects under different wind speeds	113
Table 4.5 Improvement effects on TN’s resilience (number of repair teams $n = 4$).....	118
Table 4.6 Improvement effects on EPN’s resilience (number of repair teams $n = 4$)	119
Table 5.1 Link attributes of the transportation network.....	146
Table 5.2 Statistics of random variables used in the example (all assumed to follow the normal distribution)	146
Table 5.3 Time-varying demand profile for all O-D pairs (Sbayti et al. 2007).....	147
Table 5.4 Values of parameters for the DTA model	147
Table 5.5 Probabilities and ratios of remaining capacity for the roadways blocked by fallen poles	148
Table 6.1 Notations in the problem formulation	165
Table 6.2 Notations of the DEAEGO algorithm	184
Table 6.3 Statistics of repair duration $T_{b,repair}$ (DHS 2009; Zhang et al. 2017).....	190
Table 6.5 Hyperparameters of each CNN in deep ensemble.....	192

LIST OF FIGURES

Figure 1.1 The concept of the resilience (adapted from the work of Ouyang et al. (2012) and Zhang and Wang (2016))	11
Figure 2.1 The layout of the prototype subway station.....	37
Figure 2.2 Three configurations of connection between the station platform and the exit: (a) horizontal; (b) upstairs; (c) downstairs	38
Figure 2.3 The areas in the car	39
Figure 2.4 The interface of NetLogo-based agent-based model for the subway evacuation simulation: (a) model configurations; (b) model visualization	45
Figure 2.5 Comparison of evacuation time of cases in the normal scenario.....	48
Figure 2.6 Comparison of evacuation time of cases in the emergency scenario.....	50
Figure 2.7 The effect of P_{delay} on the time of exiting from the train (high number of people and $P_{\text{train}} = 100\%$)	53
Figure 2.8 The effect of P_{train} on the time of exiting from the train (high number of people and $P_{\text{delay}} = 50\%$)	53
Figure 2.9 The effect of number of people on the time of exiting from the train ($P_{\text{delay}} = 50\%$ and $P_{\text{train}} = 100\%$).....	54
Figure 2.10 Time difference to exit from the station between cases with and without stairs	55
Figure 3.1 Illustration of the perception space of the agent.....	63
Figure 3.2 Situations of common agents aware of the incident (agents with the solid arrow are common ones who are aware of the incident): (a) personal harm from toxic gas; (b) notified by authority figures nearby; (c) informed by other common agents nearby	65
Figure 3.3 Flowchart of the simulation.....	74
Figure 3.4 Snapshots of evacuation simulation using different types of agents (in (a)-(d), red triangles represent agents being aware of the incident and green circles represent agents unaware of the incident): (a) $t = 0$ s; (b) $t = 12$ s; (c) $t = 22$ s; (d) $t = 54$ s; (e) $t = 0$ s; (f) $t = 12$ s; (g) $t = 22$ s; (h) $t = 54$ s.....	78
Figure 3.5 Time histories of number of evacuees using different types of agent models: (a) using proposed agents; (b) using omniscient agents	78
Figure 3.6 Effect of number of agents on the evacuation ($R_{i,p} = 2$ m and no authority figures are available): (a) evacuation time; (b) maximum evacuation efficiency; (c) slightly wounded agents; (d) collisions	80
Figure 3.7 Effect of perception radius on the evacuation ($N = 300$ and no authority figures are available): (a) evacuation time; (b) slightly wounded agents; (c) collisions	81
Figure 3.8 Effect of ratio of authority figures on the evacuation ($R_{i,p} = 2$ m): (a) evacuation time; (b) slightly wounded agents; (c) collisions	83
Figure 3.9 Snapshots of evacuation simulation for the room with two exits (red triangles represent agents choosing Exit 1; yellow squares represent agents choosing Exit 2; green circles represent agents unaware of the incident; pentagrams represent authority figures): (a) $t = 0$ s; (b) $t = 10$ s; (c) $t = 20$ s;	

(d) $t = 40$ s	85
Figure 3.10 Time histories of evacuation from the room with two exits: (a) the evacuation process; (b) the condition of exit using	85
Figure 3.11 Reduction effect of authority figures for the room with two exits ($R_{i,p} = 2$ m): (a) evacuation time; (b) slightly wounded agents; (c) collisions	87
Figure 4.1 Interdependencies between TN and EPN	100
Figure 4.2 Flowchart for resilience assessment of the interdependent traffic-electric power system.....	108
Figure 4.3 TN and EPN of Centerville community	109
Figure 4.4 Variations of normalized functionality metrics of both systems with time: (a) TN; (b) EPN. (Number of repair teams $n = 4$).....	114
Figure 4.5 Histograms of system resilience index with different number of repair teams: (a) TN; (b) EPN. (wind speed $v_h = 195$ km/h)	115
Figure 4.6 The variation of average system resilience index with the number of repair teams: (a) TN; (b) EPN	116
Figure 4.7 Comparison of variations of normalized functionality metrics of both systems over time with different improvement strategies: (a) TN; (b) EPN. (wind speed $v_h = 195$ km/h, number of repair teams $n = 4$, $\alpha_{\text{harden}} = 5\%$ for Case 1, and Equal repair mode for Cases 3 and 4)	118
Figure 4.8 Comparison of variation of average system resilience index with the number of repair teams in different cases: (a) TN; (b) EPN. (wind speed $v_h = 195$ km/h, $\alpha_{\text{harden}} = 5\%$ for Cases 1 and 4, and Equal repair mode for Cases 3 and 4)	123
Figure 5.1 Flowchart of the solution procedure (fp and fg are the resilience improvement)	143
Figure 5.2 The chosen area of Galveton, Texas (from Google Maps)	145
Figure 5.3 The interdependent traffic-electric power system.....	145
Figure 5.4 A typical case showing the disruption and corresponding mitigation and repair actions ($\Phi = 1$ and $B = \text{US } \$9 \times 10^4$): (a) disrupted; (b) mitigated; (c) repaired.....	152
Figure 5.5 Application of the BPSO to prioritizing mitigation and repair actions: (a) mitigation; (b) repair	153
Figure 5.6 Comparison of expected resilience improvement from BPSO and knapsack-based heuristic under mitigation and repair actions: (a) mitigation; (b) repair.....	153
Figure 5.7 The expected resilience improvements of the interdependent system under mitigation actions with different values of budget and preference parameter: (a) $\Phi = 0.0$; (b) $\Phi = 0.25$; (c) $\Phi = 0.5$; (d) $\Phi = 0.75$; (e) $\Phi = 1.0$	157
Figure 5.8 The expected resilience improvements of the interdependent system under repair actions with different values of budget and preference parameter: (a) $\Phi = 0.0$; (b) $\Phi = 0.25$; (c) $\Phi = 0.5$; (d) $\Phi = 0.75$; (e) $\Phi = 1.0$	158
Figure 5.9 Priority indices for mitigation of two components (see Figure 5.3 for locations): (a) link (14, 62) in the EPN; (b) node 15 in the TN	160
Figure 5.10 Priority indices for repair of two components (see Figure 5.3 for locations): (a) link (37, 39) in the EPN; (b) link (16, 15) in the TN	161
Figure 5.11 Comparison of priority indices for mitigation using BPSO and knapsack-based heuristic ($\Phi = 0.5$ and $B = \text{US } \$6 \times 10^4$): (a) BPSO; (b) knapsack-based heuristic	162

Figure 5.12 Comparison of priority indices for repair using BPSO and knapsack-based heuristic ($\Phi = 0.5$ and $B = \text{US } \$6 \times 10^4$): (a) BPSO; (b) knapsack-based heuristic	162
Figure 6.1 Illustration of conversion from schedule to binary image as input to deep ensemble	180
Figure 6.2 Illustration of the structure of the deep ensemble.....	182
Figure 6.3 Pseudocode of the DEAEEO algorithm	183
Figure 6.4 The selected roadway network in Southern California: (a) roadway links and all bridges; (b) the epicenter and damaged bridges (the size of blue circle indicates the experienced damage level)....	190
Figure 6.5 Variation of pre-hazard total travel cost with penetration ratio of CAVs.....	193
Figure 6.6 Evolution of optimal resilience metric with optimization iteration using BFS, GA, and DEAEEO under different penetration ratios of CAVs ($n_{\text{crews}} = 5$): (a) $\rho = 0$; (b) $\rho = 0.25$; (c) $\rho = 0.50$; (d) $\rho = 0.75$; (e) $\rho = 1$	196
Figure 6.7 Evolution of distribution of sampled resilience metrics with optimization iteration using DEAEEO under different penetration ratios of CAVs ($n_{\text{crews}} = 5$): (a) $\rho = 0$; (b) $\rho = 0.25$; (c) $\rho = 0.50$; (d) $\rho = 0.75$; (e) $\rho = 1$	198
Figure 6.8 Optimal recovery trajectories of BFS, GA, and DEAEEO under different penetration ratios of CAVs ($n_{\text{crews}} = 5$): (a) $\rho = 0$; (b) $\rho = 0.25$; (c) $\rho = 0.50$; (d) $\rho = 0.75$; (e) $\rho = 1$	199
Figure 6.9 The earliest 10 bridges being repaired from BFS, GA, and DEAEEO under different penetration ratios of CAVs ($n_{\text{crews}} = 5$): (a) $\rho = 0$; (b) $\rho = 0.25$; (c) $\rho = 0.50$; (d) $\rho = 0.75$; (e) $\rho = 1$	201
Figure 6.10 The variation of optimal resilience metric with the penetration ratio of CAVs under different number of repair crews	201
Figure 6.11 Top 30 bridges based on stochastic ranking on repair completion time under different penetration ratios of CAVs ($n_{\text{crews}} = 10$): (a) $\rho = 0$; (b) $\rho = 0.25$; (c) $\rho = 0.50$; (d) $\rho = 0.75$; (e) $\rho = 1$	203
Figure 6.12 Locations of top 30 bridges based on stochastic ranking on repair completion time under different penetration ratios of CAVs ($n_{\text{crews}} = 10$)	204
Figure 6.13 Scatterplot of the Copeland scores with the betweenness values of damaged bridges.....	205

CHAPTER 1 INTRODUCTION

1.1 Background

Humans are bound to move on a daily basis to perform different social activities, which largely shape the development of the human societies. Thus, the human mobility, referring to the movement of human beings in space and time here, has an enormous impact on the welfare of modern societies (Barbosa et al. 2018). Moreover, natural or human-made disasters, such as earthquake, tsunami, fire, and terrorist attack, can disrupt the normal daily mobility patterns, posing severe risks to human lives and resulting in tremendous economic losses. Although governments and communities have proposed a variety of disaster response and evacuation plans, it was found that insufficient consideration of human mobility behavior may render such plans ineffective in practice (Wang and Taylor 2016), as demonstrated by the huge casualties and economic losses in recent disaster events (e.g., Superstorm Sandy in 2012 and Hurricane Harvey in 2017). Meanwhile, failing to capture the human mobility patterns correctly can also lead to erroneous, ineffective, and costly disaster mitigation and recovery decisions for critical infrastructure, and then the same tragedies may reoccur when facing future disasters (Chiu et al. 2011; Marshall 2018; Nie et al. 2004; Zou and Chen 2019). Therefore, it is of great importance to correctly account for the human mobility in disaster planning to save lives, assess the safety and performance of disrupted infrastructure, and devise corresponding cost-effective disaster reduction strategies.

In the urban environment, walking and driving are two of the most common mobility modes for humans. In terms of walking, there are many important facilities with high pedestrian traffic in cities, such as airports, subway stations, stadiums, and high-rise office buildings. While these facilities provide indispensable and

critical services for the public, hazardous incidents occurring in such places and factors regarding complexity of spatial layout and heavily overcrowded population can cause a large magnitude of fatalities and injuries in emergency situations (Helbing et al. 2005; Zhang et al. 2016). For example, the crowd disaster at Love Parade in Duisburg, Germany in 2010 killed 21 people and injured more than 500 (Helbing and Mukerji 2012). The stampede in 2015 during the annual Hajj pilgrimage in Mina, Mecca, Saudi Arabia took the lives of at least 2,431 pilgrims (Manoochehry and Rasouli 2017). In the United States, a structure fire was reported every 63 s and the fires caused 15,400 civilian casualties in 2018 (National Fire Protection Association 2019). It should be noted that in many of these tragedies, a large proportion of casualties were not caused by the hazardous sources directly (e.g., fire and toxic gas), but instead attributed to the crowd behavior itself (Helbing et al. 2005). Chaos is the norm in most emergency evacuation scenarios; evacuees can be panicked due to perception of threat and social contagion. It was recognized that the panic affects the evacuees' behavior and judgement and then prompts them to act selfishly and myopically, i.e., pursuing their own safety hastily and neglecting the surroundings, which can lead to fatal consequences such as trampling and crowd crush (Abdelghany et al. 2014; Helbing et al. 2000). Given the continuing occurrence of both natural and man-made disasters in cities, the study of evacuation behavior in emergency scenarios is of particular interest since it plays a key role in proposing effective pedestrian flow regulation schemes to ensure human safety (Liu et al. 2015; Manley et al. 2016; Shi et al. 2012).

As for driving, in the U.S., the automobile is the predominant transportation mode. About 86% of daily commuting in 2013 is by private vehicle (Mckenzie 2015). And over-the-road trucking, the most-used mode of freight transport, moved \$66.5 billion of freight in 2018, accounting for 62.9% of total freight value (Bureau of Transportation Statistics 2018). Given the fundamental role of roadway driving in shaping the

modern societies, this dissertation focuses on the roadway traffic and the performance of its underlying infrastructure (e.g., highway and urban roadway systems). In fact, the U.S. Department of Homeland Security recognized the transportation infrastructure as one of sixteen critical infrastructure systems (CISs) in that they all provide essential services which support safety, economic prosperity, and social sustainability (Rinaldi et al. 2001; Zhang and Wang 2016). However, these systems, including the roadway network, are often subject to natural and human-made hazards, which can cause severe and widespread disruptions and consequences. Recent years have seen the vulnerability of our transportation system to extreme events such as Hurricane Katrina in New Orleans in 2008, Superstorm Sandy in the Northeastern United States in 2012, and Hurricanes Harvey and Maria in 2017 (Markolf et al. 2019).

Since it is not always possible to solely rely on mitigation strategies to prevent or defer these undesirable events, such as increasing the system redundancy and reliability, recent attention has been shifted to enhancing the resilience of CISs (Hosseini et al. 2016). The resilience of the CIS is about the ability to withstand or adapt to external perturbations and to recover from disruptions effectively and efficiently; therefore not only preventative strategies in the preparedness stage but also restoration strategies in response and recovery stages should be considered to maintain certain levels of performance of CISs under hazards (Fotouhi et al. 2017; Hosseini et al. 2016; Zhang and Wang 2016). Among these CISs, The performance of roadway network is important in supporting emergency humanitarian aid, distribution of essential supplies, and post-disaster restoration of other critical facilities via providing critical accessibility (Alipour and Shafei 2016; Zhang and Wang 2016). Moreover, the roadway network and many other CISs are not isolated but highly interconnected. For example, the normal functioning of traffic signals is dependent on the electricity supply of the electric power network. It was recognized that such interdependencies should be

taken into consideration in designing a more resilient community (Heracleous et al. 2017).

In light of the significant impacts of these two mobility modes on the well-being of the modern societies, this dissertation aims at modeling and assessing these two mobility modes in disaster scenarios in order to gain a better understanding of emergency human behavior, evaluate the performance of disrupted infrastructure, and help develop effective safety management and resilience enhancement strategies. The specific problems tackled focus on the crowd dynamics in hazardous scenarios and the resilience of transportation networks (TNs) against natural hazards.

1.2 Literature review

This section reviews the past research pertaining to the crowd dynamics in hazardous scenarios and the resilience of TNs against natural hazards.

1.2.1 Crowd simulation models

Many numerical models have been developed to simulate pedestrian dynamics in recent years. Generally speaking, these models can be classified into macroscopic and microscopic models. Macroscopic models, e.g., fluid dynamic model (Helbing 1992; Henderson 1971; Hughes 2002), treat the system as a whole and the evacuees as homogenous population, behaving like fluid or gas. Partial differential equations are used to describe the crowd dynamics. These models can capture the features of the whole system reasonably but neglect individual behaviors and are therefore limited to fairly simple geometries. Besides, it is also difficult to set boundary conditions for the psychological state of the crowd (Liu et al. 2017, 2015).

Microscopic models which are based on individual characteristics have broader applications. The popular microscopic models in crowd simulation mainly rely on the agent-based modeling (ABM) technique, in which the system is represented as “a collection of autonomous decision-making entities

called agents”, and each agent can assess its situation and make decisions, and respond based on preset rules (Bonabeau 2002). The rules in ABM primarily operate at the agent or individual level, but complex collective behavior can emerge from the interactions between agents. The ABM provides a reasonably realistic forecasting model that planners can use to determine effective evacuation procedures accordingly (Chen et al. 2006). Bonabeau (2002) summarized three main advantages of ABM over other modeling technique: (1) ABM captures emergent phenomena; (2) ABM provides a natural description of a system; (3) ABM is flexible. In the evacuation context, evacuee behaviors can be quite complex, and can be characterized by thresholds, if-then rules, or nonlinear coupling. Furthermore, evacuee interactions are heterogeneous and can generate network effect. Since social vulnerability to natural hazards varies within a community, individual decision-making behavior depends on factors such as gender, race and class, and age, living environment, transportation options. Gender, race and class, and age are among the most important indicators of vulnerable individuals and social groups (NRC 2006). The capability of the ABM to capture the diversity of evacuee socio-demographic characteristics, as well as decision-making modeling, can make the prediction more precise (Wang et al. 2016).

Based on the space modeling method, the microscopic or the agent-based models can be further classified into discrete models and continuous models. Cellular Automata (CA) model (Burstedde et al. 2001; Feliciani and Nishinari 2016; Kirchner and Schadschneider 2002; Zheng and Cheng 2011; Zheng et al. 2017) is a typical discrete model. In this model, space is discretized into uniform cells and each cell can be either empty or occupied by a pedestrian or an obstacle. The pedestrian can move to one of unoccupied neighbor cells at each discrete time step according to the predefined rules and certain transition probabilities. Some researchers pointed out that the CA model is more suitable to be applied in low or medium crowd

density scenarios rather than in high density scenarios in which it is likely to produce unrealistic results (Liu et al. 2015).

One of the most famous continuous models is the social force model (SFM) proposed by Helbing (Helbing et al. 2000; Helbing and Molnár 1995). In this model, pedestrians are modeled as particles with certain characteristics such as mass and size and are subjected to physical forces and virtual social forces, such as attractive force, repulsive force, body compression force, and sliding friction force. The pedestrian dynamics is governed by Newton's second law of motion. Helbing and Johansson (2013) used the SFM to investigate the crowd behavior in both normal and panic situations and found a series of self-organized patterns, such as lane formation, oscillatory flow at bottlenecks, stripe formation in intersecting flows, herding, freezing by heating, and faster-is-slower effect. Many researchers have adapted the original social force model for different complex scenarios. Yuen and Lee (2012) added the overtaking behavior to the SFM and simulated unidirectional pedestrian flow. Wang et al. (2013) modified the attractive force, repulsive force, and desired velocity to simulate the pedestrian flow in a station hall during the Spring Festival travel rush. Song et al. (2013) employed a discretized version of SFM in assessing bioterrorism in micro-spatial environments. Johansson et al. (2015) extended the SFM to include waiting pedestrians and compared the outputs of different waiting models. Li et al. (2014) proposed a five-stage trampling model based on the modified SFM to study trampling risks during escalator transfers. Existing studies suggest that the SFM is pretty flexible and convenient to be modified and incorporate psychological and sociological factors. Moreover, it is found more suitable to be applied to over-crowded situations and allows pedestrians to move around in an unrestricted manner than the CA model (Zhang et al. 2016).

1.2.2 Modeling emotion contagion and information spread in crowd dynamics

1.2.2.1 Emotion contagion

Emotion represents a kind of psychological and physiological state of an individual perceiving a certain incident, and such a state can change over time continuously (Dolan 2002; Liu et al. 2017). It has been found that emotion not only affects an individual's own behavior, but also can spread among crowds and affect the behaviors of other individuals through emotion contagion, e.g., panic in emergency scenarios. The emotion can then facilitate irrational collective behavior, which may lead to catastrophic consequences on a massive scale during emergency evacuations (Fu et al. 2014; Liu et al. 2017). Therefore, it is necessary to incorporate the effect of the emotion contagion into the simulation of crowd dynamics. There are two main computational models of emotion contagion (Tsai et al. 2013): one is a deterministic and interaction-based model similar to the concept of heat dissipation phenomena in thermodynamics (Bosse et al. 2009). The other one was developed by Durupinar (2010) which is a probabilistic threshold model based on epidemiology modeling the spread of disease. Efforts have been devoted to incorporating emotion contagion primarily based on these two models into crowd evacuation simulation. Tsai et al. (2011) simulated the evacuation in an airport considering emotional, informational, and behavioral interactions. In their multi-agent evacuation simulation tool ESCAPES, the fear level of an individual is inherited from the highest fear level of neighboring pedestrians and can be reduced when authority figures are nearby. Nguyen et al. (2014) presented the multi-agent evacuation simulation integrating emotion effects and found that emotions increase the chaos which further increases collisions between agents but can decrease the evacuation time. Fu et al. (2014) modified the epidemiological Susceptible-Infected-Recovered (SIR) model in a CA approach and found that individual movement accelerates the spread speed of emotion. Liu

et al. (2017) developed an information perception-based emotion contagion model for fire evacuation and regarded emotion contagion as a kind of information dissemination. Cao et al. (2017) constructed a modified epidemiological Susceptible-Infected-Susceptible (SIS) model P-SIS to represent the emotion contagion and coupled it with the SFM to simulate crowd evacuation with emotion contagion. Although these studies as summarized above revealed many aspects of crowd dynamics and emotion contagion, few of them considered the situation in which casualties caused by the disaster exist and how this information influences pedestrians' emotion and further affects the evacuation process.

1.2.2.2 Information transmission

The evacuees' information of the dangerous source and knowledge on the environment can influence the decision-making process and collective behavior significantly (Fu et al. 2017). For example, when the pedestrians are aware of the existence of the dangerous sources (e.g., fire and poison gas), they can become nervous and panicked, try to keep away from the dangerous sources, find an exit, and accelerate their walking speed (Qu and Dan 2014). During their evacuation process, they can encounter other pedestrians and disseminate the information of the dangerous sources, which leads to more evacuees initiating the evacuation decision-making. Meanwhile, the familiarity to the environment also plays a key role in evacuees' choices of evacuation route and exit (Tan et al. 2015). Therefore, it is of great importance to take into account the information transmission process to achieve more realistic crowd simulations. Some researchers have considered such human factor in their models. Henein and White (2010) combined the information processing and communication with the floor field pedestrian model and emphasized the necessity and importance of integrating these human factors at the microscopic level. Tsai et al. (2011) considered the spread of the knowledge about the exit and incident in their multi-agent model. Liu et al.

(2017) took into account five types of information and their effects on individual's emotion and path finding.

Fu et al. (2017) modeled the influence of information transmission on pedestrians' decision making using a fuzzy-theory-based method.

1.2.3 System resilience of TN

The TNs, as a vital part of CISs, play a key role in supporting the well-being of modern society by providing the accessibility to critical facilities (e.g., hospitals and schools) and essential transport services for indispensable resources and products (e.g., emergency humanitarian aid, food distribution, and energy supply). However, TNs are often subject to natural and human-made hazards due to their wide spatial distribution and increased frequency of disasters in recent years (Faturechi and Miller-Hooks 2014a). Research found that about 27% of all global road and railway infrastructures are exposed to at least one hazard (Koks et al. 2019); these hazards usually can cause severe structural damages to the components of the transportation infrastructure, disrupt the normal functioning of the TN, and further result in widespread and significant negative socioeconomic consequences. For example, Hurricane Harvey in 2017 paralyzed the road network of the city of Houston due to the rainwater, left tens of thousands of people displaced, and led to over \$180 billion in damage (Blake and Zelinsky 2018; Pines 2018). Hurricane Sandy in 2012 caused the damage amounted to \$7.5 billion to the New York City's transportation system (Zhou et al. 2019). Tohoku Earthquake in 2011 caused large-scale damages to the transportation infrastructure with a total length of 870 km in Japan (Kazama and Noda 2012).

It has been recognized that in order to maintain a certain level of functionality of TNs under these hazards, it is not always possible to solely rely on mitigation strategies to prevent or absorb the negative impacts induced by hazards; instead, recent attention seeks to enhance the resilience of TNs against hazards

(Hosseini et al. 2016).

The resilience of the CIS is about the ability to withstand or adapt to external perturbations and to recover from disruptions effectively and efficiently (Haimes 2009; Hosseini et al. 2016; Ouyang et al. 2012; Zhang and Wang 2016). Thus, the resilience of the CIS is often associated with the variation of the measure of its functionality over time. Figure 1.1 illustrates the concept of the resilience and its four attributes, i.e., robustness, resourcefulness, redundancy, and rapidity (Bruneau et al. 2003). It can be observed that the functionality of the system undergoes three stages: the preparedness stage ($t \leq t_d$) is from normal operation to the initial failure due to the disruptive events. In this stage, the functionality of the system can be enhanced by adopting proactive risk mitigation and preparation measures; the response stage ($t_d \leq t \leq t_0$) denotes the damage propagation process after the initial failure, and the remaining functionality reflects the robustness of the system, i.e., the ability to withstand a disruptive event and maintain a certain level of service after the event; the recovery stage ($t_0 \leq t \leq t_r$) denotes the restorative process in which repair activities are carried out and the functionality recovers to an expected level. The duration of this stage $t_r - t_0$ reflects the rapidity, i.e., the ability to recover the desired functionality in a timely manner. The shape of the recovery process reflects resourcefulness and redundancy, which are about the ability to identify problems, establish priorities, and mobilize resources and the extent to which substitutable components exist, respectively. Depending on the nature of hazards and focuses, some researchers assumed an instantaneous response stage, i.e., $t_0 = t_d$, considering that the response stage is usually much shorter than the following recovery stage (Bocchini and Frangopol 2012; Vugrin et al. 2014). Following similar concept, various measures have been established to quantify the resilience of CISs, which consider both pre- and post- disaster behavior of the system response (Hosseini et al. 2016). Based on the resilience assessment,

effective strategies to improve the CIS resilience can be further identified and implemented at different stages (Ouyang et al. 2012).

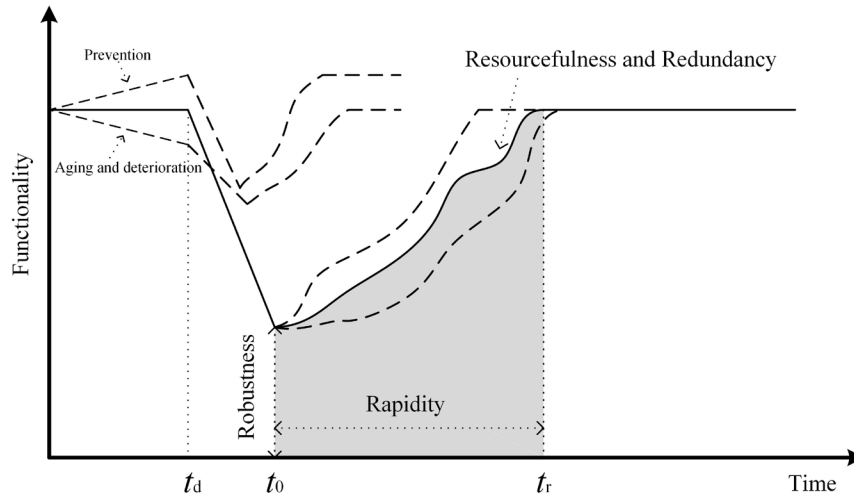


Figure 1.1 The concept of the resilience (adapted from the work of Ouyang et al. (2012) and Zhang and Wang (2016))

1.2.4 Interdependencies between TN and other CISs

The TN and many other CISs, such as electric power, gas, water, and telecommunication, do not operate separately but are highly interconnected and mutually dependent (Ouyang and Wang 2015; Rinaldi et al. 2001). The performance of those interdependent CISs collectively plays a major role in determining the community resilience subjected to major disasters (Reed et al. 2016).

Interdependencies among CISs can be classified into four main types (Rinaldi et al. 2001): (1) physical: the functionality of one CIS is dependent on the output of another; (2) cyber: the functionality of one CIS is dependent on the information transmission through the information-related CIS; (3) geographic: components of multiple CISs are in close spatial proximity and can be all affected by local events at the same time; (4) logical: CISs are linked logically via other mechanisms, e.g., policy and budget. Since the malfunction of one CIS can impact the functionality of other CISs due to these interdependencies, resilience

assessment on one CIS needs to consider the responses of its closely interconnected CISs. Rational modeling and extensive simulation are often required to study the characteristics of interdependent CISs because of the complexities and scarcity of related data (Heracleous et al. 2017). Despite the fact that many CISs in a community, such as buildings, roads, rails, electric power, gas, telecommunications, water, and economy, are interdependent, researchers usually choose some of them as the study objects depending on their research focuses and fields of expertise (Adjetej-Bahun et al. 2016; Fotouhi et al. 2017; Gong et al. 2014; Johansson and Hassel 2010). According to several review studies (Hasan and Foliente 2015; Ouyang 2014; Satumtira and Dueñas-Osorio 2010), the widely used quantitative approaches can be grouped as: agent-based (Nan and Sansavini 2017; Pumpuni-Lenss et al. 2017), system-dynamics-based (Brown et al. 2004; Stapelberg 2008), input-output-based (Haines et al. 2005; Haines and Jiang 2001; Santos and Haines 2004), network-based (Arcidiacono et al. 2012; Lee et al. 2007), etc. These approaches have their own strengths and weaknesses to fulfill different needs, but the state-of-the-art approach is still lacking and researchers are working hard to develop more efficient and effective methods (Heracleous et al. 2017).

Major natural hazards, such as earthquakes and hurricanes, can claim many human lives and cause large-scale disruptions to major infrastructures. For example, Hurricane Harvey in 2017 caused \$180 billion in damage, more than 200 thousand homes flooded, and nearly 1/3 of the city of Houston underwater (Pines 2018). Among CISs prone to natural hazards, TN and electric power network (EPN) are particularly vital. As the basic lifeline infrastructures, TN and EPN are crucial to nearly all emergency response, humanitarian relief efforts, and post-disaster emergency restoration of other critical facilities through providing essential accessibility and power supply (Zhang and Wang 2016).

Existing interdependency studies involving TN or EPN mainly adopted network-based approaches,

which can represent interdependencies using interlinks conveniently and conduct analyses with different levels of detail using topology-based or flow-based models (Mattsson and Jenelius 2015; Ouyang 2014). Arcidiacono et al. (2012) developed a methodology to describe the performance of the road network considering interdependencies with buildings under earthquakes. The measure of accessibility of the road network was used to calculate the resilience index. Feng et al. (2017) analyzed the supporting functionality of road network to the recovery process of building systems after earthquakes. The minimum-cost flow problem was solved to obtain the recovery process of buildings by delivering repair resources through the road network. Adjetey-Bahun et al. (2016) proposed a simulation model to quantify resilience in mass railway transportation systems using passenger delay and passenger load as functionality indices. Interdependencies among railway, power, telecommunication, and organization systems were considered. Johansson and Hassel (2010) modeled an electrified railway network which was dependent on four other infrastructure systems. Similarly, Zhang et al. (2014) also explored the vulnerability of the rail network with dependencies on the power and communication networks under node-based attacks. Meanwhile, some researchers have applied mathematical optimization algorithms to quantify resilience. Lee et al. (2007) established the interdependent layer network (ILN) model to explicitly identify interconnections among CISs. They demonstrated the use of the model in guiding restoration of services of the interdependent CISs of power, telecommunications, and subway. It should be pointed out that all the CISs in their study were based on a unified network maximum flow model. In fact, different CISs have different characteristics and are usually operated under different physical laws or specified conditions. For example, the performance of the electric power network may be measured by the maximum flow theory, while the traffic flows of the roadway network usually need to satisfy the user equilibrium condition. Gong et al. (2014) developed

restoration strategies aiming to aid the supply chain in recovering from a disruption based on the ILN model. The logical interdependencies between other infrastructures (power and telecommunication) and the supply chain were taken into account. Loggins and Wallace (2015) employed the ILN model to predict the vulnerability of interdependent CISs. As the closest study to the topic of this dissertation, Fotouhi et al. (2017) presented a bi-level, stochastic program to quantify the resilience of a coupled traffic-power network. Under four hypothetical damaged scenarios, they focused on the optimal preparedness actions to minimize the total travel time. The interdependencies included the traffic lights powered by EPN and repair operations dependent on the TN's state. However, their study did not consider the interdependency of the failed EPN infrastructures (e.g. poles) disrupting traffic of TN, which is very common during hurricanes. Also, the assumption in the study that repair activities can be completed simultaneously as long as the damaged sites were accessible ignored vehicle routing and repair scheduling problems in the recovery process and thus did not account for the variation of the system functionality over time.

1.2.5 Resource prioritization strategies for TN

The great risks and tremendous damages caused by human-made and natural hazards call for the needs of mitigation, repair, and maintenance actions on the CISs. However, because available financial resources are typically insufficient to cover all components of CISs simultaneously, it is necessary to devise cost-effective resource allocation strategies to prioritize limited resources to achieve the optimal balance between CIS performance and cost (Liu and Frangopol 2005; Zhang and Wang 2017).

In past decades, scholars have extensively investigated the resource prioritization scheme for single CIS. The typical way is to establish an optimization problem with the goal of maximizing the functionality of the CIS or minimizing the costs. As for the TN, Liu and Frangopol (2005) used the genetic algorithm to

find the maintenance planning to maximize the connectivity reliability of a single origin-destination (O-D) pair within a bridge network considering deterioration. Bocchini and Frangopol (2013) extended the model to multiple O-D pairs. Zhang and Wang (2017) presented a framework of determining the maintenance schedule for a degraded bridge network to minimize the total travel time considering the posted weight limit. Yan et al. (2017) formulated a pre-disaster investment optimization model to minimize the expected railway system service loss under earthquakes. As for the EPN, Romero et al. (2015) developed a two-stage stochastic program and knapsack heuristic solution procedure to optimize the seismic mitigation strategies for the electric power systems under earthquake hazards. Fang and Sansavini (2017) adopted the planner–attacker–defender model to develop decisions of capacity expansion and switch installation in electric systems that ensures optimum performance. Ghaffarpour et al. (2018) applied the genetic algorithm to find the optimal hardening planning of distribution networks.

Recent years have also seen some research progress on the resource prioritization to enhance the resilience of interdependent CISs, e.g., power and gas (Cong et al. 2018; Ouyang and Wang 2015), supply chain and telecommunication (Gong et al. 2014), and power, gas and water (González et al. 2016). To date, few studies have investigated the optimal resilience decision models for the interdependent traffic-electric power network quantitatively with adequate details to reflect their own operational characteristics. Perhaps the closest study to the topic of this dissertation is the one by Fotouhi et al. (2017). In their study, they presented a bi-level, mixed-integer, stochastic program to quantify the resilience of a coupled traffic-power network. Under four hypothetical disaster scenarios, they focused on finding the optimal preparedness and recovery decisions to minimize the total travel time. While this study provided some interesting findings, limitations still existed in their model. First, the interdependencies modeled in their study included traffic

lights powered by EPN and repair operations were dependent on the TN's state, but left out the situation of the failed EPN infrastructures (e.g. poles) disrupting traffic of TN, very likely scenarios under hazardous conditions such as hurricanes. Second, the STA algorithm was used to determine the traffic flow, which was not suitable for the congested urban roadway network and may produce unrealistic conclusions. Third, uncertainties in their study only stemmed from the possibility of occurrence of four hypothetical disaster scenarios. In fact, other factors, e.g., cost and traffic demand, may contain large uncertainties as well and it has been found essential to incorporate them in making optimal resilience-enhancing decisions (Zhang and Wang 2017). Fourth, they only sought the optimal decisions to maximize the performance of the traffic system and did not consider the decisions to enhance the resilience of traffic and electric power systems jointly. To summarize, it can be found that existing works have not examined the interactions between the traffic and electric power systems thoroughly and there is still lack of an effective decision-making framework of prioritizing limited resources to enhance the resilience of such interconnected system considering uncertainties.

1.2.6 Resilience-based recovery scheduling of TN

The recovery from hazards refers to the process of infrastructure system bouncing from the lowest functionality level back to a certain level of functionality after hazards due to recovery activities. Devising an effective schedule to accommodate these recovery activities is often a non-trivial task in that available restoration resources are typically insufficient compared to the needs arisen from large-scale disruptions caused by the hazards. Different schedules apparently will yield different recovery trajectories of infrastructure's functionality (i.e., the functionality over time). Decision maker may need to pursue some desirable recovery goals which can only be satisfied by some particular shapes of the recovery trajectories,

and finding these corresponding schedules to meet such needs is however often not easy (Bocchini and Frangopol 2012; Li et al. 2019a). The recovery scheduling of TN in literature is usually formulated as a bi-level optimization problem, in which the lower one focuses on the functionality quantification while the upper one tackles the schedule optimization. A brief review of the current practices is made for these two topics in the following.

1.2.6.1 Functionality quantification of TN

The functionality quantification is to characterize the functionality of the TN over time under a given schedule. Topology-based (Hu et al. 2016; Ulsan and Ergun 2018; Zhang and Wang 2016; Zhang et al. 2015) or flow-based functionality (Bocchini and Frangopol 2012; Li et al. 2019a; Vugrin et al. 2014; Zou and Chen 2020a) metrics for TN have been commonly adopted in existing work. In the derivations of both types of metrics, most studies only assumed a single class of users of the TN: the well-informed and rational ones who possess perfect information of the TN and always make rational route choices. However, such an assumption is often not valid, which is especially true during the recovery process of the TN. First, not all TN users are familiar with the TN to the extent of owning perfect information of the TN and the level of perceived information by the users also highly depends on communication and automation technologies equipped in road infrastructure and vehicles (Mostafizi et al. 2017; Wang et al. 2019). Second, the configuration of the TN can be in a constantly evolving environment as the recovery progresses. The fastest path connecting an origin and a destination for one day may be different from that for another; the well-informed users might adapt their travel plans pretty quickly while the ill-informed ones might not. Despite substantial research efforts on the recovery scheduling of the TN, little attention has been paid to the existence of the multiclass users in terms of their different levels of perceived knowledge and travel

behavior, and the impact on the scheduling decision also remains understudied (Ahmed et al. 2019; Bagloee et al. 2017; Faturechi and Miller-Hooks 2014b).

In fact, due to the significant advances in the information and communication technologies and wide deployment of intelligent traffic system in recent years, connected and autonomous vehicles (CAV) have emerged as the effective solution to modern mobility because of its potential benefits of facilitating safe driving, relieving traffic congestion, and reducing energy consumption (Ahmed et al. 2019; Li et al. 2019b; Mostafizi et al. 2017; Osman and Ishak 2016; Ye and Yamamoto 2018). Thanks to the vehicle-to-vehicle (V2V) and vehicle-to-infrastructure (V2I) communication systems, the CAVs can communicate with surrounding vehicles and infrastructure and thus acquire more detailed and comprehensive information about the TN's state than traditional human-driven vehicles (HDVs) (Bagloee et al. 2017; Wang et al. 2019). The CAVs are expected to be largely available on market by 2022 or 2025 (Bansal and Kockelman 2017; Ye and Yamamoto 2018). Given the considerable increase of market penetration rate of CAVs in forthcoming future and significant difference of the route-choosing behavior between the CAV and HDV users, decision makers of the infrastructure investment who fail to account for mixed traffic environment (i.e., the presence of both well-informed CAVs and less-informed HDVs) in the functionality quantification of TN may end up with ineffective and costly recovery strategies.

1.2.6.2 Recovery schedule optimization

With the functionality quantification method established in the lower level, the recovery schedule optimization in the upper level is to find the optimal schedule to restore damaged components over time to achieve the resilience-based recovery objectives subject to resource availability. To solve this NP-hard problem, various solution procedures have been proposed, which can be roughly classified into three types:

exact methods, ranking-based methods, and metaheuristics.

Due to the computational complexities, the exact methods are usually applicable to small network instances (Almoghathawi et al. 2019; Barker et al. 2013; Fang and Sansavini 2019; Gong et al. 2009; Ouyang et al. 2019; Tuzun Aksu and Ozdamar 2014; Xu et al. 2020). Ranking-based methods often require carefully handcrafting problem-specific indicators for ranking, which heavily rely on the experience and judgement of the researchers to avoid unsatisfactory results (Almoghathawi and Barker 2019; Hu et al. 2016; Li et al. 2019a; Liu et al. 2020; Özdamar et al. 2014; Uluşan and Ergun 2018; Yonca et al. 2018).

Compared to the exact and ranking-based methods, metaheuristics are a more general type of method to obtain near-optimal schedule solutions in a tractable time, such as genetic algorithm (Bocchini and Frangopol 2012; Li et al. 2019a; Ouyang and Wang 2015; Zhang et al. 2017; Zhang and Miller-Hooks 2015), approximate dynamic programming (Medury and Madanat 2013; Nozhati et al. 2019, 2020), simulated annealing algorithm (Hackl et al. 2018; Vugrin et al. 2014), and ant colony algorithm (Vodák et al. 2018). The common key step in these population-based search metaheuristics is to achieve the effective exploration in the solution space by generating and assessing sufficiently large candidate solutions. But this step in the network recovery scheduling is often associated with extensive computational burden. Because on the one hand, the evaluation of each candidate schedule needs to invoke the functionality quantification to characterize the network functionality over time under each schedule, while the functionality quantification itself in the low-level of this problem can be quite computationally expensive when more informative flow-based quantification metrics are used. In such circumstances, evaluation of a large number of generated solution samples can be prohibitive. On the other hand, the large solution space of the schedule optimization in nature usually calls for the need of enough candidate solutions for exploration, especially for large-scale

network instances. Therefore, the metaheuristics should be well-designed to reach the balance between optimization performance and computational cost before becoming feasible for large-scale network recovery scheduling problems.

1.3 Research gaps and motivations

1.3.1 Simulation of crowd dynamics in the subway station

Subway systems, as a type of popular public transportation mode, have been adopted by many large and medium-sized cities due to its advantages such as large capacity, high efficiency, and low pollution. While subway systems provide convenience in public transport, factors regarding complexity of station layout and heavily overcrowded population can pose potential risks to human safety in emergency situations. For example, fire accidents happened in underground space can cause tremendous magnitudes of injury and casualties (Shi et al. 2012; Zhang et al. 2016). Therefore, with a high number of people using subways at the same time, subway stations must be appropriately designed to allow people to move easily during both typical operations and under emergency evacuation situations.

Crowd simulation has been widely adopted to assess the potential safety risks to passengers in metro stations (Hong et al. 2016). Many microscopic numerical models have been proposed due to the flexibility, such as ABM, SFM, and CA model. Lei et al. (2012) used the SFM based FDS+Evac simulation software to study the effects of occupant density, exit width, and automatic fare gates on evacuation time. Shi et al. (2012) investigated the metro station evacuation strategies using an agent-based grid model. Song et al. (2013) employed a discretized version of the SFM in the crowd evacuation simulation for bioterrorism in subway stations. Seriani and Fernandez (2015) adopted a continuous ABM to determine the effect of pedestrian traffic management in the boarding and alighting time at metro stations. Chen et al. (2017)

embedded the SFM in their ABM for pedestrian simulation in subway stations.

Among these microscopic models, the ABM, as a general modeling concept, is flexible to incorporate advantages of other models and powerful to produce complex system behaviors through defining relatively simple local rules. This is particularly important for emergency scenarios when people may show different behavior patterns due to panic. The ABM can be effective and convenient in taking into consideration the factors that can affect their movements and evaluating how people respond and move around in such scenarios. These results can be used to improve the emergency response strategy of infrastructure systems. Therefore, ABM is adopted to simulate pedestrian dynamics in the subway station and the rules of pedestrians' destination choices and movements on different areas of the metro station, such as ticket gates, stairs, trains, and platform, are established.

It was found that most of existing studies on pedestrian evacuation usually focused on the general environment or single behavioral or environmental factor, e.g., hazardous scenarios (Song et al. 2013; Wan et al. 2014), walking on stairs (Qu et al. 2014), waiting behavior (Davidich et al. 2014), and alighting and boarding movements (Zhang et al. 2008). However, the subway station is a very complex environment and has its own unique characteristics, such as the ticket gates, the configuration of train car, the height difference between structures, and the different population densities in rush and non-rush hours. Pedestrians can exhibit different egress behavior depending on different environments and corresponding psychological and physical states. All these factors need be taken into account in order to achieve a comprehensive assessment of the egress safety of the subway station.

1.3.2 Incorporation of human factors into crowd evacuation model under toxic gas incident

Natural or human-made disasters, such as earthquake, tsunami, fire, and terrorist attack, can pose great

risks to human lives and result in tremendous economic losses. Evacuation can be the most effective and important strategy to save human lives in most emergency scenarios (Wang et al. 2016). The topic of the crowd emergency modeling and simulation has attracted much research attention in recent years. It was found that the emergency egress behavior of human is not only affected by the external environment, but also depends on internal states of evacuees, such as personality, familiarity with the environment, information perceived, and emotional responses triggered by the specific incident and casualties (Cao et al. 2017; Dossetti et al. 2017).

Many existing models focused on establishing physical movement rules of evacuees based on collision avoidance and route finding (Burstedde et al. 2001; Cao et al. 2015; Chen et al. 2012; Helbing et al. 2000). In those models, evacuees were usually assumed to be omniscient and rational, which means they can detect the disaster instantaneously and initiate the evacuation simultaneously. As a result, the internal states of the evacuees were either neglected or always remain the same as the pre-specified values during the whole evacuation process.

Many studies have confirmed that panic can occur in emergency situations and lead to irrational behavior which may cause more casualties than the actual disaster itself (Helbing et al. 2000; Helbing and Mukerji 2012; Wang et al. 2015). However, few of the existing ones considered how panic originates and propagates through the interactions among evacuees based on their personalities, emotion states, and perceived information, as well as their effects on the evacuation process and casualty. For example, Helbing and Johansson (2013) summarized the research findings of the crowd dynamics based on the classical social force model. They quantified the nervousness of evacuee using a single coefficient, which influences the movement fluctuation, desired velocity, and herding behavior for panicking evacuees. Wang et al. (2015)

incorporated panic behavior using panic indices into the multi-agent based crowd model for simulating evacuation in stadium. The panic indices were only affected by surrounding crowd density and gender and did not account for the contagion mechanism. Neto et al. (2015) applied the emotion contagion model to crowd simulation and presented evacuation results of nonemergency scenario. Nicolas et al. (2016) implemented social contagion dynamics in the cellular automata model and showed that the relations found in the contagion-free model can fail at high contagion strengths. No real danger and information spreading were included in their work. Zheng et al. (2019) carried out the emergency evacuation simulation considering the emergency diffusion. The panic level in their model was determined by the surround population density and the proximity to the danger source and the effect of emotion contagion was overlooked.

In fact, in a situation where the danger is not detected promptly and an effective warning system is lacking, evacuees usually do not initiate the evacuation immediately following the occurrence of the incident due to the delay of the information spreading and communication. Meanwhile, emotion can also be affected by surrounding environments or other evacuees through emotion contagion and vary over time. These two factors can both influence an evacuee's behavior and decision-making, which determine the whole evacuation pattern. Therefore, in order to simulate the crowd evacuation behavior more realistically, emotion contagion and information spread should be taken into account.

A typical scenario as mentioned above is the evacuation under toxic gas incident. The toxic gas incident discussed here is a general phenomenon about sudden release of toxic gas, which can be an accidental gas leakage or intentional bioterrorism attack. It is found that toxic gas attack is an attractive means for terrorists to conduct mass destruction due to devastating power, huge infection, low requirement of specialized

knowledge, and inexpensiveness to produce required materials (Henderson 1999; Wan et al. 2014). The biological weapons can not only cause tremendous casualties, such as in the 1995 Tokyo subway sarin attack, but also provoke social disruption and panic as in the 2001 anthrax attack in America. Among the methods of releasing pathogen in bioterrorism, the aerosol dissemination is the greatest concern since toxic-by-inhalation agents can be spread rapidly and influence the crowd effectively (Barrett and Adams 2011; Grundmann 2014; Song et al. 2013). Moreover, toxic gases are often hard to be detected promptly due to their invisibility, tastelessness, and odorlessness. Therefore, bioterrorism can pose a great danger to public safety of high crowd density sites such as train or metro stations, museums and airports in urban areas. This dissertation aims at presenting a method of crowd evacuation simulation under toxic gas incident considering the effects of emotion contagion and information spread.

1.3.3 Resilience modeling of interdependent traffic-electric power system subject to hurricanes

CISs provide essential services that support security, economic prosperity, and quality of life, and thus act as the bases of normal functioning of modern cities and well-being of citizens (Rinaldi et al. 2001). However, these systems can be vulnerable to natural hazards, accidents or intentional attacks, which often cause undesirable operational failures and severe consequences. Since it is not always possible to reduce the likelihood and potential impacts of undesirable events through prevention and protection strategies, such as increasing the system redundancy and reliability, recent efforts have been directed to enhancing the resilience of CISs through effective preparedness, response, and recovery (Hosseini et al. 2016). Furthermore, those CISs, such as electric power, gas, water, transportation, and telecommunication, do not operate separately but are highly interconnected and mutually dependent (Ouyang and Wang 2015; Rinaldi et al. 2001). The performance of those interdependent CISs collectively plays a major role in determining

the community resilience subjected to major disasters (Reed et al. 2016).

Although interdependencies may potentially promote the operational efficiency of CISs as a whole, they have been found to primarily increase the system vulnerability due to the increased complexities and possible cascading failures across different systems (Ouyang and Wang 2015). For example, the failure of one node of a power network can not only affect its downstream nodes but also result in power flow redistribution, which may cause more failures of overloaded nodes. On the other hand, other CISs requiring steady power supply, such as telecommunication and railway, may also lose functionality as a result of the power loss. Therefore, to design a more resilient community requires full consideration of interdependencies among those interconnected CISs when disruptions occur (Heracleous et al. 2017).

Researchers have conducted extensive studies on the resilience and vulnerability of TN (Chen and Miller-Hooks 2012; Edrissi et al. 2015; El-rashidy and Grant-muller 2014; Ip and Wang 2011; Zhang and Wang 2016) and EPN (Ouyang et al. 2017; Salman et al. 2015; Unnikrishnan and van de Lindt 2016). Nevertheless, most of the existing studies treated TN or EPN as single or isolated systems by omitting the potential interdependencies, which may lead to inaccurate conclusions (Fotouhi et al. 2017). There have been limited studies on interdependency among CISs including TN and EPN (Adjetey-Bahun et al. 2016; Gong et al. 2014; Lee et al. 2007; Loggins and Wallace 2015), and few has explicitly considered the realistic interactions of traffic flow in road networks and electric power supply on the resilience assessment with sufficient details. In fact, signalized intersections are common for urban road networks and their delays have considerable impact on the total travel time and the passengers' route choices (Mazloumi et al. 2010). The normal functioning of traffic signals relies on the electricity supply of the EPN, and the overhead distribution lines of the EPN often utilize the right-of-way for transportation systems (Ellingwood et al.

2016). In the U.S., there are still many areas with aging overhead power infrastructures (ASCE 2017). While undergrounding the distribution system can be used to harden the existing system, researchers also pointed out that burying the system is not cost effective due to the high cost (Salman et al. 2015). Thus, for these areas, hazards such as hurricanes can damage the poles supporting the distribution lines, which may block the road and interrupt the traffic flow (Alipour et al. 2018; Salman 2016). The indirect loss caused by the functionality degradation (i.e., the increase of traffic delay) of the disrupted TN can accumulate over time until the TN is fully recovered. It was found that this indirect loss usually surpasses the direct loss (i.e., the repair cost of the damaged components of the TN) (Alipour and Shafei 2016). Moreover, the disrupted TN impacts the accessibility and efficiency of recovering efforts of damaged power system, while the delayed repair of EPN in turn impacts the recovery planning of other facilities, including TN (e.g. intersection traffic lights without power). Therefore, given their importance of underpinning the resilience of other critical facilities and the whole community, the sophisticated interdependency between these two CISs need to be modeled appropriately in the resilience study.

1.3.4 Resource prioritization to enhance the resilience of interdependent traffic-electric power system

The great risks and tremendous damages caused by human-made and natural hazards call for the needs of pre-disruption mitigation and post-disruption repair actions on the CISs. The mitigation actions aim to reduce the probability of occurrence of hazardous events or alleviate the negative impacts, such as retrofitting the components, expanding the existing system, and pre-positioning resources, while the repair actions aim to restore the system functionality by repairing the damaged components (Faturechi and Miller-Hooks 2014a). However, the available resources to perform these actions are often limited, especially during the post-disruption stage. Since different CISs can be disrupted at the same time, various types of

stakeholders can be involved in the resilience enhancement planning and they may compete for limited shared resources such as machines, vehicles, and materials and make decisions based on different priorities. It is found that these critical decisions are often made from personal experiences, judgement or intuition, which may not only be ineffective but also introduce extra damages to the disrupted system (Shin et al. 2019). Therefore, it is necessary to devise science-based cost-effective resource allocation strategies to prioritize limited resources to achieve the optimal balance between CIS performance and cost (Liu and Frangopol 2005; Zhang and Wang 2017).

Based on the proposed quantification framework of the interdependencies between TN and EPN, the resilience enhancement strategies for these two systems can be devised. It is noteworthy that many urban traffic systems have already been suffering from severe daily peak-hour congestions (Ben-Akiva et al. 2012). The disruptions to TN such as roadway capacity reduction, vehicle accidents, and malfunctioning traffic signals may worsen the situation and increase traffic delay significantly (Calvert and Snelder 2018). But in modelling traffic flow, most researchers either used a general-purpose network-based method without considering the user equilibrium (UE) condition (Chang et al. 2012b; Zhang and Wang 2017) or adopted a relatively simple static traffic assignment (STA) method (Alipour and Shafei 2016; Fotouhi et al. 2017). The STA method has been criticized for its inability to accommodate the roadway capacity constraints and time-varying traffic demands and flows in congested TNs. Thus STA may yield unrealistic traffic flow patterns and has been blamed for several expensive but ineffective roadway expansion projects (Chiu et al. 2011; Marshall 2018; Nie et al. 2004). Since the traffic systems are critical to supporting some time-sensitive post-disaster emergency response activities such as medical aids and distribution of essential supplies, it is necessary to take the realistic traffic dynamics into consideration when evaluating the

performance of disrupted TNs.

While the past research yielded some insights into understanding the resilience of TN and EPN, further studies are still required on appropriately modelling the sophisticated interdependencies between these two CISs with adequate details in order to make the most cost-effective resilience investments. This dissertation aims at developing a decision-making framework for prioritization of mitigation and repair actions to enhance the resilience of an interdependent traffic-electric power system in terms of its functionality under budgetary constraints.

1.3.5 Resilience-based recovery scheduling of TN

From the perspective of resilience enhancement, post-hazard recovery strategies should be treated as equally important as pre-hazard preventative strategies to maintain a certain level of functionality of the TN and build a resilient community against hazards (Fotouhi et al. 2017; Hosseini et al. 2016; Zhang and Wang 2016).

Based on the literature review on the recovery strategies of TN in Section 1.2.6, it can be found that while the existing work as summarized above yielded some insights into understanding and application of the post-hazard recovery scheduling of TN, the limitations in the functionality quantification of TN and the solution procedure necessitate further studies. In the functionality quantification of TN, all users were assumed being able to perceive perfect information of the TN state while in reality multiclass users exist with different levels of information perception and can exhibit different route choices in the time-varying recovery process. Hence, it is necessary to account for the impact of different travel behavior on the recovery scheduling decision, especially when facing a forthcoming mixed traffic environment including both well-informed CAV and less-informed HDV users. In the solution procedure, despite their generality

and successful applications for small-scale problems in existing studies, the metaheuristics can suffer from excessive computational burden in order to explore the large solution space in tackling the large-scale network instances with complex flow-based functionality quantification methods.

1.4 Objectives

The transportation infrastructure is prone to many natural or human-made disasters and thus the normal daily mobility patterns can be disrupted. In order to help devise cost-effective disaster mitigation and recovery decisions to save human lives and ensure infrastructure safety, it is important to take into account the impact of human mobility modes in disaster scenarios. As discussed in Section 1.3, previous studies have certain limitations in theoretical considerations and modeling methodologies regarding this topic. Therefore, this dissertation focuses on modeling and assessing two important mobility modes (i.e., walking and driving) in disaster scenarios. It aims to (1) develop agent-based crowd simulation models to evaluate the crowd dynamics in complex environments and investigate the interplay between human factors and evacuation behavior; (2) develop functionality modeling and decision-making frameworks to assess and enhance the resilience of TN subject to hazards. Specifically, the objectives of this dissertation are as follows:

The first objective is to model crowd dynamics in complex environments such as subway station in both normal and emergency scenarios. Compared with most of existing studies on pedestrian evacuation which usually focused on the general environment or single behavioral or environmental factor, this study provides a more comprehensive and holistic model for assessing the egress safety of a typical subway station for people in both trains and platforms under normal and extreme conditions.

The second objective is to incorporate the effects of emotion contagion and information transmission into the crowd evacuation simulation. This study characterizes and examines the interplay among emotion contagion, information diffusion, decision-making process, and crowd dynamics; meanwhile, the casualty phenomena are taken into account. In an emergency scenario such as the toxic gas incident in which the danger is not detected promptly and an effective warning system is lacking, the proposed model considering the interactions between the human factors and crowd dynamics may lead to more realistic simulation results.

The third objective is to develop a resilience assessment framework of the interdependent traffic-electric power system. The proposed framework captures three types of interdependencies between traffic and electric power systems and covers three stages (i.e., preparedness, response, and recovery) of functionality in characterizing the resilience of this interdependent system. Different resilience improvement strategies in different stages of resilience are compared and the most effective strategies are suggested for each system.

The fourth objective is to develop a decision-making framework to optimize the resource prioritization to enhance the resilience of the interdependent traffic-electric power system. The proposed framework has the following four major contributions: (1) the formulation of mitigation and repair decision framework to support resilience enhancement of the coupled traffic-electric power system considering interdependent network functionality, uncertainties of the disruptions, traffic demands and costs, and budgetary constraint; (2) the modeling of interdependencies between traffic and electric power systems with more refined details; (3) the adoption of the simulation-based dynamic traffic assignment algorithm in characterizing traffic flow, which can capture more realistic traffic dynamics in congested urban roadway networks; (3) the application

of the binary particle swarm algorithm combined with the knapsack-based heuristic initialization to find solutions; (4) and the development of priority index ranking the importance of each component in the interdependent system for mitigation and repair efforts.

The fifth objective is to develop a decision model for the resilience-based recovery scheduling of the TN in a mixed traffic environment with connected and autonomous vehicles (CAVs) and human-driven vehicles (HDVs). The major contributions are twofold: (1) the formulation of decision framework for resilience-based restoration scheduling of the transportation network considering multiclass users' travel behavior. With the travel behavior of both CAV and HDV users captured, such a framework can help decision makers better quantify the functionality of TN with different CAV penetration ratios to support effective recovery scheduling of TN; (2) the development of an active learning approach for solving the recovery scheduling optimization of TN efficiently and effectively, which enables the consideration of more complex and realistic low-level network functionality quantification and bears the potential of being extended to general large-scale network recovery problems with different types of networks and hazards.

1.5 Outline of the dissertation

The outline of the dissertation is as follows:

Chapter 1 provides the research background for this dissertation and presents the literature review on five main research topics. Then, the research gap for each research topic are identified and the research objectives are described.

In Chapter 2, an agent-based crowd simulation model is established which enables defining both normal and emergency scenarios with realistic considerations of some critical parameters and software functions, including number of trains, number of passengers, stairs, ticket gates, number of exits, passenger

destination choices, possible delaying of exiting the train and station. Comparative studies of both normal and emergency situations are conducted on a prototype subway station. Parametric investigations show the impacts of some key parameters on evacuation time and delay and present some valuable insights for understanding the potential causes of delay of evacuations and possible improvements of the subway station design in terms of emergency response.

Chapter 3 presents a method of crowd evacuation simulation under toxic gas incident considering the effects of emotion contagion and information diffusion. It consists of four main parts: the gas dispersion model, the information diffusion model, the emotion contagion model, and the modified social force model. First, the gas dispersion model characterizing the concentration of the toxic gas is used to determine the impairment of the pedestrian. Second, the spread of the information about the incident and the exits is modeled by the information transmission model and the emotion contagion model was adopted to quantify the emotion and panic. Then the social force model is modified to integrate these effects to generate the movements in the evacuation process. Numerical simulations show that the incorporation of emotion contagion and information transmission can cause significant difference as compared to existing models in terms of evacuation time, number of casualties, and number of collisions. The influences of the number of evacuees, the perception radius, and the number of authority figures on the evacuation are examined in the parametric study.

Chapter 4 presents a framework for resilience assessment of an interdependent traffic-electric power system subject to hurricanes. The traffic and electric power systems are both characterized using the flow-based mathematical representation and three types of interdependency are captured. A modeling procedure coupled with Monte Carlo simulation is presented to assess the resilience of both systems and to integrate

different improvement strategies into corresponding stages of resilience. The traffic and electric power systems in Centerville considering three improvement strategies are studied to demonstrate the proposed framework.

In Chapter 5, a bi-level, stochastic, and simulation-based decision-making framework is proposed for prioritizing mitigation and repair resources to maximize the expected resilience improvement of an interdependent traffic-electric power system under budgetary constraints. The upper level seeks to find the optimal resource allocation plan to maximize the expected attainable functionality gain. And the lower level characterizes the functionalities of the traffic and electric power systems considering three types of interdependency based on network flow analysis methods. The dynamic traffic assignment algorithm, rather than the static traffic assignment algorithm, is used in order to capture more realistic traffic dynamics in the congested urban roadway networks. Uncertainties in disruptions, traffic demands, and costs of mitigation and repair actions are also considered in the problem formulation. The problem is solved by the binary particle swarm optimization algorithm initialized with the knapsack-based heuristic, and the priority indices of disrupted components for mitigation and repair are then established based on the solutions. The proposed decision model is demonstrated using a portion of the traffic-electric power system in Galveston, Texas.

Chapter 6 develops a bi-level decision model for the resilience-based recovery scheduling of the TN in a mixed traffic environment with CAVs and HDVs. The lower level quantifies the TN's functionality over time considering different travel behavior of CAV and HDV users arisen from their different levels of information perception. The upper level presents a novel surrogate-based active learning approach based on the deep-ensemble-assisted efficient global optimization algorithm to solve the network recovery scheduling problem. In this approach, the embedded deep convolutional neural network ensemble can assist

in exploring the large solution space sufficiently as a computationally cheap surrogate function, and the efficient global optimization algorithm updates the deep ensemble in an active learning fashion and finds improved recovery schedule solutions iteratively. The proposed methodology is demonstrated using a real-world traffic network in Southern California under earthquake considering deterministic and stochastic repair durations.

Chapter 7 concludes the dissertation by highlighting the main findings and suggesting some future research directions.

CHAPTER 2 AGENT-BASED EVACUATION SIMULATION FROM SUBWAY TRAIN AND PLATFORM¹

2.1 Introduction

Subway systems have been adopted by many large and medium-sized cities due to the advantages such as large capacity, high efficiency, and low pollution. Although subway systems provide convenience in public transport, factors regarding complexity of station layout and heavily overcrowded population can pose potential risks to human safety in emergency situations. Therefore, with a high number of people using subways at the same time, subway stations must be appropriately designed to allow people to move easily during both typical operations and under emergency evacuation situations.

This chapter aims to develop an agent-based model (ABM) covering the simulation of passengers both from trains and on platforms facing different normal and evacuation scenarios in a typical subway station. Developed based on the NetLogo platform, the proposed model enables defining both normal and emergency scenarios with realistic considerations of some critical parameters and software functions, including number of trains, number of passengers, stairs, ticket gates, number of exits, passenger destination choices, possible delaying of exiting the train and station. Comparative studies of both normal and emergency situations are conducted on a prototype subway station. Parametric investigations show the impacts of some key parameters on evacuation time and delay and present some valuable insights for understanding the potential causes of delay of evacuations and possible improvements of the subway station

¹ This chapter is adapted from a published paper by the author (Zou et al. 2019) with permission from Taylor & Francis.

design in terms of emergency response.

2.2 Model development for subway evacuation

Engineers and architects must consider unique characteristics of subway stations that are not present in many other buildings: the total number of people remaining inside the subway station can vary dynamically because of two major sources. These include (1) people being transported to and away from the subway station through subway trains, and (2) people entering and leaving the building from the exits of the subway station. To comprehensively simulate the movement of people within the whole subway station is a very important and yet challenging work that needs to incorporate time-dependent interactions among passengers on the trains, passengers entering from outside of the station, and passengers inside the station. Therefore, in this study, the focus will be remained on the movements of people on the platform, people from the arriving trains, and people who choose to exit the subway station under emergency scenarios.

2.2.1 Subway system modeling

2.2.1.1 Subway station

The prototype subway station used in this study is based on L'Enfant Metro Station in Washington DC, as shown in Figure 2.1. There are two side platforms where people wait for the subway trains moving along two adjacent tracks in the middle. Each platform has a length of 136.5 m (447.86 ft.) and a width of 4.5 m (14.76 ft.). The main station exits located around the middle points of the platform have 4.5 m of width while the other exits have 2.5 m of width. The prototype station has a maximum of six exits for the station (three on each side).

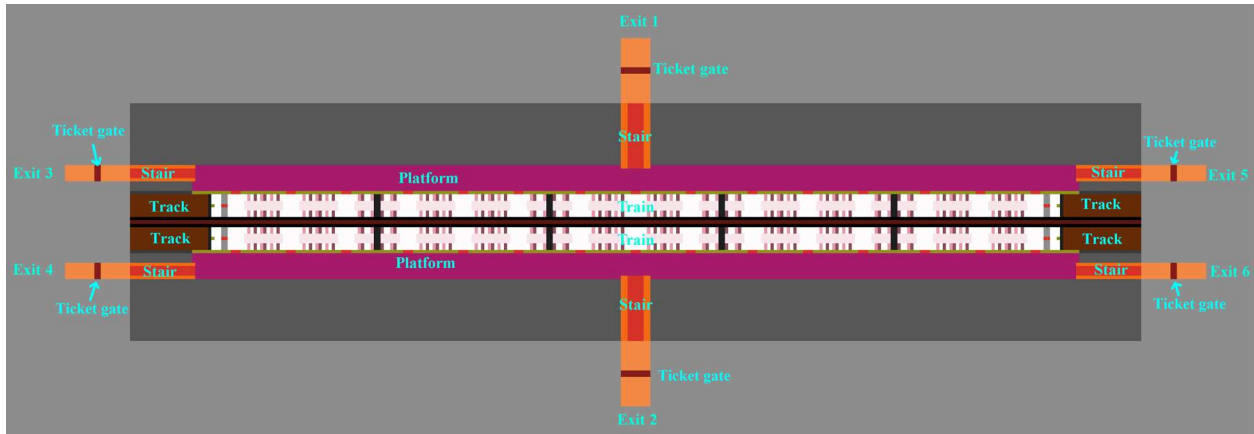


Figure 2.1 The layout of the prototype subway station

2.2.1.2 *Stairs to the exits*

In reality, the station exits can be on the same level of the platforms (i.e., horizontal and no stairs), or be lower or higher than the platform (i.e., linked by stairs or escalators). For multi-floor structures, stairs and escalators can lie on the primary evacuation paths to exits, and chaotic movements on stairs and escalators of panicking pedestrians during emergencies can lead to tragic trampling accidents (Li et al. 2014). Thus, to consider the effect of stairs on the evacuation, in this model, the path between the platform and the exit can be defined as horizontal, upstairs, or downstairs, as illustrated in Figure 2.2(a), (b), and (c), respectively. The total height of each stair in this model is set to vary between 3 and 10 meters. The inclination angle of the stairs in this simulation is assumed to be 30 degrees (Qu et al. 2014).

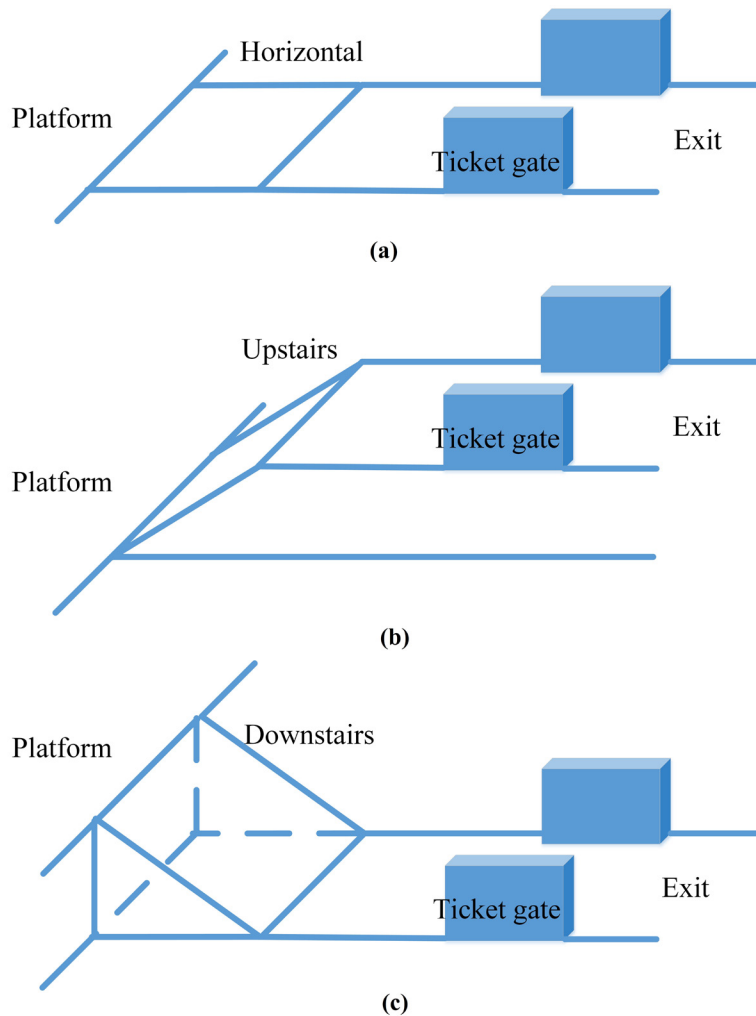


Figure 2.2 Three configurations of connection between the station platform and the exit: (a) horizontal; (b) upstairs; (c) downstairs

2.2.1.3 Ticket gates

Subway stations usually have automatic ticket gates for ticket checking located at the entrances and exits, and passengers need to lower their speeds to pass through such gates. To consider such speed reduction on the evacuation process, this model includes the ticket gates with a width of 10 m at the end of each exit (Figure 2.1). Furthermore, the speed that each agent passes the ticket gate is set to a value lower than its normal walking speed.

2.2.1.4 *Trains*

The subway train includes 5 cars following a typical train configuration. Each subway car has a similar layout with a length of 25.5 m (83.67 ft.) and a width of 3.5 m (11.48 ft.), in which there are 6 exits in total with three on each side (Roh et al. 2009). In this study, the station has two platforms on opposite sides and the two tracks are between these two platforms. The exits for each subway car will be only opened from the side next to the platform while the doors on the other side will remain closed. Therefore, there will be only three exits open for each subway car in this simulation. The areas of a typical car are classified into three categories, i.e., “Seat”, “Corridor”, and “Close-to-door”, as shown in Figure 2.3.

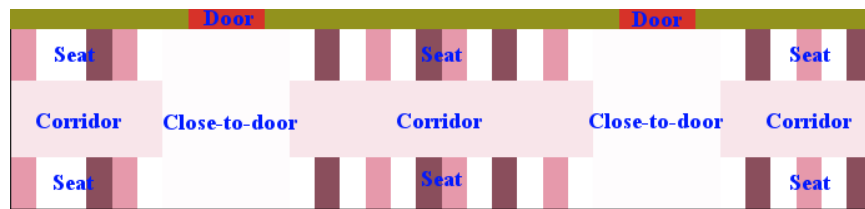


Figure 2.3 The areas in the car

In addition, this model also considers different numbers of the subway trains stopping on the tracks inside the station, which can be 0, 1, or 2, representing scenarios of no train, one train, and two trains, respectively.

2.2.2 *Pedestrian modeling*

In the model being developed, each pedestrian in the subway station is represented by an agent who can interact with surrounding environments based on predefined rules. In the following sections, the terms “pedestrian”, “passenger”, and “agent” will be used interchangeably. The model initializes all agents’ initial locations by randomly distributing them over the trains and platforms considering the passenger capacity of the station. Then, the main rule governing the agent’s movement is to determine the walking speed, destination, and walking direction in normal and emergency scenarios. It should be noted that the egress

behavior also depends on the psychological factors such as perceived emotion and stress and knowledge of spatial environment (Helbing et al. 2000; Tan et al. 2015). Vorst (2010) pointed out that the negative effects of these factors on the evacuation should be included in the evacuation model to be consistent with the reality. Although such psychological factors are not easy to be characterized using clear simulation representations, researchers have been developing models to reproduce collective behavior observed in the emergency evacuation. This study focused on the effects of perceived panic on the egress behavior: different from the behavior in normal scenarios representing the normal operation of the station, agents in emergency scenarios all try to exit from station as soon as possible and can usually exhibit typical panic characteristics (Helbing et al. 2000): (1) trying to move faster than normal; (2) starting to push and interacting more physically with people nearby; (3) being slowed down or blocked by fallen or injured people acting as “obstacles”; (4) arching and clogging near exits. These panic features are taken into account in the following rules.

2.2.2.1 Rules of walking speed

The main formulas to calculate the speed of agent are based on the Predetchenky and Milinskii method (Shi et al. 2009) and are defined as:

$$V = m \cdot \left[\frac{(112D^4 - 380D^3 + 434D^2 - 217D + 57)}{60} \right] \quad (2.1)$$

$$V_e = \mu_e \cdot V \quad (2.2)$$

where V is the standard speed (m/s) in the normal scenario, and V_e is the speed of pedestrians in the emergency scenario. Usually, V_e is higher than V (Gupta and Yadav 2004). D is the dimensionless

density:

$$D = \frac{N \cdot P}{A} \quad (2.3)$$

where N is the total number of agents; P is the area that an agent occupies, which is equal to 0.125 m^2 in this study (Almeida et al. 2012); and A is the area of where agents are located. m and μ_e in Eqs. (2.1) and (2.2) are the adjustment factors of speeds in different areas of the subway station, which are defined as follows:

For horizontal paths:

$$m = 1 \quad (2.4)$$

$$\mu_e = 1.49 - 0.36D \quad (2.5)$$

For upstairs movement:

$$m = \begin{cases} 0.785 + 0.09e^{3.45D} \sin(15.7D) & \text{when } 0 < D \leq 0.6 \\ 0.785 - 0.10\sin(7.85D + 1.57) & \text{when } 0.6 \leq D \leq 0.92 \end{cases} \quad (2.6)$$

$$\mu_e = 1.26 \quad (2.7)$$

For downstairs movement:

$$m = 0.775 + 0.44 e^{-0.39D} \sin(5.61D - 0.224) \quad (2.8)$$

$$\mu_e = 1.21 \quad (2.9)$$

2.2.2.2 Rules of destination choice

The destination choice depends on the scenario and the initial location of the agent. Generally speaking, in the normal scenario, some agents will remain in the station and other agents will exit, following the typical subway travel patterns; in the emergency scenario, all agents will try to exit from the station and will also move faster than in normal scenarios.

The initial locations of agents determine their possible destinations and moving paths. For passengers on a train arriving at a platform, they can choose either remaining on the train or getting off the train. Similarly, those passengers remaining on the platform also have different options: getting on the train, staying on the platform, transferring to another train, or exiting the station. Apparently, this information can vary significantly from station to station and from time to time. The most critical information from the evacuation simulation perspective, however, is about how many passengers will get off the train and exit the subway station. In order to define the destination choices of the passengers, two parameters are introduced: P_{train} and P_{platform} , denoting the probability of exiting from the train and the probability of exiting from the platform, respectively. For example, in the normal scenario, if P_{train} is 50%, half of agents inside the subway train will remain in the train while the other half will try to exit from the train. Similarly, if P_{platform} is 50%, half of agents on the platform will stay where they are while the other half will try to exit from the station. The P_{train} and P_{platform} can be adjusted to consider more sophisticated scenarios.

Apparently, the two percentages during normal situations usually depend on the specific travel behavior, such as how many people will get off the train at a specific station, and then how many will exit the station or transfer to another train. This data can usually be obtained from statistics of the historical data from a

specific subway station. As a general model, these two parameters P_{train} and P_{platform} are defined as variables instead of fixed numbers to allow for flexible applications with the specific data of traffic patterns. If it is in an emergency, both P_{train} and P_{platform} will become 100%, provided that all agents will choose exiting from the station.

2.2.2.3 Rules of walking direction

Once the destination of an agent is determined, the local moving direction for evacuation is needed to be assigned. For passengers initially distributed inside the train, their moving directions change with the specific areas they are located: passengers located in the “Seat” area move towards the “Corridor” area, passengers located in the “Corridor” area move towards the “Close-to-door” area, and passengers located in the “Close-to-door” area move towards the platform through the car doors (reference to Figure 2.3). For passengers on the platform, when multiple station exits exist, they tend to move towards the closest one.

To analyze the pedestrians passing through an exit, the width of the exit is divided into many 1-meter channels. It is assumed that each person has the same probability to choose any 1-meter “channel” of the exit door. In other words, for a given width of the exit, each person has the same probability to exit through the left, middle or right portions of the exit. This allows passengers to realistically move across the width of the exit.

In addition, the rule of collision avoidance is added, which states that if an agent is very close to another one, the first agent will try to avoid the contact by changing the walking direction. Again, this makes agents spread around the space because each agent will try to find a space that is not occupied by others.

2.2.2.4 Possible delays

In order to more realistically consider the movements of pedestrians, some delays should be

accommodated, including possible delays of passengers exiting the train and on the way to the exits of the subway station. The parameter P_{delay} is used to control the probability that agents (only those who will exit the station) will have some delays during the process of exiting the subway train due to several possible reasons: 1) in the normal scenario: decision-making process or delay of avoiding congestion; 2) in the emergency scenario: health condition, injury, or being unaware of emergency or evacuation needs. For example, if P_{delay} is 50%, an agent who is seated or standing inside the train has 50% chance of leaving from where the agent is for each second. Moreover, another parameter “Breaks?” is introduced to enable agents to make some stops on the way to the exits. These stops can occur because of many reasons such as falling, injury or other health conditions for those physically vulnerable people (Helbing et al. 2000). This parameter in the model can also be used to characterize the scenarios when toxic gas or other hazardous conditions exist which may impede the movement of people with more temporary stops for health reasons.

After the walking speed, destination, and walking direction are determined, the agent can start to move. The simulation stops when all agents who choose to egress have exited successfully. The ABM is established using NetLogo. Figure 2.4(a) and (b) show the interface of this model and also the model visualization of the simulated results, respectively.

For the visualization purpose, all agents are coded with different color schemes (black, green and yellow) in this model per the instantaneous status (Figure 2.4(b)): if an agent is coded in black, it will remain where it is; if an agent is coded in green or yellow, it will try to exit from the station: yellow means it is currently on the platform and green means it is inside a subway train. Different color schemes are updated in real time and allow the users to easily identify where people currently are and what their instantaneous statuses are in terms of movements.

With the proposed model, it is possible to create other different scenarios by modifying the number of people inside or outside the subway trains independently. In other words, the number of people inside the subway train has nothing to do with the number of people outside of the train. In this model, the maximum number of people inside is 1,337 for each subway train and the maximum number of people outside is 1,250 for each side of the platform, so a wide range of different numbers of people can be selected to create different scenarios.

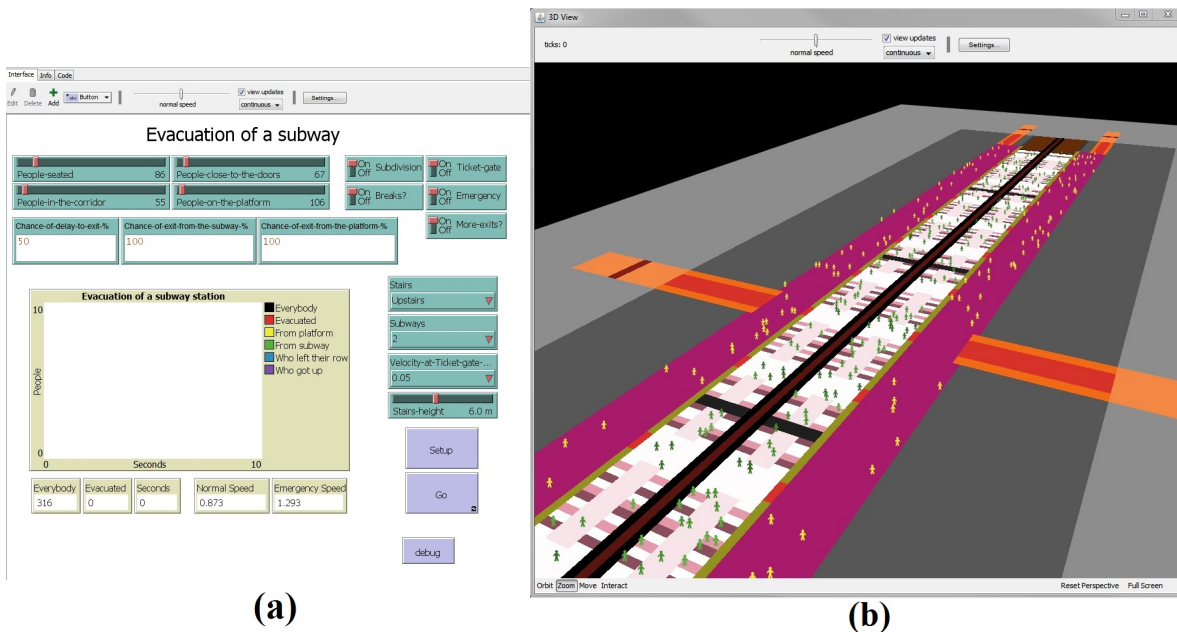


Figure 2.4 The interface of NetLogo-based agent-based model for the subway evacuation simulation: (a) model configurations; (b) model visualization

2.3 Simulation

A total of 12 cases are established in the simulation considering the variation in the scenario, the existence of ticket gate, stairs, the number of agents, and the values of P_{delay} , P_{train} , and P_{platform} . Due to the randomness of some variables (e.g., initial locations of agents, P_{delay} , and “Breaks?”), for each case, the simulations are repeated 10 times with stairs and 10 times without stairs to obtain the average evacuation

time as shown in Table 2.1. Simulations with 6 exits refer to the scenarios with all exits available while those with 2 exits imply the scenarios with only Exits 1 and 2 being open (Figure 2.1). For simulations with stairs, the stairs have inclinations of 30 degrees and vertical heights of 6 m. In emergency scenarios, it is assumed that no one tries to enter the station and the stairs are only used for moving people upstairs to evacuate. It is also assumed that people do not move between two trains by walking across the tracks. So, when two trains are on the tracks simultaneously, one train in the station would not affect the movement of people from the other one. The simulation with two trains remaining on the tracks simultaneously is to capture the evacuation scenario when two trains happen to stop at the platforms at the same time when an evacuation starts following the incident. The parameter “Breaks?” is set to be positive in this case to make the movements of people more realistic during emergencies. Two population scenarios are considered: a low number of people (885 people=360 people inside the trains + 525 people on the platforms) and a high number of people (5,174 people=2,674 people inside the trains + 2,500 people on the platforms). Considering that the ticket gate with turnstiles in subway stations can dramatically reduce the speeds of pedestrians who pass through them (Roh et al. 2009), for cases with a low number of people, the speed to pass the ticket gate is assumed to be 0.2 m/s; for cases with a high number of people, the speed to pass the ticket gate is defined as 0.05 m/s to represent the lower passing speed worsened by the clogging effects at the gate when there are many people passing through the narrow gate simultaneously. Those speed values can be further updated by observation data to reflect a more realistic scenario. Table 2.1 summarizes the simulation scenarios, associated parameters and the results.

Table 2.1 Simulation results of all cases

	Case	People in the train	People on the platform	All people	P_{delay} (%)	P_{train} (%)	P_{platform} (%)	Number of exits	Walking speed (m/s)	Time to exit from the train (s)	Time to exit outside station with stairs (s)	Time to exit outside station without stairs (s)	
Normal scenario	Without ticket gate	1	2674	2500	5174	50	45	10	6	0.32	24	268	253
		2	2674	2500	5174	50	100	10	2	0.32	27	392	371
	With ticket gate	3	2674	2500	5174	50	45	10	6	0.32	25	290	273
		4	2674	2500	5174	50	100	10	2	0.32	27	414	395
Emergency scenario	Without ticket gate	5	360	525	885	50	100	100	6	1.10	15	120	118
		6	360	525	885	50	100	100	2	1.10	15	175	174
		7	2674	2500	5174	90	100	100	6	0.43	74	216	207
		8	2674	2500	5174	90	100	100	2	0.43	74	294	278
	With ticket gate	9	360	525	885	50	100	100	6	1.10	16	122	121
		10	360	525	885	50	100	100	2	1.10	15	180	178

11	2674	2500	5174	90	100	100	6	0.43	76	232	221
12	2674	2500	5174	90	100	100	2	0.43	78	318	302

2.3.1 Normal scenarios

Case 1, 2, 3, and 4 are for normal scenarios that need to be evaluated to find out the typical daily travel pattern. In this scenario, the train stops at the station for a fixed time according to the timetable, and agents can board or alight at their normal speeds without panic behavior. Furthermore, this scenario is tested by using a high number of people to evaluate the most critical condition for a standard case. In addition, the parametric studies regarding the existence of ticket gates, P_{train} , and the number of exits in the normal scenarios are conducted to assess which variables are critical and how each variable affects the travel time. From Figure 2.5, as expected, in normal scenarios, having more exits and no stair will reduce the exit time of the passengers. The existence of ticket gates will slightly increase the exit time. More detailed comparisons are made in the following.

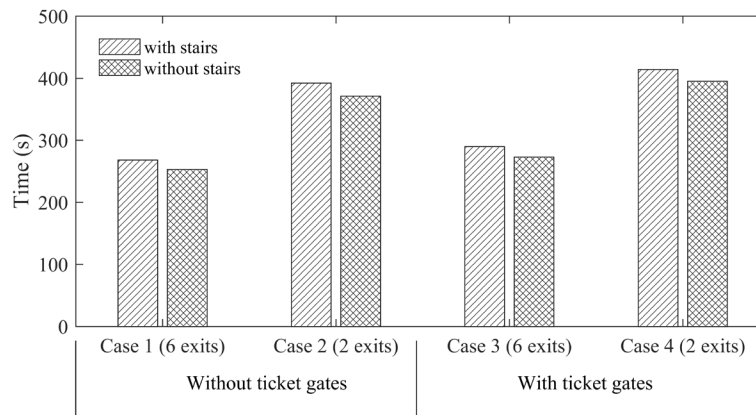


Figure 2.5 Comparison of evacuation time of cases in the normal scenario

2.3.1.1 Case 1 and 3: rush hour and six exits

The only difference between these two cases is the presence of ticket gates or not. For Case 1, there is no ticket gate, but for Case 3 there are. For Case 3, the total time to exit from the station is almost 21 s longer than that for Case 1. Since most platforms have exits at the ends, this phenomenon suggests that the ticket gates have quite considerable impacts on the evacuation time.

2.3.1.2 Case 2 and 4: rush hour and two exits

For Case 2 and 4, the same number of passengers as Case 1 and 3 are applied representing rush hour scenarios. With only two exits (Cases 2 and 4), the final time to exit from the station becomes higher (122 s longer) than the scenario with six exits (Case 1 and 3). For Case 2, there is no ticket gate, but for Case 4 there are. For Case 4, the total time to exit from the station is almost 23 s longer than that for Case 2. To evaluate the additional time people would need to exit from the subway train due to an increase in the number of people that want to get off the train, the ratio of people who leave the subway is increased to 100% of 2,674 individuals while for Case 1 and 3 the ratio is 45% of 2,674 individuals. As a result, the time to exit from the subway is increased by 2.5 s (average) for Case 2 and 4 than those of Case 1 and 3.

2.3.2 Emergency scenarios

Case 5, 6, 7, 8, 9, 10, 11, and 12 are for emergency scenarios. During an emergency, such as a fire or a terrorist attack, all people will try to exit and the probability of trying to exit from the train and the platform, i.e., P_{train} and P_{platform} , both become 100%. Those eight cases differ in the number of people in the train, the number of people on the platform, the total number of people, the existence of ticket gate, P_{delay} , and the number of exits. Different impacts of these parameters on the evacuation time can be found out and based

on which, the critical parameters can be identified. Figure 2.6 illustrates the results of the eight cases.

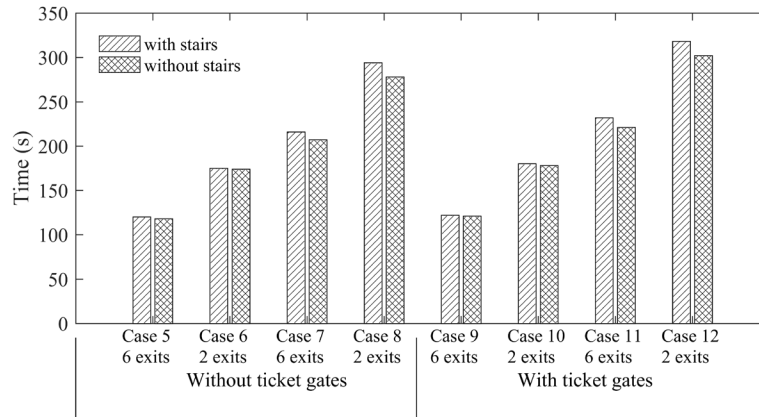


Figure 2.6 Comparison of evacuation time of cases in the emergency scenario

2.3.2.1 Case 5, 6, 9, and 10: low number of people

For Case 5 and 6, there is no ticket gate, but for Case 9 and 10, there are ticket gates. For Case 9, the average total time for all agents to exit from the station is 2.5 s longer than that for Case 5. For Case 10, the average total time for all agents to exit from the station is 4.5 s longer than that for Case 6. There is just difference of a few seconds between Cases 5 and 9 and there is also a small difference of total time to exit between Cases 6 and 10. This is because there are only a few people that are passing through ticket gates and only a little delay was observed. The difference between Case 5 and 6 is the number of exits. For Case 6 with only two exits, the total time for all people to exit from the station is 55.5 s longer than that of Case 5 with six exits. Similarly, for Case 10 with two exits, the total time for everybody to exit from the station is almost 57.5 s more than that for Case 9 with six exits.

2.3.2.2 Case 7 and 11: high number of people and six exits

To evaluate more critical scenarios during an emergency, some parameters are varied to conduct numerical simulations. It is assumed that the incident occurs during rush hours with a higher number of

people inside the subway train and station. People will also spend more time to exit from the train due to obstacles (e.g. debris, fallen people), smoke, or possible injury, and accordingly the probability of delay to exit P_{delay} is increased to 90% for each second. For Case 11 with ticket gates, the total time for all individuals to exit from the station is 15 s longer than the time for Case 7 without ticket gates. There remains such significant difference because of the speed reduction effects caused by ticket gates located near the exits. Moreover, it is also found that the results between the scenarios with stairs and without stairs have considerable difference, which is more significant than that when the number of people is low (Case 5 and 9).

2.3.2.3 Case 8 and 12: high number of people and two exits

The most critical condition is probably when only two exits are available during rush hours. Two exits for many people will increase the evacuation time considerably. As in Case 7 and 11, the P_{delay} is set to 90%, and the difference between Case 8 and 12 are only about the existence of ticket gates. For Case 12 with ticket gates, the total time for everybody to exit from the station is 24 s longer than the time for Case 8 without ticket gates. The higher number of people increases the time to pass through ticket gates. For cases of rush hour with two exits (Case 8 and 12), the average time for all agents to exit from the station is 79 s higher than the time of cases of rush hour and six exits (Case 7 and 11). The reduction of the number of exits increases the total time to exit from the station. The comparison between the results with and without stairs for both Case 8 and 12 suggests that the existence of stairs will cause a significant difference to the total evacuation time as compared to the rest cases when there are a high number of people and only two exits.

2.3.3 Discussion about factors influencing exit time

Based on the parametric studies, some discussions are made in terms of the factors influencing exit time.

2.3.3.1 Effects of P_{delay} , P_{train} , and number of people in the train

By analyzing the results above, it is found that there are several critical variables affecting the evacuation time to exits from the subway. The first one is P_{delay} , which indicates the probability of delay when evacuating from the subway trains.

For normal scenarios, P_{delay} is assumed to be 50% (per second before starting to move) to characterize an expected delay that people exhibit daily. This delay happens because some individuals can spend time thinking about where they need to get off the train or trying to get up from the seat, etc. This is apparently a minor delay because each agent inside the train will start to move most likely in the following a couple seconds. In other words, in this model, that P_{delay} being 50% reflects that in normal scenarios, there is sufficient time for all individuals to exit the subway train before the doors close and the train departs for the next station.

For emergency scenarios with a high number of people, P_{delay} is assumed to be 90% (per second before starting to move) to study an extreme delay. Such a severe delay can happen due to, for example, people not being aware of the emergency situations or physical constraints such as injury and congestion. Under this situation, the delay becomes considerable because each agent on a seat will most likely start to move during the next 20 s. Therefore, P_{delay} of 90% reflects that the time for the last agent to get off the train can be long (more than 1 minute), which can put people who experience delay in danger for emergency scenarios. Figure 2.7 shows the effect of P_{delay} on the time of exiting from the train. When P_{delay} is 90%, the

time for the last agent to get off the train can be as high as almost 80 s. In contrast, for the same number of people (2,674 people) but P_{delay} being 50%, the time to exit from the subway train is much lower: 27 s.

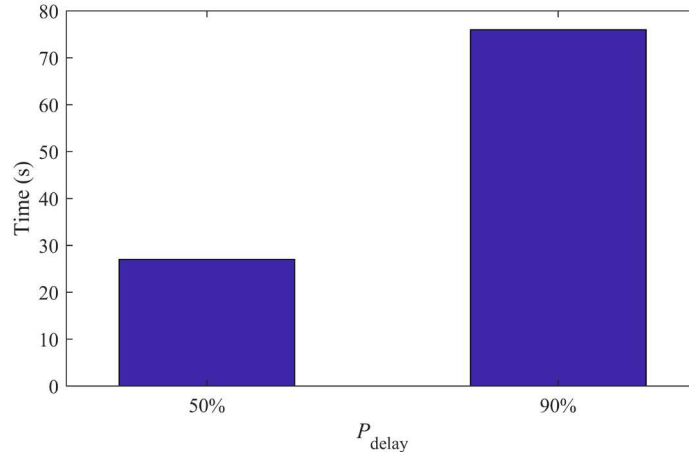


Figure 2.7 The effect of P_{delay} on the time of exiting from the train (high number of people and $P_{\text{train}} = 100\%$)

Other parameters that also considerably increase the time to exit from the subway train are P_{train} and the number of people in the train. With the same values for the number of people in the train and P_{delay} , when P_{train} is increased to 100%, the time to exit from the train becomes 27 s. When other conditions remain the same and P_{train} is 45%, the time to exit from the subway is 2 s less than that with P_{train} being 100% (Figure 2.8).

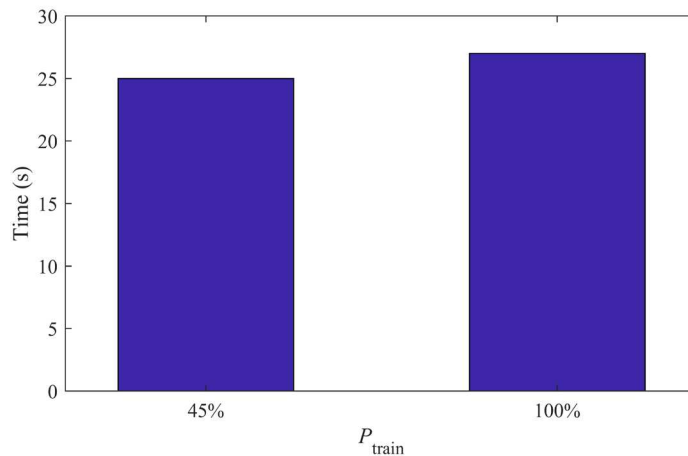


Figure 2.8 The effect of P_{train} on the time of exiting from the train (high number of people and $P_{\text{delay}} = 50\%$)

When all other parameters remain the same, the scenario with a high number of people can cause the

time to exit from the train to be 12 s more than that with a low number of people. For this situation, the results are 15 s for a low number of people and 27 s for a high number of people (Figure 2.9).

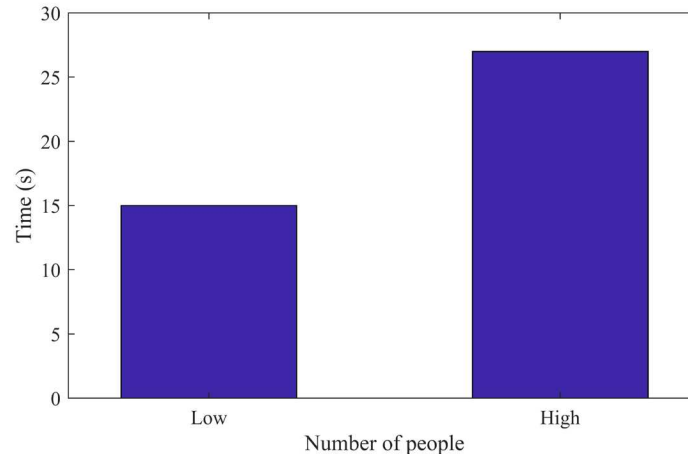


Figure 2.9 The effect of number of people on the time of exiting from the train ($P_{\text{delay}} = 50\%$ and $P_{\text{train}} = 100\%$).

2.3.3.2 *Effects of stairs*

Comparisons are also made between the results with and without stairs. With a high number of people and stairs, the average time for all the people to exit is 16 seconds higher than the situation with no stair. With the low numbers of people and stairs, the average time for everybody to exit is just 1 second higher than the situation where there is no stair (Figure 2.10). The results suggest that many people trying to exit through stairs at the same time can cause some delay that can put people's lives at risk. The challenge is how to avoid stairs on those subway platforms that are often not at the street level. Given the fact that it is nearly impossible to eliminate the stairs, some more effective evacuation measures are needed, such as designing faster emergency vertical evacuation venues, etc.

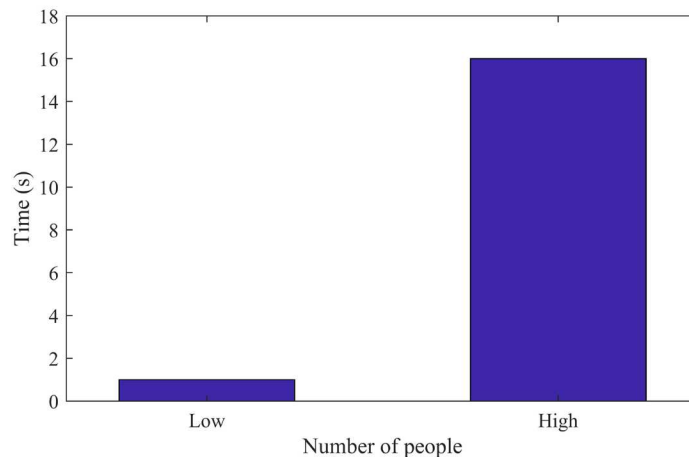


Figure 2.10 Time difference to exit from the station between cases with and without stairs

2.3.3.3 Effects of number of exits

Six exits are apparently very helpful during an emergency as compared to fewer exits (e.g., 2 exits) by substantially decreasing the time to exit from the station. As can be seen from Table 2.1, the additional time for all individuals to exit from the station due the reduction of exits is around 60 s for a low number of people and between 80 and 120 s for a high number of people. The reduction of exits is found to be the main reason that causes the exit time to increase. Therefore, creation of additional emergency exits will allow for a more effective evacuation from the station during an emergency by minimizing the time for all people to exit.

2.3.3.4 Effects of ticket gates

Another important issue is the ticket gates. Although the existence of ticket gates does not increase as much additional evacuation time as the reduction of exits does, the magnitude (around 20 s) is still something that should be seriously considered depending on the nature of the emergency. In addition, during an emergency with a high number of people, the presence of ticket gates could create an extremely high density of people gathering around these gates, leading to clogging. This is very dangerous because people

may push each other, fall or be trampled. In some situations, people could die because of the high concentration of panicking people trying to escape rather than from the emergency incident itself. If the ticket gates are essential, it will be very helpful to develop “smart” gate systems which can automatically open all the ticket gates at the same time during an emergency without causing any further delay.

2.3.3.5 Effects of crowd density

When the crowd density is low, people can walk normally due to the ample space around them. The time that someone requires to exit from a subway station will be less because people will usually have sufficient room to move around and the chance of suffering from the “bottleneck” effects around the exits will be low. In contrast, with a high number of people, people will start to clog around the exits. Although in normal scenarios the station space usually can accommodate all the people to exit rather quickly, the “bottleneck” phenomenon can decrease the speeds of people exiting the subway station considerably. During rush hours and under emergency with two doors, the “bottleneck” effect becomes more severe and people lose precious time around the exit doors without being evacuated quickly.

Meanwhile, the pedestrian’s speed is a function of crowd density due to the clogging effect. Therefore, a high number of people will decrease the average walking speed. On the other hand, an emergency incident may also motivate people to move faster because of the urgency they feel to save their lives (Tsai et al. 2013). Thus, the actual speed of the pedestrian depends on the tradeoff between these two factors. Ideally, the station management team should control the population size not to go beyond the critical point without jeopardizing an effective evacuation and causing significant delay, casualties and injuries. By appropriately defining desired evacuation performance, risk-informed management plan for possible emergency scenarios of any subway station can be made.

For evacuations involving subway trains, another important issue that can considerably decrease the movement speed of the public is the possible delays on the path to the exits. As discussed earlier, if the probability of delay to the exits from the subway trains is high because of some specific reasons, such as injury, toxic gas or smoke, fire, or health conditions, the time spent for all the people to escape from the subway trains can be as high as those listed in Case 7, 8, 11, and 12. More refined assessment can be made based on more detailed characterization of the specific emergency incident, subway station environment and possible health and psychological conditions of the passenger population both inside the subway trains and on the platforms.

2.4 Conclusions

A study to simulate passenger movements under normal conditions and evacuations under extreme conditions is carried out including people from both the subway trains and platform. Some detailed configurations of the station and pedestrians' different behavior are considered. Parametric studies including some main variables are conducted and the impacts of several major variables on the evacuation time are also discussed. Different from the previous studies focusing on some single aspects of the evacuation of people inside the subway station, this study provides a more comprehensive and holistic model for assessing the egress safety of a typical subway station for people in both trains and platforms under normal and extreme conditions. Further experimental and observation data can be used to calibrate some key parameters to achieve more realistic and site-specific simulation results. Some valuable insights are made from the demonstration and parametric study to understand the major causes of delay of evacuations and possible improvements of the subway system design in terms of emergency response. It is also found that more comprehensive studies based on specific emergency events are needed to provide more

customized analysis, which can provide the site- and event-specific emergency response plan including optimal routes and potential design improvements for different emergency incidents.

CHAPTER 3 SIMULATION OF CROWD EVACUATION UNDER TOXIC GAS INCIDENT CONSIDERING EMOTION CONTAGION AND INFORMATION TRANSMISSION²

3.1 Introduction

The emergency egress behavior of human is not only affected by damages caused by dangerous sources directly, but also depends on time-varying internal states of evacuees, such as the familiarity with the environment, the information perceived, and the emotional responses triggered by the incident and casualties. This chapter presents a method of crowd evacuation simulation under toxic gas incident considering the effects of emotion contagion and information diffusion, which consists of four main parts: the gas dispersion model, the information diffusion model, the emotion contagion model, and the modified social force model. The concentration of the toxic gas described by the gas dispersion model determines the casualty and the impairment of the pedestrian mobility. The spread of the information about the incident and the exits is modeled by the information diffusion model, and the emotion contagion model quantifies the emotion and panic. Then the social force model is modified to integrate these effects to govern the movements of people in the evacuation process. Numerical simulations show that the incorporation of emotion contagion and information transmission can cause significant difference as compared to existing models in terms of evacuation time, number of casualties, and number of collisions. The influences of the number of evacuees, the perception radius, and the number of authority figures on the evacuation are examined in the parametric study.

3.2 Model descriptions

² This chapter is adapted from a published paper by the author (Zou and Chen 2020b) with permission from ASCE.

In this section, the gas dispersion model is first introduced and the four damage states of pedestrians are defined. Agents are designed with certain attributes to represent pedestrians allowing for considering information transmission and emotional contagion. The effects of toxic gas, information transmission, and emotional contagion on the movements of agents are integrated into the social force model to simulate the evacuation process.

3.2.1 Hazardous environment: gas dispersion model

The toxic gas attack studied here is assumed to be an instantaneous chlorine attack, which means the concentration of chlorine is formed instantaneously once the attack happens since the time of release is much shorter than the dispersion time. The Gaussian Puff Model is a classical model to calculate the concentration of instantaneous sources (Hanna et al. 2008). When the wind speed is no more than 1 m/s as assumed in this study for indoor environment, the concentration of the gas can be calculated as

$$C(x, y, z) = \frac{2Q}{(2\pi)^{3/2} \sigma_x \sigma_y \sigma_z} \exp\left(-\frac{x^2}{2\sigma_x^2}\right) \exp\left(-\frac{y^2}{2\sigma_y^2}\right) \exp\left(-\frac{z^2}{2\sigma_z^2}\right) \quad (3.1)$$

where $C(x,y,z)$ is the gas density at the spatial location (x,y,z) ; Q is the total mass of toxic gas; and σ_x , σ_y , and σ_z are dispersion coefficients along the x , y , z -axis, respectively. Since the chlorine concentration level does not vary much from $z = 0$ m to the typical height of the pedestrian (approximately 1.60–1.80 m), here only the concentration level at $z = 0$ m is computed, which reduces the gas dispersion model to a 2D model. Suppose the total amount of leaked chlorine is 5 kg in the study and the maximum concentration at location (x, y, z) near the ground is (Wan et al. 2014):

$$C(x, y, z) = 26.15 \exp[-2.2635(x^2 + y^2)] \quad (3.2)$$

After the concentration of chlorine gas is known, the casualties due to the toxic load can be determined and are classified into four categories as listed in Table 3.1 (Wan et al. 2014).

Table 3.1 Damage states of pedestrians caused by chlorine concentration

Distance to gas source (m)	Damage state	Speed reduction factor γ (%)
≤ 2.025	Dead	100
[2.025, 2.34]	Seriously injured	50
[2.34, 2.435]	Slightly wounded	10
> 2.435	Normal	0

3.2.2 Agent design

To allow for interaction dynamics of pedestrians from information and emotion perspectives and consider the heterogeneity, pedestrians are designed to be intelligent agents who can possess certain degrees of knowledge about the environment and their neighbors and act accordingly based on the perceived information and emotion. Table 3.2 lists relevant attributes used for modeling information transmission and emotion contagion, including both time-dependent (defined as functions of time t) and time-independent attributes. For time-dependent attributes, they will be recalculated in each time step during the simulation, while the time-independent attributes remain constants once they are initialized at the beginning of the simulation. The detailed explanations about the parameters in Table 3.2 can be found in the following sections introducing the information transmission and emotion contagion models.

Table 3.2 Pedestrian's attributes related with information transmission and emotion contagion

Parameter	Value	Description	Reference
$R_{i,P}$	Depending on the environment	Perception radius	(Ma et al. 2016)
$S_{i,D}(t)$	{Dead, Injured, Wounded, Normal}	Damage state	(Wan et al. 2014)
$S_{i,E}(t)$	{Infected, Susceptible}	Emotional state	(Cao et al. 2017)
$S_{i,I}(t)$	{True, False}	Indicating whether the agent knows the incident or not	–
$\alpha_i(t)$	{0.2, 0.5}	Tendency of herding	(Helbing et al. 2002)
$t_{i,reaction}$	1 s	Reaction time after know incident and before initiating evacuation	(Shields and Boyce 2000)
$EC_i(t)$	Exit number	Exit choice	–
P_i	Uniform random number within [0,1]	Personal sensitivity index	(Cao et al. 2017; Fu et al. 2017)
$T_{i,E}$	Uniform random number within [0,1]	Emotion threshold	(Cao et al. 2017)
$E_i(t)$	Uniform random number within [0,1]	Emotion value	(Durupinar 2010)
$E_{i,init}$	Random number greater than $T_{i,E}$	Initial emotion value once changing from susceptible state to infected state	(Cao et al. 2017)
$d_i(t)$	Lognormal random number ($\mu_d=0.5, \sigma_d^2=1.5^2$)	Panic dose released	(Cao et al. 2017; Durupinar 2010)
$D_i(t)$	Summation of $d(t)$ of neighbors	Accumulated panic dose received	(Cao et al. 2017; Durupinar 2010)
$T_{i,P}$	Lognormal random number ($\mu_{TP}=4, \sigma_{TP}^2=2.8^2$)	Threshold of accumulated panic dose	(Durupinar 2010)
β	0.2	Emotion decay coefficient	(Cao et al. 2017)

Note: the subscript i indicates the agent number; μ_d and σ_d^2 are the mean and variance of $d_i(t)$, respectively; μ_{TP} and σ_{TP}^2 are the mean and variance of $T_{i,P}$, respectively.

Each agent in the simulation has its own independent perception space defined by a circular area with the perception radius R_p , as shown in Figure 3.1. The small circles represent the pedestrians, within which

the arrow indicates the current moving direction. The agents can only perceive information within the perception space, i.e., the solid circular area, via its vision and hearing. In this study, the visual information includes the building information, other agents' moving speeds and directions, panic based on others' facial expressions, body languages, dangerous sources and casualties. The auditory information indicates the emergency information, the exit information, and other knowledge and experience that the agent is able to share with its neighbors using verbal language while passing by each other. The possible activities of information exchange and emotion contagion are all assumed to occur within the perception space. The perception radius depends on the agent's physiological condition and the surrounding environment. Two types of agents are considered here: common pedestrians and authority figures. The authority figures are typically security officials or evacuation leaders who are familiar with the environment and can calm the panic emotion of evacuees nearby. They differ from general public in terms of the behavior of information transmission and emotion contagion, which is elaborated in following subsections.

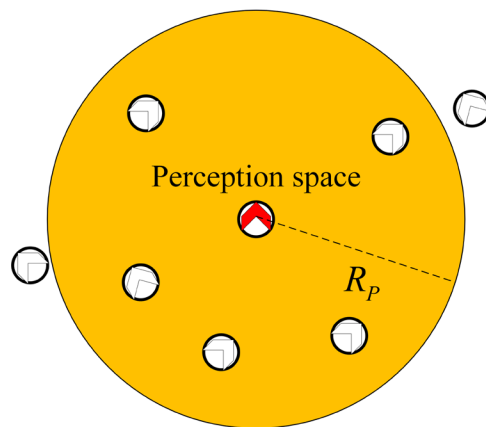


Figure 3.1 Illustration of the perception space of the agent

3.2.3 Interactions among the agents: information transmission and emotion contagion

The information transmission and emotion contagion models are constructed based on the OCEAN personality model and the epidemiological SIS model (Cao et al. 2017; Durupinar 2010). The OCEAN personality model includes five dimensions: openness, conscientiousness, extroversion, agreeableness, and neuroticism (Wiggins 1996). Among them, the neuroticism refers to emotional sensitivity and susceptibleness to the mood swings (Durupinar 2010), and can play a significant role in crowd behavior in emergency scenarios. Therefore, only this type of personality “neuroticism” is considered in this study and is denoted using the personal sensitivity index P_i in Table 3.2. The higher the value of the P_i , the more sensitive the agent is to the external informational or emotional signals.

3.2.3.1 Information transmission

When a disastrous incident occurs, it is important to detect the dangerous sources, isolate affected areas, distribute emergency information, and initiate emergency responses (Fu et al. 2017; Wan et al. 2014). Meanwhile, the familiarity level with the facility information can vary among pedestrians in places such as an airport and contributes to the pedestrian’s exit choice during the evacuation (Tsai et al. 2011). Therefore, two types of information are considered here: the incident information and the exit information.

The incident information refers to whether the agent is aware of the disastrous event, which is represented by a state variable $S_{i,1}(t)$. Provided that the toxic gas is often hard to be detected by common agents without being directly harmed and an effective warning system is lacking, common agents can detect the toxic gas attack under three situations, as illustrated in Figure 3.2.

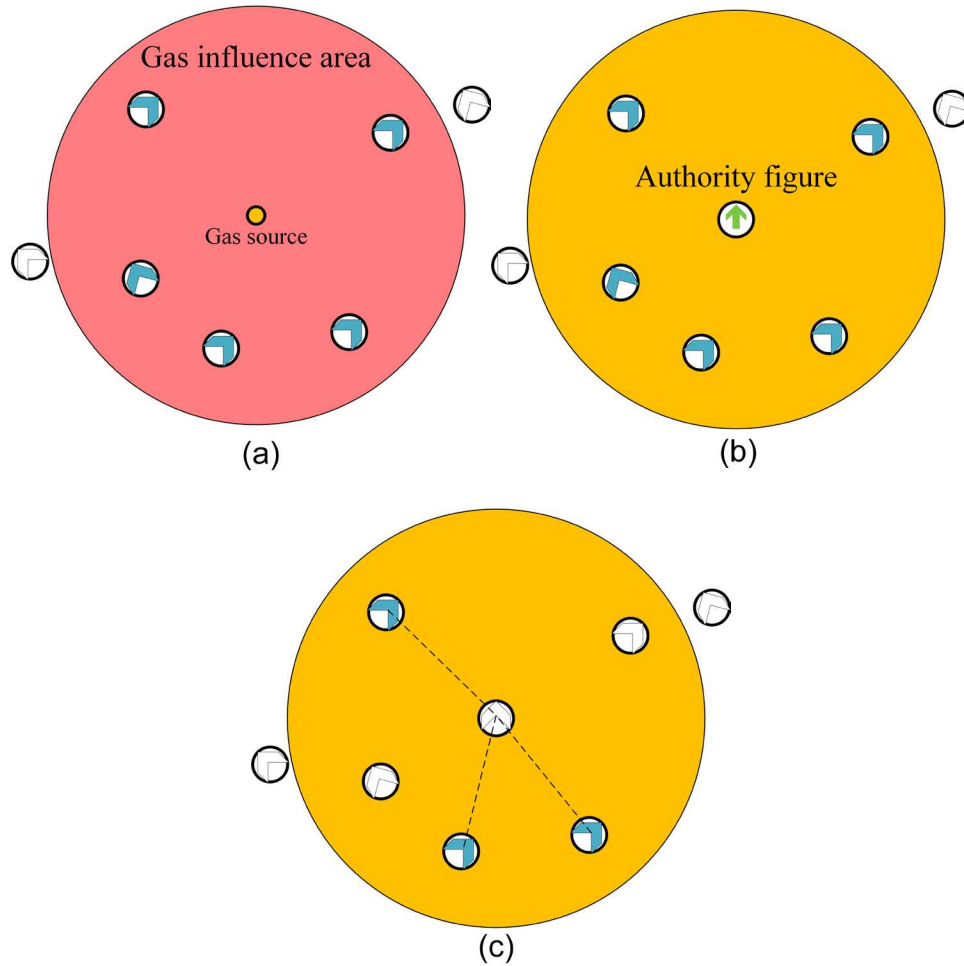


Figure 3.2 Situations of common agents aware of the incident (agents with the solid arrow are common ones who are aware of the incident): (a) personal harm from toxic gas; (b) notified by authority figures nearby; (c) informed by other common agents nearby

Figure 3.2(a) indicates that if the common agents are in the gas influence area, i.e., harmed by the toxic gas, they know the incident deterministically. Figure 3.2(b) shows that common agents can also become aware of the incident if the authority figures who know the incident are nearby, such as through voice directions. Since authority figures such as security guards usually have distinctive features, e.g., special uniform, and can be easily distinguished and capture others' attention, it is assumed that the authority figures can always deliver the incident information to common agents nearby successfully (Ma et al. 2016). However, the success of information transmission among common agents in Figure 3.2(c) depends on the

probability related to the agents' personality. Due to the variation of personalities, each person can be affected by surrounding environment in a different way (Cao et al. 2017). A sensitivity index P_i is used here to represent the sensitivity of the agent to surrounding stimuli, including information and emotion, which can also be interpreted as the probability of changing its own mind and accepting external information. Therefore, the algorithm of information transmission in Figure 3.2(c) is as follows:

Algorithm 3.1 Information transmission among agents

```

1: Input: sensitivity index  $P_i$ , perception radius  $R_{i,p}$ 

2: for each agent  $a_i$  do
3:   Initialized set  $A_{ik}=\emptyset$ 
4:   for other common agents  $a_j$  do
5:     if distance  $(a_i, a_j) < R_{i,p}$  and  $S_{j,1}(t) = \text{True}$  then
6:        $A_{ik} = A_{ik} \cup a_j$ 
7:     end if
8:   end for
9:   for each agent  $a_j$  in  $A_{ik}$  do
10:    Generate a uniform random number  $u$  within  $[0,1]$ 
11:    if  $u \leq P_i$  then
12:      The information is delivered successfully  $S_{i,1}(t) = \text{True}$ 
13:      break
14:    end if
15:  end for
16: end for

```

It is noteworthy that each common agent in set A_{ik} has and only has a single chance to deliver the information to agent a_i , either successfully or unsuccessfully. The rationale of this assumption is twofold. First, the information transmission model is based on the Independent Cascade Model, one of the most basic and prevalent diffusion models (Kempe et al. 2003). This model stipulates that in the social network, one active node has only one single chance to activate each inactive neighbor. Second, the information transmission here needs to account for the crowd dynamics. Suppose agent a_i becomes aware of the incident

and initiates its evacuation. Along its evacuation route, it can encounter other agents who are not aware of the incident and send the message about incident by the way. Suppose agent a_j is not aware of the incident and encounters agent a_i . If agent a_j successfully receives the incident information based on its sensitivity, then agent a_j will also begin to egress. However, if agent a_j fails to receive the incident information, agent a_j still continues its random walking within the room while agent a_i moves towards the chosen exit. In the simulation, it was found that these two agents are unlikely to encounter each other again. It should be pointed out that although agent a_j has little possibility to encounter the same agent a_i , it can still encounter other agents being aware of the incident and then get to know the incident since the crowd is always in motion. In other words, the set of nearby agents A_{jk} who can potentially deliver the information to agent a_j , defined in Algorithm 3.1, is time dependent. It is also assumed that once the common agents receive the incident information, they are fully aware of the distribution of toxic gas and can avoid the gas influence area during the evacuation.

For authority figures, apart from receiving the incident information from common agents using the algorithm above, they are assumed to be able to recognize the attack by detecting the gas influence area directly without being harmed. And once one authority agent knows the incident, all authority figures can instantly know this incident as well, which simulates an immediate radio communication among the authority figures (Tsai et al. 2011).

Once agents obtain the incident information, they initiate their evacuation and make their own exit choices after a short reaction time t_{reaction} . The exit information can also spread among evacuees, especially for those who enter the environment for the first time and have incomplete knowledge of exit locations (Tsai et al. 2011). The exit information combined with the agent's emotion state can finally determine its

exit choice behavior. Authority figures are assumed to be familiar with all exit locations and always choose the nearest or specified exit to evacuate. The common agent a_i uses the following algorithm to determine its exit choice:

Algorithm 3.2 Exit choice for common agents

```

1: Input: perception radius  $R_{i,p}$ , current emotion value  $E_i(t)$ 

2: for each common agent  $a_i$  do
3:   if distance ( $a_i$ , authority figures)  $< R_{i,p}$  then
4:     Choose the exit choice of one of the authority figures
5:   else
6:     Generate a uniform random number  $u$  within  $[0,1]$ 
7:     if  $u \geq E_i(t)$  then
8:       if distance ( $a_i$ , exits)  $< R_{i,p}$  then
9:         Choose the nearest exit
10:      else
11:        Choose the exit which the agent is most familiar with
12:      end if
13:    else
14:      if distance ( $a_i$ , other common agents with exit choices being made)  $< R_{i,p}$  then
15:        Choose the exit choice of one of them randomly
16:      else
17:        Choose the exit which the agent is most familiar with
18:      end if
19:    end if
20:  end if
21: end for

```

It should be noted that the exit choice in this model also depends on the agent's emotion state as shown in Algorithm 3.2. The emotion value $E_i(t)$, reflecting the panic level, is used to determine whether an individual either makes its own decision or follows others' strategies, i.e. the herding behavior (Helbing et al. 2000; Lovreglio et al. 2016). In addition, similar to the algorithm for the incident information transmission, each agent can have and only have a single chance to follow the exit choice from other common agents, which avoids the unrealistic phenomenon where an agent changes its exit choice too

frequently. But if the agent only forms its exit choice based on its own familiarity or other common agents' exit choice, it still has the second chance to change its mind if it encounters authority figures or exits within its perception space. In other words, the priority of exit information sources from high to low follows the following sequence: from authority figures > from perception > from its own familiarity or from other common agents.

3.2.3.2 Emotion contagion

The emotion contagion is simulated by a modified P-SIS model which combines the personality model and the epidemiological SIS model (Cao et al. 2017). From the emotion perspective, an agent in the simulation can be in either susceptible state or infected state, which is defined by a state variable $S_E(t)$. If the agent a_i is in the infected state, the emotion value $E_i(t)$ is above the emotion threshold $T_{i,E}$, and it reflects more panicking behavior and can also generate a random panic dose $d_i(t)$. If the agent a_i is in the susceptible state, the emotion value $E_i(t)$ is below the emotion threshold $T_{i,E}$, and it reflects less panicking behavior. And it has the probability of changing into the infected state based on the surrounding environment or the accumulated panic doses perceived (i.e., $d_i(t)$ and $T_{i,P}$). For authority figures, it is assumed that they always stay calm and rational and are not affected by others' emotion; meanwhile they can have a calming effect on common infected agents nearby and enable them to change from infected state to susceptible state, which is represented by an emotion decay coefficient β . The algorithm for emotion contagion among common agents is shown in Algorithm 3.3.

Algorithm 3.3 Emotion contagion among common agents

1: **Input:** Before the toxic gas attack, for each agent, initialize P_i , $T_{i,E}$, and $E_{i,init}$ according to their distributions in Table 3.2. Set $t = 0$, $E_i(0) = 0$, $D_i(t)=0$, and $S_{i,E}(0) = \text{Susceptible}$

2: **for** each time step t **do**

```

3:   for each common agent  $a_i$  do
4:       update  $S_{i,I}(t)$  first based on the information transmission model (Algorithm 3.2)
5:   end for

6:   for each common agent  $a_i$  do
7:       if  $S_{i,I}(t)=\text{True}$  then
8:           if distance ( $a_i$ , the gas influence area or any casualties)  $< R_{i,P}$  and
9:               distance ( $a_i$ , authority figures)  $> R_{i,P}$  then
10:                  set  $S_{i,E}(t) = \text{Infected}$ ,  $D_i(t)=0$ , and  $E_i(t) = E_{i,\text{init}}$ 
11:              end if
12:          end if

13:          if  $S_{i,I}(t)=\text{False}$  then
14:              if distance ( $a_i$ , any casualties)  $< R_{i,P}$  and ( $a_i$ , authority figures)  $> R_{i,P}$  then
15:                  set  $E_i(t) = P_i$ 
16:                  if  $E_i(t) > T_{i,E}$  then
17:                      set  $S_{i,E}(t) = \text{Infected}$  and  $D_i(t)=0$ 
18:                  end if
19:              end if
20:          end if
21:      end for

22:   for each common agent  $a_i$  do
23:       if distance ( $a_i$ , the gas influence area and casualties)  $> R_{i,P}$  then
24:            $A_{i,p}$  = the infected agents nearby,  $n$  = the total number of infected agents in  $A_{i,p}$ 
25:           for each common agent  $a_j$  in  $A_{i,p}$  do
26:               Generate random panic dose  $d_j(t)$ 
27:           end for

28:           set  $D_i(t) = \sum_{j=1}^n d_j(t)$  ,

29:           if  $D_i(t) > T_{i,P}$  then
30:               set  $S_{i,E}(t) = \text{Infected}$ ,  $D_i(t)=0$ , and  $E_i(t) = E_{i,\text{init}}$ 
31:           end if
32:       end if
33:   end for

34:   for each infected common agent  $a_i$  ( $S_{i,I}(t) = \text{True}$ ) do
35:       if distance ( $a_i$ , authority figures)  $< R_{i,P}$  then
36:           set  $E_i(t) = (1 - \beta)E_i(t - \Delta t)$ 

```

```

37:         if  $E_i(t) \leq T_{i,E}$  then
38:             set  $S_{i,E}(t) = \text{Susceptible}$  and  $D_i(t)=0$ 
39:         end if
40:     end if
41: end for
42: end for

```

In the Algorithm 3.3, lines 6–33 imply that the conditions of changing from susceptible state into infected state depend on both the incident information and emotion perceived, while lines 34–41 show that whether the infected agent can enter the susceptible state only depends on the calming effect of the nearby authority figures.

3.2.4 Crowd dynamics: modified social force model

The social force model is modified to simulate the crowd dynamics incorporating the effects of toxic gas, information transmission, and emotion contagion. Each agent is represented by a circle with a radius of r_i and a mass of m_i and the motion of each agent is governed by the following equation:

$$m_i \frac{d\vec{v}_i}{dt} = m_i \frac{v_i^0(t)\vec{e}_i^0(t) - \vec{v}_i(t)}{\tau} + \sum_{j \neq i} \vec{f}_{ij} + \sum_w \vec{f}_{iw} + \sum_g \vec{f}_{ig} \quad (3.3)$$

where the subscript i, j are the agent numbers; $v_i^0(t)$ and $\vec{e}_i^0(t)$ are the desired moving speed and direction, respectively; $\vec{v}_i(t)$ is the actual moving velocity; τ is the relaxation time; f_{ij}, f_{iw} , and f_{ig} represent the repulsive forces used to maintain a safety distance from other pedestrians j , walls w , and gas source g , respectively, which have a similar form:

$$f_{ix} = \begin{cases} A_{ix} e^{-(d_{ix}-r_{ix})/B_{ix}} (\lambda_{ix} + (1-\lambda_{ix}) \frac{1+\cos\varphi_{ix}}{2}) \vec{n}_{ix} & \text{when } d_{ix} > r_{ix} \\ A_{ix} e^{-(d_{ix}-r_{ix})/B_{ix}} (\lambda_{ix} + (1-\lambda_{ix}) \frac{1+\cos\varphi_{ix}}{2}) \vec{n}_{ix} + k_{ix} g(r_{ix} - d_{ix}) \vec{n}_{ix} + \kappa_{ix} g(r_{ix} - d_{ix}) \Delta v_{xi} \vec{t}_{ix} & \text{when } d_{ix} \leq r_{ix} \end{cases} \quad (3.4)$$

where the subscript x can be j , w , or g , referring to pedestrians, walls and gas source, respectively; d_{ix} is the distance between the centers of mass of agent and object; r_{ix} equals $r_i + r_j$ when $x = j$ and equals r_i when $x = w$ or g ; A_i and B_i define the strength and range of the social force, respectively; λ_i controls the anisotropy of the social force; \vec{n}_{ix} is the unit vector pointing from object x to agent i ; \vec{t}_{ix} is the unit vector pointing the tangential direction; φ_{ix} denotes the angle between the direction of moving motion and the direction vector $-\vec{n}_{ix}$; $\Delta v_{xi}^t = (\vec{v}_x - \vec{v}_i) \cdot \vec{t}_{ix}$ is the tangential velocity difference; k_{ix} and κ_{ix} are constants related to the body compression and sliding friction, respectively.

The pedestrian's tendency of keeping away from the toxic gas is represented by a repulsive force term \vec{f}_{ig} in Eq. (3.3). It should be noted that only those agents who are aware of the incident are able to perceive this repulsive force. Those agents who do not know the incident can enter the toxic gas influence area and result in different levels of damage, which can lead to the speed reduction factor γ on $v_i^0(t)$ as listed in Table 3.1.

The information transmission mainly affects the agent's decision on whether to initiate the evacuation and the exit choice from a global perspective as discussed previously, which can be represented by the desired moving direction:

$$\vec{e}_i^0 = \begin{cases} \text{pointing the chosen exit,} & \text{when } S_{i,1} = \text{True} \\ \text{pointing the random target,} & \text{when } S_{i,1} = \text{False} \end{cases} \quad (3.5)$$

The emotion contagion can influence the agent's local moving behavior at each time step, more specifically, the original desired speed $v_i^0(t)$ and the desired moving direction $\vec{e}_i^0(t)$, which are modified as follows:

$$v_{i,\text{new}}^0(t) = \begin{cases} (1-\gamma)v_i^0(t) & \text{when in "Seriously injured" or "Slightly wounded" state} \\ (1-E_i(t))v_i^0(t) + E_i(t)v_i^{\text{max}} & \text{when in "Normal" state} \end{cases} \quad (3.6)$$

$$\vec{e}_{i,\text{new}}^0(t) = (1-\alpha_i(t))\vec{e}_i^0 + \alpha_i(t) \langle \vec{v}_j(t) \rangle_i \quad (3.7)$$

where $v_{i,\text{new}}^0(t)$ and $\vec{e}_{i,\text{new}}^0(t)$ are modified desired speed and direction, respectively; $v_i^0(t)$ is the desired speed in normal condition; $E_i(t)$ is the current emotion value; γ is the speed reduction factor based on the damage state; v_i^{max} is the maximum speed the agent wants to achieve in emergency scenarios; $\langle \vec{v}_j(t) \rangle_i$ is the average moving direction of agent i 's neighbors within its perception space; $\alpha_i(t)$ is the herding tendency, which is assumed to be 0.2 when $S_{i,E}(t) = \text{Susceptible}$ and 0.5 when $S_{i,E}(t) = \text{Infected}$.

Eq. (3.6) suggests that the higher the emotion value is or the more panic the agent is, the higher desired speed the agent tends to adopt. Eq. (3.7) represents the herding behavior that the infected agents tend to weigh more on the choices by other people than the susceptible ones. It should be noted that some researchers pointed out that the herding behavior is always present (Lovreglio et al. 2016), and that is the reason that a relatively low $\alpha_i(t)$ is also adopted for the susceptible agents.

The whole simulation procedure as described previously can be summarized as Figure 3.3.

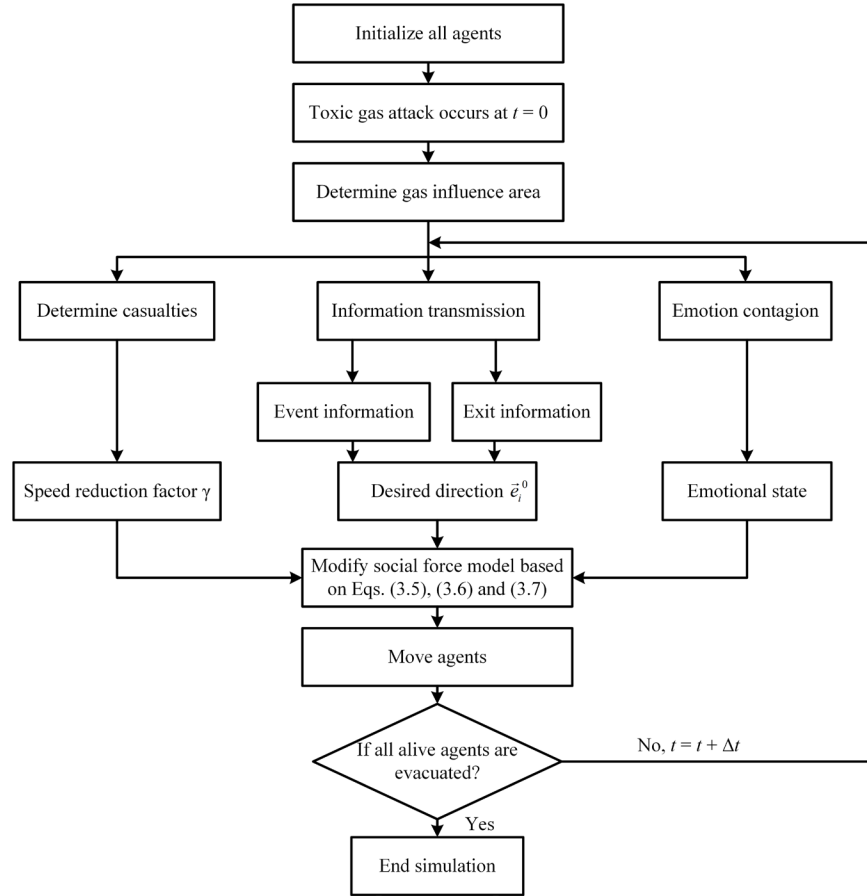


Figure 3.3 Flowchart of the simulation

3.3 Simulations

In this section, a computer code was developed based on software NetLogo and two cases, i.e., room with one and two exits, were used to demonstrate the simulation framework. The layout of the square room with the side length of 27 m is shown in Figure 3.4(a). The exit with the width of 3 m is located in the middle of the side wall. Only one toxic gas source is considered, and the corresponding gas influence area is a circular area with a radius of 2.435 m (Table 3.1). It is assumed that pedestrians' initial positions are randomly distributed over the room space, and those pedestrians who do not know the gas attack keep walking randomly in the room (the black area). These agents are classified into male and female based on the gender and young and old based on the age since these characteristics can account for the heterogeneity

in mobility. And it is assumed that two-thirds of the crowd are young adults and one-third to be old adults; 44% are male and 56% are female (Liu et al. 2015). Table 3.3 summarizes the parameters for the social force model used in the simulation. Values of parameters related to the information transmission and emotional contagion models can be found in Table 3.2. It should be noted that although values of some parameters (i.e., $\alpha_i(t)$, $t_{i,\text{reaction}}$, $T_{i,E}$, $d_i(t)$, and β) in Table 3.2 were chosen based on the literature, existing studies pertaining to this topic are still mainly simulation-based, indicating that these chosen values may be possible, but can also vary from case to case and no agreement has been made. Therefore, these possible values were only chosen in order to demonstrate the proposed methodology.

Table 3.3 Values of parameters related with the social force model

Parameter	Value	Reference
r_i (m)	Young female	Uniform [0.22, 0.26]
	Young male	Uniform [0.25, 0.29]
	Old female	Uniform [0.23, 0.27]
	Old male	Uniform [0.23, 0.27]
$v_i^0(t)$ (m/s)	Young female	1.42
	Young male	1.52
	Old female	0.91
	Old male	1.12
$v_i^{\max}(t)$ (m/s)	3	-
m_i (kg)	Gaussian ($\mu_m = 80$, $\sigma_m^2 = 10^2$)	-
τ (s)	Uniform [0.8, 1.2]	(Korhonen 2016)
A_i (N)	2×10^3	(Korhonen 2016)
B_i (m)	0.04	(Korhonen 2016)
λ_i	0.5	(Korhonen 2016)
A_{iw} (N)	2×10^3	(Korhonen 2016)
B_{iw} (m)	0.08	(Korhonen 2016)
λ_{iw}	0.2	(Korhonen 2016)
A_{ig} (N)	4×10^3	-
B_{ig} (m)	0.9	-
λ_{ig}	0.9	-
k (kg m ⁻²)	1.2×10^5	(Cao et al. 2017)

κ (kg s ⁻¹)	2.4×10 ⁵	(Cao et al. 2017)
Δt (s)	0.04	-

3.3.1 Room with one exit

In this case, the toxic gas source is placed at the center of the room. Since only one exit is available which is located at the middle of the side wall and is familiar to all agents, only the incident information is transmitted among agents. Figure 3.4 presents the comparative results of evacuation simulations of 350 agents with different models, where $R_{i,p} = 3$ m, and no authority figure is available. Figure 3.4(a)–(d) show the simulation results using the proposed agents considering information transmission and emotion contagion, and agents being aware of the incident are represented by triangles and those unaware of the incident represented by circles. Figure 3.4(e)–(h) show the results using the omniscient agent who can detect the incident and initiate the evacuation instantaneously and always behave rationally. Figure 3.5 gives the time histories of the number of evacuees with these two types of agent models.

It can be seen that when the proposed agents are used, after the toxic gas attack occurs, the agents in the gas influence area first detect the incident, and then distribute the incident information and propagate the emotion to others. After that, those receiving the incident information initiate their evacuation, and their movements further enable the incident information to be received by other agents they encounter. Thus, the numbers of agents who know the incident and who are infected both increase, as shown in Figure 3.5(a) during the time range 0–12 s. As most agents in the room who are aware of the information move towards the exit and the evacuation rate becomes stable. The curve of the number of accumulated agents who are aware of the incident flattens and the number of infected agents in the room decreases when more agents have escaped from the room, as shown in Figure 3.5(a) during the time range 12–60 s. Figure 3.4(b) also

illustrates the snapshot when most agents know the incident and are infected at $t = 12$ s. For the omniscient agents, they initiate the evacuation as soon as the attack begins, as shown in Figure 3.5(b), which has no first 10-second delay due to information transmission and emotion contagion (Figure 3.5(a)). It can also be observed that the solid curve in Figure 3.5(a) has a longer upper tail than that in Figure 3.5(b), which can be explained by the fact that as most agents evacuate successfully, some agents who are unaware of the incident can still linger in the room for some time. Because of the decrease of crowd density, the chance of detecting the incident under such low crowd density is small, which may prolong the simulation unnecessarily, and these scattered lingering agents are less likely to induce significant disaster during evacuation such as trampling and overtaking in practice (Wang et al. 2015). Therefore, the evacuation time with the proposed agents is limited to the time instant with 95% of agents who have already escaped from the room in order to make a better comparison with the simulation with omniscient agents. In this example, the evacuation time with the proposed agents is 61 s which is smaller than 70 s with omniscient agents. Meanwhile, from the perspective of the maximum evacuation efficiency, defined as the maximum evacuated agents per second, the case with the proposed agents is 6.5 while that with omniscient agents is 4.5. This phenomenon is due to the fact that the infected agents because of emotion contagion tend to adopt higher moving speeds, which may shorten the whole evacuation process.

Further parametric study is conducted to show the effects of number of agents, perception radius, and proportion of authority figures on the evacuation process.

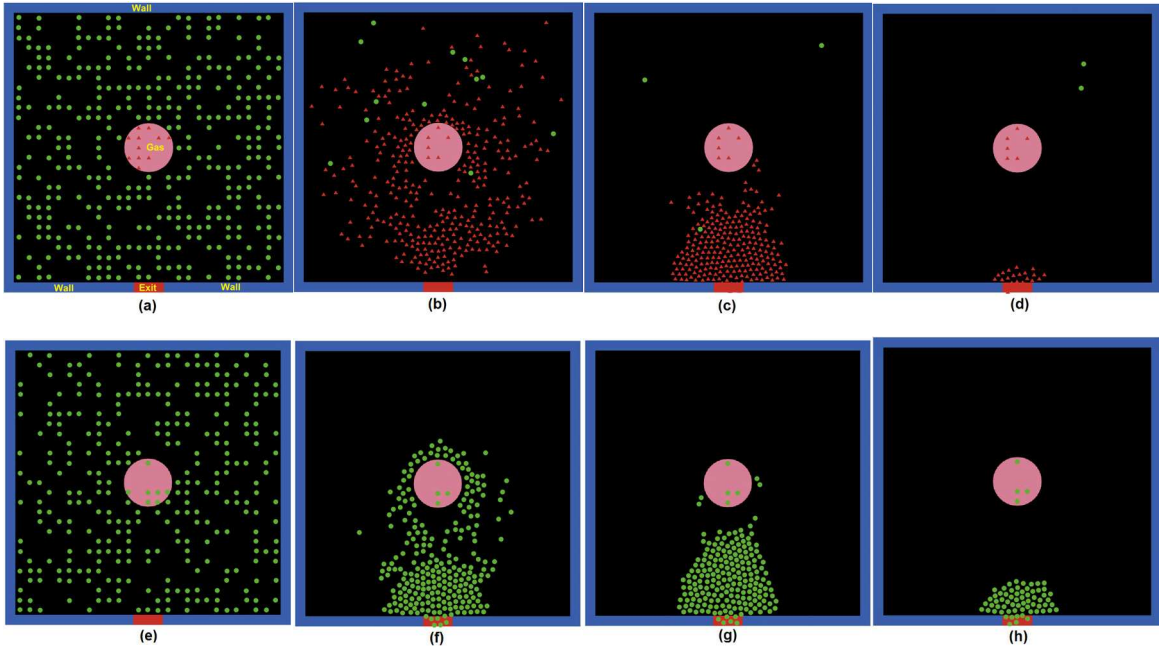


Figure 3.4 Snapshots of evacuation simulation using different types of agents (in (a)–(d), red triangles represent agents being aware of the incident and green circles represent agents unaware of the incident): (a) $t = 0$ s; (b) $t = 12$ s; (c) $t = 22$ s; (d) $t = 54$ s; (e) $t = 0$ s; (f) $t = 12$ s; (g) $t = 22$ s; (h) $t = 54$ s

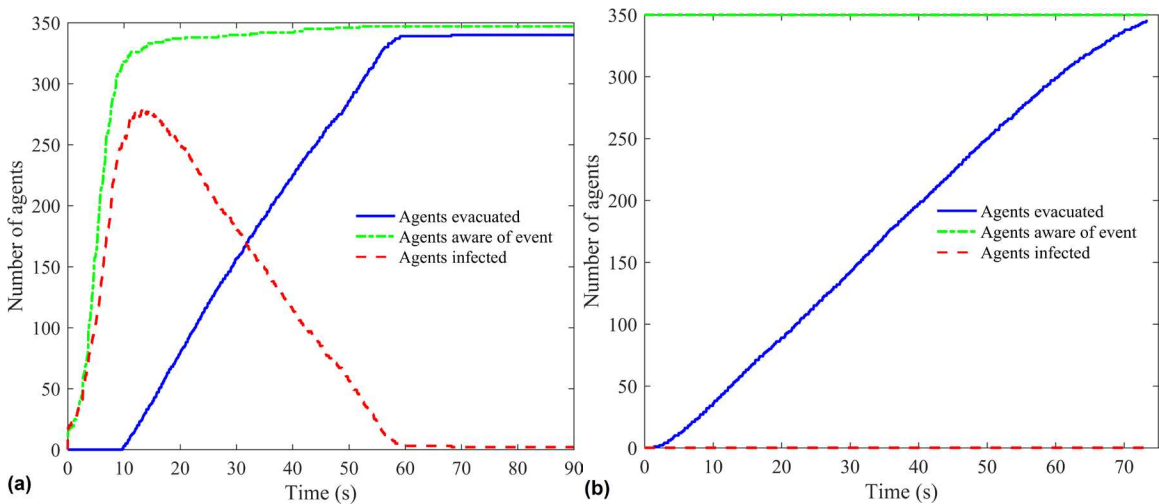


Figure 3.5 Time histories of number of evacuees using different types of agent models: (a) using proposed agents; (b) using omniscient agents

3.3.1.1 *Effect of number of agents*

Figure 3.6 shows the results about different numbers of agents N on the evacuation using the proposed agents or omniscient agents. It can be found from Figure 3.6(a) and (b) that larger N does not necessarily lead to longer evacuation time when the proposed agents are used. In fact, when N is low, the evacuation

speed of omniscient agents is faster than that of the proposed agents, while when N is high, the opposite is true. The reason is that when the crowd density is low, the chance of agents encountering the gas source or each other is low, leading to a relatively long period of transmission of the incident information, and thus agents can have a longer delay to initiate their evacuation; when the crowd density is high, on the one hand the incident information can spread more rapidly, while on the other hand agents can get infected more easily due to emotion contagion and thus move faster, which decreases the evacuation time as compared to the omniscient agents.

In addition to evacuation speed, casualty is another concern. It should be noted that once an agent unaware of the incident enters the outermost layer of the gas influence area, it can be in the “slightly wounded” state as defined in Table 3.1. The agent can become aware of the incident and then keep away from this area and will not likely be further harmed to the “seriously injured” or “dead” states. This implies that apart from those agents whose initial positions are within the gas influence area, the agents who get harmed during the evacuation are usually in the “slightly wounded” state and the number may accumulate. Figure 3.6(c) shows the total number of agents being slightly wounded in the evacuation. Meanwhile, the collision among evacuees is another source of causing damages, which is shown in Figure 3.6(d) (Zhao et al. 2017). The collision is defined as the occurrence of the physical contact among agents, i.e., $d_{ix} \leq r_{ix}$ in Eq.(3.4).

It can be observed in Figure 3.6(c) that the number of slightly wounded agents is relatively stable under different numbers of total agents. This is also because the way of getting incident information under the low crowd density mainly relies on the direct contact with the gas influence area. While under the high crowd density, more frequent occurrence of information transmission acts as another important means of

distributing the incident information, which explains why a higher number of agents does not necessarily lead to a larger number of wounded agents. However, in terms of the collision, the number of collisions among proposed agents is much higher than that among omniscient agents and rises with the increase of N . When the infected agents tend to have higher desired speeds, higher driving forces and thus collisions will occur.

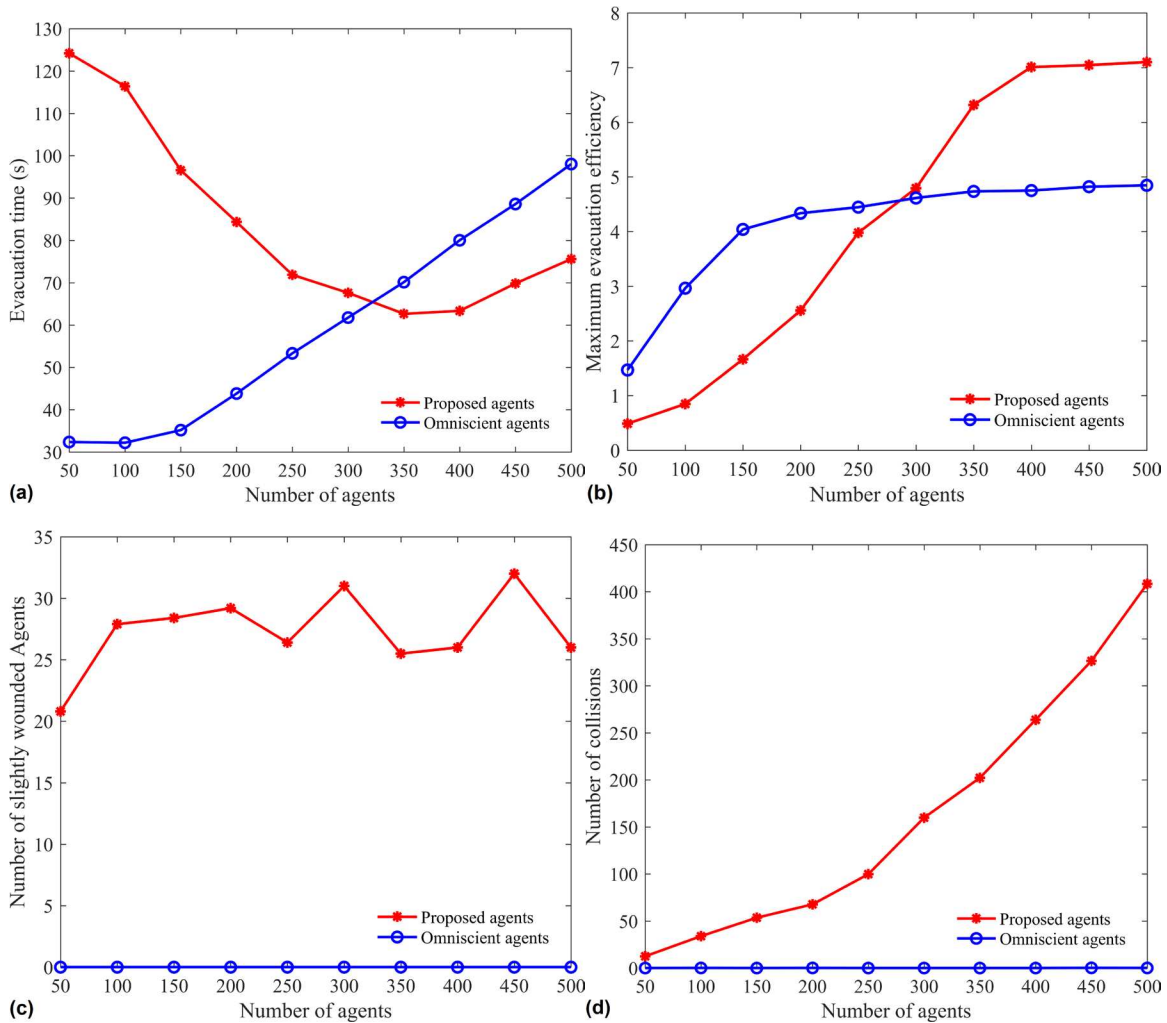


Figure 3.6 Effect of number of agents on the evacuation ($R_{i,P} = 2$ m and no authority figures are available): (a) evacuation time; (b) maximum evacuation efficiency; (c) slightly wounded agents; (d) collisions

3.3.1.2 Effect of perception radius

Due to the specific environments and physiological conditions, pedestrians can have different perception radii $R_{i,p}$. Figure 3.7 shows the effect of perception radius on the evacuation and all agents are assumed to have the same value of $R_{i,p}$ for the illustrative purpose. It can be seen that larger $R_{i,p}$ can lead to reductions in the evacuation time, the number of slightly wounded agents, and the number of collisions. This is because larger $R_{i,p}$ enables each agent to interact with more agents and perceive more information, which accelerates the incident information transmission and moving speed and also decreases the collisions. Such a finding highlights the importance of visibility in evacuation, which can be critical in some occasions such as heavy smoke or power loss (Jeon et al. 2011).

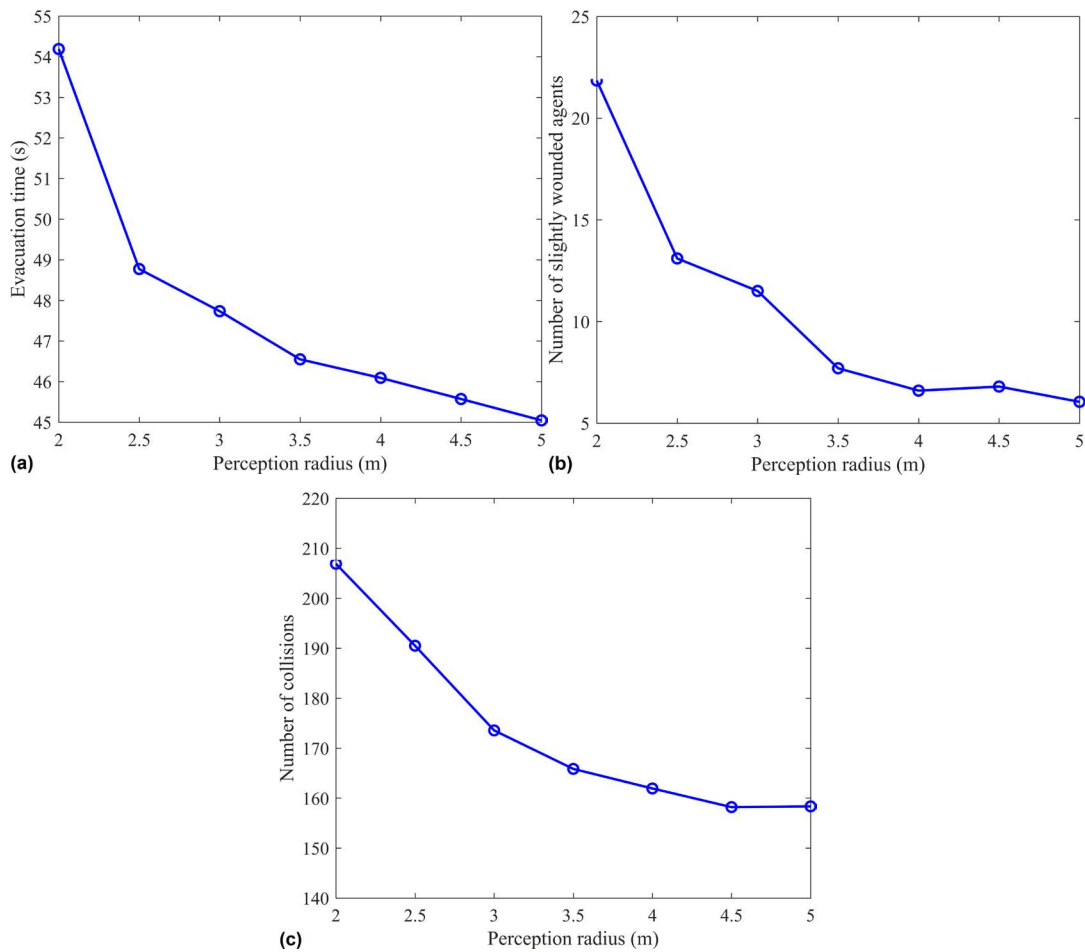


Figure 3.7 Effect of perception radius on the evacuation ($N = 300$ and no authority figures are available): (a) evacuation time; (b) slightly wounded agents; (c) collisions

3.3.1.3 *Effect of ratio of authority figures*

As discussed earlier, authority figure is a special kind of agents with following features: (1) can detect the toxic gas attack without being harmed; (2) can always stay calm, i.e., $E_i(t) = 0$; (3) can transmit the incident information instantaneously among themselves; (4) can always deliver the incident and exit information successfully to common agents nearby; and (5) has a calming effect on the emotion of common agents nearby. Therefore, authority figures can act as leaders of the evacuation to guide common agents to exits. Figure 3.8 depicts the effect of varying the ratio of authority figures on the evacuation and it is assumed that the initial positions of authority figures are all beyond the boundary of the gas influence area.

It can be found from Figure 3.8(a) that adding more authority figures can reduce the evacuation time, and such reduction is more significant for the low crowd numbers than for the high crowd numbers. This is because authority figures reduce the evacuation time mainly by delivering the incident information effectively and decreasing the pre-evacuation delay. Under the high crowd density case, the more frequent communications among common agents also contribute to the incident information transmission, which weakens the effect of authority figures. This also confirms the finding that a large ratio of authority figures is needed to increase the evacuation speed effectively for a small crowd size (Ma et al. 2016). Moreover, due to the calming effect on common agents, the increase of ratio of authority figures greatly reduces the numbers of slightly wounded agents and collisions, as shown in Figure 3.8(b) and (c). This phenomenon implies that the authority figures can effectively help soothe the chaos and maintain the evacuation order.

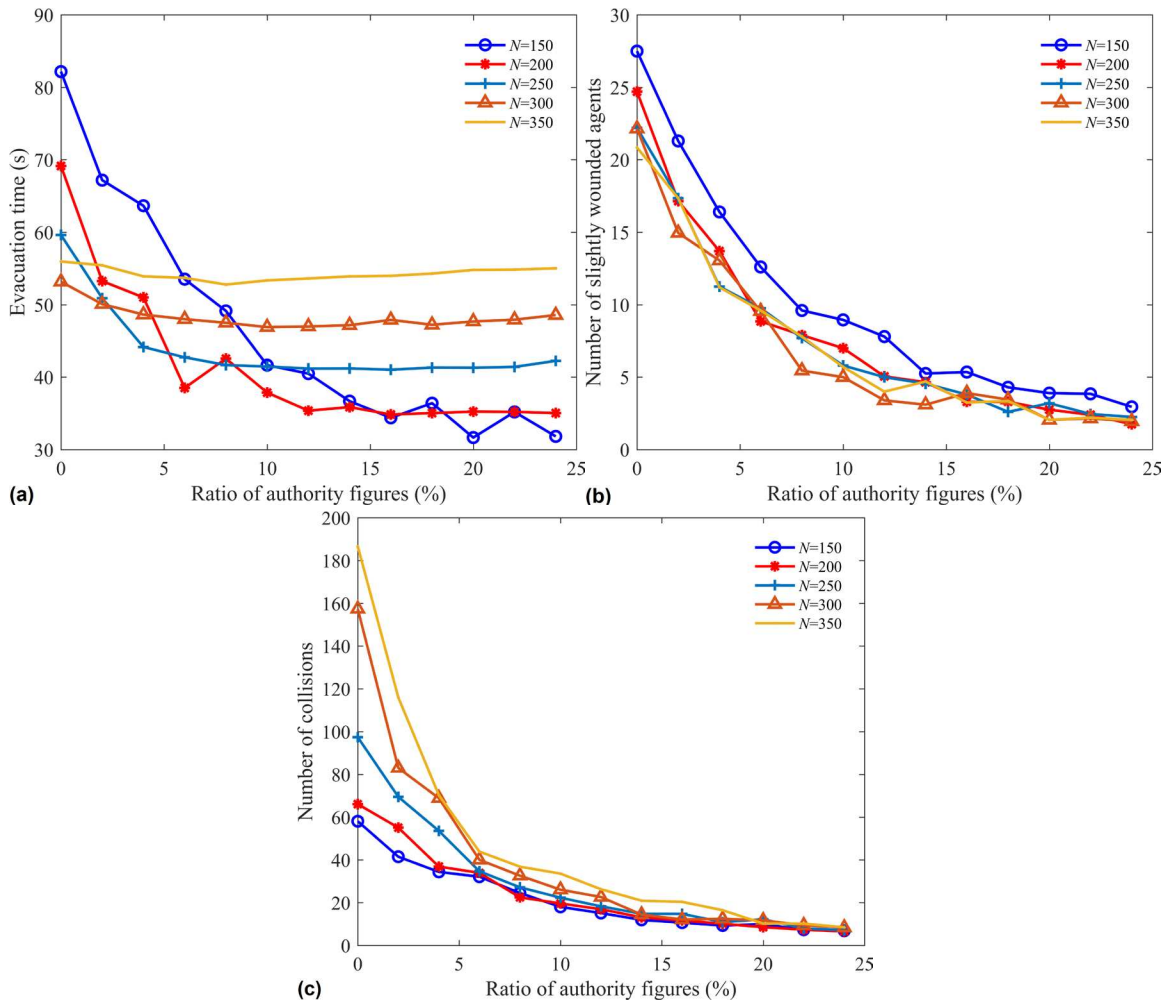


Figure 3.8 Effect of ratio of authority figures on the evacuation ($R_{t,p} = 2$ m): (a) evacuation time; (b) slightly wounded agents; (c) collisions

3.3.2 Room with two exits

The example of a room with two exits is presented to demonstrate the impact of having more exits on the simulation results. The room has Exit 1 and Exit 2, locating at the lower and upper side walls, respectively and other dimensions are the same as the room with one exit (Figure 3.9(a)). The location of the toxic gas attack is near Exit 1, and common agents are assumed to enter the room through Exit 1 and thus are only familiar with Exit 1, while authority figures, which are represented by pentagams in Figure 3.9(a), are familiar with both exits.

Figure 3.9 and Figure 3.10 list the simulation results of 350 agents where $R_{i,p} = 2$ m and 5 authority figures are available. In Figure 3.9, the agents choosing Exit 1 are represented by triangles and those choosing Exit 2 are represented by squares. Because the toxic gas source is close to Exit 1, the exit choices of all authority figures are assumed to be Exit 2 in order to keep away from the dangerous source and guide common agents safely through evacuation. But since common agents in this case are only familiar with Exit 1, after they are aware of the incident, the exit priority becomes Exit 1 when Exit 2 is out of perception space or they are panicked, and no authority figure is nearby. Once they encounter authority figures or other informed common agents, they may change their choices. Such behavior about exit choices is illustrated in Algorithm 2. At the time $t = 10$ s in Figure 3.9(b), several clusters of agents around authority figures (marked in yellow) all move towards Exit 2 with the help from the authority figures. Meanwhile, common agents near the gas influence area (marked in red) can detect the incident more easily and thus choose the nearest and most familiar Exit 1 to evacuate. During the movements of agents choosing Exit 2, they can pass by other common agents and change their minds about exit choice due to information transmission, as shown in Figure 3.9(c) (the red turned yellow). Therefore, eventually the final number of the agents using Exit 2 can be greater than that of the agents using Exit 1 (see Figure 3.9(d) and Figure 3.10(b)). As expected, the total evacuation time (45 s) for the room with two exits is less than the evacuation time (61 s) for the room with only one exit.

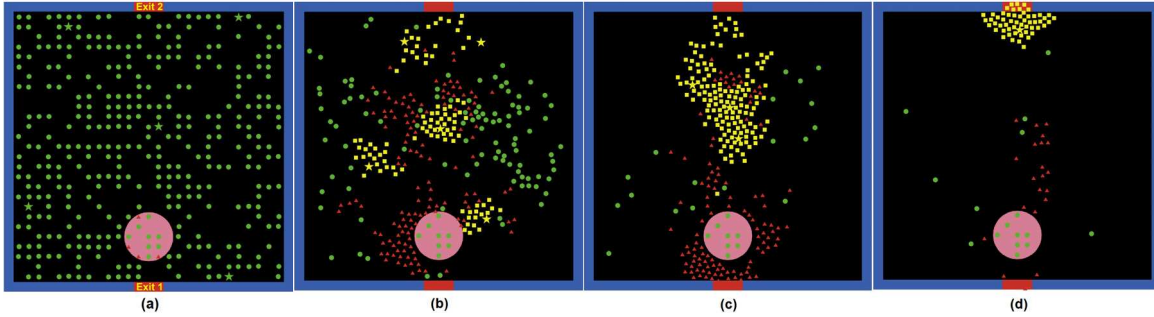


Figure 3.9 Snapshots of evacuation simulation for the room with two exits (red triangles represent agents choosing Exit 1; yellow squares represent agents choosing Exit 2; green circles represent agents unaware of the incident; pentagrams represent authority figures): (a) $t = 0$ s; (b) $t = 10$ s; (c) $t = 20$ s; (d) $t = 40$ s

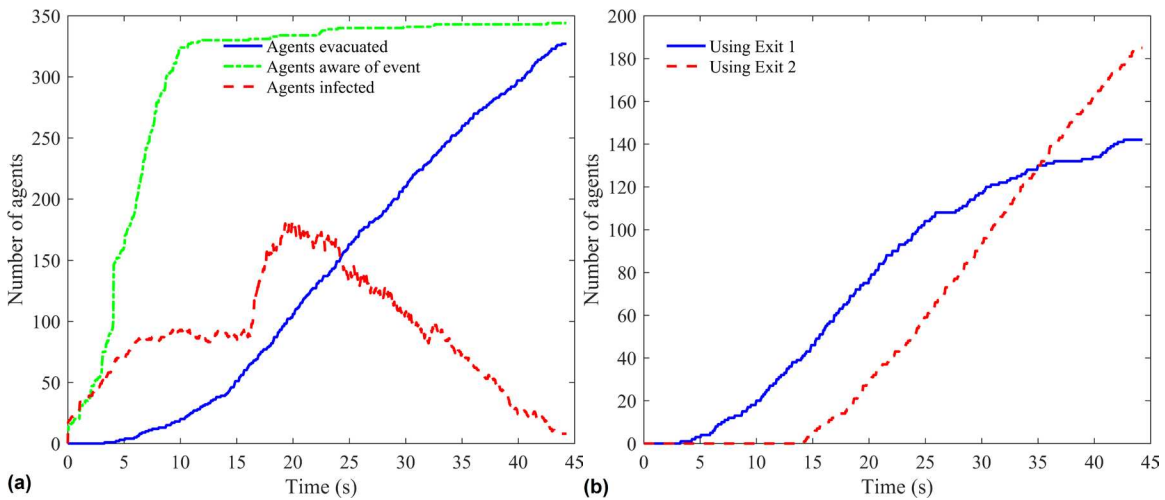


Figure 3.10 Time histories of evacuation from the room with two exits: (a) the evacuation process; (b) the condition of exit using

The effects of the number of authority figures on the evacuation time, number of casualties, and number of collisions for the room with two exits are also studied. The reduction ratio in Figure 3.11 is computed as follows:

$$RR = \frac{m_n - m_0}{m_0} \times 100\% \quad (3.8)$$

where RR is the reduction ratio, i.e., the y -axis in Figure 3.11; m is the measure, i.e., the evacuation time, the number of slightly wounded agents, and the number of collisions; subscript n indicates the number of authority figures, i.e., the x -axis in Figure 3.11.

Similar to the room with one exit, it is also found in the results of the room with two exits that increasing the number of authority figures in the simulation can reduce the evacuation time, the number of slightly wounded agents, and the number of collisions. Comparatively such reduction effect is more significant for the small crowd size than the large one. Once again, this is because the higher the crowd density is, the more frequently the agents can encounter each other and the information transmission occurs, leading to faster spreading of the incident information and weakening the effect of authority figures. It is noteworthy that when the number of authority figures is greater than 4, the reductions in the evacuation time and the number of slightly wounded agents stay stable. This implies that a critical number of authority figures may exist for a certain environment to achieve the best evacuation outcome (Tsai et al. 2011). Increasing the number of authority figures beyond this threshold would not produce better results because the evacuation efficiency is also governed by other environmental factors such as the width of the exit (Ma et al. 2016).

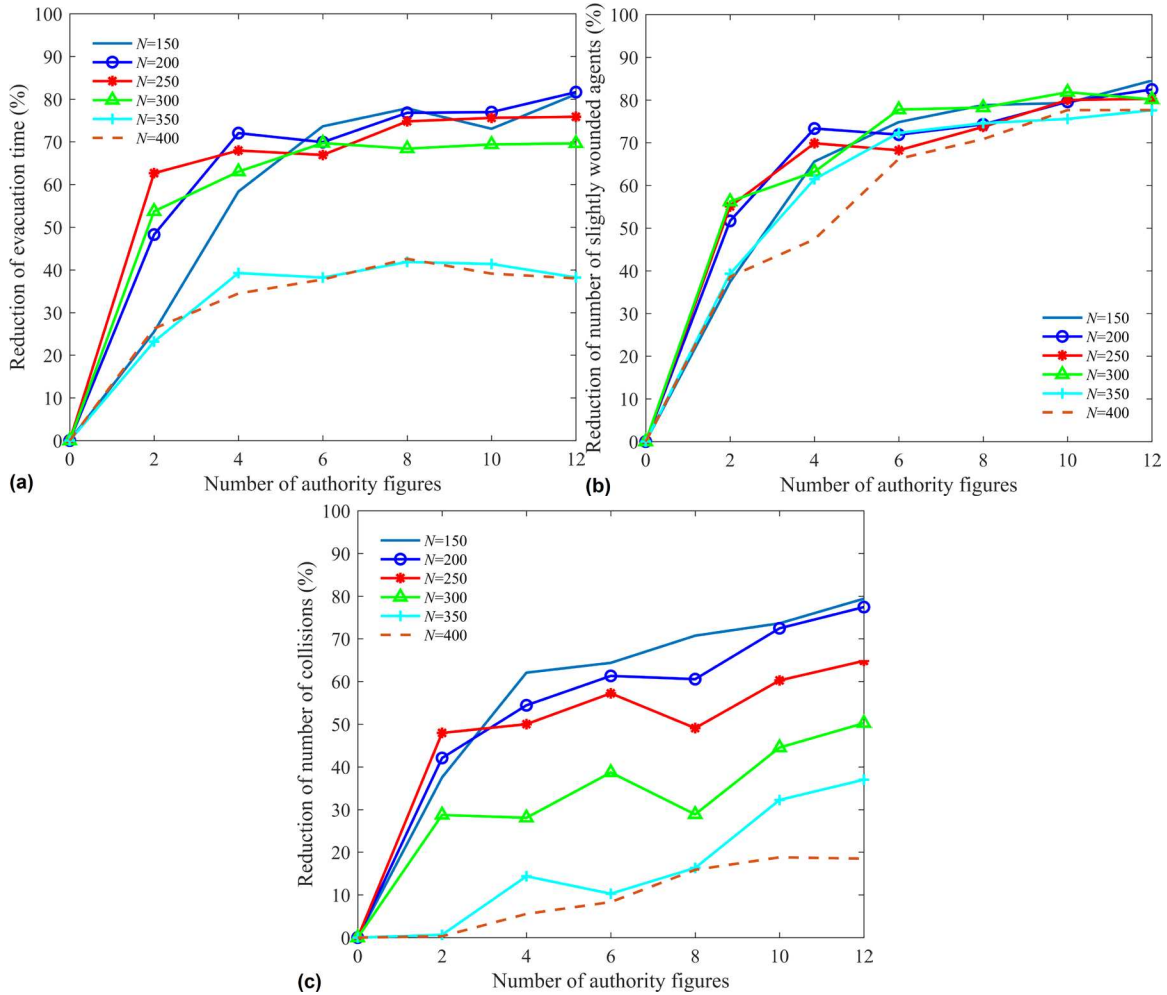


Figure 3.11 Reduction effect of authority figures for the room with two exits ($R_{i,p} = 2$ m): (a) evacuation time; (b) slightly wounded agents; (c) collisions

3.4 Conclusions

This study presents a method of crowd evacuation simulation under toxic gas incident considering the effects of emotion contagion and information transmission. The concentration of the toxic gas quantified by the gas dispersion model determines the casualty and the impairment of the pedestrian mobility. The spread of the information about the incident and the exits is modeled by the information diffusion model. The emotion contagion model quantifies the emotion and panic. Then the social force model is modified to integrate these effects to govern the movements of people in the evacuation process. Two cases, i.e., room with one and two exits, are used to demonstrate the proposed simulation framework. The effects of number

of agents, perception radius, and ratio of authority figures on the evacuation process are further examined.

Conclusions based on the simulation results are drawn as follows:

- (1) Compared to using omniscient agents, using agents considering emotion contagion and information transmission can cause considerable difference in the evacuation outcome in terms of the evacuation time, the number of casualties, and the number of collisions;
- (2) Increasing the perception radius can accelerate the evacuation and reduce the potential physical threats to evacuees;
- (3) Adding authority figures improves the overall evacuation performance, and such improvement is more significant for a small crowd size and tends to remain stable when the number of authority figures surpasses a certain value.

These findings from the quantitative model not only underline the necessity of incorporating human factors into crowd simulation but also provide some suggestions for emergency management in practice. Since the evacuation safety and efficiency can be improved by increasing the perception radius and knowledge of the environment, it can be critical to establishing effective early warning systems (e.g., by means of smart sensors and intelligent information sharing systems) in public areas in order to detect the dangers, issue evacuation orders, and disseminate emergency messages to public in time. Maintaining good illumination in emergency scenarios can provide sufficient visibility for evacuees and reduce possible collisions of evacuees. The emergency signage can be placed at important locations to inform evacuees of alternative exits and help them make better choices of egress routes. It was also found that the authority figures can be helpful in alleviating the anxiety and accelerating the evacuation speed, even for a small crowd size. The quantity, deployed locations, and patrol routes of authority figures may be further optimized

to deliver evacuation guidance more effectively and efficiently according to the crowd density distribution and the environment layout.

This study highlights the importance of human factors, i.e., emotion and perception, on the crowd evacuation simulation in emergency scenarios. The proposed model and findings can help implement more effective emergency evacuation planning strategy, including adopting some smart sensing and information sharing technology through artificial intelligence and incorporating more realistic modeling of pedestrians' behavior.

CHAPTER 4 RESILIENCE MODELING OF INTERDEPENDENT TRAFFIC-ELECTRIC POWER SYSTEM SUBJECT TO HURRICANES³

4.1 Introduction

As the basic lifeline infrastructures, transportation networks (TNs) and electric power networks (EPNs) are crucial to nearly all emergency response, humanitarian relief efforts, and post-disaster emergency restoration of other critical facilities through providing essential accessibility and power supply. And these two systems have strong interdependencies. However, little attention has been paid to the realistic interactions of traffic flow in road networks and electric power supply on the resilience assessment with sufficient details.

In fact, signalized intersections are common for urban road networks and their delays have considerable impact on the total travel time and the passengers' route choices (Mazloumi et al. 2010). The normal functioning of traffic signals relies on the electricity supply of the EPN, and the overhead distribution lines of the EPN often utilize the right-of-way for transportation systems (Ellingwood et al. 2016). In the U.S., there are still many areas with aging overhead power infrastructures (ASCE 2017). While undergrounding the distribution system can be used to harden the existing system, researchers also pointed out that burying the system is not cost effective due to the high cost (Salman et al. 2015). Thus, for these areas, hazards such as hurricanes can damage the poles supporting the distribution lines, which may block the road and interrupt the traffic flow (Alipour et al. 2018; Salman 2016). The indirect loss caused by the functionality degradation (i.e., the increase of traffic delay) of the disrupted TN can accumulate over

³ This chapter is adapted from a published paper by the author (Zou and Chen 2020a) with permission from ASCE.

time until the TN is fully recovered. It was found that this indirect loss usually surpasses the direct loss (i.e., the repair cost of the damaged components of the TN) (Alipour and Shafei 2016). Moreover, the disrupted TN impacts the accessibility and efficiency of recovering efforts of damaged power system, while the delayed repair of EPN in turn impacts the recovery planning of other facilities, including TN (e.g. intersection traffic lights without power). Therefore, given their importance of underpinning the resilience of other critical facilities and the whole community, the sophisticated interdependency between these two CISs need to be modeled appropriately in any resilience study.

This chapter presents a holistic resilience assessment framework for the traffic-electric power system by capturing three typical types of interdependencies under hurricanes over different phases of hazard resilience. Based on the graph theory, the traffic and electric power systems are represented by two directed graphs. In the TN, the traffic flow pattern is determined by solving the traffic assignment problem, in which the link delay and intersection delay functions are affected by the state of the electric power system. In the EPN, fragility functions are used to estimate the damage level of components, and the functionality of the whole EPN is determined considering cascading effects. Since the accessibility of the damaged components for emergency recovery depends on the state of the TN, some effective strategies of improving the system resilience of both TN and EPN in preparedness, response, and recovery stages are investigated. The proposed framework is demonstrated using a numerical example based on the virtual community called Centerville.

4.2 Framework description

In this framework, the traffic and electric power systems are both characterized using the flow-based mathematical representation and three types of interdependency are captured. A procedure coupled with

Monte Carlo simulation is presented to assess the resilience of both systems. Improvement strategies in corresponding stages of resilience are also integrated into this framework.

4.2.1 Transportation network

The transportation network focuses on the roadway networks, in which both topology and traffic flow performance are important to assessing the ability of the system to cope with disasters. While the topology defines the ability of maintaining connectivity among critical facilities, the traffic flow reflects the throughput of the roadway network, and traffic efficiency between origins and destinations. The transportation network is represented as a directed graph $G^T = (V^T, A^T)$, where V^T and A^T are the set of nodes and arcs, respectively (Sheffi 1985; Vugrin et al. 2014). The nodes define origins, destinations, and the arcs (i,j) where $i,j \in V^T$ and $i \neq j$ are all roadway links. Given the set of origins O and the set of destinations D and the traffic demand between each origin-destination (O-D) pair, the traffic flow pattern of the network at time t can be determined by solving the user equilibrium traffic assignment problem (Sheffi 1985):

$$\text{minimize } \sum_{(i,j) \in A^T} \int_0^{x_{ij}(t)} t_{ij}(w) dw \quad (4.1)$$

subject to:

$$\sum_k f_k^{od} = q_{od} \quad \forall o \in O, d \in D \quad (4.2)$$

$$x_{ij}(t) = \sum_o \sum_d \sum_k f_k^{od} \delta_{ij,k}^{od} \quad \forall (i,j) \in A^T, k \in K_{od}, o \in O, d \in D \quad (4.3)$$

$$f_k^{od} \geq 0 \quad \forall k \in K_{od}, o \in O, d \in D \quad (4.4)$$

where $x_{ij}(t)$ is the total flow from node i to node j on arc (i,j) ; $t_{ij}(\cdot)$ is the arc cost function that is separable,

convex, and strictly increasing; q_{od} , f_k^{od} and K_{od} are the traffic demand, the flow on path k , and the set of paths between o and d , respectively; $\delta_{ij,k}^{od}$ is the path-arc incidence indicator (for paths between o and d , if arc (i,j) belongs to path k , $\delta_{ij,k}^{od} = 1$, else $\delta_{ij,k}^{od} = 0$). Eq. (4.1) is the objective function to achieve user equilibrium condition; the constraint in Eq. (4.2) indicates that the flow on all paths connecting each O-D pair has to equal the O-D travel demand; the constraint in Eq. (4.3) is the path-arc incidence relationship; and the constraint in Eq. (4.4) stipulates that all flow should be nonnegative.

The key part as shown above is the definition of the arc cost function $t_{ij}(\cdot)$ calculating the travel delay from node i to node j , which depends on both the traffic flow $x_{ij}(t)$ and the road configuration. For those arcs with ending nodes belonging to the set of intersections $V_{\text{intersection}}^T \subseteq V^T$, this function should account for not only the driving time spent by vehicles from node i to node j , but also the possible intersection delay at node j , which is defined as:

$$t_{ij}(x_{ij}(t)) = \begin{cases} t_{ij}^1(x_{ij}(t)) & \forall j \in V^T - V_{\text{intersection}}^T \\ t_{ij}^1(x_{ij}(t)) + t_j^2(x_{ij}(t)) & \forall j \in V_{\text{intersection}}^T \end{cases} \quad (4.5)$$

$$t_{ij}^1(x_{ij}) = \frac{l_{ij}}{v_{ij}^0} [1 + 0.15 (\frac{x_{ij}(t)}{\delta_{ij}^T(t) C_{ij}^T})^4] \quad (4.6)$$

$$t_j^2(x_{ij}(t)) = sig_j \cdot [y_j^T(t) \cdot delay_{sig,j}(x_{ij}(t)) + (1 - y_j^T(t)) \cdot delay_{unsig,j}(x_{ij}(t))] + (1 - sig_j) \cdot delay_{unsig,j}(x_{ij}(t)) \quad (4.7)$$

$$delay_{sig,j}(x_{ij}(t)) = \frac{0.5 \cdot Cycle_j \cdot (1 - Green_j / Cycle_j)}{1 - [\min(1, \frac{x_{ij}(t)}{\delta_{ij}^T(t) C_{ij}^T}) \cdot Green_j / Cycle_j]} + \frac{900}{4} [(\frac{x_{ij}(t)}{\delta_{ij}^T(t) C_{ij}^T} - 1) + \sqrt{(\frac{x_{ij}(t)}{\delta_{ij}^T(t) C_{ij}^T} - 1)^2 + \frac{16x_{ij}(t)}{(\delta_{ij}^T(t) C_{ij}^T)^2}}] \quad (4.8)$$

$$delay_{\text{unsig},j}(x_{ij}(t)) = t_{s,j} + \frac{900}{4} \left[\frac{x_{ij}(t)h_d}{3600} - 1 + \sqrt{\left(\frac{x_{ij}(t)h_d}{3600} - 1\right)^2 + \frac{x_{ij}(t)h_d^2}{450 \cdot 3600 / 4}} \right] + 5 \quad (4.9)$$

where $t_{ij}^1(x_{ij}(t))$ is the travel delay for arc (i, j) and is characterized by the famous Bureau of Public Roads (BPR) function in Eq. (4.6); l_{ij} , v_{ij}^0 , and C_{ij}^T are the distance, free flow speed, and original flow capacity for arc (i, j) , respectively; $\delta_{ij}^T(t)$ indicates the ratio of the remaining capacity of arc (i, j) to its original capacity C_{ij}^T and is also referred to as the functionality level of arc (i, j) ; $t_j^2(x_{ij}(t))$ is the intersection delay at node j as shown in Eq. (4.7); sig_j indicates the type of signalization of intersection node j (signalized: $sig_j=1$; unsignalized: $sig_j=0$); $y_j^T(t)$ indicates the condition of the traffic light for a signalized interstation (functional: $y_j^T(t)=1$; failed: $y_j^T(t)=0$); $delay_{sig,j}(\cdot)$ and $delay_{\text{unsig},j}(\cdot)$ are functions from Highway Capacity Manual (HCM) to approximate the time delays for signalized intersections and all-way stop intersections, respectively (unit: second) (Transportation Research Board (TRB) 2000); $Cycle_j$ is the cycle length (unit: second); $Green_j$ is the green time (unit: second); $t_{\text{service},j}$ is the service time (unit: second); h_d is the departure headway (unit: second). More detailed information about Eqs. (4.8) and (4.9) can be found in HCM (Transportation Research Board (TRB) 2000). For the signalized intersections, this study assumes that traffic signal lights are pre-timed and operated in the isolated mode.

It should be noted that the intersection delay in Eq. (4.7) depends on both the design of signalization and the functionality of traffic signal. For a particular intersection, if and only if it is signalized ($sig_j=1$) and the traffic light operates normally ($y_j^T(t)=1$), the intersection delay can be defined as $t_j^2(x_{ij}(t)) = delay_{sig,j}(x_{ij}(t))$; otherwise, this intersection is assumed to work as an unsignalized one, i.e., $t_j^2(x_{ij}(t)) = delay_{\text{unsig},j}(x_{ij}(t))$. Therefore, given the traffic demand input (e.g., O-D pairs and q_{od}) and the

roadway state (e.g., sig_j , $y_j^T(t)$, $\delta_{ij}^T(t)$, C_{ij}^T , $Cycle_j$, and $Green_j$), the traffic pattern $x_{ij}(t)$ for the roadway network can be solved using Eqs. (4.1)-(4.4), and then the TN's state $s_T(t)=\{x_{ij}(t), y_j^T(t), \delta_{ij}^T(t)\}$ at time t is determined.

To study the resilience of the system, it is important to use appropriate metrics to quantify the functionality of the roadway network. For the TN, those metrics can be classified into topology-based and flow-based. Topology-based metrics often describe the number of immediately available arcs after the disaster or the accessibility of the network (i.e., the probability to maintain at least one path between O-D pairs of interest) (Zhang and Wang 2017; Zhang et al. 2015), which are often used to evaluate the functionality of disrupted networks. Flow-based metrics, e.g., flow capacity and travel time, focus on the efficiency aspect of the network functionality. It should be noted that since the flow pattern also relies on the network topology, the flow-based metrics can also imply the topological characteristics of the network. For example, the losses of connectivity among nodes may result in the increase of travel time. Further, the disaster may not cause full damage of some nodes (e.g. bridges) or full closure of some arcs (roads), and partial traffic may still be allowed which cannot be well reflected with topology-based metric. Therefore, flow-based metrics can provide more comprehensive information of the functionality of TN in both normal and disrupted conditions than the topology-based ones. The following flow-based metrics for TN in state $s_T(t)$ are used:

$$Q_{total}^T(t) = \frac{1}{\sum_{(i,j) \in A^T} x_{ij}(t) t_{ij}(x_{ij}(t))} \quad (4.10)$$

where $Q_{\text{total}}^T(t)$ represents the reciprocal of total travel time for all users and measures the overall travel efficiency of the TN.

4.2.2 Electric power network

The EPN's main function is to deliver electric power from the power plant to end users, and it contains three subsystems: generation, transmission, and distribution. For the generation system, the power plants produce electricity and generation substations step up the voltage to transmission levels. The transmission system, consisting of transmission lines and substations, is responsible for carrying electricity from generation substations over long distance to the distribution system. It often adopts mesh-like design from the topological perspective to ensure redundancy and reliability. In the distribution system, the electricity is stepped down at the distribution substations and then flows through the distribution lines to end users. Distribution networks usually have a radial topology, i.e., a unique path exists from a substation to each end user. It has been found that since generation and transmission systems are specially designed to resist high wind loads, the distribution system is often the one particularly susceptible to hurricanes (Salman 2016). This is because overhead distribution systems are widely used due to economic reasons, and distribution towers and poles can be knocked down by hurricane winds, which can cause large scale blackouts considering its radial topology. Therefore, this study focuses on the distribution part of the EPN subject to hurricanes.

Models simulating the behavior of EPNs can be classified into two main categories (Fang et al. 2015): those based on complex network theory and those based on the power flow analysis. While the power flow analysis, which uses the power flow equations to describe the flow dynamics, may give more detailed information, it requires more parameter settings and computational efforts, limiting its application mainly

to small networks and operational analyses of energy industry. In this study, the EPN is modeled using the complex network theory, which is more computationally economic but can provide sufficiently detailed results for the resilience assessment (Dueñas-osorio and Vemuru 2009; Ouyang et al. 2014).

The EPN is also represented as a directed graph $G^E = (V^E, A^E)$, where the set of nodes V^E consists of the union of the set of supply nodes $V^{E, \text{supply}}$, the set of transshipment nodes $V^{E, \text{transship}}$, and the set of demand nodes $V^{E, \text{demand}}$ (i.e., $V^E = V^{E, \text{supply}} \cup V^{E, \text{transship}} \cup V^{E, \text{demand}}$) (Lee et al. 2007; Loggins and Wallace 2015).

The structurally hurricane-vulnerable components are assumed to be only power towers and poles and the failure of power line is determined based on the failure patterns of the corresponding towers and poles (Salman et al. 2015; Unnikrishnan and van de Lindt 2016). The structural damages to the distribution towers and poles, which can be nodes or lie on the arcs, can be estimated by performing structural analysis explicitly or implementing the fragility functions. Then, given the structurally affected components, a network flow model based on (Loggins and Wallace 2015) is established to calculate the state $s_E(t) = \{y_i^E(t), y_{ij}^E(t), \delta_i^E(t), \delta_{ij}^E(t), x_{ij}^E(t)\}$ of the EPN at time t due to cascading effects as follows:

$$\text{maximize} \quad \sum_{i \in V^{E, \text{demand}} \cup V^{E, \text{transship}}} y_i^E(t) + \sum_{(i,j) \in A^E} y_{ij}^E(t) \quad (4.11)$$

subject to

$$\sum_{(i,j) \in A^E} x_{ij}^E(t) - \sum_{(j,i) \in A^E} x_{ji}^E(t) \leq C_{s,i} \quad \forall i \in V^{E, \text{supply}} \quad (4.12)$$

$$\sum_{(i,j) \in A^E} x_{ij}^E(t) - \sum_{(j,i) \in A^E} x_{ji}^E(t) \geq 0 \quad \forall i \in V^{E, \text{transship}} \quad (4.13)$$

$$\sum_{(i,j) \in A^E} x_{ij}^E(t) - \sum_{(j,i) \in A^E} x_{ji}^E(t) \leq C_{t,i} \quad \forall i \in V^{E, \text{transship}} \quad (4.14)$$

$$\sum_{(i,j) \in A^E} x_{ij}^E(t) - \sum_{(j,i) \in A^E} x_{ji}^E(t) = -p_i \quad \forall i \in V^{E,\text{demand}} \quad (4.15)$$

$$0 \leq p_i \leq d_i \quad \forall i \in V^{E,\text{demand}} \quad (4.16)$$

$$0 \leq \sum_{(i,j) \in A^E} x_{ij}^E(t) \leq \delta_i^E(t) C_i^E y_i^E(t) \quad \forall i \in V^E \quad (4.17)$$

$$0 \leq \sum_{(j,i) \in A^E} x_{ji}^E(t) \leq \delta_i^E(t) C_i^E \quad \forall i \in V^E \quad (4.18)$$

$$0 \leq x_{ij}^E(t) \leq \delta_{ij}^E(t) C_{ij}^E y_i^E(t) \quad \forall (i,j) \in A^E, i \in V^E \quad (4.19)$$

$$y_i^E(t) \leq 100 \delta_i^E(t) \quad \forall i \in V^E \quad (4.20)$$

$$y_{ij}^E(t) \leq 100 \delta_{ij}^E(t) \quad \forall (i,j) \in A^E \quad (4.21)$$

$$y_{ij}^E(t) \leq y_i^E(t) \quad \forall i \in V^E, (i,j) \in A^E \quad (4.22)$$

$$y_i^E(t) \leq \sum_{(j,i) \in A^E} x_{ji}^E(t) \quad \forall i \in V^{E,\text{transship}} \quad (4.23)$$

$$y_i^E(t) \leq p_i / d_i \quad \forall i \in V^{E,\text{demand}} \quad (4.24)$$

$$x_{ij}^E(t) \in \mathbb{Z}, y_{ij}^E(t) \in \{0,1\}, 0 \leq \delta_{ij}^E \leq 1 \quad \forall (i,j) \in A^E \quad (4.25)$$

$$y_i^E(t) \in \{0,1\}, 0 \leq \delta_i^E(t) \leq 1 \quad \forall i \in V^E \quad (4.26)$$

where $y_i^E(t)$ and $y_{ij}^E(t)$ denote the functional states of node i and arc (i,j) , respectively (functional: $y_i^E(t) = 1$, $y_{ij}^E(t) = 1$; failed: $y_i^E(t) = 0$, $y_{ij}^E(t) = 0$); $x_{ij}^E(t)$ denotes the flow on arc (i,j) ; $\delta_i^E(t)$ and $\delta_{ij}^E(t)$ denote the experiencing functionality levels for node i and arc (i,j) at time t , respectively; $C_{s,i}$ and $C_{t,i}$

are the supply flow capacity and the transshipment flow capacity of node i , respectively; C_i^E and C_{ij}^E are the total flow capacities of node i and arc (i, j) , respectively; p_i and d_i are the actual supplied and required flows of demand node i .

The objective function of this model (Eq. (4.11)) is to maximize the number of survival components after the hurricane. The constraints in Eqs. (4.12)–(4.16) regulate the electricity flowing with respect to supply, transshipment, and demand flow levels. The constraints in Eqs. (4.17)–(4.19) ensure that the flows respect the disrupted capacities for both nodes and arcs. The constraints in Eqs. (4.20)–(4.24) describe the relationship between the state of components and the flow pattern. It is noteworthy that the constraints in Eqs. (4.20) and (4.21) introduce the coefficients of 100 which are arbitrarily set to handle the partially functional components, i.e., when $0 < \delta_i^E(t) < 1$, the component i is not totally disrupted and its functional state $y_i^E(t)$ can still be 1; Only when $\delta_{ij}^E(t) = 0$, the component i is totally disrupted and its functional state $y_i^E(t)$ should be 0.

The inputs of this model are the network topology, the flow parameters such as $C_{s,i}$, $C_{t,i}$, C_i^E , C_{ij}^E , and d_i , and the structurally damaged states $\delta_i^E(t)$ and $\delta_{ij}^E(t)$. It can be also found that when the data of electricity supply and demand is not available, this model can also be adapted for the connectivity analysis which only depends on the network topology (i.e., $C_{s,i}$, $C_{t,i}$, C_i^E , and C_{ij}^E are set to large constants, d_i is set to equal to p_i , $x_{ij}^E(t)$, $\delta_i^E(t)$, and $\delta_{ij}^E(t)$ are set to be binary, and the constraint Eq. (4.13) is omitted). The following metric characterizing the ratio of the number of functional components to the number of total components is used to evaluate the functionality of the EPN in state $s_E(t)$:

$$Q_{\text{survival}}^E(t) = \frac{\sum_{i \in V^E} y_i^E(t) + \sum_{(i,j) \in A^E} y_{ij}^E(t)}{|V^E| + |A^E|} \quad (4.27)$$

where $|\cdot|$ is the cardinality of the set.

4.2.3 Interdependencies between TN and EPN

Three types of interdependency between TN and EPN are considered, as shown in Figure 4.1:

- (1) Type I (physical and geographic interdependency): The function of traffic lights at signalized intersections in TN depends on the electricity supply of EPN;
- (2) Type II (geographic interdependency): The function of some roadway arcs in TN depends on whether the fallen towers or poles due to hurricanes in EPN can block the roadway;
- (3) Type III (physical interdependency): The accessibility to damaged sites in EPN in the recovery process depends on the function of TN.

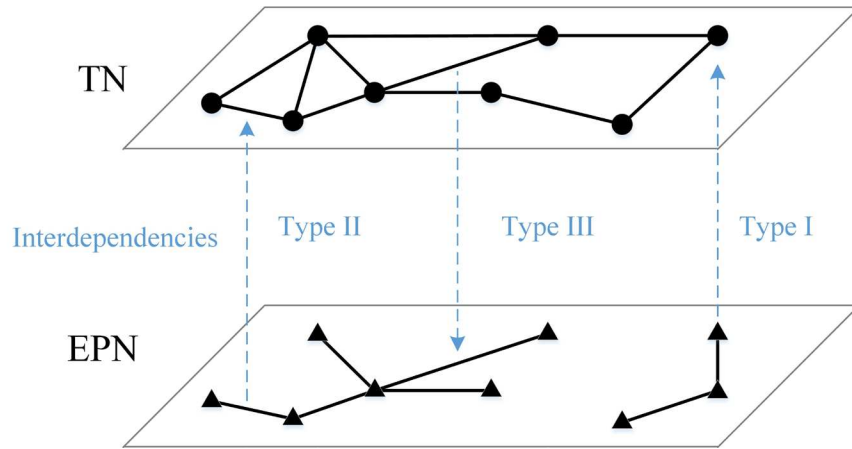


Figure 4.1 Interdependencies between TN and EPN

These three types of interdependency can be delineated using following constraints:

4.2.3.1 Type I

Type I interdependency denotes the relationship mapping from nodes in EPN to nodes in TN. For a

signalized intersection node i in TN, its functional state depends on its power supply node j in EPN. Those poles supporting power lines which are directly connected to the traffic lights are explicitly modeled as nodes in the EPN. In other words, no additional poles exist between these poles and the traffic lights, and the state of the traffic lights only depends on the state of these poles. Let $F_V(T,E)$ denote the set of such node pairs (i,j) where $i \in V_{\text{intersection}}^T$ and $sig_i=1$, and $j \in V^E$. Then the following equation must hold:

$$y_i^T(t) = y_j^E(t) \quad \forall (i,j) \in F_V(T,E) \quad (4.28)$$

4.2.3.2 Type II

Type II interdependency denotes the relationship mapping from nodes and arcs in EPN to nodes in TN and occurs in the damage propagation stage. The towers or poles, which can be the nodes or lie on the arcs of EPN, may be knocked down and block the traffic in TN. Let $F_{VA}(T,E)$ denote the set of such component pairs $((i,j),r_{ij})$ where $(i,j) \in A^T$ and r_{ij} is the corresponding set of nodes and arcs of EPN affecting arc (i,j) of TN. R_{ij} is determined based on the geographical proximity in this study. This interdependency is represented as:

$$\delta_{ij}^T(t_0) = f_{\text{block}}(r_{ij}) \quad \forall ((i,j),r_{ij}) \in F_{VA}(T,E) \quad (4.29)$$

where $f_{\text{block}}(\cdot)$ is the function mapping the potential blockages caused by damaged components of EPN to the TN's state. The blockage is reflected in the capacity reduction of the roadway using $\delta_{ij}^T(t_0)$ in Eq. (4.6).

4.2.3.3 Type III

Type III interdependency occurs in the recovery stage. In this study, two types of recovery activities

are considered: (1) removing debris for TN; (2) repairing damaged components for EPN. These activities both involve the route choices of delivering repair resources to designated sites which depend on the TN's state. Once part of the blockage is cleared and some traffic lights are recovered, the travel time may be reduced and the disrupted EPN sites can be accessed and recovered sooner. Thus, this section describes the recovery process in which the Type III interdependency is embedded.

It is assumed that Rc denotes a set of available generic recovery resource units with a number of n and they are located at some depot nodes of TN before hurricanes. The recovery resource, also referred to as a repair team here, is generic enough to capture the required personnel, equipment and material to conduct the necessary recovery activities. Each damaged component is assumed to only require one unit of resource for recovery (Ouyang and Wang 2015). Let $\Theta \subseteq A^T \cup V^E \cup A^E$ denote the set of damaged components (nodes and arcs) needed to be repaired in TN and EPN, Pr denote the set of precedence relationships for components pairs (i,j) where $i,j \in \Theta$, τ_i is repair duration for component i in Θ , and $T_{\text{span}} = \{t_0, t_1, \dots, t_k\}$ denotes the set of time ticks for the recovery process where $t_0 \leq t_1 \leq \dots \leq t_k$ and the difference between any adjacent time ticks is a constant increment Δt . For each component $i \in \Theta$, the decision variable $u_i(t)$ is 1 if the repair activity starts on the component i at time t , and 0 otherwise. Accordingly, following constraints should be satisfied:

$$\sum_{t \in T_{\text{span}}} u_i(t) \leq 1 \quad \forall i \in \Theta \quad (4.30)$$

$$\sum_{i \in \Theta} \sum_t^{t+\tau_i-\Delta t} u_i(z) \leq n \quad \forall t \in T_{\text{span}} \quad (4.31)$$

$$\sum_{t \in T_{\text{span}}} (t + \tau_i) u_i(t) \leq \sum_{t \in T_{\text{span}}} t \cdot u_j(t) \quad \forall (i, j) \in Pr \quad (4.32)$$

where the constraint in Eq. (4.30) indicates that any damaged component can only be scheduled to be repaired no more than once; the constraint in Eq. (4.31) indicates that at any time, the number of damaged components under repair is limited by the total number of available resources; and the constraint Eq. (4.32) states that any precedence relationship in Pr must be respected (e.g., the repair for component i must be completed before the repair for component j can begin). It is also assumed here that the repair scheduling is non-preemptive, i.e., the repair team should complete the repair task on the currently assigned component before it moves to next component.

It should be noted that the repair duration τ_i consists of two parts:

$$\tau_i = \tau_{i,\text{travel}} + \tau_{i,\text{repair}} \quad (4.33)$$

where $\tau_{i,\text{repair}}$ is the repair time required for component i to recover to a desired functionality level; and $\tau_{i,\text{travel}}$ is the travel time for a repair team from its current position to component i . While $\tau_{i,\text{repair}}$ can be pre-estimated based on the empirical data, $\tau_{i,\text{travel}}$ depends on the TN's state which may change over time as the recovery process progresses. Two assumptions are made to calculate $\tau_{i,\text{travel}}$: (1) the repair team will try to utilize the roadways in TN as much as possible to reach the damaged component; (2) once the repair team finishes the repair task, it becomes available for next task with its waiting position being assumed to be the TN node which is geographically closest to its last repaired component.

Suppose at time t , there exists at least one repair team which is unassigned. $\tau_{i,\text{travel}}$ is determined as the minimum travel cost among all available repair teams to reach component i :

$$\tau_{i,\text{travel}} = \min_{r \in R_c} \{f_{\text{shortest}}(pos_r(t), i, s_T(t))\} \quad \text{with } i \in \Theta, pos_r(t) \in V^T \quad (4.34)$$

where $pos_r(t)$ denotes the current waiting position of available repair team r at time t ; and $f_{\text{shortest}}(\cdot)$ is the function to calculate the shortest path from $pos_r(t)$ to component i based on the TN's states. And $f_{\text{shortest}}(\cdot)$ is defined as:

$$f_{\text{shortest}}(pos_r(t), i, s_T(t)) = \begin{cases} f_{\text{TN}}(pos_r(t), ctn(i), s_T(t)) & i \in A^T \\ f_{\text{TN}}(pos_r(t), ctn(i), s_T(t)) + 2 \cdot dist(i, ctn(i)) / v_{\text{out}} & i \in V^E \cup A^E \end{cases} \quad (4.35)$$

where $ctn(i)$ is the TN node which is closest to component i (specifically, if i is the arc in TN, $ctn(i)$ is the closest one in its two endpoints; if i is the node in EPN, $ctn(i)$ is the closest TN node; and if i is the arc in EPN, $ctn(i)$ is the closest TN node considering its two endpoints); $f_{\text{TN}}(\cdot)$ finds the lowest time cost from $pos_r(t)$ to $ctn(i)$ within the TN using the shortest path finding algorithm such as Dijkstra's algorithm; $dist(i, ctn(i))$ calculates the straight line distance between i and $ctn(i)$; and v_{out} is the travel speed for the repair team outside of TN. It should be noted that in Eq. (4.35): (1) since emergency repair vehicles are usually not expected to follow traffic signals in the emergency response stage, $f_{\text{TN}}(\cdot)$ only uses the free flow time without considering the effects of traffic flow and traffic signals to compute the shortest path in the emergency response stage (i.e., defined as in the 72 h immediately after the disruption) (Nikoo et al. 2018); after the emergency response stage, $f_{\text{TN}}(\cdot)$ utilizes the travel time caused by other traffic with the traffic signals to find the shortest path; (2) the term $2 \cdot dist(i, ctn(i)) / v_{\text{out}}$ is used to handle the additional travel cost for reaching the components of EPN located outside of the TN.

As the recovery process progresses, the functionality level of the component $i \in A^T \cup V^E \cup A^E$ at any time t can be expressed as:

$$\delta_i^{\text{CIS}}(t) = \delta_i^{\text{CIS}}(t_0)[t \leq \sum_{t \in T_{\text{span}}} (t + \tau_i)u_i(t)] + \delta_i^{\text{CIS}}(t_d)[t > \sum_{t \in T_{\text{span}}} (t + \tau_i)u_i(t)] \quad \forall t \in T_{\text{span}} \quad (4.36)$$

where $[\cdot]$ is the Iverson bracket, which returns 1 if the statement is true and 0 otherwise; and the superscript of CIS can be T or E, indicating TN or EPN, respectively; $\delta_i^{\text{CIS}}(t_0)$ is the functionality level of component i at time t_0 ; and $\delta_i^{\text{CIS}}(t_d)$ is the normal functionality level of component i before the hurricane at time t_d . Eq. (4.36) states that component i maintains its initial functionality level $\delta_i^{\text{CIS}}(t_0)$ before its scheduled repair activity is completed, and returns to its normal functionality level $\delta_i^{\text{CIS}}(t_d)$ after the completion of the repair works.

4.2.4 Resilience assessment

The analytical definition of resilience in this study is adopted from (Cimellaro et al. 2016) as follows:

$$R^{\text{CIS}} = \frac{1}{T_{\text{LC}}} \int_{t_0}^{t_0 + T_{\text{LC}}} Q^{\text{CIS}}(t) / Q^{\text{CIS}}(t_d) dt \quad \forall \text{CIS} \in \{\text{T}, \text{E}\} \quad (4.37)$$

where R^{CIS} is the dimensionless resilience index of the CIS; T_{LC} is the control time for the period of interest; and $Q^{\text{CIS}}(t)$ is the chosen functionality metric of the CIS such that the larger $Q^{\text{CIS}}(t)$ is, the better functionality level the CIS is at; and $Q^{\text{CIS}}(t_d)$ indicates the normal functionality level before the hazard. Note that this definition of resilience relates itself with the shaded area in Figure 1.1 (Bocchini and Frangopol 2012).

Based on the aforementioned models quantifying states of TN and EPN and their interdependencies, the simulation procedure to calculate R^{CIS} for the interdependent traffic-electric power system is shown in Figure 4.2. The three stages of the functionality level in Figure 1.1 are considered in this procedure. At every time point t , the functionality level of each component $\delta_i^{\text{CIS}}(t)$ in TN and EPN is evaluated and then used to update the two networks' states ($s_{\text{T}}(t)$ and $s_{\text{E}}(t)$) and their functionality level at the system level

($Q_{\text{total}}^T(t)$, $Q_{\text{critical}}^T(t)$, and $Q_{\text{survival}}^E(t)$). When all the damaged components are repaired, the resilience indices for TN and EPN can be obtained using Eq. (4.37) based on the chosen functionality metrics. It should be noted that similar to the reliability analysis, the resilience assessment should also account for uncertainties within the hazards and the system. Apart from the load and resistance uncertainties from the structural perspective, the uncertainties in functionality-related variables, e.g., the supply and demand of service flow, the quantity of available resources, and the repair duration, can also play an important role in affecting three stages of the system-level functionality. Given the probabilistic information of these variables, Monte Carlo simulation can be employed to generate input random samples and coupled with the resilience assessment framework.

Different strategies can be implemented in three stages to improve CIS's resilience. In the context of TN and EPN, the following strategies are considered:

- (1) Preparedness stage: the key components in EPN can be strategically and proactively strengthened to increase their resistances to hurricanes and reduce the probability of severe damage, which may cause serious consequences in the following stages;
- (2) Response stage: backup power generators can be deployed at strategic nodes of EPN, which can provide power for some critical locations for a certain period $t_{i,b}^E$ after supply nodes failed. These locations are identified to achieve the best resilience outcome of the two interdependent CISs. The functionality of node i in the set of nodes equipped with backup generators V_{backup}^E can be expressed as:

$$\delta_i^E(t) = \delta_i^E(t_d)[t \leq t_{i,b}^E] + \delta_i^E(t_0)[t > t_{i,b}^E \cap t \leq \sum_{t \in T_{span}^E} (t + \tau_i)u_i(t)] + \delta_i^E(t_d)[t > \sum_{t \in T_{span}^E} (t + \tau_i)u_i(t)] \quad (4.38)$$

$\forall i \in V_{backup}^E, \forall t \in T_{span}^E$

Similarly, backup batteries can be equipped for traffic lights at critical signalized intersections and provide power for a certain period $t_{i,b}^T$ after power supply nodes failed. The constraint for Type I interdependency can be modified to be:

$$y_i^T(t) = [t \leq t_{i,b}^T] + y_j^E(t)[t > t_{i,b}^T] \quad \forall (i, j) \in F_V(T, E) \quad (4.39)$$

Compared with Eq. (4.36), incorporating the backup generators and backup batteries is expected to lower the negative impact of infrastructure interdependency and can delay the functionality losses of the two systems;

- (3) Recovery stage: advanced decisions can be made to improve the effectiveness and efficiency of restorative efforts. Objective functions can be established based on needs (e.g., minimizing the makespan of restoration and maximizing resilience indices of CISs) and optimization techniques can be applied to find optimal resource allocation strategies and repair schedules.

It should be stressed that these strategies are only based on the TN and EPN, the main study objects of this research. Such strategies may need to be modified if other interdependent CISs are included.

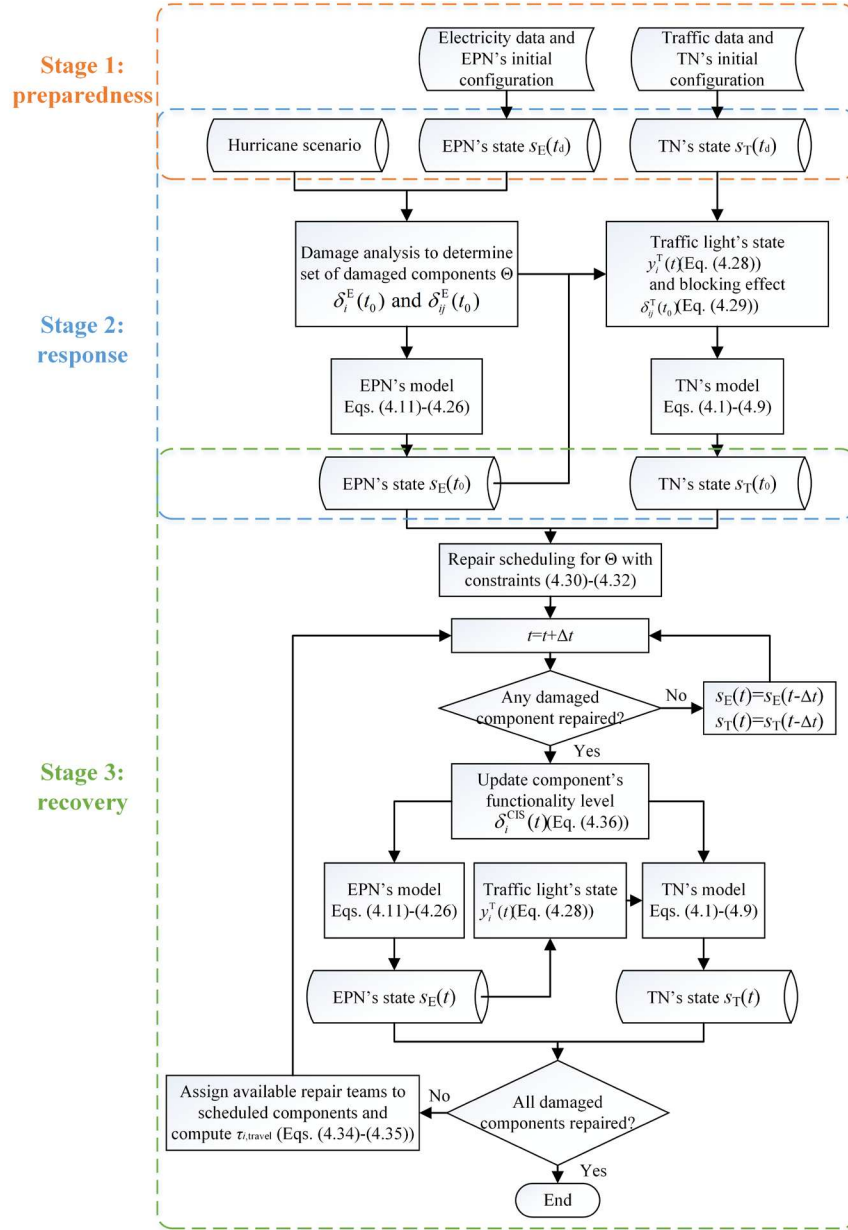


Figure 4.2 Flowchart for resilience assessment of the interdependent traffic-electric power system

4.3 Illustrative example

The TN and EPN in the Centerville Virtual Community Testbed (Ellingwood et al. 2016) subject to hurricanes are used here to illustrate the proposed framework. Figure 4.3 depicts the layout of these two CISs of Centerville, which locate in an approximately $13 \text{ km} \times 8 \text{ km}$ rectangular region and Table 4.1 lists the descriptions of components of two networks. In the EPN, EP1 and EP25 are two source nodes and

provide power for the left and right parts of the EPN, respectively. It is assumed that the transmission lines are supported by steel towers with the spacing of 320 m, and the distribution lines are supported by wooden poles with the spacing of 46 m (Salman 2016).

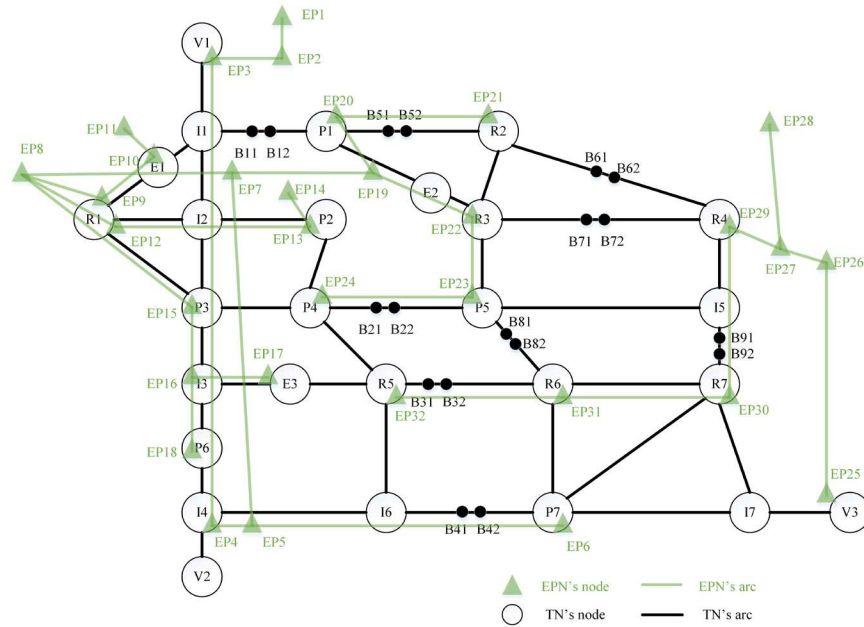


Figure 4.3 TN and EPN of Centerville community

Table 4.1 Descriptions of TN and EPN of Centerville

CIS	Component	Description
TN	P1–P7, R1–R7, and V1–V3	Major origins and destinations
	I1–I7	Major intersections
	E1–E3	Critical facilities
	(B11, B12),..., (B91, B92)	Bridge arcs
EPN	EP1	Power plant
	EP2, EP5	Transmission substations
	EP6, EP7, EP8, EP19, EP27	Distribution substations
	Other nodes (EP2, EP3), (EP3, EP4), (EP4, EP5), (EP25, EP26), (EP26, EP27)	Towers or poles
	Other arcs	Transmission lines
	Other arcs	Distribution lines

In this example, the whole region is assumed to be under the same wind speed and the same wind

direction and five typical wind speeds representing five hurricane categories based on the Saffir-Simpson hurricane wind scale are used (Table 4.2). To determine the state of EPN immediately following the hurricane at time t_0 , the structural damages on towers and poles are simulated using the fragility functions in Table 4.3. Specifically, given the experienced wind speed v_h , the failure probability $p(v_h)$ is compared with a uniformly distributed random variable $\xi \in [0,1]$: the tower or pole is assumed to fail completely if $\xi \leq p(v_h)$ and experience no damage otherwise. It should be pointed out that the assumption of independent fragilities for adjacent towers and poles, which have been adopted in many studies (Mensah and Dueñas-osorio 2016; Ouyang and Dueñas-osorio 2014; Salman and Li 2015; Unnikrishnan and van de Lindt 2016), might not always hold since they may be correlated due to structural couplings. Further research is needed to quantify the conditional probabilities of failure of adjacent towers and poles (Darestani et al. 2018; Salman et al. 2015).

Table 4.2 Values of parameters instantiating the resilience assessment of illustrative example

Parameter	Value
Wind speed v_h (km/h)	135, 165, 195, 225, 255
Free flow speed v_{ij}^0 (mph)	Uniform[50, 55, 60, 65, 75]
Traffic demand q_{od}	Normal (mean: 500, COV: 0.8)
Length of cycle $Cycle_j$ (s)	70
Green time $Green_j$ (s)	42
travel speed outside of TN v_{out} (km/h)	50
Set of signalized intersections	{I1, I2, I4, I5, I6, I7}
Set of depot nodes dispatching repair teams	{P5}

Note: COV is the coefficient of variation; the free flow speed v_{ij}^0 and traffic demand q_{od} are only sampled once to initialize the network and then treated as deterministic in following resilience assessment.

Table 4.3 Probabilistic information for attributes of tower and pole (Unnikrishnan and van de Lindt 2016)

Support structure	Attribute	Distribution	Parameter
-------------------	-----------	--------------	-----------

Tower	Fragility	Lognormal	Median: 304 km/h, COV: 0.15
	Repair duration	Normal	Mean: 72 h, COV: 0.5
	Clean duration	Normal	Mean: 1 h, COV: 0.5
Pole	Fragility	Lognormal	Median: 188 km/h, COV: 0.15
	Repair duration	Normal	Mean: 5 h, COV: 0.5
	Clean duration	Normal	Mean: 0.5 h, COV: 0.5

And the functionality level of each EPN's component $\delta_i^E(t)$ is assumed to be either 0 or 1, and the connectivity criteria of EPN model as defined in Eqs. (4.11)–(4.26) are used. When the towers or poles happen to be the nodes in the EPN, the corresponding $\delta_i^E(t_0)$ are assigned 0 or 1; when the towers or poles lie on the arcs of EPN, the failure probabilities of towers or poles are assumed to be independent. The arc is assumed to be out of service ($\delta_{ij}^E(t_0) = 0$) if no fewer than two towers or poles fail, and operate normally ($\delta_{ij}^E(t_0) = 1$) otherwise (Salman et al. 2015). For the TN, the settings of related parameters are summarized in Table 4.2. It is noted that the data on the change of traffic demand after hazards is often very hard to be collected, and the post-disaster traffic demand is assumed to be the same as the pre-disaster level in this study. In reality, the hazard can significantly change the traffic demand because the infrastructures essential for some social and economic activities may be damaged and therefore some post-hazard activities can be either reduced or relocated to other places. As a result, travelers may alter their travel plans, such as canceling their trips and changing destinations. Furthermore, as the infrastructures recover and the everyday activities return to normality gradually, the post-hazard traffic demand can also evolve correspondingly (Alipour and Shafei 2016; Kilanitis and Sextos 2019).

However, predicting the post-hazard traffic demand and its evolution during recovery stage is very complicated because many uncertain socio-economic and behavioral aspects are involved and thus remains as a common challenge in transportation resilience research (Chang et al. 2012a; Khademi et al. 2015).

Researchers on the effect of the earthquake on the TN typically propose to use the modified pre-earthquake traffic demand by applying trip reduction factors to the original-destination matrix to approximate the post-earthquake traffic demand (Alipour and Shafei 2016; Bocchini and Frangopol 2011; Guo et al. 2017). But estimating the trip reduction factors still requires related data and socio-economic analysis. Since the data for the post-hurricane traffic demand change is lacking and the socio-economic analysis can introduce additional level of uncertainty, this study does not explicitly address this issue, but rather adopts the same traffic demands for both before and after the hurricane. Similar procedures can also be found in literature (Bocchini and Frangopol 2011, 2012; Guo et al. 2017). It is noted that the proposed framework can accommodate the updated post-hurricane traffic demand once such data is available.

To simulate the blocking effects $f_{\text{block}}(\cdot)$ on the traffic flow caused by the damaged towers and poles, it is assumed here that each damaged tower or pole can cause three levels of blocking impact on the traffic on the flow capacity of related TN's arc, i.e., $\delta_{ij}^T(t_0) = 0, 0.5, \text{ or } 1$, corresponding to fully blocked, partially blocked, and no impact, respectively and the corresponding probabilities under different wind speeds are given in Table 4.4. This is based on the assumption that the higher the wind speed is, the more likely the fully blocked and partially blocked are to occur. More detailed simulation can be adopted to refine the above structural damage analysis at time t_0 , e.g., using the simulation tool such as HAZUS-MH 4.0 to generate more realistic hurricane scenarios, and performing detailed structural and statistical analyses to investigate the blocking effects of fallen towers and poles. In addition, for the recovery stage, the recovery activities are set to begin after a period of delay $\tau_{\text{delay}} = 4 \text{ h}$ when the hurricane occurs (Ouyang et al. 2012), and no precedent constraints are imposed on the repair sequences of the damaged components. In fact, to evaluate all possible disrupted scenarios for a large infrastructure system under natural hazards such as earthquakes

and hurricanes is often impractical and computationally expensive. So some researchers developed a methodology to select a small set of realistic hazard cases associated with corresponding hazard-consistent probabilities to approximate all the cases (Chang et al. 2000; Romero et al. 2015). Since this study aims to propose a framework to explore the interdependencies between TN and EPN, the application of scenario selection methodology is beyond the scope. In this study, a simple Monte Carlo method is applied: for a given wind speed and a number of repair teams, the simulation procedure in Figure 4.2 is repeated 200 times independently so the average resilience indices converge and are recorded (Ouyang et al. 2012; Ouyang and Wang 2015).

Table 4.4 Probabilities of three blocking effects under different wind speeds

Blocking effect	Wind speed (km/h)				
	135	165	195	225	255
Fully blocked	0.13	0.20	0.33	0.40	0.47
Partially blocked	0.27	0.27	0.33	0.40	0.40
No impact	0.60	0.53	0.33	0.20	0.13

4.3.1 Resilience assessment of the original systems

Figure 4.4 shows the variations of the functionality metrics of both systems with time. The repair sequences are assumed to be random and still satisfy the repair scheduling constraints as listed in Eqs. (4.30) and (4.31). It can be seen that with the increase of the wind speed, the functionality levels of both systems decrease, and the total recovery time increases. While the functionality levels of the two interdependent systems remain almost unchanged (near 1.0) when the wind speed v_h is 135 km/h, they both decrease significantly when v_h exceeds 135 km/h. Specifically, at time $t = 0$ h, the hurricane with v_h higher than 135 km/h can decrease the functionality of EPN by more than 50% of its normal level. Although the hurricane does not affect TN directly according to the assumption, the functionality of TN can still drop below 20%

of the normal level due to the Type I and II interdependencies with EPN. Meanwhile, the Type III interdependency determines the rapidity of the recovery stage by the repair planning and all three types of interdependency contribute to the shapes of functionality curves of two systems in the recovery stage.

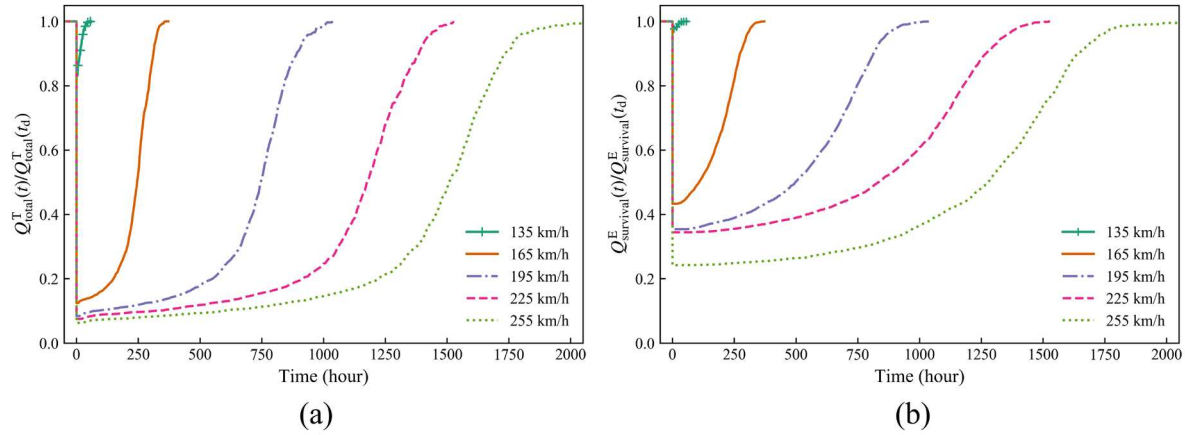


Figure 4.4 Variations of normalized functionality metrics of both systems with time: (a) TN; (b) EPN. (Number of repair teams $n = 4$)

Based on the functionality variations, the resilience indices of both systems can be obtained by integrating the functionality curves over time based on Eq. (4.37). The control time for the period of interest T_{LC} is set to be $30 \times 24 = 720$ h for the purpose of comparing different hurricane scenarios. Figure 4.5 depicts the distribution of resilience indices of two systems based on 200 simulation results of each scenario. With the increase of the number of repair teams, the distribution of resilience index shifts rightward and the mean value increases, indicating that more recovery resources can enhance the resilience of both systems. To better demonstrate this trend, Figure 4.6 shows the variation of the mean system resilience index with the number of repair teams. It can be observed that the resilience indices of both systems decrease with the increase of the wind speed and both systems can withstand hurricanes with the wind speed as high as 135 km/h. Increasing the number of repair teams generally improves the system resilience, and such improvement effect becomes more significant when the number of repair teams n is low and turns stable

when n surpasses a certain value. This is partly because when n is less than the number of the damaged components, increasing n can allow more damaged components to be repaired at the same time and thus shorten the total recovery time. When n is greater than the number of the damaged components, the repair scheduling becomes less important as all damaged components can be repaired in parallel with sufficient resources. As a result, the total recovery time would be same as the longest time of those components taking to repair. It should be noted that in reality, due to budget constraint and severity of major natural hazards, available resource is often scarce compared to the needs, as evidenced by many historical hazards. It is therefore important to have appropriate decision-making tools to prioritize repair, assist on resource allocation and make the optimal scheduling to enhance the system resilience.

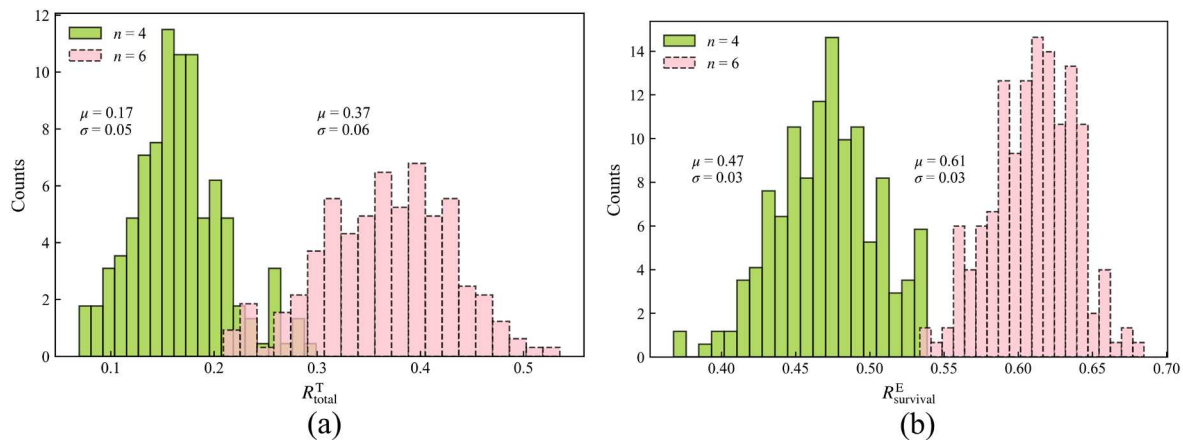


Figure 4.5 Histograms of system resilience index with different number of repair teams: (a) TN; (b) EPN. (wind speed $v_h = 195$ km/h)

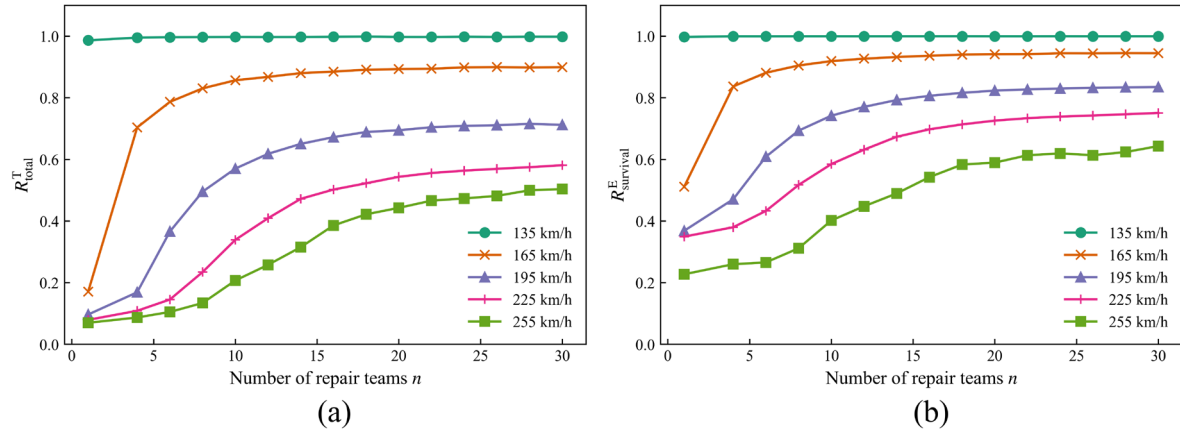


Figure 4.6 The variation of average system resilience index with the number of repair teams: (a) TN; (b) EPN

4.3.2 Effects of resilience improvement strategies

To investigate the effects of different improvement strategies in three stages of the system resilience, four cases are studied to be compared with the original interdependent system (denoted as Case 0). Case 1 focuses on enhancing the resistance of components to hurricane in the preparedness stage. It is assumed that all towers and poles in the EPN vulnerable to hurricanes are strengthened, reflected as increasing the median values in their fragility functions by a ratio α_{harden} of 1%, 5%, and 10%, respectively. Such a strategy is also shown in the damage analysis of the flowchart in Figure 4.2. Case 2 focuses on improving the robustness in the response stage. It is assumed that all substation nodes in EPN are equipped with backup generators which can still provide power for 24 hours after they fail (Ouyang et al. 2012). All signalized intersection nodes in TN are equipped with backup batteries which can still provide power for traffic lights for 10 hours after the main power loss. This strategy is characterized in Eqs. (4.38) and (4.39).

Compared with Cases 0, 1, and 2, Case 3 focuses on improving the repair scheduling in the recovery stage. First, the delay time for the repair activities to be initiated is reduced from 4 hours to 1 hour to represent an emergency/fast response. Second, better repair sequences of damaged components are

determined, instead of being randomly arranged in Cases 0, 1, and 2. An objective function aiming at maximizing the resilience of the interdependent system can be established as follows (Ouyang and Wang 2015):

$$\text{maximize } w^T R^T + w^E R^E \quad (4.40)$$

where w^T and w^E are weight coefficients for the resilience indices of TN and EPN, respectively, and satisfy $w^T + w^E = 1$. The values of w^T and w^E can be adaptively set depending on which system is deemed more important and should be recovered first under a particular situation in the view and judgment of the decision-makers. In this demonstrative study, three repair modes are adopted: Equal ($w^T = w^E = 0.5$), TN-first ($w^T = 1$ and $w^E = 0$), and EPN-first ($w^T = 0$ and $w^E = 1$). It should be noted that the final resilience indices can only be determined when the whole recovery process completes. Typical recovery process takes time and during the duration of recovery, the topology of the network and the service flows will dynamically change. So the stochastic scheduling optimization with the objective function in Eq. (4.40) and the constraints in Eqs. (4.30) and (4.31) is essentially a type of dynamic job shop problem and also known to be NP-hard. The approximate solutions are often obtained based on heuristics, such as rule-based, genetic, and simulated annealing algorithms (Bocchini and Frangopol 2012; Vugrin et al. 2014).

Here, a heuristic method based on the importance ranking is adopted to improve the repair scheduling.

First, the important measure IM_i for each component i is computed as follows:

$$IM_i = w^T \cdot \frac{Q^T(t_d) - Q^T(t_0 | i)}{Q^T(t_d)} + w^E \cdot \frac{Q^E(t_d) - Q^E(t_0 | i)}{Q^E(t_d)} \quad \forall i \in V^T \cup A^T \cup V^E \cup A^E \quad (4.41)$$

where $Q^T(t_0 | i)$ and $Q^E(t_0 | i)$ denote the functionality of TN and EPN after only removing component i ,

respectively. Under the chosen repair mode (w^T and w^E), the IM_i directly reflects the impact of removing component i on the functionality of the two systems. The larger the IM_i is, the more important the component i is to the functionality of the two systems. Then the repair sequences of the damaged components are determined based on the ranking of their IM_i 's from high to low. Further, Case 4 combines all strategies in Cases 1, 2, and 3 to improve the original systems (the α_{harden} is set to be 5% and all three repair modes are considered).

Figure 4.7 shows the functionality curves of different cases for a typical scenario, and Table 4.5 and Table 4.6 summarize the improvement ratios of average resilience indices for improved TN and EPN as compared to the original ones, respectively.

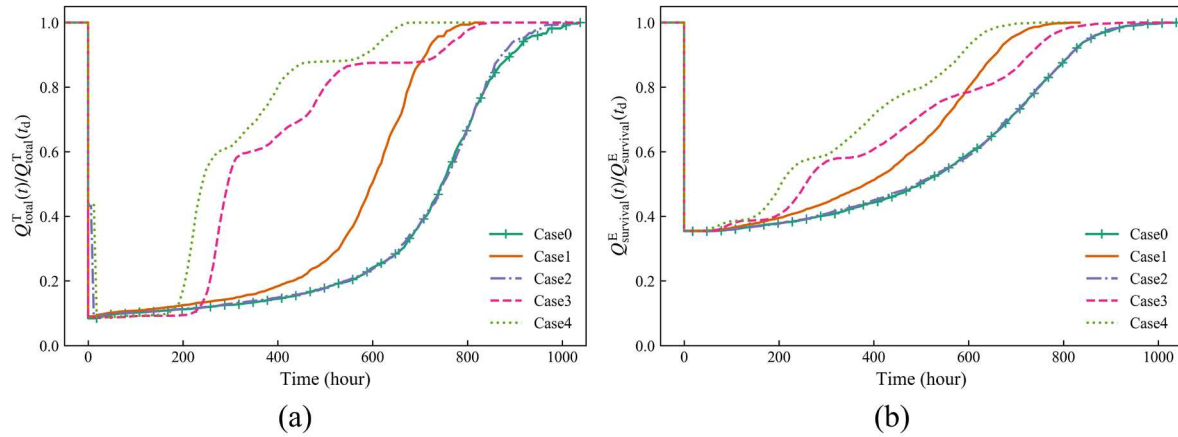


Figure 4.7 Comparison of variations of normalized functionality metrics of both systems over time with different improvement strategies: (a) TN; (b) EPN. (wind speed $v_h = 195$ km/h, number of repair teams $n = 4$, $\alpha_{\text{harden}} = 5\%$ for Case 1, and Equal repair mode for Cases 3 and 4)

Table 4.5 Improvement effects on TN's resilience (number of repair teams $n = 4$)

Case	Improvement strategy	Wind speed (km/h)				
		135	165	195	225	255
Case 0	None	0.00%	0.00%	0.00%	0.00%	0.00%
Case 1	1%	0.24%	4.49%	5.69%	0.40%	2.14%
	5%	0.35%	16.87%	66.06%	4.96%	7.09%
	10%	0.45%	30.96%	161.88%	11.77%	9.69%

Case 2	Backup power	0.17%	0.25%	3.14%	0.44%	1.00%
Case 3	Equal	0.41%	22.60%	202.99%	178.64%	97.66%
	TN-first	0.42%	22.83%	243.10%	241.45%	166.96%
	EPN-first	0.25%	5.62%	-2.89%	-7.94%	-13.04%
Case 4	Equal	0.60%	32.86%	260.95%	225.80%	154.03%
	TN-first	0.60%	34.87%	292.27%	280.29%	232.54%
	EPN-first	0.55%	22.85%	79.10%	4.47%	-5.48%

Table 4.6 Improvement effects on EPN's resilience (number of repair teams $n = 4$)

Case	Improvement strategy	Wind speed (km/h)				
		135	165	195	225	255
Case 0	None	0.00%	0.00%	0.00%	0.00%	0.00%
Case 1	1%	0.03%	2.33%	2.29%	2.40%	2.42%
	5%	0.06%	9.77%	19.12%	4.08%	23.66%
	10%	0.07%	16.15%	42.25%	8.82%	39.30%
Case 2	Backup power	0.00%	-0.36%	0.46%	-1.20%	0.55%
Case 3	Equal	0.17%	5.40%	25.74%	27.86%	47.01%
	TN-first	0.16%	4.15%	18.47%	16.11%	19.49%
	EPN-first	0.18%	6.15%	30.43%	29.96%	49.13%
Case 4	Equal	0.21%	13.74%	42.28%	33.72%	70.09%
	TN-first	0.20%	12.62%	34.33%	22.06%	50.45%
	EPN-first	0.21%	14.23%	47.00%	36.19%	73.09%

It can be observed that for Case 1, hardening (strengthened) towers and poles in EPN can reduce the number of the damaged components and thus shorten the recovery stage and enhance the resilience of both systems. It should be pointed out that the reason the functionality of EPN for Case 1 is almost equal to that

for Case 0 at time $t = 0$ in Figure 4.7(b) is that the adopted functionality metric $Q_{\text{survival}}^E(t)$ represents the ratio of number of functional components in EPN rather than the ratio of number of structurally intact components. This is based on the fact that a structurally intact component may still not be able to provide service due to the failure of its upstream components. It is true however, that a higher number of structurally intact components due to the pre-disaster hardening usually means lower overall post-disaster repair workloads and faster recovery process.

In Case 2, it can be found from Table 4.5 and Table 4.6 that that adopting backup generators and batteries does not enhance the resilience of interdependent TN and EPN significantly. The first reason is that the EPN used in the demonstrative example is a star-like distribution network with nearly no redundancy. Through the unique failure path to the demand node, the upstream substations cannot deliver the power successfully even with backup generators equipped. The second reason is that, for the TN, although the backup generators for some substations which directly power traffic lights and the backup batteries at signalized intersections can delay the failure of traffic lights temporally (note the delayed drop of functionality level immediately after $t = 0$ h for Case 2 in Figure 4.7(a)), the lasting time of backup generators (i.e., 24 h) and batteries (i.e., 10 h) are relatively short compared with the whole recovery process. Since the resilience index is calculated based on the integration of functionality level over the control time $T_{LC} = 30$ days, the effect of backup generators and batteries on the resilience is not significant. This is also reflected in Figure 4.7: except for some small difference immediately after $t = 0$ h, the functionality curves for Case 2 are almost identical to those for Case 0.

The effect of repair scheduling on the resilience can be clearly reflected in Case 3. From Table 4.5 and Table 4.6, the improvement ratios of TN and EPN are found to vary under different repair modes. The most

effective repair mode for each single network is always the “selfish” one (i.e., the TN-first mode is the best for improving the resilience of TN, and the EPN-first mode is the best for improving the resilience of EPN), and apparently the worst repair mode for each single network is always the “unselfish” one (i.e., the EPN-first mode is the worst for improving the resilience of TN, and the TN-first mode is the worst for improving the resilience of EPN). The result of the equal mode lies in between the results of the “selfish” and “unselfish” modes.

It can also be seen that from Table 4.5, the negative ratios in Case 3 indicate that using EPN-first mode actually impairs the resilience of TN, but from Table 4.6 even using TN-first mode can still improve the resilience of EPN. This is because the durations for repair activities (i.e., debris cleaning) on TN are much shorter than the durations for repair activities (i.e., towers and poles repairing) on EPN (see Table 4.3). If most repair teams are first assigned to repair EPN under EPN-first mode, they need to take a relatively longer time to finish their repair work before moving to the next task. And again, due to the star-like EPN, the first repaired components (i.e., with high value of IM_i) under EPN-first mode are located near the power source nodes, which had little contributions to TN (i.e., not directly powering the traffic lights). Thus, the functionality of TN remains at a low level for an extended time, resulting in reduced resilience. But if the most repair teams are assigned first to repair TN under TN-first mode, the debris cleaning on important roadways could be quickly finished and the overall TN state could be improved at an earlier time, which resulted in shorter travel time and faster moving to next assigned tasks. Meanwhile, due to Type I interdependency, some EPN’s components can also be important to TN’s functionality and be scheduled for repairing first, which explains the improvement of EPN’s resilience under TN-first mode in Table 4.6.

Equal mode balances the importance of different components to each system and thus can achieve an

in-between improvement for individual systems. It can be seen from Figure 4.7(a) that for the TN, the functionality of Case 3 is lower than that of Case 0 in the early duration of recovery stage but surpasses the functionality of Case 0 in the later duration and results in a shorter recovery stage. As a result, the equal-mode strategy can effectively enhance the resilience of both systems. This result also underlines the importance of the TN's state to the recovery processes of both systems. The faster the TN's functionality can be recovered, the more efficiently the repair activities can be conducted and thus the greater resilience can be achieved for both systems.

When all the improvement strategies are combined in Case 4, the resilience of both systems is significantly improved as expected. Different repair modes can still generate similar effects on the improvement ratios as in Case 3 but all have positive numbers. By comparing the result of Case 4 to those of Cases 1, 2, and 3, the most effective single strategy to improve the system resilience can be determined. For the TN, adopting a better repair schedule ranks first, and hardening EPN's components is the second, and setting up backup generators and batteries gives the least improvement. But for the EPN, hardening EPN's components and adopting a better repair schedule both work well while setting backup generators and batteries barely improves the resilience of this star-like EPN.

Figure 4.8 depicts the variations of average system resilience indices with the increase of the number of repair teams in all five cases. The overall trend is similar to that of the original system: more repair resources result in larger resilience indices. It also clearly shows the ranking of improvement of different strategies. Note that in Figure 4.8(a), when the number of repair teams was less than 12, the components were not hardened in Case 3 and the number of damaged components in Case 3 may be larger than that in Case 1. However, adopting a better repair schedule (Case 3) still outperformed hardening EPN's

components (Case 1), which highlights the benefit of using an improved repair sequence in the non-trivial repair scheduling problem (when the number of repair team is less than the number of damaged components). And it can be also found that the improvement levels for EPN were smaller than those of TN; however, the economic variation may be significant. This is because if the actual data on customer demand for electricity was available, the functionality metric for the EPN can be represented as the proportion of customers affected by outages which is strongly correlated with the fraction of functional nodes being used. For large networks, even a small change in resilience index based on the functionality in this study could mean millions of dollars in economic saving or loss (Ouyang et al. 2012).

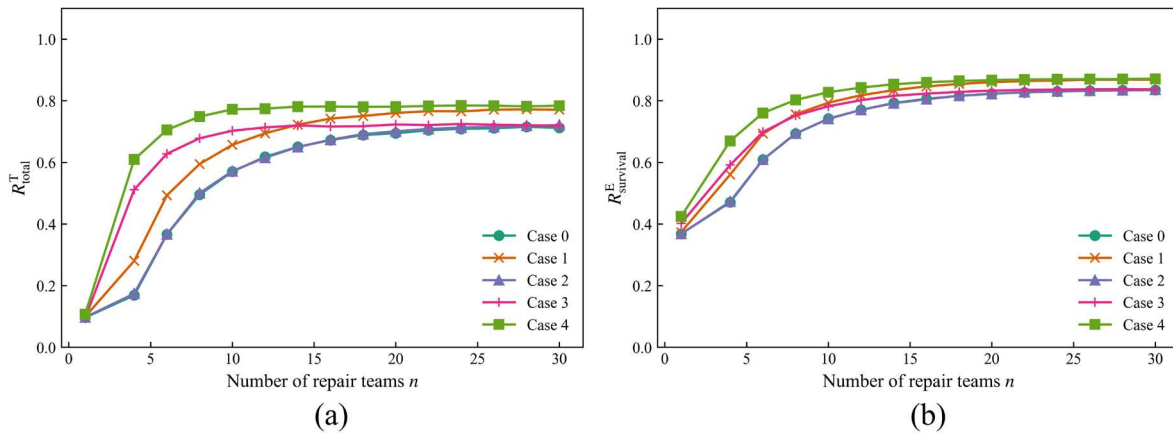


Figure 4.8 Comparison of variation of average system resilience index with the number of repair teams in different cases: (a) TN; (b) EPN. (wind speed $v_h = 195$ km/h, $\alpha_{harden} = 5\%$ for Cases 1 and 4, and Equal repair mode for Cases 3 and 4)

4.3.3 Computational cost

All analyses in this chapter were coded using Python and conducted on a desktop computer with Intel core i7-6700 3.40 GHz CPU, 16 GB RAM, and 64-bit Windows 7 operating system. The running time of each sample in the simulation varies from 20 s to 60 s depending on the wind speed and the number of repair team, i.e., higher wind speed leads to more damaged components and fewer number of repair teams leads to longer recovery time, which both increase the running time. For the importance ranking algorithm,

it took 26 minutes to obtain importance measures of all components of the TN and EPN used. The importance ranking algorithm aims to provide a heuristic solution of recovery schedule for maximizing the resilience of the TN and EPN since the original problem is NP-hard and its efficiency depends on the size of the networks. For larger instances of TN and EPN, ranking all components may be computationally expensive and the efficiency of this framework can be further improved from the perspectives of computational setting (e.g., implementing parallel computing) and algorithm (e.g., using topology-based measures for ranking or applying optimization to the recovery scheduling problem directly).

4.4 Conclusions

This chapter presents a framework of resilience assessment for the interdependent traffic-electric power system subject to hurricane. Flow-based mathematical models are established to describe the traffic and electric power systems. Three types of interdependencies were captured: type I interdependency describes the traffic lights at signalized intersection nodes in TN requiring power supply from relevant nodes in EPN; type II interdependency is the potential blocking effects induced by the failed components of EPN on the traffic flow in TN; and type III interdependency is the effect of accessibility of TN on the recovery processes of both systems. A procedure coupled with Monte Carlo simulation is proposed to assess the resilience of the two systems. The TN and EPN in a virtual community named Centerville considering three improvement strategies are studied as a demonstration. It is found that interdependencies can significantly affect the resilience of both systems and each system corresponds to different most effective single strategy. While hardening hurricane-vulnerable components and adopting a better repair schedule both improve the resilience of the electric power system significantly, adopting a better repair schedule works best for the resilience of the traffic system. The equal repair mode can achieve the resilience

improvement in a balanced fashion. The results also highlight the importance of repair scheduling to the resilience improvement for these two interdependent systems when the available recovery resources were limited. Due to the interdependencies, the faster the functionality of traffic system can recover, the more efficiently the repair activities can be conducted and thus the greater resilience of both systems can be achieved. It is noted the specific findings in terms of resilience and recovery strategies are highly dependent on the specific network configurations. Therefore, some specific findings about Centerville may be different from another community.

CHAPTER 5 ENHANCING RESILIENCE OF INTERDEPENDENT TRAFFIC-ELECTRIC POWER SYSTEM BY PRIORITIZING MITIGATION AND REPAIR RESOURCES⁴

5.1 Introduction

TN and EPN are critical lifelines underpinning the normal functioning of the modern society and the investigation in Chapter 4 suggests that these two systems can be strongly interdependent. Characterizing the interdependencies among these two highly interconnected critical infrastructure systems with adequate details is critical in devising cost-effective resilience improvement strategies. In addition, the available resources to perform pre-disruption mitigation and post-disruption repair actions are often limited, especially during the post-disruption stage. However, these crucial decisions on the resource allocation are often made from personal experiences, judgement or intuition, which may not only be ineffective but also introduce extra damages to the disrupted system. Therefore, it is necessary to devise science-based cost-effective resource allocation strategies to prioritize limited resources to achieve the optimal balance

⁴ This chapter is adapted from a published paper by the author (Zou and Chen 2019) with permission from Elsevier.

between CIS performance and cost.

This chapter develops a decision-making framework for prioritization of mitigation and repair actions to enhance the resilience of an interdependent traffic-electric power system in terms of its functionality under budgetary constraints. A bi-level, stochastic, and simulation-based optimization problem is established with the objective of maximizing the expected resilience improvement of the interdependent system. The upper level of this framework seeks to find the optimal plan of allocating limited mitigation and repair resources to multiple disrupted components to estimate the maximum attainable functionality gain. And at the lower level, the functionalities of the traffic and electric power systems considering their interdependencies are measured based on network analysis methods. Moreover, the dynamic traffic assignment algorithm is adopted to overcome the shortcomings of the static traffic algorithm and capture more realistic traffic dynamics in congested urban roadway networks. Uncertainties in disruptions, traffic demands, and mitigation and repair costs are considered in the problem formulation. The problem is solved by the binary particle swarm optimization algorithm combined with the knapsack-based heuristic initialization and based on which, the mitigation and repair priorities of disrupted components are then further established.

5.2 Network representation and functionality

5.2.1 Transportation network

The transportation network here refers to the urban roadway network and is represented as a directed graph $G^T = (V^T, A^T)$, where V^T and A^T are the set of nodes and links, respectively. The nodes define origins, destinations, and the links (i, j) where $i, j \in V^T$ and $i \neq j$ are all roadways. Since the static traffic assignment (STA) model cannot capture traffic dynamics (e.g., queue spillback, and speed variations), a simulation-

based mesoscopic dynamic traffic assignment (DTA) model is developed to determine the traffic flow pattern of the TN by solving the dynamic user equilibrium (DUE) traffic assignment problem. The period of interest is discretized into a set of small intervals, $S = \{0, \Delta t, 2\Delta t, \dots, M\Delta t\}$, where Δt is a small time interval during which no considerable variation in traffic conditions may occur, and M is a large integer such that the intervals from 0 to $M\Delta t$ covers the period of interest. Given the set of origins O and the set of destinations D and the time-varying traffic demand between each O-D pair, the traffic flow pattern of the network should satisfy the following DUE condition (Sbayti et al. 2007):

$$c_k^{od}(\tau) - \pi^{od}(\tau) \geq 0 \quad \forall o \in O, d \in D, k \in K_{od}, \tau \in T \quad (5.1)$$

$$f_k^{od}(\tau)(c_k^{od}(\tau) - \pi^{od}(\tau)) \geq 0 \quad \forall o \in O, d \in D, k \in K^{od}(\tau), \tau \in T \quad (5.2)$$

$$f_k^{od}(\tau) \geq 0 \quad \forall o \in O, d \in D, k \in K^{od}(\tau), \tau \in T \quad (5.3)$$

$$\sum_{k \in K^{od}(\tau)} f_k^{od}(\tau) = q^{od}(\tau) \quad \forall o \in O, d \in D, \tau \in T \quad (5.4)$$

where T is the set of departure time intervals, $T \subseteq S$; $K^{od}(\tau)$ is the set of feasible paths from o and d in departure time τ ; $q^{od}(\tau)$ is the traffic demand from o to d in departure time τ ; $f_k^{od}(\tau)$ is the flow on path k from o to d in departure time τ ; $c_k^{od}(\tau)$ is the path travel time for travelers on path k from o to d in departure time τ ; and $\pi^{od}(\tau)$ is the minimum path travel time for travelers from o to d in departure time τ .

Compared with the STA model, the DTA model does not have nice mathematical properties (e.g., highly nonlinear and non-differentiable objective function) to be exploited easily (Chiu et al. 2011; Sbayti et al. 2007). As a result, if the DTA model is implemented in the following decision optimization model,

the whole bi-level problem cannot be linearized and converted to an equivalent single-level problem as in the work by Fotouhi et al. (Fotouhi et al. 2017). To achieve such DUE conditions, the DTA method usually contains a dynamic network loading model simulating traffic dynamics to obtain the actual experienced travel time, a time-dependent shortest path algorithm which finds the new shortest routes, and a path assignment adjustment algorithm to iteratively update the routes for travelers to approximate the DUE condition (Chiu et al. 2011). A mesoscopic and simulation-based dynamic network loading model is adopted here, in which vehicles in each departure time interval τ are divided into a number of packets and loaded onto the network (Tong and Wong 2000; Zhou and Taylor 2014).

The travel time for a packet of vehicles traversing a link (i, j) consists of two parts: the cruise time along the link and the queuing time at the end of the link. The cruise time depends on the length of the link l_{ij} , the traffic density $k_{ij}(t)$, and the following speed-density relationship (Ben-Akiva et al. 2012):

$$v_{ij}(t) = \max \{v_{ij}^{\min}, v_{ij}^0 (1 - (\frac{\max \{k_{ij}(t) - k_{ij}^0, 0\}}{k_{ij}^{\text{jam}} - k_{ij}^0})^\beta)^\alpha\} \quad \forall t \in \mathcal{S} \quad (5.5)$$

$$k_{ij}^0 = \delta_{ij}^T C_{ij}^0 / v_{ij}^0 \quad (5.6)$$

where $v_{ij}(t)$ is the current cruise speed on link (i, j) at time interval t ; v_{ij}^{\min} , v_{ij}^0 , k_{ij}^0 , k_{ij}^{jam} and C_{ij}^0 are the minimum speed, free flow speed, optimal density, jam density, and original flow capacity for link (i, j) , respectively; α and β are parameters; and δ_{ij}^T indicates the ratio of the remaining capacity of link (i, j) to its original capacity C_{ij}^0 and is also referred to as the functionality level of link (i, j) , and the original functionality level in the intact TN is 1 (i.e., $\delta_{ij}^{T,0} = 1$).

Once vehicles arrive at the end of the link and yet reach their destinations, they may experience

additional queuing delay before they can enter the downstream link because of congestion or signalization of intersection. A modified point queue model with the spatial storage capacity and first-in-first-out (FIFO) constraints is adopted here to account for queue spillbacks (Zhou and Taylor 2014). Thus, at each time interval t , for vehicles arriving at the end of the link, the condition for entering the downstream link (j, k) is that the outflow capacity of the current link C_{ij}^{out} and the physical space availability $k_{jk}^{\text{jam}} - k_{jk}(t)$ of the downstream link (j, k) can both accommodate these vehicles. Otherwise, the vehicles would form or enter the queue at the end of the current link (i, j) .

Two types of signalization of intersection are considered here: signalized and unsignalized. For the signalized intersections, traffic signal lights are assumed to be pretimed and operated in the isolated mode and the effect of traffic signal is reflected in the outflow capacity of the link (i, j) with the signalized interstation node j (Zhou and Taylor 2014):

$$C_{ij}^{\text{out}} = y_j^{\text{T}} C_{ij}^{\text{saturation}} \frac{\text{Green}_j}{\text{Cycle}_j} + (1 - y_j^{\text{T}}) C_{ij}^{\text{saturation}} \quad \forall j \in V_{\text{signalized}}^{\text{T}} \subseteq V^{\text{T}} \quad (5.7)$$

where $C_{ij}^{\text{saturation}}$ is the saturation flow of link (i, j) ; and Green_j and Cycle_j denote the effective green time and cycle length of the traffic signal for node j , respectively; $V_{\text{signalized}}^{\text{T}}$ is the set of signalized nodes in TN; the binary variable y_j^{T} is introduced to indicate the condition of the traffic light for a signalized node j (functional: $y_j^{\text{T}} = 1$; failed: $y_j^{\text{T}} = 0$).

The unsignalized intersections are assumed to be all-way-stop intersections and their impact is considered by forcing all vehicles about to enter the downstream link through the unsignalized intersection to stop and wait at the end of the current link for a specified length of time τ_{stop} , which aims to mimic the

behavior of drivers encountering stop signs. It is assumed that if the traffic light of the signalized intersection fails (i.e., $y_j^T = 0$), the intersection would operate as an unsignalized one.

Once the dynamic network loading model produces the actual experienced travel time by each traveler, the time-dependent shortest path algorithm computes the shortest paths for each departure time interval and then the flows of paths are adjusted using the method of successive averages. This process is repeated iteratively until the DUE condition is reached with acceptable accuracy. More information of the DTA model can be found in relevant literature (Chiu et al. 2011; Sbayti et al. 2007; Tong and Wong 2000; Zhou and Taylor 2014).

To summarize, given the time-varying traffic demand input (e.g., O-D pairs and $q^{od}(\tau)$) and the roadway state (e.g., y_j^T and δ_{ij}^T) and characteristics (e.g., v_{ij}^{\min} , v_{ij}^0 , k_{ij}^{jam} , l_{ij} , C_{ij}^0 , $Cycle_j$, and $Green_j$), the DTA model can yield the state of the TN, $s_T = \{y_j^T, \delta_{ij}^T, f_k^{od}(\tau), c_k^{od}(\tau)\}$, where $f_k^{od}(\tau)$ and $c_k^{od}(\tau)$ represent the traffic flow pattern over the period of interest S satisfying Eqs. (5.1)–(5.4).

The resilience of the CIS is usually characterized by measuring the variation of the functionality of the system and various functionality metrics have been proposed based on the research focuses. The functionality metrics of TN can be classified into topology-based and flow-based ones. While the topology-based metrics concern about the ability of maintaining connectivity after disruption (Bocchini and Frangopol 2013; Freiria et al. 2015; Liu and Frangopol 2005; Reggiani et al. 2015; Zhang et al. 2015), the flow-based metrics reflect the throughput of the roadway network, and traffic efficiency between origins and destinations (Fotouhi et al. 2017; Guo et al. 2017; Liao et al. 2018; Nogal and Honfi 2019; Zhang and Wang 2017). It should be noted that since the flow pattern also relies on the network topology, the flow-based metrics also imply the topological characteristics of the network. In this study, as the disruption to

the TN is congestion due to partial capacity loss and traffic signal outage, the following flow-based metric for TN is used (Fotouhi et al. 2017; Zhang and Wang 2017):

$$Q_{\text{total}}^T = \frac{1}{\sum_{\tau \in T} \sum_{o \in O, d \in D} \sum_{k \in K^{od}(\tau)} f_k^{od}(\tau) c_k^{od}(\tau)} \quad (5.8)$$

where Q_{total}^T represents the reciprocal of total travel time for all users over the period of interest. The total travel time is computed by the summation of all users' travel time from their origins to destinations and reflects the overall travel efficiency of the TN.

5.2.2 Electric power network

In the EPN, the electric power is first generated from power plants, then carried through transmission lines to distribution substations, and finally delivered to end users through distribution lines. The EPN can experience many different types of disruptions: random failures (e.g., short circuit and failure of some devices), natural hazards (e.g., hurricane and earthquake), and intentional attack (e.g., sequential or synchronous attacks) (Abedi et al. 2019). As in Chapter 4, this chapter also focuses on the distribution networks, which usually have a radial topology and are installed along the urban roadways. Compared to power generation and transmission systems, the power distribution system is particularly susceptible to hurricanes because overhead distribution lines are widely used due to economic reasons, and the support structures (i.e., towers and poles) can be knocked down by hurricane winds, which can induce sizable blackouts considering its radial topology (Salman 2016).

The EPN here is also represented as a directed graph $G^E = (V^E, A^E)$, where the set of links A^E denotes the distribution lines and the set of nodes V^E consists of the union of the set of supply nodes $V^{E, \text{supply}}$, the set

of transshipment nodes $V^{E, \text{transship}}$, and the set of demand nodes $V^{E, \text{demand}}$ (i.e., $V^E = V^{E, \text{supply}} \cup V^{E, \text{transship}} \cup V^{E, \text{demand}}$). The only structurally vulnerable components are assumed to be distribution towers and poles, which can be nodes or lie on the links. The failure of power line is determined based on the failure patterns of the corresponding towers and poles (Salman et al. 2015; Unnikrishnan and van de Lindt 2016). The EPN's state, $s_E = \{y_i^E, y_{ij}^E, \delta_i^E, \delta_{ij}^E, x_{ij}^E\}$, is not only affected by the structural failure pattern of towers and poles but also determined by the following network flow model to account for cascading effects, which is the same as the model in Section 4.2.2 in Chapter 4 (Loggins and Wallace 2015):

$$\text{maximize} \quad \sum_{i \in V^{E, \text{demand}} \cup V^{E, \text{transship}}} y_i^E + \sum_{(i,j) \in A^E} y_{ij}^E \quad (5.9)$$

subject to

$$\sum_{(i,j) \in A^E} x_{ij}^E - \sum_{(j,i) \in A^E} x_{ji}^E \leq C_{s,i} \quad \forall i \in V^{E, \text{supply}} \quad (5.10)$$

$$\sum_{(i,j) \in A^E} x_{ij}^E - \sum_{(j,i) \in A^E} x_{ji}^E \geq 0 \quad \forall i \in V^{E, \text{transship}} \quad (5.11)$$

$$\sum_{(i,j) \in A^E} x_{ij}^E - \sum_{(j,i) \in A^E} x_{ji}^E \leq C_{t,i} \quad \forall i \in V^{E, \text{transship}} \quad (5.12)$$

$$\sum_{(i,j) \in A^E} x_{ij}^E - \sum_{(j,i) \in A^E} x_{ji}^E = -p_i \quad \forall i \in V^{E, \text{demand}} \quad (5.13)$$

$$0 \leq p_i \leq d_i \quad \forall i \in V^{E, \text{demand}} \quad (5.14)$$

$$0 \leq \sum_{(i,j) \in A^E} x_{ij}^E \leq \delta_i^E C_i y_i^E \quad \forall i \in V^E \quad (5.15)$$

$$0 \leq \sum_{(j,i) \in A^E} x_{ji}^E \leq \delta_i^E C_i^E y_i^E \quad \forall i \in V^E \quad (5.16)$$

$$0 \leq x_{ij}^E \leq \delta_{ij}^E C_{ij}^E y_i^E \quad \forall (i, j) \in A^E, i \in V^E \quad (5.17)$$

$$y_i^E \leq \lambda \delta_i^E \quad \forall i \in V^E \quad (5.18)$$

$$y_{ij}^E \leq \lambda \delta_{ij}^E \quad \forall (i, j) \in A^E \quad (5.19)$$

$$y_{ij}^E \leq y_i^E \quad \forall i \in V^E, (i, j) \in A^E \quad (5.20)$$

$$y_i^E \leq \sum_{(j,i) \in A^E} x_{ji}^E \quad \forall i \in V^{E, \text{transship}} \quad (5.21)$$

$$y_i^E \leq p_i / d_i \quad \forall i \in V^{E, \text{demand}} \quad (5.22)$$

$$x_{ij}^E \in \mathbb{Z}, y_{ij}^E \in \{0, 1\}, 0 \leq \delta_{ij}^E \leq 1 \quad \forall (i, j) \in A^E \quad (5.23)$$

$$y_i^E \in \{0, 1\}, 0 \leq \delta_i^E \leq 1 \quad \forall i \in V^E \quad (5.24)$$

where y_i^E and y_{ij}^E denote the functional states of node i and link (i, j) , respectively (functional: $y_i^E = 1, y_{ij}^E = 1$; failed: $y_i^E = 0, y_{ij}^E = 0$); x_{ij}^E denotes the flow on link (i, j) ; δ_i^E and δ_{ij}^E denote the experiencing functionality levels for node i and link (i, j) , respectively, and the original functionality levels in intact EPN are 1 (i.e., $\delta_i^{E,0} = 1$ and $\delta_{ij}^{E,0} = 1$); $C_{s,i}$ and $C_{t,i}$ are the supply flow capacity and the transshipment flow capacity of node i , respectively; C_i^E and C_{ij}^E are the total flow capacities of node i and link (i, j) , respectively; p_i and d_i are the actual supplied and required flows of demand node i .

The objective function of this model (Eq. (5.9)) is to maximize the number of survival components after the disruption. The constraints shown in Eqs. (5.10)–(5.14) regulate the electricity flowing with respect to supply, transshipment, and demand flow levels. The constraints shown in Eqs. (5.15)–(5.17)

ensure that the flows respect the disrupted capacities for both nodes and arcs. The constraints shown in Eqs. (5.18)–(5.22) describe the relationship between the state of components and the flow pattern. The coefficients of λ in Eqs. (5.18) and (5.19) are introduced to handle the partially functional components and are set to 100 here, i.e., when $0 < \delta_i^E < 1$, the component i is not totally disrupted and its functional state y_i^E can still be 1; only when $\delta_i^E = 0$, the component i is totally disrupted and its functional state y_i^E should be 0.

The inputs of this model include the network topology, the flow parameters such as $C_{s,i}$, $C_{t,i}$, C_i^E , C_{ij}^E , and d_i , and the structurally damaged states δ_i^E and δ_{ij}^E . If the data of electricity supply and demand is not available, this model can also be adapted for the connectivity analysis which only depends on the network topology (i.e., $C_{s,i}$, $C_{t,i}$, C_i^E , and C_{ij}^E are set to large constants; d_i equals p_i ; x_{ij}^E , δ_i^E , and δ_{ij}^E are set to be binary, and the constraint Eq. (5.11) is omitted). The same metric in Section 4.2.2 in Chapter 4 characterizing the ratio of the number of functional components to the number of total components is used to evaluate the functionality of the EPN in state $s_E(t)$ (Loggins and Wallace 2015; Ouyang and Dueñas-osorio 2014; Panteli et al. 2017):

$$Q_{\text{survival}}^E = \frac{\sum_{i \in V^E} y_i^E + \sum_{(i,j) \in A^E} y_{ij}^E}{|V^E| + |A^E|} \quad (5.25)$$

where $|\cdot|$ is the cardinality of the set.

5.2.3 Interdependencies between TN and EPN

The same three types of interdependency between TN and EPN as described in Section 4.2.3 in Chapter 4 are considered:

- (1) Type I: The function of traffic lights at signalized intersections in TN depends on the electricity supply of EPN;
- (2) Type II: The function of some roadway links in TN depends on whether the fallen towers or poles along the roadways in EPN will block the roadways;
- (3) Type III: The accessibility to damaged sites in EPN depends on the function of TN.

Type I interdependency denotes the relationship mapping from nodes in EPN to nodes of signalized intersections in TN, which can be expressed as the following equation:

$$y_i^T = y_j^E \quad \forall (i, j) \in F_V(T, E) \quad (5.26)$$

where node $i \in V_{\text{signalized}}^T$ is the signalized intersection in TN, and node $j \in V^E$ in EPN directly supplies electricity to node i , and $F_V(T, E)$ is the set of all such node pairs (i, j) .

Type II interdependency denotes the relationship mapping from the nodes and links in EPN to the links in TN. The towers or poles, which are the nodes or lie on the links of EPN, may be knocked down and therefore disrupt the traffic of nearby roadways in TN. The remaining capacity of roadways after disruption is denoted using $\delta_{ij}^{T,d}$:

$$\delta_{ij}^{T,d} = f_{\text{block}}(r_{ij}) \quad \forall ((i, j), r_{ij}) \in F_{VA}(T, E) \quad (5.27)$$

where $f_{\text{block}}(\cdot)$ is the function mapping the potential blockages caused by the damaged components of EPN to the TN's state; $(i, j) \in A^T$ and r_{ij} is the corresponding set of nodes and links of EPN affecting link (i, j) of TN, which is determined based on the geographical proximity; and $F_{VA}(T, E)$ denotes the set of all such

component pairs $((i,j), r_{ij})$.

Type III interdependency mainly impact the repair actions on the EPN after the disruption occurs. It is assumed that the repair resources, also referred to as repair teams here, are located at some depot nodes of TN before disruption. After disruption, the repair teams will utilize the roadways in TN to access the damaged components to perform repair activities (e.g., removal of fallen towers and poles from roadways and restoration of the distribution lines). If the locations of damaged components are accessible (i.e., at least one path exists for the repair teams to reach the location), all repair actions are assumed to be completed instantaneously (Fotouhi et al. 2017). Otherwise, the damaged components cannot be restored.

5.3 Problem formulation and solution procedure

With the network representations, the functionality metrics, and the interdependencies introduced above, the bi-level, stochastic optimization problem of prioritizing mitigation and repair actions under budgetary constraints can be formulated. The definition of resilience adopted in this study is adapted from (Chen and Miller-Hooks 2012; Fotouhi et al. 2017; Miller-Hooks et al. 2012; Zhang et al. 2015): the coping capacity of the system considering the effects of pre-disruption mitigation and the post-disruption repair actions, which can be measured as the ratio of the post-disruption system functionality to the pre-disruption one. The objective is to maximize the expected resilience improvement RI of this interdependent traffic-electric power system, in terms of the increase of the functionality, over all selected disrupted scenarios:

$$\text{maximize } RI = E\left[\phi \cdot \frac{Q^T - Q_d^T}{Q_0^T - Q_d^T} + (1 - \phi) \cdot \frac{Q^E - Q_d^E}{Q_0^E - Q_d^E}\right] \quad (5.28)$$

where $E[\cdot]$ is the mean operator; Q^T and Q^E are the functionality levels of TN and EPN after disruption

with mitigation or repair actions, respectively; Q_d^T and Q_d^E are the functionality levels of TN and EPN after disruption without taking mitigation or repair actions, respectively; Q_0^T and Q_0^E are the functionality levels of intact TN and EPN before disruption, respectively; $(Q^T - Q_d^T)/(Q_0^T - Q_d^T)$ and $(Q^E - Q_d^E)/(Q_0^E - Q_d^E)$ are the normalized functionality improvements of TN and EPN after taking mitigation or repair actions, respectively; ϕ and $1-\phi$ are weight coefficients for the resilience improvements of TN and EPN, respectively. The value of ϕ , which is referred to as the preference parameter here, can be adaptively set depending on which system is deemed more important and should be assigned more mitigation or repair resources under a particular situation in the view and judgment of the decision makers.

The upper level of this problem is to find an optimal plan of allocating limited mitigation or repair resources to vulnerable components. In this study, the mitigation resources here refer to the following pre-disaster actions: (1) hardening the distribution poles or towers, which can protect nodes and links of the EPN; (2) pre-installing battery backup systems for the traffic signals in TN. The repair resources refer to the following post-disaster actions: (1) repairing the distribution poles or towers; (2) restoring affected roadway capacity by removing fallen poles and towers. It is noted that considering the detailed process of mitigation and repair actions can be challenging since it involves coordinating and dispatching many different resources, such as crews, equipment, and materials, this study simplifies this process by assuming that these mitigation and repair actions are only under limited budgetary constraints (i.e., transforming all types of available resources into the equivalent monetary values) (Fang and Sansavini 2019; Fotouhi et al. 2017; Romero et al. 2015; Zhang and Wang 2017). These actions can affect the states of components directly or through interdependencies, which are expressed using following constraints:

Under mitigation actions with decision variable ξ_i^{CIS} :

$$\delta_i^{\text{E}} = \xi_i^{\text{E}} \delta_i^{\text{E},0} + (1 - \xi_i^{\text{E}}) \delta_i^{\text{E},\text{d}} \quad \forall i \in V^{\text{E},\text{vul}} \cup A^{\text{E},\text{vul}} \quad (5.29)$$

$$y_i^{\text{T}} = \xi_i^{\text{T}} + (1 - \xi_i^{\text{T}}) y_j^{\text{E}} \quad \forall i \in V_{\text{signalized}}^{\text{T},\text{vul}}, (i, j) \in F_V(\text{T}, \text{E}) \quad (5.30)$$

$$\delta_{ij}^{\text{T}} = \left(\prod_{k \in r_{ij}} \xi_k^{\text{E}} \right) \delta_{ij}^{\text{T},0} + \left(1 - \prod_{k \in r_{ij}} \xi_k^{\text{E}} \right) \delta_{ij}^{\text{T},\text{d}} \quad \forall (i, j) \in A^{\text{T},\text{vul}}, ((i, j), r_{ij}) \in F_{VA}(\text{T}, \text{E}) \quad (5.31)$$

$$\sum_{i \in V^{\text{E},\text{vul}} \cup A^{\text{E},\text{vul}}} c_i^{\text{E},\text{m}} \xi_i^{\text{E}} + \sum_{i \in V_{\text{signalized}}^{\text{T},\text{vul}}} c_i^{\text{T},\text{m}} \xi_i^{\text{T}} \leq B \quad (5.32)$$

$$\xi_i^{\text{CIS}} \in \{0, 1\} \quad \forall i \in V^{\text{E},\text{vul}} \cup A^{\text{E},\text{vul}} \cup V_{\text{signalized}}^{\text{T},\text{vul}} \quad (5.33)$$

Under repair actions with decision variable η_i^{CIS} :

$$\delta_i^{\text{E}} = \eta_i^{\text{E}} (\delta_i^{\text{E},0} \Lambda_i + \delta_i^{\text{E},\text{d}} (1 - \Lambda_i)) + (1 - \eta_i^{\text{E}}) \delta_i^{\text{E},\text{d}} \quad \forall i \in V^{\text{E},\text{vul}} \cup A^{\text{E},\text{vul}} \quad (5.34)$$

$$\delta_{ij}^{\text{T}} = \eta_{ij}^{\text{T}} (\delta_{ij}^{\text{T},0} \Lambda_{ij} + \delta_{ij}^{\text{T},\text{d}} (1 - \Lambda_{ij})) + (1 - \eta_{ij}^{\text{T}}) \delta_{ij}^{\text{T},\text{d}} \quad \forall (i, j) \in A^{\text{T},\text{vul}}, ((i, j), r_{ij}) \in F_{VA}(\text{T}, \text{E}) \quad (5.35)$$

$$\sum_{i \in V^{\text{E},\text{vul}} \cup A^{\text{E},\text{vul}}} c_i^{\text{E},\text{r}} \eta_i^{\text{E}} + \sum_{i \in A^{\text{T},\text{vul}}} c_i^{\text{T},\text{r}} \eta_i^{\text{T}} \leq B \quad (5.36)$$

$$\eta_i^{\text{CIS}} \in \{0, 1\} \quad \forall i \in V^{\text{E},\text{vul}} \cup A^{\text{E},\text{vul}} \cup A^{\text{T},\text{vul}} \quad (5.37)$$

where the superscripts of CIS can be T or E, indicating TN or EPN, respectively; the superscript vul represents the set of vulnerable components, which are disrupted in at least one considered scenario; the superscripts m and r in Eqs. (5.32) and (5.36) denote mitigation and repair actions, respectively; ξ_i^{CIS} and η_i^{CIS} are binary decision variables indicating whether mitigation and repair actions are assigned to the

vulnerable component i , respectively; $\delta_i^{\text{CIS},0}$ and $\delta_i^{\text{CIS},d}$ are the original and disrupted functionality levels of component i without mitigation or repair actions, respectively; Λ_i (or Λ_{ij}) in Eqs. (5.34) and (5.35) is a binary variable indicating the accessibility for repair teams to reach component i (accessible: $\Lambda_i = 1$; inaccessible: $\Lambda_i = 0$); $c_i^{\text{CIS},m}$ and $c_i^{\text{CIS},r}$ in Eqs. (5.32) and (5.36) are costs for mitigation and repair actions on component i , respectively; B in Eqs. (5.32) and (5.36) is the total available budget for mitigation or repair actions.

Finding optimal mitigation and repair resources allocation plans are treated as two separate problems to investigate their different impacts on the resilience improvement. For mitigation actions, Eq. (5.29) indicates that the components in the EPN can be directly protected by the pre-disaster hardening; Eq. (5.30) modifies the original dependency of the traffic signals on the EPN in Eq. (5.26) due to installation of the backup battery systems; Eq. (5.31) represents that hardening relevant nodes and links of the EPN can prevent the blockages on the roadways, which are assumed to only arise from the fallen poles and towers, and the reason of using product notation is that there are many possible poles or towers affecting the same roadway, and unless they are all hardened, the possibility of blockage remains; Eq. (5.32) stipulates that the costs of feasible mitigation shall not exceed the available budget.

Compared to the pre-disaster mitigation actions, the main difference of the post-disaster repair actions is the need to account for the aforementioned Type III interdependency. Eqs. (5.34) and (5.35) states that disrupted component i can be repaired and return to original functionality level only if the decision maker allocates the repair resource to it ($\eta_i^{\text{CIS}} = 1$) and the disruption location is accessible ($\Lambda_i = 1$); otherwise, the component i remains as disrupted.

Therefore, by introducing these constraints above, the effects of feasible mitigation and repair actions

on the states of components in the coupled system are determined. The lower level of this optimization problem is to evaluate the functionality levels of the TN and EPN in Eqs. (5.8) and (5.25), as well as the resilience improvement in Eq. (5.28) under given mitigation and repair actions using the corresponding network analysis. It should be noted that the DTA model for the TN and the network analysis model in Eqs. (5.9)–(5.24) for the EPN are both optimization problems. Such optimization problems can also be viewed as the adaptability of the coupled system (one important property of the system resilience (Fotouhi et al. 2017; Hosseini et al. 2016)), i.e., the travelers on the TN and the power flows on the EPN both seeking alternative routes to adapt to the changing environment. To account for uncertainties, disrupted scenarios, traffic demand (q^{od}), and costs of mitigation and repair actions ($c_i^{E,m}$, $c_i^{T,m}$, $c_i^{E,r}$, and $c_i^{T,r}$) are modeled as random variables in the optimization problems.

The bi-level binary optimization problems are highly nonlinear involving extensive simulation due to DTA model used and the interdependencies between TN and EPN. Therefore, the exact methods, e.g., branch and bound, are very difficult to be implemented and would be computationally expensive, which may only be limited to small problem instances. So the metaheuristic methods are often adopted to obtain the approximate optimal solution, such as genetic algorithm (Bocchini and Frangopol 2013), simulated annealing (Vugrin et al. 2014), and ranking-based approach (Romero et al. 2015). Among them, the binary particle swarm optimization (BPSO), as the binary version of the traditional particle swarm optimization method, has been found suitable to solve discrete optimization problem with superior performance than the genetic algorithm in several studies (Chiu et al. 2012; Elbeltagi et al. 2005; Panda and Padhy 2008) and therefore is adopted in the present study.

In the original BPSO procedure, the position of a particle represents a solution, which is expressed as

a vector containing binary decision variables (i.e., ξ_i^{CIS} and η_i^{CIS}); all possible positions of particles denote the feasible solution space (i.e., governed by the budgetary constraint); the positions of particles are first randomly initialized and then iteratively updated to find new solutions with better fitness values (i.e., larger resilience improvement) based on the BPSO mathematical formulation (Kennedy and Eberhart 1997). The uncertainties in disrupted scenarios, such as traffic demand (q^{od}), and costs of mitigation and repair actions ($c_i^{\text{E,m}}$, $c_i^{\text{T,m}}$, $c_i^{\text{E,r}}$, and $c_i^{\text{T,r}}$), can be considered by employing simple Monte Carlo simulation to generate samples or other advanced sampling methods to construct a reduced number of representative samples (Chang et al. 2000; Romero et al. 2015).

In addition, this study uses a knapsack-based heuristic (Barker et al. 2013; Romero et al. 2015) in the initialization stage of the BPSO in order to accelerate the convergence and also for comparison. The main idea is to obtain the following importance measure IM_i for each component i :

$$IM_i = \phi \cdot \frac{Q_0^{\text{T}} - Q_d^{\text{T}}(i)}{Q_0^{\text{T}}} + (1 - \phi) \cdot \frac{Q_0^{\text{E}} - Q_d^{\text{E}}(i)}{Q_0^{\text{E}}} \quad \forall i \in V_{\text{signalized}}^{\text{T,vul}} \cup A^{\text{T,vul}} \cup V^{\text{E,vul}} \cup A^{\text{E,vul}} \quad (5.38)$$

where $Q_d^{\text{T}}(i)$ and $Q_d^{\text{E}}(i)$ denote the functionality levels of TN and EPN after only removing component i , or changing the signalized intersection to a unsignalized one, respectively; $Q_0^{\text{T}} - Q_d^{\text{T}}(i)$ and $Q_0^{\text{E}} - Q_d^{\text{E}}(i)$ are the functionality losses of TN and EPN after only component i fails, respectively; $(Q_0^{\text{T}} - Q_d^{\text{T}}(i)) / Q_0^{\text{T}}$ and $(Q_0^{\text{E}} - Q_d^{\text{E}}(i)) / Q_0^{\text{E}}$ are the normalized functionality losses of TN and EPN after only component i fails, respectively, and both are within the range $[0,1]$. It is noted that the failure of component in one system may also affect the other system due to the interdependencies. The importance measure IM_i represents the importance of component i of the interdependent system under the given value of preference parameter ϕ .

Under a chosen ϕ , IM_i reflects the impact of failed component i on the functionality of the interdependent system. The larger IM_i is, the more important the component i is to the functionality of the system. So IM_i can also provide guidance on selecting which components for mitigation and repair actions. Specifically, under the budgetary constraints, the plan of allocating mitigation and repair resources to the vulnerable components is determined based on the ranking of their IM_i values (in descending order) and costs (in ascending order). And the allocation plan is provided as an initial solution in the BPSO for further possible improvement and the whole solution procedure is summarized in Figure 5.1.

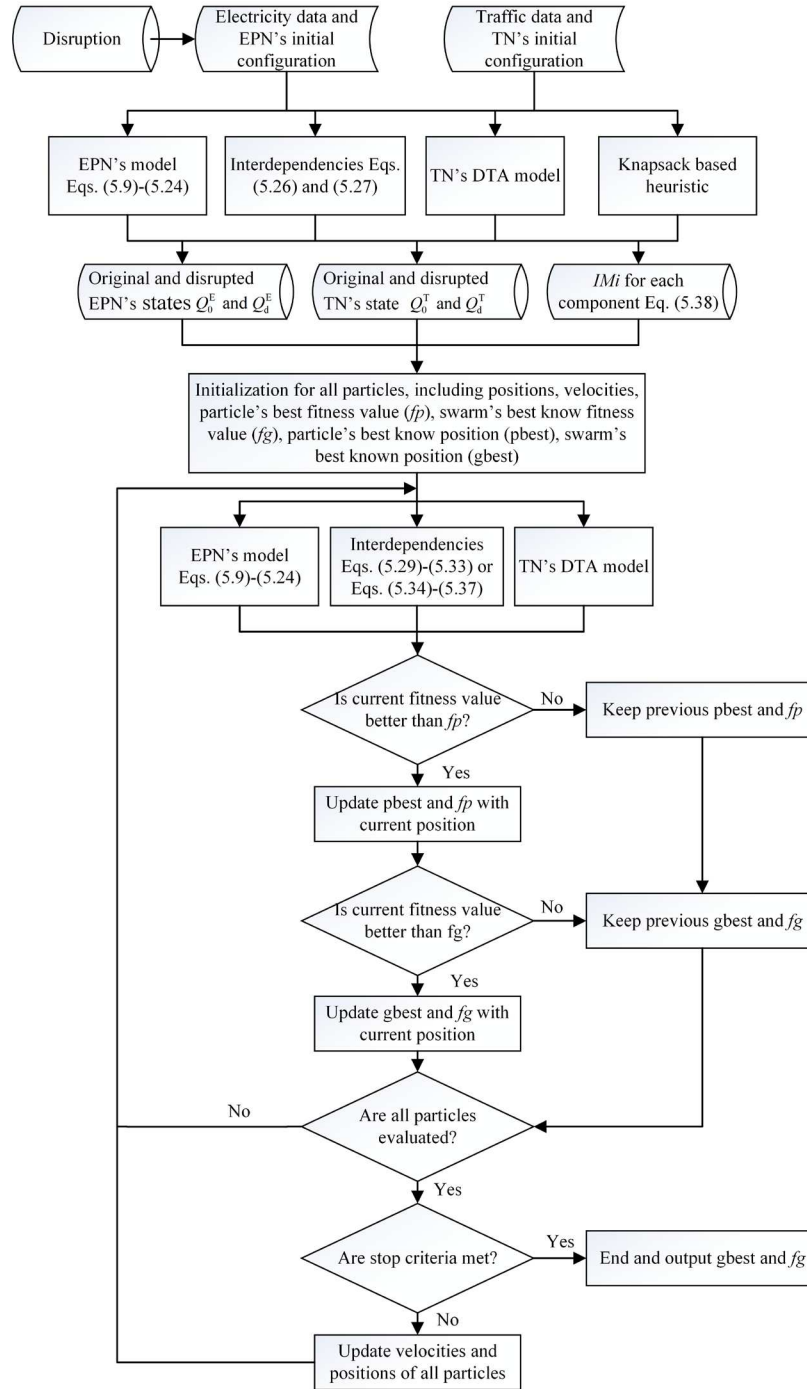


Figure 5.1 Flowchart of the solution procedure (fp and fg are the resilience improvement)

5.4 Illustrative example

A portion of real-world traffic-electric power system in Galveston, Texas is used here to demonstrate the proposed methodology. Figure 5.2 depicts this chosen area and Figure 5.3 shows the TN and EPN. The

TN has 16 nodes and 44 links and the EPN has 62 nodes and 70 links. The links of TN only include main and minor streets and the nodes are all signalized intersections (Table 5.1). The period of interest for simulating traffic dynamics in the DTA model is set to 2 hours and the repair team is located at node 3. Table 5.2 gives the assumed total traffic demands for O-D pairs, which are all assumed to follow the normal distribution. Table 5.3 lists the time-varying demand profile for all O-D pairs, which are used to construct time-dependent O-D demand matrices as inputs for the DTA model. Values of other parameters in the DTA model are summarized in Table 5.4. Detailed configuration of the EPN is usually classified and not open to the public due to security reasons. The construction of the EPN here mostly relies on the observation in Google Street View, assumptions and the connectivity criteria of EPN model as defined in Eqs. (5.9)–(5.24) are used. Since the EPN at the distribution level usually has a radial topology, the only one substation found in this area (see Figure 5.3) is assumed to supply electric power for all other nodes. The distribution lines are all supported by wooden poles. The traffic lights at the signalized intersections are assumed to be powered by the closest pole, which are used to construct the set $F_V(T, E)$ in Eq. (5.26). The roadways can be affected by all the roadside fallen poles, as represented by the set $F_{VA}(T, E)$ in Eq. (5.27).

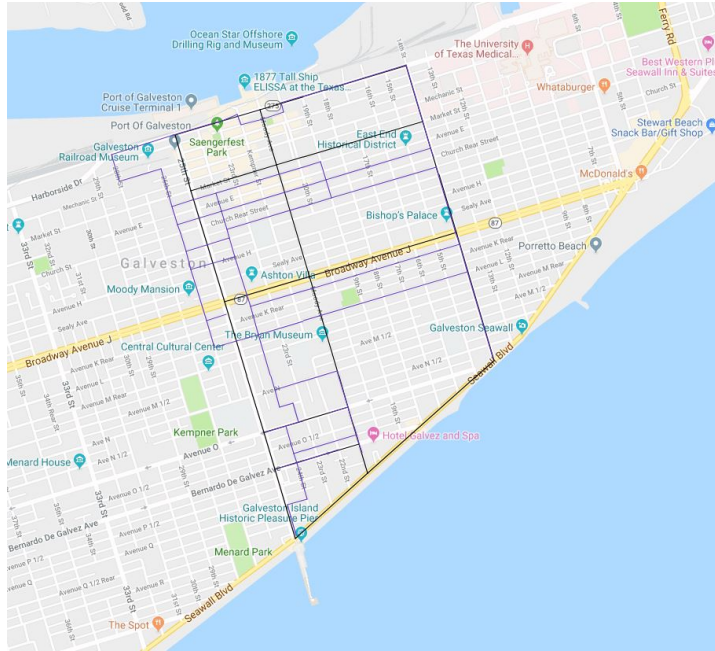


Figure 5.2 The chosen area of Galveston, Texas (from Google Maps)

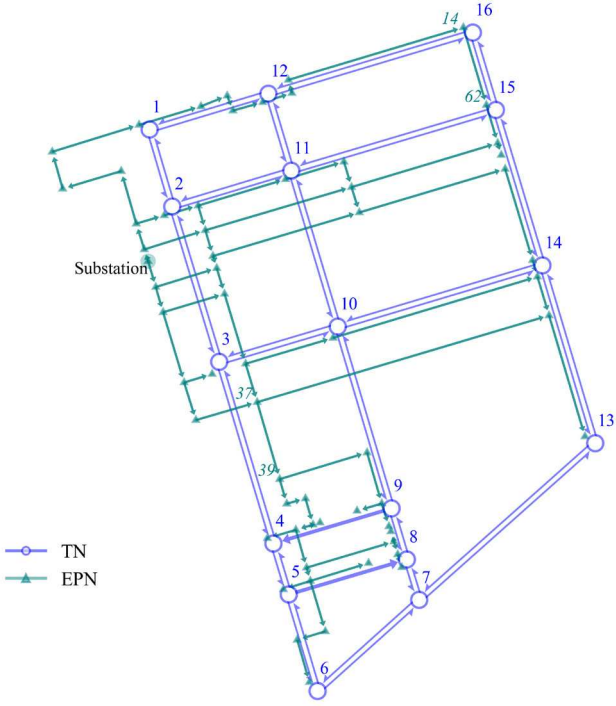


Figure 5.3 The interdependent traffic-electric power system

Table 5.1 Link attributes of the transportation network

Link	Number of lanes	Length l_{ij} (m)	Free flow speed v_{ij}^0 (km/h (mph))	Capacity C_{ij}^0 (vehicles/h)
(1, 2) and (2, 1)	2	304.91	48.28 (30)	3600
(2, 3) and (3, 2)	2	616.05	48.28 (30)	3600
(3, 4) and (4, 3)	2	720.14	48.28 (30)	3600
(4, 5) and (5, 4)	2	202.10	48.28 (30)	3600
(5, 6) and (6, 5)	2	382.56	48.28 (30)	3600
(6, 7) and (7, 6)	2	518.05	56.33 (35)	3600
(7, 8) and (8, 7)	1	160.36	48.28 (30)	1800
(8, 9) and (9, 8)	1	202.45	48.28 (30)	1800
(9, 10) and (10, 9)	1	720.12	48.28 (30)	1800
(10, 11) and (11, 10)	1	617.59	48.28 (30)	1800
(11, 12) and (12, 11)	1	304.95	48.28 (30)	1800
(13, 14) and (14, 13)	1	704.28	48.28 (30)	1800
(14, 15) and (15, 14)	1	616.22	48.28 (30)	1800
(15, 16) and (16, 15)	1	306.59	48.28 (30)	1800
(1, 12) and (12, 1)	2	470.46	56.33 (35)	3600
(12, 16) and (16, 12)	2	809.31	56.33 (35)	3600
(2, 11) and (11, 2)	1	471.55	48.28 (30)	1800
(11, 15) and (15, 11)	1	809.37	48.28 (30)	1800
(3, 10) and (10, 3)	3	469.00	56.33 (35)	5400
(10, 14) and (14, 10)	3	810.36	56.33 (35)	5400
(7, 13) and (13, 7)	2	894.44	56.33 (35)	3600
(9, 4)	2	467.60	48.28 (30)	3600
(5, 8)	2	466.97	48.28 (30)	3600

Table 5.2 Statistics of random variables used in the example (all assumed to follow the normal distribution)

Parameter	Mean	Coefficient of variance (COV)	Reference
Traffic demand of O-D pair (1, 13)	600	0.05	–
Traffic demand of O-D pair (13, 1)	800	0.05	–
Traffic demand of O-D pair (6, 16)	800	0.05	–
Traffic demand of O-D pair (16, 6)	600	0.05	–
Cost of hardening a pole, $c_i^{E,m}$ (US Dollar)	718	0.1	–
Cost of installing a backup battery system, $c_i^{T,m}$ (US Dollar)	3250	0.05	(Wallace et al. 2009)

Cost of repairing a pole, $c_i^{E,r}$ (US Dollar)	1435	0.1	(Unnikrishnan and van de Lindt 2016)
Cost of removing a fallen pole (US Dollar)	100	0.1	–

Table 5.3 Time-varying demand profile for all O-D pairs (Sbayti et al. 2007)

Time interval (min)	Ratio of number of departed vehicles to O-D demand (%)
[0, 15]	8
[15, 30]	10
[30, 45]	16
[45, 60]	21
[60, 75]	18
[75, 90]	13
[90, 105]	10
[105, 120]	4

Table 5.4 Values of parameters for the DTA model

Parameter	Value
Jam density, k_{ij}^{jam}	75 vehicles/km/lane
Minimum speed, v_{ij}^{min}	16.09 km/h (10 mph)
Green time / Cycle length, $Green_j / Cycle_j$	0.5
Stop delay, τ_{stop}	7 s
Saturation flow, $C_{ij}^{saturation}$	1800 vehicles/h/lane
α	1.6
β	0.5
Simulation time interval, Δt	0.1 min
The length of period of interest, $M\Delta t$	120 min

To generate disrupted scenarios, hurricane hazard is taken for example here and the whole area is assumed to be under the same wind speed of 195 km/h with same wind direction, which corresponds to category 3 hurricane wind based on the Saffir-Simpson hurricane wind scale. The structural damages on

wooden poles are simulated using the fragility functions (Ouyang and Dueñas-osorio 2014; Salman et al. 2015). Specifically, given the experienced wind speed, the failure probability $p_f = 0.597$ (Salman et al. 2015) is compared with a uniformly distributed random variable $\varphi \in [0, 1]$: the pole is assumed to fail completely if $\varphi \leq p_f$ and experience no damage otherwise. And the functionality level of each EPN's component δ_i^E is assumed to be either 0 or 1. When the poles happen to be the nodes in the EPN, the corresponding δ_i^E are assigned with 0 or 1; when the poles lie on the links of EPN, the failure probabilities of poles are assumed to be independent. The link is assumed to be out of service ($\delta_{ij}^E = 0$) if no fewer than two poles fail, otherwise operate normally ($\delta_{ij}^E = 1$) (Salman et al. 2015). The blocking effects $f_{\text{block}}(\cdot)$ on the traffic flow caused by the fallen poles are simplified by assuming probabilities of different levels of capacity reduction on the traffic considering the number of lanes, the distance from the pole to the roadway, and the typical height of the pole, as shown in Table 5.5 (Smith et al. 2003).

Table 5.5 Probabilities and ratios of remaining capacity for the roadways blocked by fallen poles

Number of lanes	Ratio of remaining capacity δ_{ij}^T	Probability
1	1	0.33
	0.25	0.33
	0	0.33
2	1	0.33
	0.81	0.33
	0.35	0.33
3	1	0.33
	0.83	0.33
	0.5	0.33

The post-disaster traffic demand is assumed to be the same as the pre-disaster level. It is noted that the data on the change of traffic demand after hazards is often very hard to be collected, and the post-disaster traffic demand is assumed to be the same as the pre-disaster level in this study. In reality, the hazard may

considerably change the traffic demand because the infrastructures essential for some social and economic activities may be damaged and therefore some post-hazard activities can be either reduced or relocated to other places. As a result, travelers may alter their travel plans, such as canceling their trips and changing destinations. Furthermore, as the infrastructures recover and the everyday activities return to normality gradually, the post-hazard traffic demand can also evolve correspondingly (Alipour and Shafei 2016; Kilanitis and Sextos 2019).

However, predicting the post-hazard traffic demand and its evolution during recovery stage is very complicated and challenging because many uncertain socio-economic and behavioral aspects are involved and thus remains as a common challenge in transportation resilience research (Chang et al. 2012a; Khademi et al. 2015). Researchers on the effect of the earthquake on the TN typically propose to use the modified pre-earthquake traffic demand by applying trip reduction factors to the original-destination matrix to approximate the post-earthquake traffic demand (Alipour and Shafei 2016; Bocchini and Frangopol 2011; Guo et al. 2017). But estimating the trip reduction factors still requires related data and socio-economic analysis. Since the data for the post-hurricane traffic demand change is lacking and the socio-economic analysis can introduce additional level of uncertainty, this study does not explicitly address this issue, but rather adopts the same traffic demands for both before and after the hurricane. Similar procedures can also be found in literature (Bocchini and Frangopol 2011, 2012; Guo et al. 2017). It is noted that the proposed framework can accommodate the updated post-hurricane traffic demand once such data is available.

It should be noted that this simplified example is only for demonstration purpose and more detailed simulation methods and field data can be incorporated to refine the quantification of the disruptions to the networks, e.g., using the simulation tool such as HAZUS-MH 4.0 to generate more realistic hurricane

scenarios, performing detailed structural and statistical analyses to investigate the blocking effects of fallen poles, and calibrating the parameters of the DTA model with collected traffic data. The statistics of the costs of mitigation and repair actions are reported in Table 5.2. The cost of hardening and repairing the distribution line (i.e., $c_{ij}^{E,m}$ and $c_{ij}^{E,r}$) and the cost of cleaning the roadway (i.e., $c_{ij}^{T,r}$) all depend on the number of the related poles since only poles are deemed vulnerable components of the EPN.

To evaluate all possible disrupted scenarios under natural hazards such as earthquakes and hurricanes is often impractical and computationally expensive, some researchers developed a methodology to select a small set of realistic hazard cases associated with corresponding hazard-consistent probabilities to approximate all the cases (Chang et al. 2000; Romero et al. 2015). Since this study aims to propose and test the decision model to prioritize mitigation and repair actions, the application of scenario selection methodology is beyond the scope. In the present study, the Monte Carlo simulation regarding the random variables above is adopted here to generate 50 samples as the representative cases with equal occurrence probability to be used in the optimization process. For each case, the BPSO is applied, in which the number of particles is 16, the Von Neumann topology is used, the coefficients of the update functions (i.e., w , c_1 , and c_2) are set to 0.689343, 1.42694, and 1.42694, respectively (Lee et al. 2008), and the maximum iteration is 50. An additional stop criterion is also implemented which terminates the search when the objective value is not improved for 5 consecutive iterations.

5.4.1 Solutions of the decision model

A typical disrupted scenario without mitigation and repair actions is depicted in Figure 5.4(a). It can be seen that due to the high failure probability of the pole under the given wind speed and the radial topology of the EPN, most components of the EPN, except small parts near the substation, are not functional.

Moreover, the Type I and II interdependencies propagate the disruptions to the TN: traffic lights at all signalized intersections experience the power outage and the roadways, along which the poles are located, experience capacity reductions. The average relative functionality decreases for the EPN $E[(1 - Q_d^E / Q_0^E)]$ is as high as 0.97 while that for the TN $E[(1 - Q_d^T / Q_0^T)]$ is 0.21. The reasons that the TN has much less functionality loss than the EPN include: (1) the hurricane is assumed to damage the EPN directly and only affect the TN through interdependencies; (2) the functionality metric of the TN is based on the total travel time of all travelers instead of the topology as for the EPN. So, the travelers in the DTA model will adapt to the disrupted TN and try to find alternative routes to minimize their travel time.

It should be noted that although the functionality loss of the TN seems small here, the indirect economic loss can be substantial because such indirect loss considering the contribution of socioeconomic factors can accumulate over time until the functionality of the TN is restored (Alipour and Shafei 2016). Figure 5.5(a) and (b) show the iterations during the BPSO in prioritizing mitigation and repair actions for a disrupted scenario, respectively. In most cases, the objective value, i.e., the resilience improvement described in Eq. (5.28), increases gradually with the increase of the number of iterations and becomes stable within 20 iterations, which indicates that convergence of the BPSO for this optimization problem.

Meanwhile, it is found that since the BPSO is initialized with the solutions of the knapsack-based heuristic, which can yield better or even the optimal results at the first iteration compared with the randomly initialized positions of particles, the required iterations to achieve convergence in some cases can be reduced, as shown by the line for $\phi = 1.0$ in Figure 5.5(a) and the line for $\phi = 0.75$ in Figure 5.5(b). Figure 5.6 further compares the quality of the solutions from the BPSO and from the knapsack-based heuristics over all cases. It has been found that the expected resilience improvements obtained from the BPSO are greater

than those from the knapsack-based heuristic, except under large budget levels for mitigation actions when they are almost equal. Therefore, such knapsack-based heuristic can provide a convenient but not necessarily the optimal solution for this problem and can be used as an initialization method to accelerate the convergence of the BPSO.

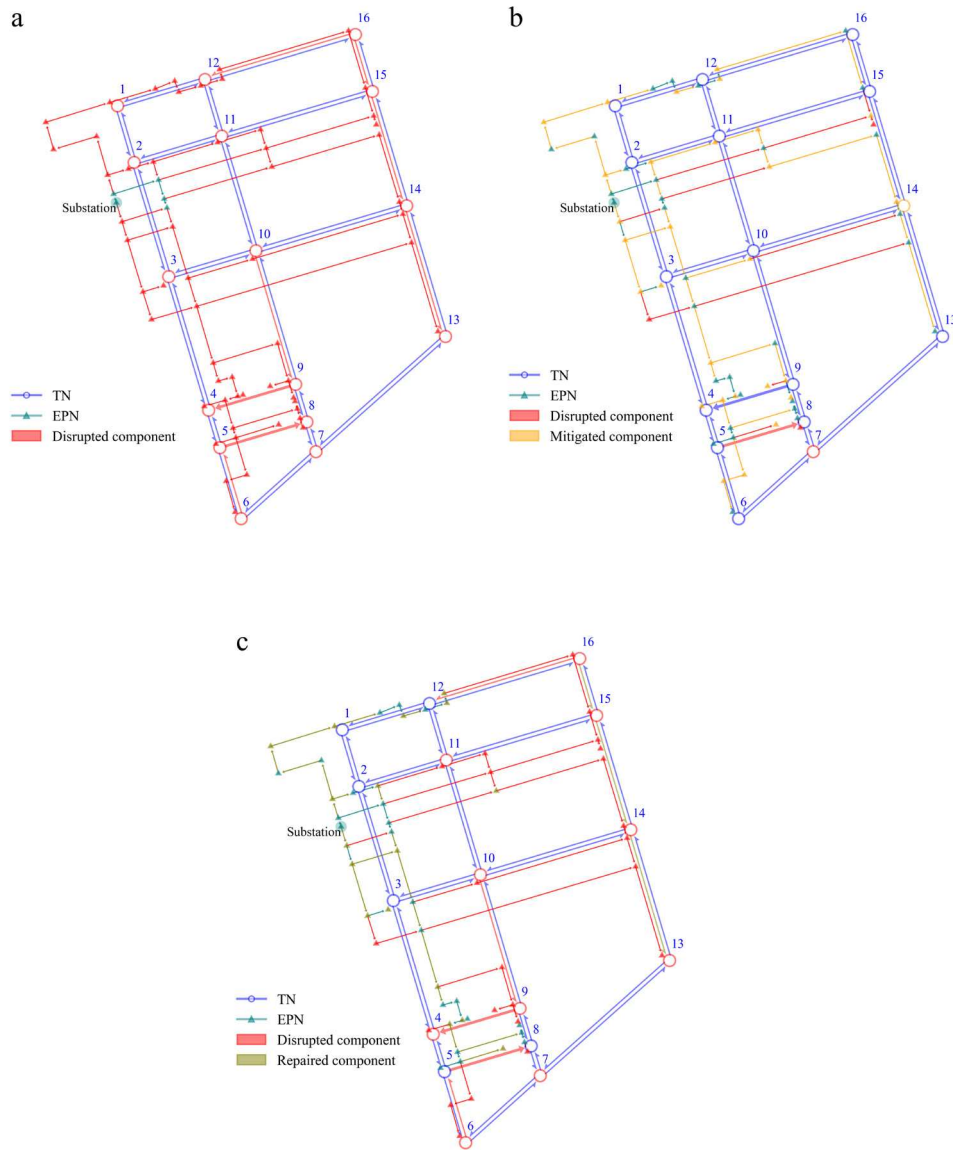


Figure 5.4 A typical case showing the disruption and corresponding mitigation and repair actions ($\Phi = 1$ and $B = \text{US } \$9 \times 10^4$): (a) disrupted; (b) mitigated; (c) repaired

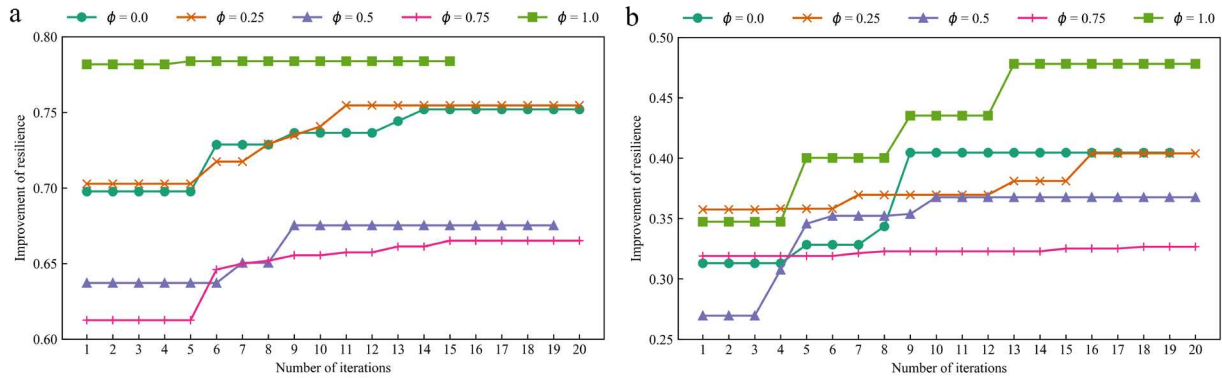


Figure 5.5 Application of the BPSO to prioritizing mitigation and repair actions: (a) mitigation; (b) repair

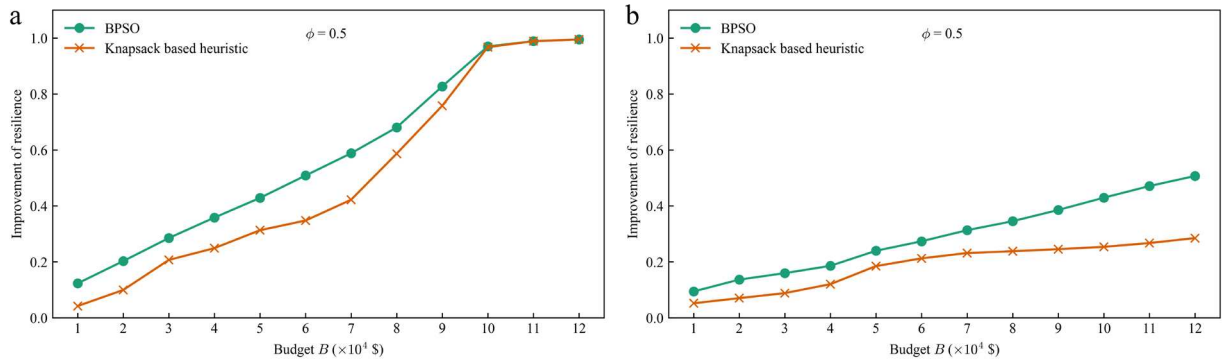


Figure 5.6 Comparison of expected resilience improvement from BPSO and knapsack-based heuristic under mitigation and repair actions: (a) mitigation; (b) repair

The chosen components for mitigation and repair actions for one study case are illustrated in Figure 5.4(b) and (c), respectively. It can be observed that the number of chosen components for mitigation is more than that for repair because the cost for pre-disaster hardening of poles is only half of that of post-disaster repair of damaged poles (see Table 5.2) and the budget level (US 9×10^4) is sufficient to cover the cost for hardening most of the components in the EPN. In addition, the preference parameter ϕ is set to 1.0, indicating that the decision maker chooses improving the resilience of the TN as the priority; with this objective, the solution of the decision model for mitigation covers most distribution lines, which are either along the roadways or include at least one path to the traffic lights, as shown in Figure 5.4(b). As a result, the TN becomes nearly unaffected by the hazard.

As for the repair actions, it should be pointed out that such actions are only carried out after the disaster. Therefore, the blockages induced by the fallen poles on the roadways already exist in the disrupted scenarios through the Type II interdependency, so the actions of repairing damaged distribution lines cannot prevent the blockages, which can only be eliminated by the actions of road debris removal on the TN. As can be seen in Figure 5.4(c), although the budget level is insufficient to repair as many distribution lines following the hazard as would mitigate before the hazard, some signalized intersections in the left part of the network, which are closer to the substation, are still recovered. In contrast, those intersections in the right part of the network remain as unsignalized ones because the longer distance of distribution lines indicates higher repair cost. Meanwhile, several roadway links (16, 15), (15, 14), and (14, 13) in the right part of the network have been identified for debris removal actions in the optimization to achieve the TN-first repair mode ($\phi=1$).

To further investigate the effects of the budget level B and the preference parameter ϕ on the expected resilience improvement, multiple values of budget and preference parameter are tested. Figure 5.7 and Figure 5.8 show the variation of the expected resilience improvement RI under mitigation and repair actions, respectively, where not only the objective, i.e., the weighted sum of resilience improvements of two system, but also resilience improvement of each system, are plotted. It can be observed that for both mitigation and repair actions, the expected resilience improvement shows the overall ascending trend with the increase of the budget level under different ϕ values, which is as expected. Also by comparing Figure 5.7 to Figure 5.8, the RI of the coupled system achieved by the mitigation actions is found larger than that by the repair actions, which is once again due to the lower costs of mitigation costs. As the budget level exceeds a certain level (US $\$1 \times 10^5$ as shown in Figure 5.7), the RI under mitigation actions becomes stable and approaches 1.0, meaning that the budget level is no longer a constraint anymore and has become sufficient to enable

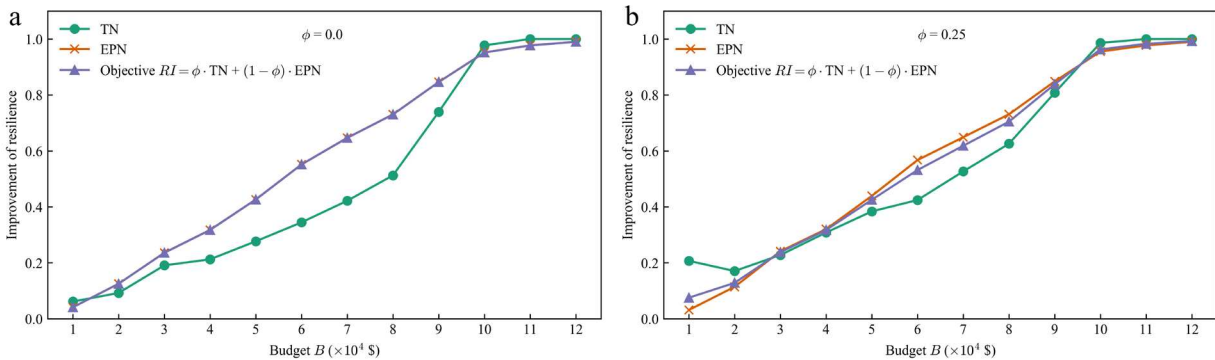
the functionality of the coupled system to be nearly restored to the level of its intact state.

When the pre-hazard mitigation cost is still lower than post-hazard repair cost, the results suggest that well-planned mitigation efforts could provide more cost-effective approaches to improve the coupled system resilience. Effective pre-disaster mitigation planning is very challenging, which depends on rational prediction of the resilience performance and optimization offered by some advanced modeling like the proposed one in this study. It should be pointed out, however, that this does not mean the repair actions are less important than the mitigation actions since it is not always practical to foresee or prevent undesirable consequences using pre-disaster mitigation actions and the post-disaster recovery planning remains to be one of the key approaches in developing more resilient CISs.

Furthermore, although the *RI* of the coupled system goes up when the budget increases, the *RI* of single system does not always increase monotonously and can stagnate (e.g., the *RI* of TN during the budget interval US \$[5×10^4 , 7×10^4] in Figure 5.7(c)) or even decrease (e.g., the *RI* of TN from budget level US $\$1 \times 10^4$ to US $\$2 \times 10^4$ in Figure 5.7(b)). This can be explained by the fact that the objective of the optimization problem is the form of the weighted sum of the *Ris* of two systems and does not guarantee the monotonous increase of the *RI* of single systems. Instead, the two systems can compete for the limited resources and have different levels of contribution to the weighted sum of *Ris*; therefore, when more budget becomes available, one system may ‘sacrifice’ itself, i.e., the *RI* stops growth or even drops, to let the other system use the budget more effectively to achieve the increase of the overall *RI* of the coupled system. On the other hand, the value of ϕ reflects the priority of the TN in the resource allocation. When $\phi = 0.0$, the line denoting the EPN is on top of the line denoting the TN, as shown in Figure 5.7(a) and Figure 5.8(a). When $\phi = 1.0$, the line denoting the TN is on top of the line denoting the EPN, as shown in Figure 5.7(e)

and Figure 5.8(e). As the value of ϕ changes from 0.0 to 1.0, meaning the resource allocation priority changing from the EPN-first to the TN-first gradually, it can be found that the line denoting the TN moves up and the line denoting the EPN goes down, as illustrated in both Figure 5.7(a)–(e) and Figure 5.8(a)–(e), which indicates that this preference parameter ϕ can successfully guide the resource allocation in the optimization to obtain desirable mode of resilience improvement for each system.

In addition, it is interesting to note that since the disruptions to the TN all originate from the EPN through the Type I and II interdependencies, the pre-disaster mitigation actions of hardening the poles in the EPN can also prevent the TN from disruptions. As can be observed in Figure 5.7(e) when $\phi = 1.0$ (TN-first mode), when the budget is less than US $\$8 \times 10^4$, all mitigation actions are applied to the TN and the EPN performance is not improved at all. When the budget exceeds US $\$8 \times 10^4$, part of the mitigation resources is now directed to the EPN and the *RI* of the EPN increases greatly. As a result, the *RI* of the TN also goes up since fewer disruptions are propagated from the hardened EPN.



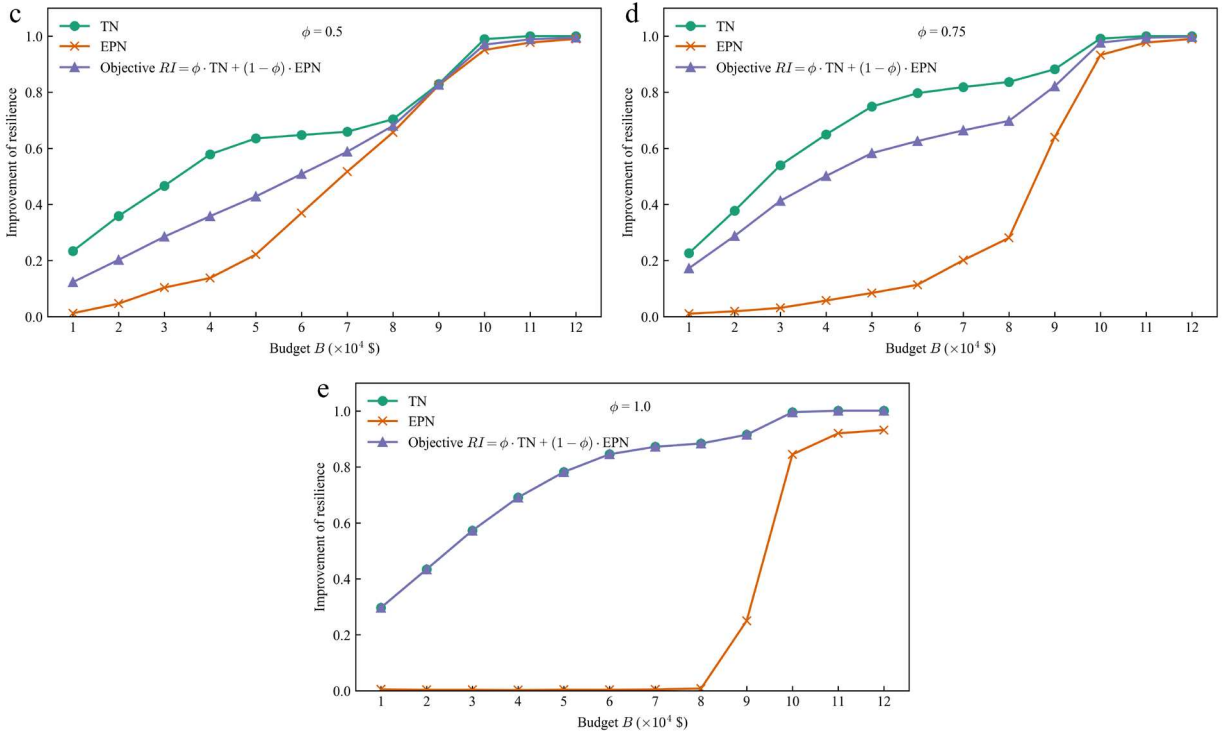
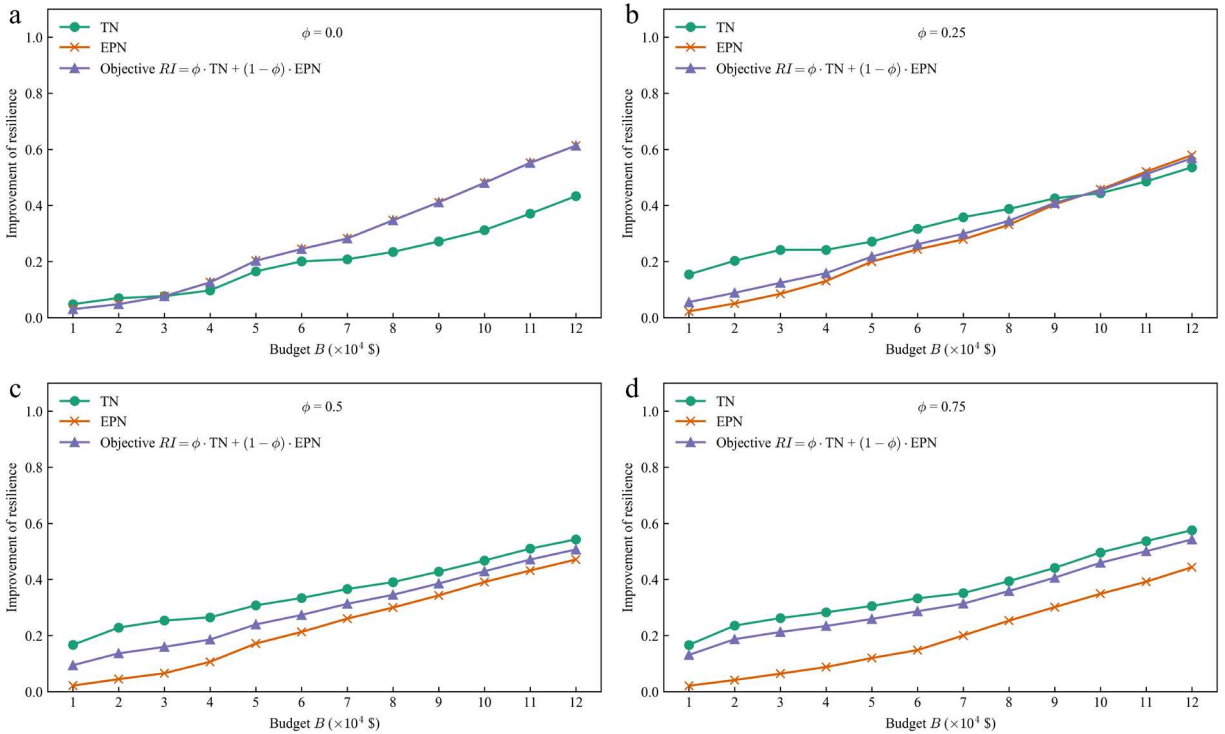


Figure 5.7 The expected resilience improvements of the interdependent system under mitigation actions with different values of budget and preference parameter: (a) $\Phi = 0.0$; (b) $\Phi = 0.25$; (c) $\Phi = 0.5$; (d) $\Phi = 0.75$; (e) $\Phi = 1.0$



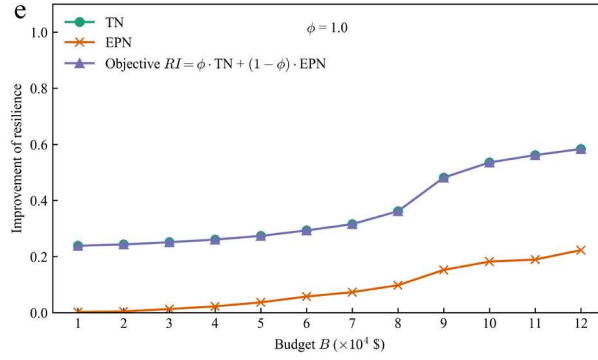


Figure 5.8 The expected resilience improvements of the interdependent system under repair actions with different values of budget and preference parameter: (a) $\Phi = 0.0$; (b) $\Phi = 0.25$; (c) $\Phi = 0.5$; (d) $\Phi = 0.75$; (e) $\Phi = 1.0$

5.4.2 Component priority indices for mitigation and repair actions

Based on the solutions from the proposed optimization model, a type of priority index (PI) at the component level is introduced here to measure the relative importance of each component under mitigation and repair actions to the resilience improvement of the interdependent system. The PI is defined as the likelihood of a component being selected for mitigation or repair actions under given budget level and preference parameter value when the uncertainties in the interdependent system are considered (Zhang and Wang 2017):

$$PI_i^m = \left\{ \frac{\sum_n^N \xi_i^{\text{CIS}} RI_n}{\sum_n^N RI_n} \middle| B, \phi \right\} \quad \forall i \in V^{\text{E,vul}} \cup A^{\text{E,vul}} \cup V_{\text{signalized}}^{\text{T,vul}} \quad (5.39)$$

$$PI_i^r = \left\{ \frac{\sum_n^N \eta_i^{\text{CIS}} RI_n}{\sum_n^N RI_n} \middle| B, \phi \right\} \quad \forall i \in V^{\text{E,vul}} \cup A^{\text{E,vul}} \cup A^{\text{T,vul}} \quad (5.40)$$

where PI_i^m and PI_i^r are the priority indices for mitigation and repair actions, respectively; N is the number

of representative cases; n is the case index; and RI_n is the resilience improvement for case n . It should be pointed out that although both PI_i here and IM_i in Eq. (5.38) for the knapsack-based heuristic can reflect the importance of the single component, the derivations are very different. To obtain the IM_i , the disrupted scenario was based on the disruption of only component i and no optimization on mitigation or repair actions was considered. The PI_i depends on the disrupted scenarios of failure of multiple components, the available budget, and the optimal mitigation and repair actions. In contrast, the solutions from the knapsack-based heuristic are often less optimal than those from the BPSO in calculating the PI_i . So the PI_i can be more effective to measure the contribution of single component to the optimal resilience improvement under the given budget level.

Priority indices for mitigation of two components with different values of budget and preference parameters are demonstrated in Figure 5.9. From Figure 5.3, node 15 in the TN is found to be a signalized intersection which is powered by node 62 of link (14, 62) in the EPN. In addition, link (16, 15) in the TN can also be affected by the fallen poles of link (14, 62) in the EPN. So for the budget level less than US $\$9 \times 10^4$, with the increase of the value of ϕ , the PI values of link (14, 62) in the EPN and node 15 in the TN both increase, suggesting increased likelihood to be selected for mitigation to support the TN-first mitigation resource allocation. For the budget level larger than US $\$9 \times 10^4$, link (14, 62) in the EPN is always selected, which in return reduces the likelihood of node 15 in the TN being selected.

It is noteworthy that the PI value of node 15 in the TN does not always increase when the budget level goes up, as shown in Figure 5.9(b). This shows that the increase of the resilience improvement with the increase of the budget in Figure 5.7 and Figure 5.8 is not simply due to adding more components to the solutions of the lower budget. In the optimization process, the likelihood of some components such as node

15 in the TN being selected can actually decrease when the budget increases because other components may be better options with more budgets to achieve larger resilience improvement of the coupled system.

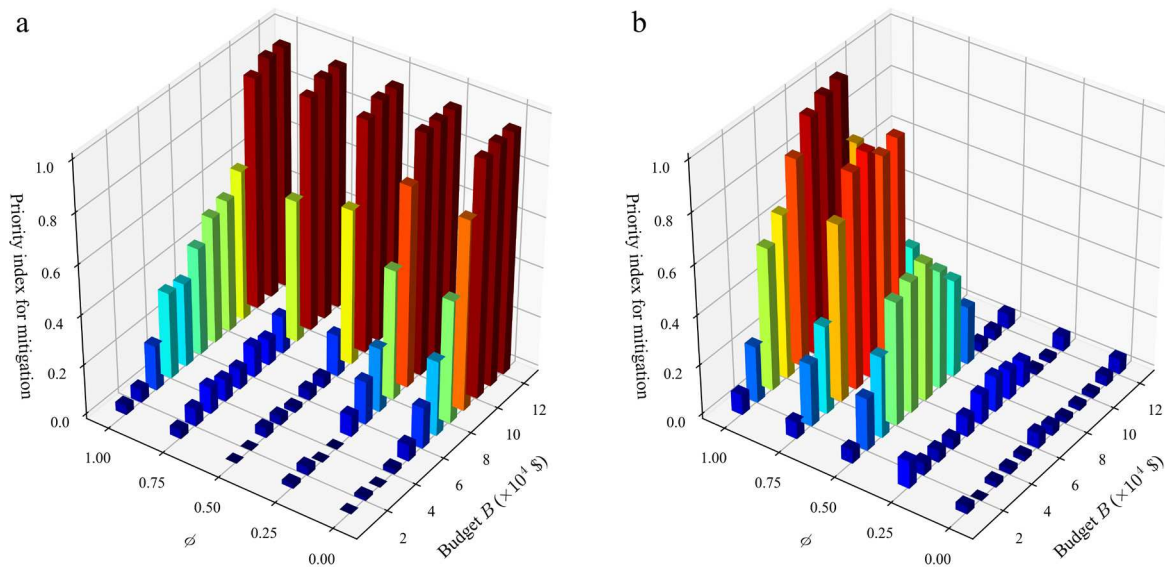


Figure 5.9 Priority indices for mitigation of two components (see Figure 5.3 for locations): (a) link (14, 62) in the EPN; (b) node 15 in the TN

Similarly, Figure 5.10 depicts priority indices for repair of another two components with different values of budget and preference parameters. As shown in Figure 5.3, unlike link (14, 62) in the EPN for the mitigation resource allocation problem, link (37, 39) in the EPN has weaker interdependencies with the TN in the repair resource allocation problem. However, since link (37, 39) is the only distribution line responsible for transmitting electric power to the lower part of the EPN, it has significant contribution to the resilience improvement of the EPN. This is reflected in Figure 5.10(a): the *PI* value decreases when ϕ changes from 0.0 to 1.0. Link (16, 15) in the TN directly starts from the origin (node 16) and can significantly impact the functionality of the TN, so the *PI* value increases with the increase of ϕ in Figure 5.10(b). It is also observed that the *PI* value does not always increase with the increase of the budget level.

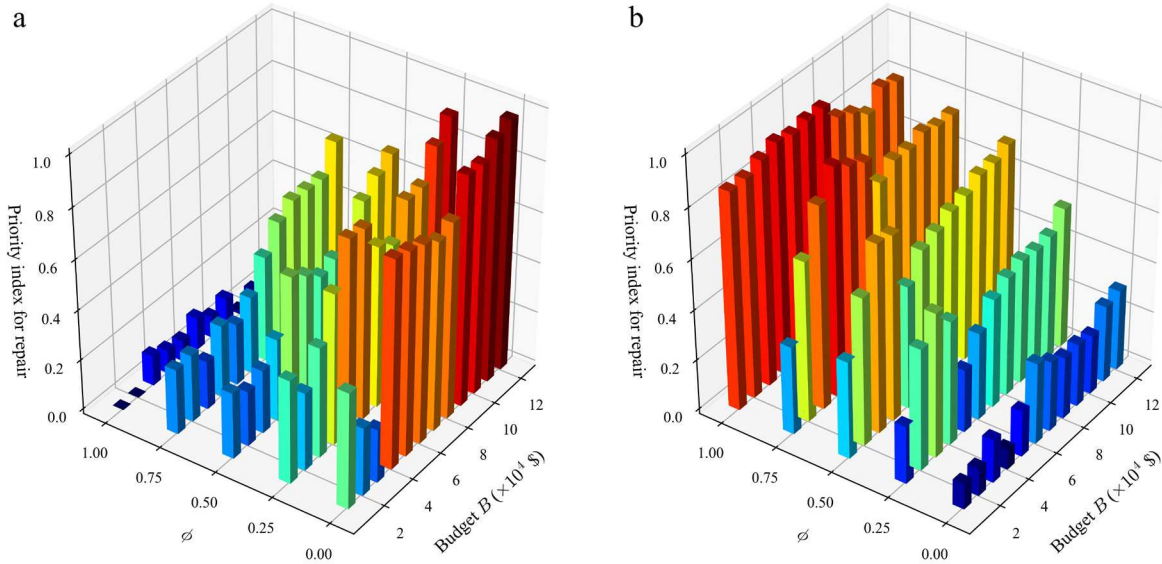


Figure 5.10 Priority indices for repair of two components (see Figure 5.3 for locations): (a) link (37, 39) in the EPN; (b) link (16, 15) in the TN

The solutions from the knapsack-based heuristic are also used to calculate the PI values in order to be compared with the PI values obtained from the BPSO. Figure 5.11 and Figure 5.12 illustrate the ranking results of top 25 components for mitigation actions and repair actions respectively, based on the PI values from the BPSO and the knapsack-based heuristic. For the tick labels of the horizontal axis, E and T denote EPN and TN, respectively, (i, j) denotes the link between node i and j , and single number refers to the node.

It can be seen that the ranking of components for mitigation actions is different from that for repair actions and the PI values from the BPSO and the knapsack-based heuristic can also result in different component selections and ranking results for both mitigation and repair actions. The larger resilience improvement from the BPSO once again shows that the BPSO can produce better solutions than the knapsack-based heuristic.

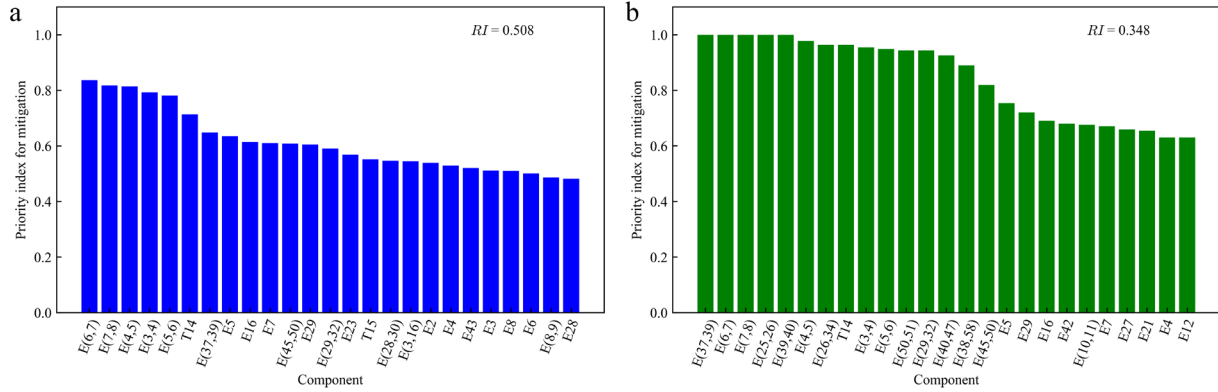


Figure 5.11 Comparison of priority indices for mitigation using BPSO and knapsack-based heuristic ($\Phi = 0.5$ and $B = \text{US } \$6 \times 10^4$): (a) BPSO; (b) knapsack-based heuristic

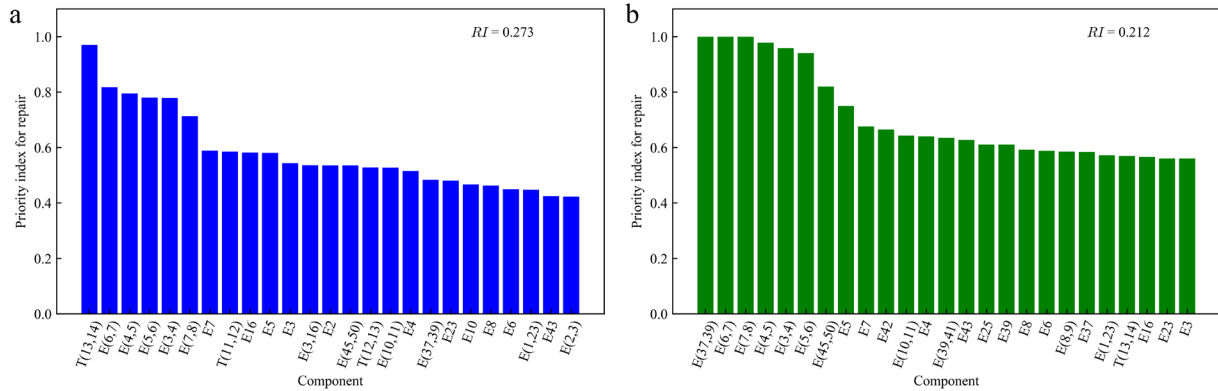


Figure 5.12 Comparison of priority indices for repair using BPSO and knapsack-based heuristic ($\Phi = 0.5$ and $B = \text{US } \$6 \times 10^4$): (a) BPSO; (b) knapsack-based heuristic

5.5 Conclusions

This chapter proposes a decision-making framework for prioritization of mitigation and repair actions to enhance the resilience of an interdependent traffic-electric power system in terms of functionality of the system under budgetary constraints. A bi-level, stochastic, simulation-based optimization problem is established with the objective of maximizing the expected resilience improvement of this interdependent system. The upper level of this framework tries to find the optimal plan of allocating limited mitigation and repair resources to multiple disrupted components to estimate the maximum attainable functionality gain. At the lower level, the functionalities of the traffic and electric power systems are obtained based on

network analysis methods. Three types of interdependencies have been considered: Type I interdependency describes the traffic lights at signalized intersection nodes in TN requiring power supply from relevant nodes in EPN; Type II interdependency is the potential blocking effects induced by the fallen poles of EPN on the traffic flow in TN; and Type III interdependency is the effect of accessibility of TN on the repair actions to both systems. Moreover, the dynamic traffic assignment (DTA) algorithm is used in order to overcome the shortcomings of the static traffic assignment method and capture more realistic traffic dynamics in the congested urban roadway networks. Uncertainties in disruptions, traffic demands, and mitigation and repair costs are considered in the problem formulation. The problem is solved by the binary particle swarm optimization combined with the knapsack-based heuristic and mitigation and repair priorities of disrupted components are then established based on the solutions.

The main findings of this study include: (1) the preference parameter in the objective function can be set to different values to obtain corresponding mitigation and repair resource allocation plan according to the decision-maker's preference or needs; (2) the priority indices can reflect the importance and contribution of components to the resilience improvement of the coupled system in both mitigation and repair actions; (3) the BPSO can produce better resource allocation plan than the knapsack-based heuristic to achieve greater resilience improvement.

CHAPTER 6 RESILIENCE-BASED RECOVERY SCHEDULING OF TRANSPORTATION NETWORK IN MIXED TRAFFIC ENVIRONMENT: A DEEP-ENSEMBLE-ASSISTED ACTIVE LEARNING APPROACH⁵

6.1 Introduction

Devising effective post-hazard recovery strategies is critical in enhancing the resilience of TNs. However, existing work does not consider the multiclass users' travel behavior in network functionality quantification and the metaheuristic solution procedures often suffer from extensive computational burden due to the exploration need in large solution space and the expensive functionality quantification. This study develops a bi-level decision-making framework for the resilience-based recovery scheduling of the transportation network in a mixed traffic environment with connected and autonomous vehicles (CAVs) and human-driven vehicles (HDVs).

The lower level quantifies the functionality of TN over time considering two types of users with different levels of information perception and travel behavior: the CAV users can acquire more detailed and accurate information of the TN, which justifies the user equilibrium model for their route choice behavior; while the HDV users are less-informed with only limited knowledge of the TN and their behavior is captured using the cross-nested logit model. The upper level presents a novel surrogate-based active learning approach based on the deep-ensemble-assisted efficient global optimization algorithm. The proposed approach is applied to solve the network recovery scheduling optimization problem by balancing the tradeoff between optimization performance and computational cost. Specifically, the embedded deep

⁵ This chapter is submitted to a journal in a paper that is currently under review (Zou and Chen 2020c).

convolutional neural network (CNN) ensemble acts as a computationally cheap surrogate function facilitating exploring the large schedule solution space and in the meantime, the efficient global optimization algorithm updates the deep ensemble in an active learning fashion and lead the optimization search in the right direction.

This framework can help decision makers better quantify the TN’s functionality to support effective recovery scheduling of TN with different mixed traffic scenarios ranging from HDV-only to future CAV-dominant traffic. The optimization approach bears the potential to be extended to solving general large-scale network recovery scheduling problems effectively and efficiently. The proposed methodology is demonstrated using a real-world traffic network in Southern California under earthquake considering deterministic and stochastic repair durations.

6.2 Problem formulation

The optimization problem of resilience-based recovery scheduling of the TN is formulated in this section in a bi-level structure, in which the lower level takes care of the functionality quantification of TN over time in a mixed traffic environment with both CAVs and HDVs while the upper level centers on the resilience-based optimization objectives and resource constraints. Relevant notations are defined in Table 6.1.

Table 6.1 Notations in the problem formulation

Notation	Description
t	Superscript referring to the recovery timestep
U	Subscript referring to the user class, the CAV user (A) or the HDV user (H), $U \in \{A, H\}$
t_0	Beginning of recovery horizon
t_r	End of recovery horizon

Δt	Time interval
n_{crews}	Number of repair crews
s_{bt}	Binary decision variable in scheduling optimization formulation (=1 if component b is initiated repair at time t and =0 otherwise)
\mathbf{s}	Schedule solution in matrix form, of which s_{bt} is the element
T	Number of time steps of recovery scheduling horizon
V	Set of all nodes (origins and destinations) in the TN
\mathcal{B}	Set of damaged components
\mathcal{B}_e	Set of damaged components on link e
$T_{b,\text{repair}}$	Repair duration for damaged component b
$T_{b,\text{completion}}$	Completion time for repairing damaged component b
TTC_{pre}	Total travel costs of users of pre-hazard, intact TN
TTC_t	Total travel costs of users of TN
Q_t	Normalized functionality metric of TN
W_U	Set of OD pairs for user class U
K_U^w	Set of feasible paths connecting OD pair $w \in W_U$
q_U^w	Traffic demand of OD pair w for user class U
$g_{k,U}^{w,t}$	Generalized travel cost of path k connecting OD pair w for user class U
$c_{k,U}^{w,t}$	Travel cost of path k connecting OD pair w for user class U
$f_{k,U}^{w,t}$	Traffic flow of user class U on path k connecting OD pair w
$f_{k,U}^{w,t*}$	Traffic flow of user class U on path k connecting OD pair w at equilibrium
l_e	Length of link $e \in E$
v_e^{FFS}	Free flow speed of link e
t_e^t	Travel time of traversing link e
F_e^t	The amount of fuel consumption for traversing link e
η	Unit price of fuel

VOT_U	Value of time of user class U
$\tau_{e,U}^t$	Travel cost of traversing link e for user class U
$v_{e,U}^t$	Traffic flow of user class U on link e
$\Delta_{e,k}^{w,U}$	Link-path incidence indicator for OD pair w and user class U (=1 if link e is in path k and =0 otherwise)
δ_e^t	Remaining ratio of original flow capacity of link e
δ_b^t	Remaining ratio of original flow capacity of component b
C_e^t	Remaining link capacity for mixed traffic flow of link e
$C_{e,U}$	Link capacity for pure flow of the user class U of link e in intact state
$\alpha_{e,k}^w$	Inclusion coefficient in CNL model
u	Degree of nesting in CNL model
λ	Dispersion parameter in CNL model

6.2.1 Functionality quantification of TN in mixed traffic environment

The TN in this study, which is represented as a directed graph $G = (V, E)$, refers to the roadway network. The nodes include the set of origins O and the set of destinations D , and the links $e \in E$ include all roadway segments. The functionality of TN at any time step t of recovery horizon is quantified based on the two classes of users: the well-informed CAV users and the less-informed HDV users, who differ in the levels of perceived knowledge and route choice behavior. Based on the work of Wang et al. (2019), the route choice behavior of CAV and HDV users can be characterized using user equilibrium and cross-nested logit traffic assignment models, respectively.

In order to better quantify the advantages of the CAVs over the HDVs and draw a fair comparison of

travel behavior between these two classes of users, the generalized link travel cost functions $\tau_{e,A}^t$ and $\tau_{e,H}^t$ consider two parts, i.e., travel time and fuel consumption, which are both converted into equivalent monetary values (Levin and Boyles 2015):

$$\tau_{e,U}^t = t_e^t \cdot VOT_U^t + \eta \cdot F_e^t \quad \forall U \in \{A, H\}, e \in E \quad (6.1)$$

It is noteworthy that due to the improved travel comfort and productivity during commuting time, the CAV users tend to have lower value of time than the HDV users (i.e., $VOT_A^t \leq VOT_H^t$) (Zhong et al. 2020).

In addition, t_e^t in Eq. (6.1) is assumed to follow the Bureau of Public Roads function (Wang et al. 2019):

$$t_e^t(v_{e,A}^t, v_{e,H}^t, C_e^t) = \frac{l_e}{v_e^{FFS}} \left[1 + \left(\frac{v_{e,A}^t + v_{e,H}^t}{C_e^t} \right)^4 \right], \quad \forall e \in E \quad (6.2)$$

$$v_{e,U}^t = \sum_{w \in W_U} \sum_{k \in K_U^w} f_{k,U}^{w,t} \Delta_{e,k}^{w,U}, \quad \forall U \in \{A, H\}, e \in E \quad (6.3)$$

where the term $v_{e,A}^t + v_{e,H}^t$ in Eq. (6.2) accounts for the mixed traffic flow in the presence of both CAVs and HDVs on link e ; and Eq. (3) describes the relationship between the link flow and the path flow. The remaining link capacity C_e^t for the mixed traffic flow at time t is affected not only by the disruption or the recovery progress but also by the different driving behavior between CAV and HDV users. Due to the automation technologies, the CAV users can have shorter reaction time and thus are expected to follow leading vehicles with smaller headway distance than the HDV users (Zhao et al. 2020). This also means, given the same certain period of time, the link can accommodate more CAVs than HDVs, i.e., $C_{e,A} \geq C_{e,H}$. On the other hand, the impacts of the disruption by the hazard or the repair by the recovery efforts on $C_{e,A}$

and $C_{e,H}$ are assumed to be the same, so $C_{e,A}$ and $C_{e,H}$ are both modified by δ_e^t as $\delta_e^t C_{e,A}$ and $\delta_e^t C_{e,H}$ to reflect the remaining capacity for 100% CAV and 100% HDV flows at time t , respectively.

The link capacity C_e^t for the mixed traffic flow is then somewhat in between $\delta_e^t C_{e,A}$ and $\delta_e^t C_{e,H}$ dependent on the proportions of CAVs and HDVs (Levin and Boyles 2016; Wang et al. 2019).:

$$C_e^t = \frac{\delta_e^t}{\frac{v_{e,A}^t}{v_{e,A}^t + v_{e,H}^t} \frac{1}{C_{e,A}} + \frac{v_{e,H}^t}{v_{e,A}^t + v_{e,H}^t} \frac{1}{C_{e,H}}}, \quad C_{e,A} \geq C_{e,H} \quad (6.4)$$

It can be seen from Eq. (6.4) that the link capacity for the mixed traffic increases with the rise of the proportion of CAVs since more vehicles can have smaller headways. Therefore, the increase of the link travel time function as defined in Eq.(6.2) due to the increase of the CAV ratio is no greater than that due to the increase of the same amount of the HDV ratio, i.e., the impacts of HDVs and CAVs on link travel time are asymmetric.

The fuel consumption F_e for a vehicle traversing the link e in Eq. (6.1) can be estimated based on the model of Zhang et al. (2014) for the gasoline-fueled light duty passenger vehicles:

$$F_e^t = 147.92 \left(\frac{l_e}{t_e^t} \right)^{-0.689} l_e \quad (6.5)$$

where F_e^t , l_e , and t_e^t are measured in liter, kilometer, and hour, respectively. Eq. (6.5) suggests that the fuel consumption F_e^t depends on the length of link l_e and average traffic speed l_e / t_e^t .

With the definition of the generalized link travel cost in Eqs. (6.1)–(6.5), the user equilibrium (UE) and cross-nested logit (CNL) traffic assignment models can be established for the CAV and HDV users, respectively. Due to the V2V and V2I technologies, the CAV users are assumed to possess perfect

information of the TN condition and thus can always choose the right paths to minimize their travel costs—meeting the classical static UE assumption (Sheffi 1985). Therefore, the CAV path flows at UE $f_{k,A}^{w,t*}$ can be obtained by solving the following variational inequality (VI) problem:

$$\sum_{w \in W_A} \sum_{k \in K_A^w} g c_{k,A}^{w,t} (f_{k,A}^{w,t*}) (f_{k,A}^{w,t} - f_{k,A}^{w,t*}) \geq 0 \quad (6.6)$$

subject to:

$$g c_{k,A}^{w,t} = \begin{cases} \min_{k \in K_A^w} g c_{k,A}^{w,t}, & \text{if } f_{k,A}^{w,t*} > 0 \\ \geq \min_{k \in K_A^w} g c_{k,A}^{w,t}, & \text{if } f_{k,A}^{w,t*} = 0 \end{cases} \quad \forall k \in K_A^w, w \in W_A \quad (6.7)$$

$$g c_{k,A}^{w,t} = c_{k,A}^{w,t} = \sum_{e \in k} \tau_{e,A}^t \quad \forall k \in K_A^w, w \in W_A \quad (6.8)$$

$$\sum_{k \in K_A^w} f_{k,A}^{w,t} = q_A^w \quad \forall k \in K_A^w, w \in W_A \quad (6.9)$$

$$f_{k,A}^{w,t} \geq 0 \quad \forall k \in K_A^w, w \in W_A \quad (6.10)$$

Eq. (6.7) states that under the UE condition, the generalized travel costs of the used paths for the CAV users between any OD pair are equal and no CAV user can unilaterally reduce his/her travel cost by switching to another route. Eq. (6.8) defines that the generalized path travel cost for the CAV user $g c_{k,A}^{w,t}$ is same as the path travel cost $c_{k,A}^{w,t}$, which also equals the summation of the generalized travel costs of the corresponding links for the CAV user along the path. Eqs. (5.4) and (6.10) impose the flow conservation and nonnegative constraints on the path flow $f_{k,A}^{w,t}$, respectively.

In contrast to the well-informed CAV users, who can choose the least costly path deterministically, the less-informed HDV users only receive limited knowledge of the TN's state and perceive travel costs based on higher levels of uncertainty in traffic information, which leads to the randomness in their final decisions on the preferred paths for trips. Such stochastic route choosing behavior is better to be described using the stochastic user equilibrium (SUE) model, which uses a probabilistic route choice model to account for the non-zero probability of choosing other costlier routes over the least costly route (Daganzo and Sheffi 1997; Prashker and Bekhor 2004). The CNL model, as a modified SUE model to address the route overlapping problems (Prashker and Bekhor 1999), is adopted here to characterize the traffic patterns of the HDV users. The HDV path traffic flows at SUE in the CNL model can be obtained by solving the following VI problem:

$$\sum_{w \in W_H} \sum_{k \in K_H^w} g c_{k,H}^{w,t} (f_{k,H}^{w,t*}) (f_{k,H}^{w,t} - f_{k,H}^{w,t*}) \geq 0 \quad (6.11)$$

subject to:

$$g c_{k,H}^{w,t} = \begin{cases} \min_{k \in K_H^w} g c_{k,H}^{w,t}, & \text{if } f_{k,H}^{w,t*} > 0 \\ \geq \min_{k \in K_H^w} g c_{k,H}^{w,t}, & \text{if } f_{k,H}^{w,t*} = 0 \end{cases} \quad \forall k \in K_H^w, w \in W_H \quad (6.12)$$

$$c_{k,H}^{w,t} = \sum_{e \in k} \tau_{e,H}^t \quad \forall k \in K_H^w, w \in W_H \quad (6.13)$$

$$g c_{k,H}^{w,t} = c_{k,H}^{w,t} - \frac{u}{\lambda} H_{k,H}^{w,t} + \frac{u}{\lambda} \ln \left(\frac{f_{k,H}^{w,t}}{q_H^w} \right) \quad \forall k \in K_H^w, w \in W_H \quad (6.14)$$

$$H_{k,H}^{w,t} = \ln \left[\sum_{e \in E} (\alpha_{e,k}^w)^{1/u} \left(\sum_{p \in K_H^w} (\alpha_{e,p}^w \exp(-\lambda c_{p,H}^{w,t}))^{1/u} \right)^{u-1} \right] \quad \forall k \in K_H^w, w \in W_H \quad (6.15)$$

$$\alpha_{e,k}^w = \left(\frac{l_e}{l_k^w} \right) \Delta_{e,k}^{w,H} \quad \forall e \in E, k \in K_H^w, w \in W_H \quad (6.16)$$

$$\sum_{k \in K_H^w} f_{k,H}^{w,t} = q_H^w \quad \forall k \in K_H^w, w \in W_H \quad (6.17)$$

$$f_{k,H}^{w,t} \geq 0 \quad \forall k \in K_H^w, w \in W_H \quad (6.18)$$

Eq. (6.12) states that under the SUE condition, the generalized travel costs of the used paths for the HDV users between any OD pair are equal and no HDV user can unilaterally reduce his/her travel cost by switching to another route. Eq. (6.13) suggests that the path travel cost for the HDV user $c_{k,H}^{w,t}$ equals the summation of the generalized travel costs of corresponding links for the HDV user in this path. Eq. (6.14) defines the generalized path travel cost for the HDV user $gc_{k,H}^{w,t}$ in the CNL model. Eq. (6.15) introduces the generalized path travel cost correction term $H_{k,H}^{w,t}$ to tackle route overlapping issues in the CNL model. Eq. (6.16) defines the inclusion coefficient $\alpha_{e,k}^w$. Eqs. (6.17) and (6.18) impose the flow conservation and nonnegative constraints on the path flow $f_{k,H}^{w,t}$, respectively. It can be found that the UE model in Eqs. (6.6)–(6.10) and the CNL model in Eqs. (6.11)–(6.18) look very much alike in terms of the VI formulations except for the definitions of the generalized path travel cost for two classes of users. By some mathematical manipulations, the probability of choosing path k for OD pair w for the HDV user can be shown as:

$$p_H^{w,t}(k) = \frac{f_{k,H}^{w,t}}{q_H^w} = \frac{\exp(-\frac{u}{\lambda} c_{k,H}^{w,t} + H_{k,H}^{w,t})}{\sum_{p \in K_H^w} \exp(-\frac{u}{\lambda} c_{p,H}^{w,t} + H_{p,H}^{w,t})} \quad (6.19)$$

For the HDV users with limited perception of the TN's state, the possibilities of choosing all available routes instead of only using the least costly one are therefore captured by the probabilistic route choice model defined in Eq. (6.19). Particularly, when $u = 1$, $H_{k,H}^{w,t} = 0$ and the CNL model reduces to the multinomial-logit-based SUE model (Guo and Huang 2016; Liu et al. 2009).

It should be noted that the UE model and CNL model established above are only for 100% CAV users scenario and 100% HDV users scenario, respectively. In order to consider the mixed traffic environment in the presence of both CAV and HDV users, the multiclass user traffic assignment in the VI formulation can be developed by combining Eqs. (6.6) and (6.11) into the following one:

$$\sum_{w \in W_A} \sum_{k \in K_A^w} g c_{k,A}^{w,t} (f_{k,A}^{w,t*}, f_{k,H}^{w,t*}) (f_{k,A}^{w,t} - f_{k,A}^{w,t*}) + \sum_{w \in W_H} \sum_{k \in K_H^w} g c_{k,H}^{w,t} (f_{k,A}^{w,t*}, f_{k,H}^{w,t*}) (f_{k,H}^{w,t} - f_{k,H}^{w,t*}) \geq 0 \quad (6.20)$$

subject to Eqs. (6.7)–(6.10) and Eqs. (6.12)–(6.18).

This type of path-flow-based traffic assignment is often solved by the path-swapping algorithm: starting with an initial non-equilibrium solution, the path flows within each OD pair are iteratively redistributed over available paths until the equilibrium condition is reached with acceptable accuracy (Liu et al. 2009; Lu et al. 2009; Sbayti et al. 2007).

Once the path travel costs ($c_{k,A}^{w,t}$ and $c_{k,H}^{w,t}$) and path flows ($f_{k,A}^{w,t}$ and $f_{k,H}^{w,t}$) for the CAV and HDV users at time t are determined, the functionality of the whole TN at time t is measured by the total travel costs of all CAV and HDV users as below:

$$TTC_t = \sum_{w \in W_A} \sum_{k \in K_A^w} c_{k,A}^{w,t} f_{k,A}^{w,t} + \sum_{w \in W_H} \sum_{k \in K_H^w} c_{k,H}^{w,t} f_{k,H}^{w,t} \quad (6.21)$$

And the functionality metric of TN at time t is defined as TTC_t normalized by pre-hazard total travel cost

TTC_{pre} :

$$Q_t = \frac{TTC_{pre}}{TTC_t} \quad (6.22)$$

Since typically the intact TN in the pre-hazard stage has the best functionality level, so $TTC_{pre} \leq TTC_t$

and Q_t falls into the interval $(0, 1)$. Immediately after the hazard, the TN drops to its lowest functionality

level and Q_t is equal to the minimum value of TTC_{pre} / TTC_0 over the recovery horizon; as the recovery

progresses under the given schedule, Q_t gradually increases until approaching the maximum value 1.0.

6.2.2 Problem formulation of resilience-based recovery scheduling of TN

The analytical definition of system resilience as the optimization objective function in the recovery scheduling is defined as below (Bocchini and Frangopol 2012; Cimellaro et al. 2016; Vugrin et al. 2014):

$$R = \frac{1}{(t_r - t_0)} \int_{t_0}^{t_r} Q_t dt \quad (6.23)$$

The recovery scheduling horizon $[t_0, t_r]$ is divided into a sequence of $T + 1$ time steps

$\{t_0, t_0 + \Delta t, t_0 + 2\Delta t, \dots, t_0 + T\Delta t\}$ with an interval of Δt , and the corresponding Q_t at each time step t is

obtained using functionality quantification; then the resilience metric R in Eq. (6.23) can be computed

using numerical integration. Without loss of generality, the recovery scheduling horizon $[t_0, t_r]$ is set to $[0,$

$T\Delta t]$ hereafter.

At time step $t = 0$, a hazardous event occurs and a set of components of links (e.g., bridges) \mathcal{B} can sustain different levels of damages. The damaged components of \mathcal{B} can cause disruptions to the traffic on their own links or nearby ones, which are quantified as the degraded remaining ratios of original flow capacities (i.e., $\delta_b^0 < 1.0, \forall b \in \mathcal{B}$). The corresponding links associated with these damaged components also experience reductions in their traffic flow capacities (i.e., $\delta_e^0 < 1.0$). Thus, the functionality level of whole TN is also decreased (i.e., Q_0) due to the possible travel delays for the CAV and HDV users. The recovery activities refer to utilizing recovery resources to restore the affected components from the damaged states to the intact states (i.e., the transition from δ_b^0 to 1.0) in which the functionality of the disrupted TN can be recovered gradually.

The recovery resource is assumed to be generic enough to capture the required personnel, equipment, and material to perform the necessary recovery activities. Each damaged component is assumed to only require one unit of resource for recovery (i.e., also referred to as one repair crew here). Since the post-hazard recovery resources can be very limited, the number of repair crews n_{crews} during the recovery horizon can be far lower than the number of damaged components to be repaired $|\mathcal{B}|$ (i.e., $n_{\text{crews}} \ll |\mathcal{B}|$), which makes the scheduling optimization non-trivial (Nozhati et al. 2019; Ouyang and Wang 2015). It is also assumed that the repair crews work in a non-preemptive mode, i.e., a repair crew should complete the repair task on the currently assigned component before it moves to next component.

Given the number of damaged components $|\mathcal{B}|$, the repair duration of each damaged component $T_{b,\text{repair}}$, and available recovery resources n_{crews} , the scheduling is concerned with arranging these recovery activities in a particular order ($\mathbf{s} = (s_{bt}) \in \mathbb{R}^{|\mathcal{B}| \times T}$); the resulting optimal recovery trajectory

$(Q_t, \forall t \in \{0, 1, \dots, T\})$ over the recovery horizon is expected to maximize the resilience-based objective R in Eq. (6.23). This is formulated as the following bi-level optimization problem:

$$\max R \quad (6.24)$$

subject to:

$$T_{b,completion} = \sum_{t=1}^T (t + \lceil T_{b,repair} / \Delta t \rceil - 1) s_{bt} \quad (6.25)$$

$$\delta_b^t = \delta_b^0 \left[t \leq T_{b,completion} \right] + \left[t > T_{b,completion} \right], \quad \forall b \in \mathcal{B}, t \in \{1, 2, \dots, T\} \quad (6.26)$$

$$\delta_e^t = \min_{b \in \mathcal{B}_e} \delta_b^t, \quad \forall e \in E, t \in \{1, 2, \dots, T\} \quad (6.27)$$

$$Q_t = g(\{\delta_e^t\}_{e=1}^{|E|}), \quad \forall t \in \{0, 1, 2, \dots, T\} \quad (6.28)$$

$$\sum_{t=1}^T s_{bt} \leq 1, \quad \forall b \in \mathcal{B} \quad (6.29)$$

$$\sum_{b \in \mathcal{B}} \sum_{\tau=t}^{\min(t + \lceil T_{b,repair} / \Delta t \rceil - 1, T)} s_{b\tau} \leq n_{crews}, \quad \forall t \in \{1, 2, \dots, T\} \quad (6.30)$$

$$s_{bt} \in \{0, 1\}, \quad \forall b \in \mathcal{B}, t \in \{0, 1, 2, \dots, T\} \quad (6.31)$$

where $\lceil \cdot \rceil$ in Eq. (6.26) is Iverson bracket, which returns 1 if the statement is true and 0 otherwise;

$\{\delta_e^t\}_{e=1}^{|E|}$ in Eq. (6.28) denotes the set of δ_e^t for all links in E ; and $\lceil \cdot \rceil$ in Eqs. (6.25) and (6.30) is the

ceiling function. Eq. (6.24) is the objective function, i.e., to maximize the resilience metric R . Eq. (6.25)

defines the repair completion time for component b . Eq. (6.26) indicates the component states varying with

the recovery progress. When component b is not being scheduled to be repaired or undergoing the repair (i.e., $t \leq T_{b,completion}$), its remaining ratio of original flow capacity δ_b^t stays the same as the disrupted one δ_b^0 and when the repair on component b is completed (i.e., $t > T_{b,completion}$), δ_b^t is set to 1.0. Eq. (6.27) suggests that when more than one damaged components exist on link e , the remaining ratio of original flow capacity of link e equals the minimum of the remaining capacity ratios of these components in \mathcal{B}_e , which implies a series system (Chang et al. 2000; Guo et al. 2017). Eq. (6.28) states that the functionality of TN at time t (Q_t) can be obtained based on the state of all links at time t ($\{\delta_e^t\}_{e=1}^{|E|}$); $g(\cdot)$ denote the functionality quantification model introduced in Eqs. (6.7)–(6.10), (6.12)–(6.18), and (6.20). Eq. (6.29) stipulates that any damaged component can only be scheduled to be repaired no more than once. Eq. (6.30) is the recovery resource constraint and indicates that at any time, the number of damaged components under repair is limited by the total number of available resources n_{crews} . Eq. (6.31) is the binary constraint for decision variable s_{bt} .

In this bi-level formulation, the upper level aims to construct the schedule solution considering the recovery resource constraint to maximize the resilience metric, as described in Eqs. (6.29)–(6.31); the lower level evaluates the given schedule solution from the upper level using functionality quantification, in which the time-dependent states of damaged components and links are deduced from the repair schedule and then the corresponding recovery trajectory can be obtained, as described in Eqs. (6.25)–(6.28).

The formulation introduced above is for the deterministic case where the repair durations $T_{b,repair}$ are assumed to be certain. However, in some cases, due to the insufficient preparedness for the hazards and the long-term recovery process for a large TN, accurately estimating repair durations for damaged components beforehand can be difficult and the estimated repair durations tend to contain uncertainty (Li et al. 2019a;

Zhang et al. 2017). In such cases, $T_{b,repair}$ is treated as a random variable, and the objective function in the recovery scheduling optimization can be expressed as:

$$\max E(R) \quad (6.32)$$

where $E(\cdot)$ is the expectation operator.

6.3 Solution procedure

This study employs the metaheuristics to find the near-optimal solutions to this NP-hard problem. As mentioned in the introduction, population-based metaheuristics relies on generating and evaluating a large number of candidate schedule samples to explore the solution space sufficiently, especially when dealing with the large network instances. Generating candidate solutions is computationally cheap but evaluating them all can be cost prohibitive. Evaluation of the candidate schedule $\mathbf{s}_i = (s_{bt}^i) \in \mathbb{R}^{|\mathcal{B}| \times (T+1)}$ here refers to obtaining the corresponding resilience metric R_i based on Eqs. (6.25)–(6.28), and is denoted using the back-box function $f(\cdot)$:

$$R_i = f(\mathbf{s}_i) \quad (6.33)$$

Recall that this evaluation includes computing the recovery trajectory using the lower-level functionality quantification model, i.e., obtaining the functionality level Q_t at each time step t , where $t = 0, 1, \dots, T$. In infrastructure recovery scheduling optimization, the lower-level functionality quantification model can be very complex and computationally expensive even it is just for the lower-level multiclass user traffic assignment model.

One well-known issue of the path-swapping algorithm used in the lower-level traffic assignment is its

slow convergence; it often requires many iterations to achieve convergence so the traffic assignment process may be time-consuming, especially when a large number of path flows exist in the TN (Jayakrishnan et al. 1994; Liu et al. 2009; Peeta and Yang 2003). So, performing the traffic assignment once may be already expensive, and repeating the algorithm for $T+1$ times to obtain the recovery trajectory greatly exacerbates the computational burden. Therefore, it becomes infeasible to evaluate all generated schedule samples in the metaheuristics using the exact functionality quantification model with reasonable computational resource.

To resolve this issue, this study proposes a deep-ensemble-assisted active learning approach for the general network recovery scheduling optimization, in which the deep ensemble acts as a computationally cheap surrogate function to evaluate large candidate solutions and assist in finding the promising solutions. In addition, the efficient global optimization (EGO) is adopted to lead the optimization direction and update the deep ensemble by enriching the training data adaptively to reach the tradeoff between exploration and exploitation.

6.3.1 Deep ensemble

Since it can be expensive to evaluate all generated schedule samples using the exact functionality quantification model, a surrogate model of $f(\cdot)$ in Eq. (6.33) can be introduced to relieve the computational burden. By observing that the high dimensional schedule solution can be converted into an image representing the component states over time, a deep learning model—the deep CNN ensemble is adopted as the surrogate model to leverage the CNN’s capability in image learning (Krizhevsky et al. 2012; Lecun et al. 2015; Szegedy et al. 2015) and deep ensemble’s capability in uncertainty quantification (Beluch et al. 2018; Lakshminarayanan et al. 2017; Leibig et al. 2017).

First, a schedule $\mathbf{s}_i = (s_{bt}^i) \in \mathbb{R}^{|\mathcal{B}| \times (T+1)}$ is converted into an image, namely a 2-dimensional binary tensor $\mathbf{x}_i = (x_{bt}^i) \in \mathbb{R}^{|\mathcal{B}| \times (T+1)}$, in which $|\mathcal{B}|$ rows and $T+1$ columns represent $|\mathcal{B}|$ damaged components and $T+1$ time steps, respectively. The element x_{bt} is binary which equals 1 if component b is repaired at time t under given \mathbf{s}_i otherwise 0. A toy example of this conversion is illustrated in Figure 6.1. With this conversion, the schedule \mathbf{s}_i is converted into the binary image \mathbf{x}_i , which can be fed into the deep CNN ensemble.

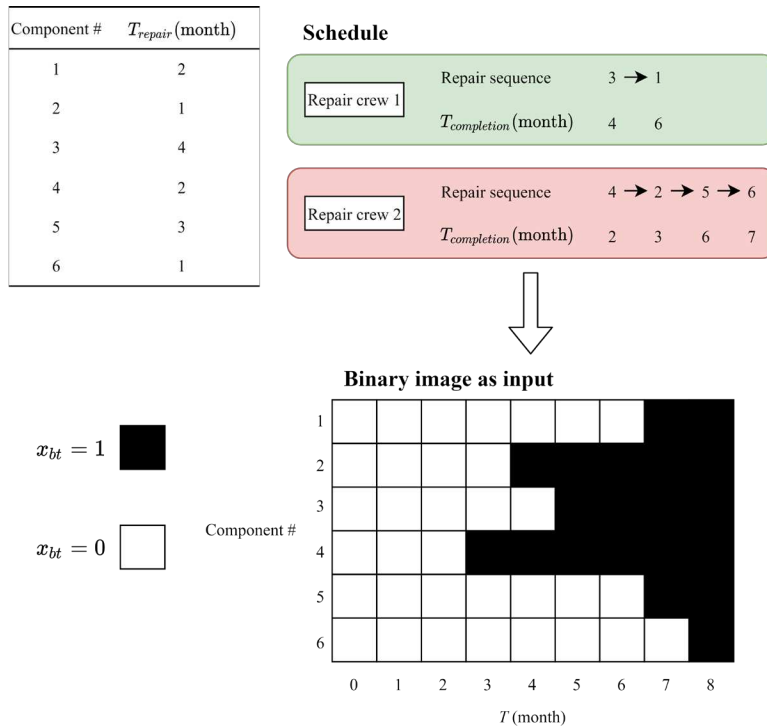


Figure 6.1 Illustration of conversion from schedule to binary image as input to deep ensemble

Although the CNN has achieved unprecedented successes on extensive image processing tasks, training a deep CNN still requires a very large amount of labeled training data or it can quickly overfit and demonstrate poor generalization behavior on unseen data due to its large number of parameters. In addition, the normal CNN only provides point estimates of predictions and lacks the uncertainty information, which makes assessment of the model quality difficult and acquisition of labeled data costly (Gal 2016; Janet et

al. 2019). In this study, the labeled training set consists of data pairs (\mathbf{x}_i, R_i) , and labeling a high amount of such data (i.e., using $f(\cdot)$ in Eq. (6.33) to evaluate \mathbf{x}_i) can be very expensive. And since the optimization is an iterative process, it is also desirable to obtain the uncertainty information of predictions, which can be used to determine the surrogate model's most applicable region in the solution space, so that only data of most interest is labeled and the surrogate model can be enhanced iteratively with a reduced data acquisition effort.

The deep ensemble serves as a simple yet effective solution to this regression task, which improves the generalization behavior and enables the uncertainty quantification of deep CNNs (Lakshminarayanan et al. 2017). As depicted in Figure 6.2, the deep ensemble consists of M CNNs, which all share the same neural network structure but with different initializations of parameters. In each CNN_m , the input \mathbf{x}_i is first processed by deeply stacked convolutional and pooling layers to extract the important features, and then two heads at the top, which consist of some fully-connected layers, output the mean prediction and standard deviation of the prediction based on the extracted features:

$$(\mu_{im}, \sigma_{im}) = \text{CNN}_m(\mathbf{x}_i), \quad \forall m = 1, 2, \dots, M \quad (6.34)$$

By assuming a Gaussian mixture distribution, the results from all CNNs are ensembled as follows:

$$(\mu_{i,ens}, \sigma_{i,ens}) = \text{ens}(\mathbf{x}_i) \quad (6.35)$$

where

$$\mu_{i,ens} = \frac{1}{M} \sum_{m=1}^M \mu_{im} \quad (6.36)$$

$$\sigma_{i,ens} = \sqrt{\frac{1}{M} \sum_{m=1}^M \sigma_{im}^2 + \frac{1}{M} \sum_{m=1}^M (\mu_{im} - \mu_{i,ens})^2} \quad (6.37)$$

Therefore, the deep ensemble is able to give not only the mean prediction of R_i ($\mu_{i,ens}$) but also the standard deviation (i.e., uncertainty information) of R_i ($\sigma_{i,ens}$). If the input \mathbf{x}_i is associated with larger $\sigma_{i,ens}$, it means that the model ens is more uncertain about its prediction at \mathbf{x}_i , which may be due to the sparsity of training data around \mathbf{x}_i ; otherwise, the model ens is confident about its prediction at \mathbf{x}_i . To train this deep ensemble is to minimize the following loss function using the stochastic gradient descent algorithm or its variants:

$$\mathcal{L} = \frac{\ln \sigma_{i,ens}^2(\mathbf{x}_i)}{2} + \frac{(R_i - \mu_{i,ens}(\mathbf{x}_i))^2}{2\sigma_{i,ens}^2(\mathbf{x}_i)}, \quad (6.38)$$

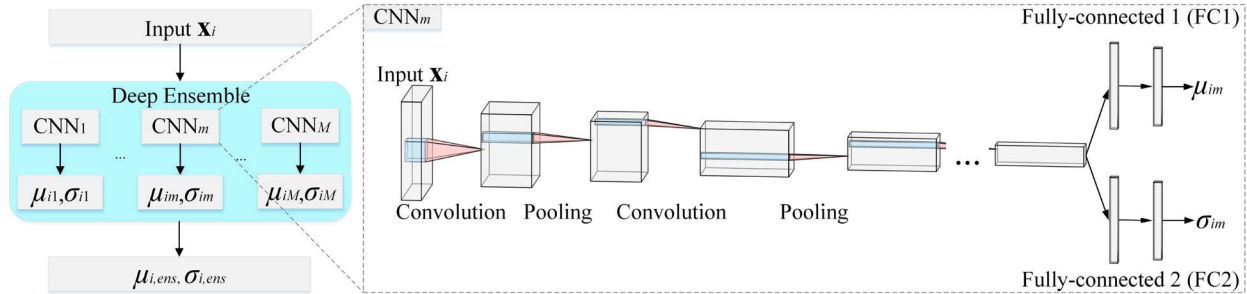


Figure 6.2 Illustration of the structure of the deep ensemble

6.3.2 Deep-ensemble-assisted efficient global optimization

The uncertainty quantification capability of the deep ensemble facilitates solving the recovery scheduling optimization in an active learning fashion. With the notation in Eq. (6.33), the original recovery scheduling optimization can be rewritten in a more general form as below:

$$\mathbf{x}^* = \arg \max f(\mathbf{x}) \quad (6.39)$$

where \mathbf{x}^* is the optimal schedule to be solved and the each corresponding \mathbf{s} still needs to satisfy the constraints in Eqs. (6.29)–(6.31). To solve this problem, a deep-ensemble-assisted efficient global optimization (DEAEGO) approach is developed, where the efficient global optimization (EGO) is employed as the active learning scheme to be combined with the deep ensemble to find the optimal schedule solution iteratively. The pseudocode of the whole algorithm is detailed in Figure 6.3 and relevant notations are listed in Table 6.2.

Algorithm DEAEGO: deep-ensemble-assisted efficient global optimization

- 1: **Input:** $a(\cdot)$ - acquisition function; $f(\cdot)$ - evaluation function; \mathcal{U}_0 - initial unevaluated schedule samples; $GAScheduleGenerator(\cdot)$ - genetic-algorithm-based schedule sample generator; n_{start} - size of starting training set; n_{eval} - number of evaluated schedule samples of each iteration; n_{new} - number of newly generated schedule samples of each iteration; K - total number of optimization iterations; M - total number of neural networks in deep ensembles.
- 2: **Initialize:** $k = 0, \mathcal{U}_0 \leftarrow \emptyset$
- 3: Randomly generate n_{start} schedule samples $\mathcal{X}_0 \leftarrow \{\mathbf{x}_i\}_{i=1}^{n_{start}}$
- 4: Evaluate $\mathbf{x}_i \in \mathcal{X}_0^{new}$ using functionality quantification $\mathcal{R}_0 \leftarrow \{R_i = f(\mathbf{x}_i) | \mathbf{x}_i \in \mathcal{X}_0\}_{i=1}^{n_{start}}$
- 5: Prepare initial training set $\mathcal{E}_0 \leftarrow \{(\mathbf{x}_i, R_i) | \mathbf{x}_i \in \mathcal{X}_0, R_i \in \mathcal{R}_0\}_{i=1}^{n_{start}}$
- 6: **while** $k \leq K$ **do**
- 7: $R_{opt} \leftarrow \max\{R_i | R_i \in \mathcal{R}_k\}, \mathbf{x}_{opt} \leftarrow \arg \max\{R_i | \mathbf{x}_i \in \mathcal{X}_k, R_i \in \mathcal{R}_k\}$
- 8: Train each member of deep ensembles $CNN_m (m = 1, 2, \dots, M)$ from scratch given \mathcal{E}_k
- 9: Form ensemble model $ens_k = ensemble(CNN_1, CNN_2, \dots, CNN_M)$
- 10: Generate n_{new} new schedule samples $\mathcal{U}_k^{new} \leftarrow \{\mathbf{x}_i\}_{i=1}^{n_{new}} = GAScheduleGenerator(\mathcal{E}_k, n_{new})$
- 11: $\mathcal{U}_k \leftarrow \mathcal{U}_k \cup \mathcal{U}_k^{new}$
- 12: $\hat{R}_{opt} = \max\{\mu_{i,ens} = ens_k(\mathbf{x}_i) | \mathbf{x}_i \in \mathcal{X}_k\}$
- 13: **for** \mathbf{x}_i in \mathcal{U}_k **do**
- 14: Obtain $(\mu_{i,ens}, \sigma_{i,ens}) = ens_k(\mathbf{x}_i)$
- 15: Calculate expected improvement $EI_i = a(\mu_{i,ens}, \sigma_{i,ens}; \hat{R}_{opt})$
- 16: **end for**
- 17: Sort $\mathbf{x}_i \in \mathcal{U}_k$ according to EI_i in descending order $index_j = argsort(EI_j)$
- 18: Obtain top n_{eval}^{th} samples $\mathcal{X}_k^{new} \leftarrow \{\mathbf{x}_z | z \in index_j[1 : n_{eval}]\}$
- 19: Evaluate $\mathbf{x}_i \in \mathcal{X}_k^{new}$ using functionality quantification $\mathcal{R}_k^{new} \leftarrow \{R_i = f(\mathbf{x}_i) | \mathbf{x}_i \in \mathcal{X}_k^{new}\}_{i=1}^{n_{eval}}$
- 20: $\mathcal{Q}_k \leftarrow \{(\mathbf{x}_i, R_i) | \mathbf{x}_i \in \mathcal{X}_k^{new}, R_i \in \mathcal{R}_k^{new}\}_{i=1}^{n_{eval}}$
- 21: $\mathcal{U}_{k+1} \leftarrow \mathcal{U}_k \setminus \mathcal{X}_k^{new}$
- 22: $\mathcal{X}_{k+1} \leftarrow \mathcal{X}_k \cup \mathcal{X}_k^{new}, \mathcal{R}_{k+1} \leftarrow \mathcal{R}_k \cup \mathcal{R}_k^{new}$
- 23: $\mathcal{E}_{k+1} \leftarrow \mathcal{E}_k \cup \mathcal{Q}_k$
- 24: $k \leftarrow k + 1$
- 25: **end while**
- 26: **Return** $(\mathbf{x}_{opt}, R_{opt})$

Figure 6.3 Pseudocode of the DEAEGO algorithm

Table 6.2 Notations of the DEAEEO algorithm

Parameter	Description
k	The k th optimization iteration
K	Total number of optimization iterations
n_{start}	Size of starting training set $ \mathcal{R}_0 $
n_{eval}	Number of evaluated schedule samples of each iteration
n_{new}	Number of newly generated schedule samples of each iteration
m	The m^{th} neural network in deep ensembles
M	Total number of neural networks in deep ensembles
ens_k	The trained deep ensembles of iteration k
\mathbf{x}_i	The i^{th} schedule sample
\mathbf{x}_{opt}	The optimal schedule solution
$\mu_{i,ens}$	Mean prediction of resilience metric of \mathbf{x}_i by ens_k
$\sigma_{i,ens}$	Standard deviation of prediction of resilience metric of \mathbf{x}_i by ens_k
R_i	Resilience metric of \mathbf{x}_i by functionality quantification
R_{opt}	The optimal resilience metric found
\hat{R}_{opt}	The optimal mean prediction of resilience metric by ens_k
EI_i	Expected improvement of \mathbf{x}_i
\mathcal{X}_k	Set of evaluated schedule samples of iteration k
\mathcal{X}_k^{new}	Set of newly evaluated schedule samples of iteration k
\mathcal{R}_k	Set of resilience metrics of schedule samples of iteration k
\mathcal{R}_k^{new}	Set of resilience metrics of newly evaluated schedule samples of iteration k
\mathcal{E}_k	Set of training set for deep ensembles of iteration $k \{(\mathbf{x}_i, R_i) \mathbf{x}_i \in \mathcal{X}_k, R_i \in \mathcal{R}_k\}$
\mathcal{U}_k	Set of unevaluated schedule samples of iteration k
\mathcal{Q}_k	Set of newly generated training set of iteration $k \{(\mathbf{x}_i, R_i) \mathbf{x}_i \in \mathcal{X}_k^{new}, R_i \in \mathcal{R}_k^{new}\}$

In the beginning of this approach, two datasets exist, i.e., a relatively small initial training set \mathcal{E}_0 containing the data pairs (\mathbf{x}_i, R_i) and a unlabeled set \mathcal{U}_0 containing only unevaluated schedule samples \mathbf{x}_i . The deep ensemble is first trained on this small training dataset \mathcal{E}_0 and then perform prediction and uncertainty quantification on sample \mathbf{x}_i in \mathcal{U}_0 . Since the deep ensemble is computationally cheaper than the actual evaluation function $f(\cdot)$, an extensive search becomes affordable to allow for a large size of \mathcal{U}_0 .

What follows is the key of this active learning approach, relying on an acquisition function $a(\cdot)$ (or an infill criterion) to decide which \mathbf{x}_i in \mathcal{U}_0 should be actually evaluated using the expensive evaluation function $f(\cdot)$ based on the optimization objective. The acquisition function $a(\cdot)$ is usually built on the surrogate model's uncertainty. Based on the Gaussian distribution assumption on the outputs of the deep ensemble, the expected improvement (EI) is adopted as the acquisition function for this maximization problem as follows (Jones et al. 1998; Lizotte 2008; Shahriari et al. 2016):

$$EI_i = a(\mu_{i,ens}, \sigma_{i,ens}; \hat{R}_{opt}) = \begin{cases} (\mu_{i,ens} - \hat{R}_{opt} - \xi) \Psi\left(\frac{\mu_{i,ens} - \hat{R}_{opt} - \xi}{\sigma_{i,ens}}\right) + \sigma_{i,ens} \psi\left(\frac{\mu_{i,ens} - \hat{R}_{opt} - \xi}{\sigma_{i,ens}}\right), & \text{if } \sigma_{i,ens} \geq 10^{-10} \\ 0, & \text{if } \sigma_{i,ens} < 10^{-10} \end{cases} \quad (6.40)$$

where $\Psi(\cdot)$ and $\psi(\cdot)$ are the cumulative distribution function (CDF) and probability density function of the standard Gaussian distribution, respectively; ξ is the small explorative parameter which is usually set to 0.01.

The optimization is about the process to balance exploiting accumulated knowledge of the function $f(\cdot)$ from the historical evaluations with exploring other uncertain regions where the training data is sparse and better solutions may exist. Therefore, the EI as defined in Eq.(6.40) can tradeoff between exploration

and exploitation and thus lead the optimization in right direction. Note that the EI is high where the mean prediction $\mu_{i,ens}$ is high (exploitation) and where the prediction uncertainty $\sigma_{i,ens}$ is high (exploration); so with this acquisition function, it is reasonable that only sample \mathbf{x}_i in \mathcal{U}_0 which maximizes the EI and may be potentially a better solution than the existing one, can be chosen as the one to be evaluated using the expensive function $f(\cdot)$ and further update the deep ensembles.

However, this infill criterion is originally designed for the Gaussian process (GP) surrogate model and needs to be modified to be extended to the deep ensembles. First, analytically finding the solution \mathbf{x}_i to maximize EI is not an easy task as in continuous optimization with GP model, because the deep ensemble does not have the same mathematical properties with the GP model, and the schedule solution space is discrete so the gradient-based methods cannot be used. Second, the deep ensemble has many parameters and is trained using minibatch training data, adding only single one sample has statistically little impact on deep ensemble's parameter updating (Sener and Savarese 2018).

To apply this infill criterion to the deep ensemble, this algorithm allows adding top n_{eval} samples ranked by their EI values in descending order to achieve statistical significance on the deep ensemble's training. Instead of solving the \mathbf{x}_i to maximize EI directly, this study adopts a simple strategy: just calculate EI values of all \mathbf{x}_i in \mathcal{U}_0 based on the trained deep ensemble model ens , and pick the top n_{eval} samples \mathbf{x}_i . In order to further encourage the exploration in the large solution space, the unevaluated data set \mathcal{U}_0 is, instead of fixed, increased on the fly with the optimization iteration. Here the crossover and mutation operations in the genetic algorithm are incorporated to generate n_{new} new unevaluated solution samples in each iteration, which is denoted as $GAScheduleGenerator(\cdot)$ in line 10 in Figure 6.3. Other schedule solution generation methods such as the local search can also be adopted. It should be noted that in each iteration,

the deep ensemble should be retrained from scratch based on the current training set \mathcal{E}_k , as described in line 8 in Figure 6.3.

These steps are repeated themselves until the stop criteria are met (i.e., the total number of optimization iterations K in Figure 6.3). With this DEAEEO algorithm, starting with only a few evaluated schedule samples, the deep ensemble is trained to assist in finding potentially better solutions based on the acquisition function. The infill criterion can adaptively decide which samples are of interest and should be evaluated using the expensive function and then added to the training set to update the deep ensemble. It is expected that more high-quality schedule solutions (i.e., with larger R here) can be found within an affordable computational cost as the optimization progresses.

6.3.3 Recovery priority ranking for stochastic case

When dealing with the stochastic case of the recovery scheduling optimization in Eq. (6.32), sampling methods are often used to draw N samples of $T_{b,repair}$ for each component from its distribution, and thus N realizations of deterministic optimization problems are created and each can be solved using the DEAEEO separately. A recovery priority ranking at the component level is introduced to aggregate the results of these N realizations and establish the relative priority of each damaged component in the recovery scheduling to improve the whole TN's resilience. This ranking is made by comparing the Copeland score (CS), which is a nonparametric ranking tool in the field of voting and has also been applied in the field of infrastructure resilience (Baroud and Barker 2018; Fang et al. 2016; Xu et al. 2020).

Specifically, the objects in the CS ranking are the distributions of random variables, and in this study refer to the CDFs of the completion times $T_{b,completion}$ of all damaged components, which are derived from the optimal solutions of N deterministic optimization problems. The CDF of component b 's completion

time is characterized using D percentiles denoted as $q_d(i)$ ($d = 1, 2, \dots, D$), where $q_d(i)$ represents the d^{th} percentile of the CDF of component b . The CS score is computed by pairwise comparison of percentiles of the CDF of $T_{b,completion}$ between any two damaged components and is defined for each component b as the difference between the number of times that CDF of $T_{b,completion}$ of component b is better than the CDFs of other components' $T_{b,completion}$ and the number of times that it is worse than others. The Copeland score $CS_d(i, j)$ indicating pairwise comparison between the CDFs of $T_{b,completion}$ for component i and component j with respect to $q_d(i)$ ($d = 1, 2, \dots, D$) is computed as follows:

$$CS_d(i, j) = \begin{cases} CS_{d-1}(i, j) + 1, & \text{if } q_d(i) < q_d(j) \\ CS_{d-1}(i, j) + 0.5, & \text{if } q_d(i) = q_d(j), \\ CS_{d-1}(i, j), & \text{if } q_d(i) > q_d(j) \end{cases} \quad \forall i, j \in \mathcal{B}, i \neq j, d = 1, 2, \dots, D \quad (6.41)$$

where $CS_0(i, j)$ is initialized as 0 for the first percentile. Then, the Copeland score for CDF of $T_{b,completion}$ of each component i is obtained by summation as below:

$$CS(i) = \sum_{j \in \mathcal{B}, j \neq i} CS_D(i, j), \quad \forall i \in \mathcal{B} \quad (6.42)$$

The priorities for components in the recovery scheduling are finally established by ranking these Copeland scores of all components from high to low: the higher the score, the higher the priority of component to the overall resilience-based recovery of the TN.

6.4 Illustrative example

A portion of real-world traffic network in Southern California is used here to demonstrate the proposed methodology. The chosen TN is distributed over Los Angeles and Orange counties and only includes freeway and state highways, which is represented as a directed graph consisting of 476 links and 154 nodes.

Since this TN is located in a high seismic region, the earthquake is chosen as the scenario hazard under investigation. The vulnerable components of TN are taken as only those bridges located on the links (Alipour and Shafei 2016; Bocchini and Frangopol 2012; Zhang et al. 2017) and a total of 2,027 bridges are considered here, as shown in Figure 6.4(a).

To create a post-earthquake damage scenario for recovery scheduling, an earthquake with magnitude of 8.5 and epicenter of depth of 15 km is assumed to occur in the eastern north of this region, as marked using pentagram in Figure 6.4. The ground motion attenuation relationship is used to estimate the peak ground acceleration (PGA) at each bridge's location (Campbell 1997; Lee et al. 2011). To estimate the damages on bridges, based on the National Bridge Inventory data (NBI 2016), these 2,027 bridges are further classified into 28 types of standard highway bridges specified by the HAZUS-MH manual (DHS 2009). Then the damage states of bridges under given PGA can be determined using the fragility curves for the corresponding standard bridges. Following the definitions in HAZUS-MH (DHS 2009), four damages states of the bridge are considered (from less severe degree to more severe degree): slight, moderate, extensive, and complete, and the corresponding degraded remaining ratios of traffic flow capacity δ_b^0 are assumed to be 0.75, 0.50, 0.25, and 0.00, respectively (Alipour and Shafei 2016; Lee et al. 2011). As a result, a total of 152 bridges sustain at least "slight" damage, which are depicted in Figure 6.4(b). The repair duration of a damaged bridge is dependent on its damage state and is assumed as a normal random variable with the statistics summarized in Table 6.3.

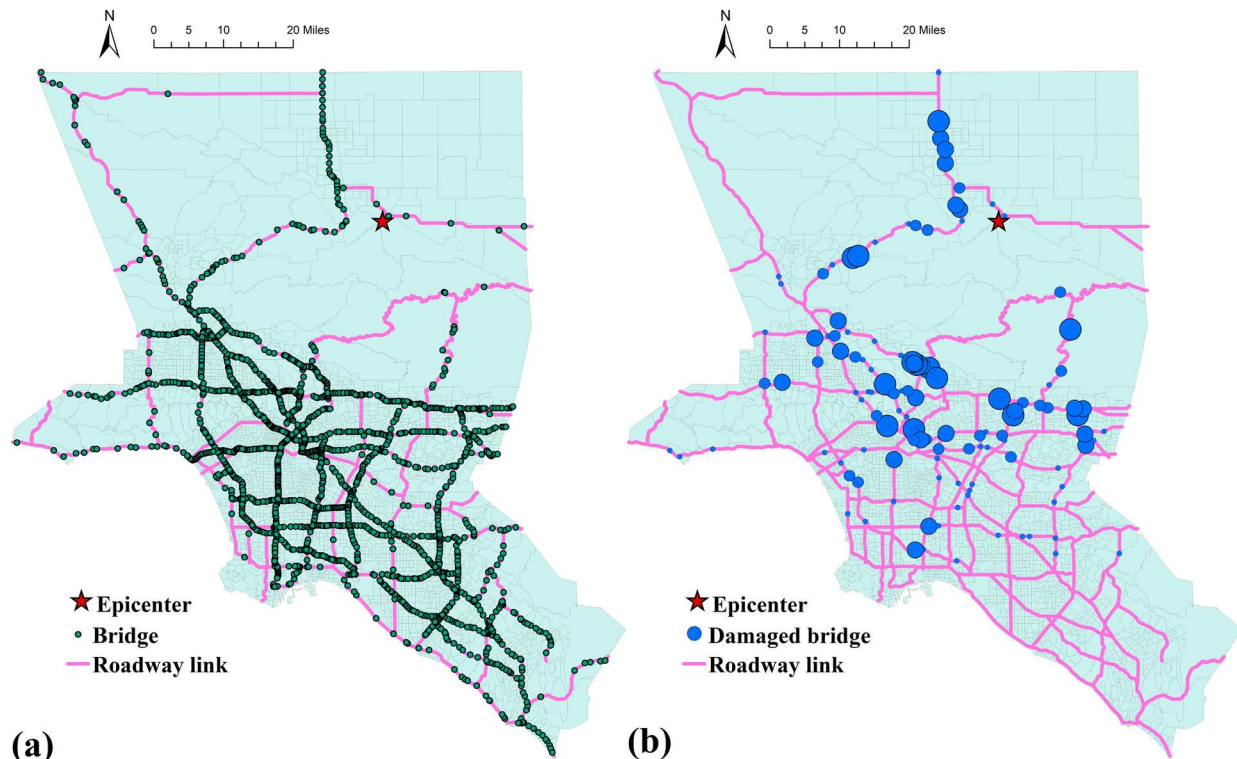


Figure 6.4 The selected roadway network in Southern California: (a) roadway links and all bridges; (b) the epicenter and damaged bridges (the size of blue circle indicates the experienced damage level)

Table 6.3 Statistics of repair duration $T_{b,repair}$ (DHS 2009; Zhang et al. 2017)

Damage state	Mean (month)	Coefficient of variation
Slight	[1.25, 2.50]	0.05
Moderate	[3.30, 5.25]	0.05
Extensive	[4.75, 6.55]	0.05
Complete	[6.65, 10.25]	0.05

The traffic demand data for the traffic assignment model is obtained from Southern California Association of Governments (SCAG 2016). A total of 2,794 OD pairs and 27,388 paths are considered for this TN. To account for the mixed traffic consisting of CAVs and HDVs, the penetration ratios of CAVs ρ in the traffic demands of all OD pairs are assumed to remain the same and are defined with the following equation:

$$\rho = q_A^w / (q_A^w + q_H^w), \quad \forall w \in W_A \cup W_H \quad (6.43)$$

where q_A^w and q_H^w are traffic demands of OD pair w for CAV and HDV users, respectively. ρ is set to a series of values, i.e., 0.00, 0.25, 0.50, 0.75, and 1.00, to investigate the effect of the penetration ratios of CAVs on the scheduling. The values of time for CAVs VOT_A and HDVs VOT_H are set as 10 and 5, respectively. The price of gasoline per liter η is set to 0.793 and the degree of nesting u and the dispersion parameter λ are set to 1 and 0.5, respectively.

Regarding the recovery scheduling optimization, three different numbers values (5, 10, and 15) of repair crews n_{crews} are considered. The recovery horizon is set as $[0, 60]$ (unit: month), and the time interval set as 1 month, i.e., $T = 60$ and $\Delta t = 1$. This means that to evaluate a single schedule sample \mathbf{x}_i to obtain the resilience metric R_i , the function $f(\cdot)$ in Eq. (6.39) needs to invoke the multiclass user traffic assignment model $T + 1 = 61$ times, which can be very computationally expensive considering the large number of paths in the traffic assignment model.

In the DEAEGO algorithm, the deep ensemble consists of $M = 5$ CNNs sharing the same structure, which is detailed in Table 6.4. Note that the dimension of the input tensor \mathbf{x}_i is $(1, 152, 61)$, corresponding to the number of channel, number of damaged bridges $|\mathcal{B}|$, and number of recovery time steps $T + 1$, respectively. The size of initial training set n_{start} , training epochs, learning rate, and batch size for training the deep ensemble are set to 200, 150, 0.001, and 20 based on some experiments. The *GAScheduleGenerator*(\cdot) in line 10 in Figure 6.3 uses the position-based crossover operator with probability of 0.7, and the two-point swapping mutation operator with probability of 0.1 to generate $n_{new} = 1,000$ new unevaluated schedule samples in each iteration (Li et al. 2019a; Murata et al. 1996). The number of

schedules being evaluated with $f(\cdot)$ in each iteration n_{eval} is set as 4 and the total number of optimization iterations K is set as 50 considering the available computational resources.

Although this example only demonstrates earthquake hazard and bridge damages, it is noted that the formulation and methodology are general enough to be applied to other types of hazards or infrastructure damages with some modifications.

Table 6.4 Hyperparameters of each CNN in deep ensemble

Layer	Name	Parameters	Dimensions
Input	—	—	(1, 152, 61)
Conv1	Convolution	(4, 3, 3)	(4, 152, 61)
	Batch Normalization	—	—
	Activation (ReLU)	—	—
	Dropout	$p = 0.1$	—
	Max-Pooling	(2, 2)	(4, 76, 30)
Conv2	Convolution	(8, 3, 3)	(8, 76, 30)
	Batch Normalization	—	—
	Activation (ReLU)	—	—
	Dropout	$p = 0.1$	—
	Max-Pooling	(2, 2)	(8, 38, 15)
Conv3	Convolution	(16, 3, 3)	(16, 38, 15)
	Batch Normalization	—	—
	Activation (ReLU)	—	—
	Dropout	$p = 0.1$	—
	Max-Pooling	(2, 2)	(16, 19, 7)
Conv4	Convolution	(32, 3, 3)	(32, 19, 7)
	Batch Normalization	—	—
	Activation (ReLU)	—	—
	Dropout	$p = 0.1$	—
	Max-Pooling	(2, 2)	(32, 9, 3)
Conv5	Convolution	(64, 3, 3)	(64, 9, 3)
	Batch Normalization	—	—
	Activation (ReLU)	—	—
	Average-Pooling	(9, 3)	(64, 1, 1)
Flatten	—	—	(64,)
FC1	Fully Connected	(64, 1)	(1,)
FC2	Fully Connected	(64, 1)	(1,)

Note: ReLU is the rectified linear unit activation function.

6.4.1 Deterministic case

The deterministic case shows the result of the recovery scheduling optimization within one sampled repair duration. First, the pre-hazard total travel costs of the intact TN TTC_{pre} under different penetration ratios of CAVs ρ are presented in Figure 6.5 since the TTC_{pre} is required by the normalized functionality metric of the TN Q_t in Eq.(6.22) to compute the resilience metric R in Eq. (6.23). It can be observed that when the total traffic demand is fixed, increasing the penetration ratio of CAVs can reduce the TN's total travel costs monotonically and significantly due to the lower value of time and increased link flow capacity, which indicates that replacing more traditional HDVs with the CAVs can be beneficial to the overall system's functionality improvement.

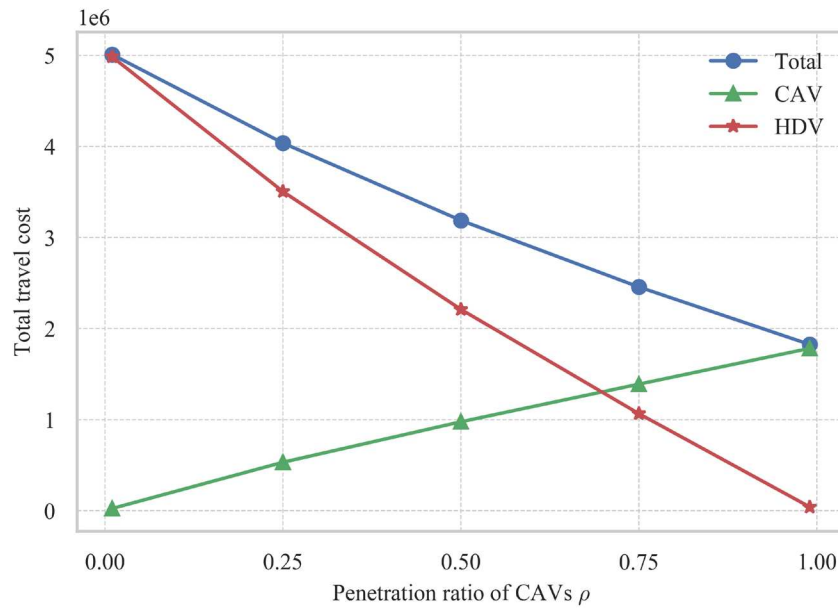


Figure 6.5 Variation of pre-hazard total travel cost with penetration ratio of CAVs

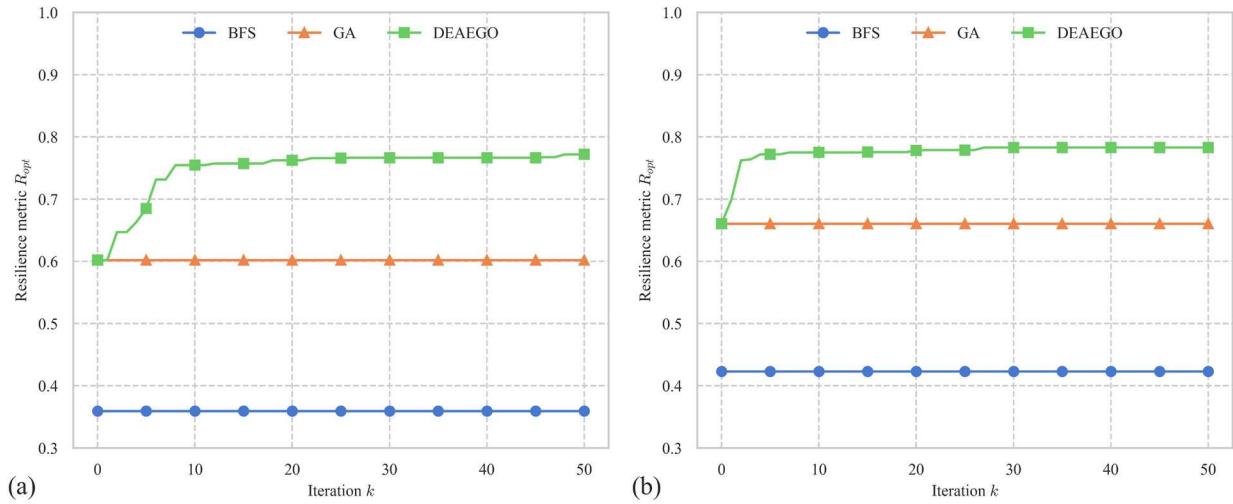
With TTC_{pre} being computed, the resilience-based scheduling optimization problem is established and solved with the proposed DEAEGO. In addition, for comparison purposes, two other methods introduced

in literature are also implemented (Fang et al. 2016; Li et al. 2019a): the betweenness-first strategy (BFS) and the GA. In the BFS, the betweenness of each damaged bridge is calculated and used as the indicator of the recovery priority, which is defined as the number of all shortest paths between all OD pairs that pass through this bridge, and the recovery schedule is constructed by arranging these bridges according to their betweenness values in descending order. In the GA, all generated schedule samples should be evaluated by the expensive function $f(\cdot)$; to draw a fair comparison with the DEAEEO and considering the computational cost, the same initial population set and crossover and mutation operators as in the *GascheduleGenerator*(\cdot) in DEAEEO are used and the number of samples to be generated and evaluated in each generation is also set to be the same value $n_{eval} = 4$ as in the DEAEEO.

Figure 6.6 shows the improvement process of the optimal resilience metric with iterations using these three methods under different penetration ratios of CAVs. It can be seen that the DEAEEO can rapidly find better schedule solutions resulting larger resilience objective R than the BFS and GA. Generally, the DEAEEO finishes the large part of the improvement in R in the first 10 iterations and thereafter R remains relatively steady. Except for the scenario with $\rho = 0.50$ in Figure 6.6(c), R is not increased significantly during the whole optimization due to the fact the high-quality solutions have already been found in the randomly generated initial training set. It should be noted that the recovery scheduling is for the whole TN, and for a large network, even a small improvement in the resilience metric based on the functionality could mean millions of dollars in economic saving (Ouyang et al. 2012; Zou and Chen 2020a).

In comparison, the GA, with the same setting as the *GascheduleGenerator*(\cdot) in DEAEEO, fails to improve the initial solution during the optimization process. This is because due to the very small number

of new samples to be generated and evaluated in each iteration ($n_{eval} = 4$), there is no guarantee that the GA can generate enough diverse and promising samples to explore the large solution space. By contrast, the assistance of the deep ensemble enables the DEAEGO to generate a sufficiently large number of samples ($n_{new} = 1,000$) for exploration and choose the only top $n_{eval} = 4$ most promising ones for evaluation which can greatly reduce the required computation effort. The BFS results in the worst resilience-based recovery schedule because the betweenness only considers topological characteristics of the TN but leaves out the traffic flow information, which indicates that the computationally simple betweenness cannot be a reliable indicator in devising the recovery plan.



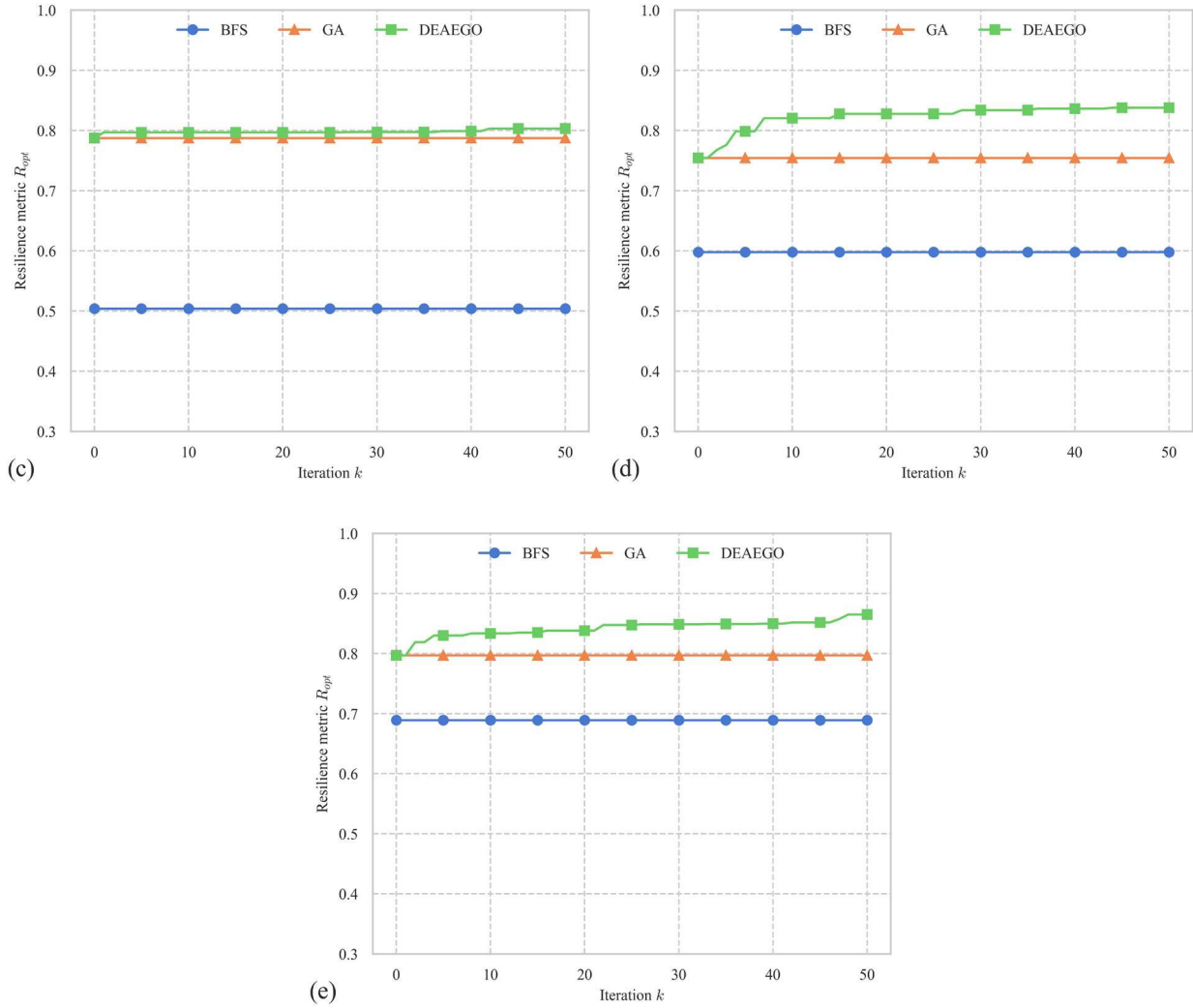
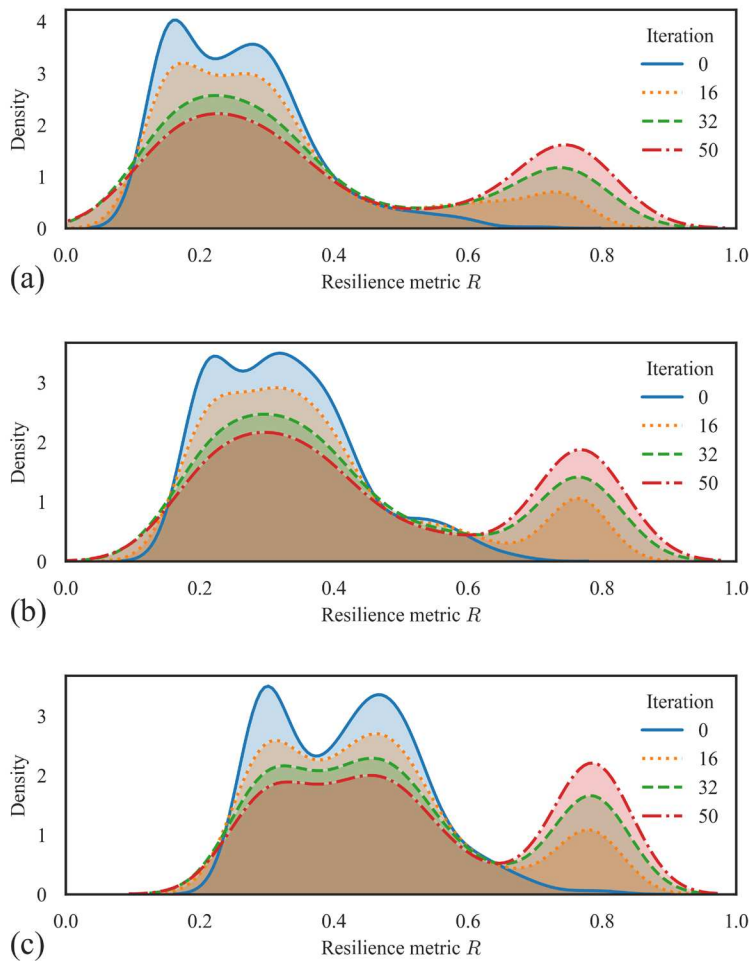


Figure 6.6 Evolution of optimal resilience metric with optimization iteration using BFS, GA, and DEAEGO under different penetration ratios of CAVs ($n_{crews} = 5$): (a) $\rho = 0$; (b) $\rho = 0.25$; (c) $\rho = 0.50$; (d) $\rho = 0.75$; (e) $\rho = 1$

To further illustrate that the DEAEGO actually generates more higher-quality samples over the optimization process, Figure 6.7 depicts the evolution of distribution of sampled resilience metrics with optimization iteration under different penetration ratios of CAVs. It can be found that in all scenarios, in the beginning of the optimization, some peaks exist in the range of lower values, representing that the resilience metrics of randomly generated initial training set concentrates in this range; as the optimization progresses, a new peak emerges gradually in the range of higher values, indicating that more samples corresponding to

higher resilience metrics are found and accumulated and thus impact the distribution shape of sampled resilience metrics. It is also observed from Figure 6.7(a)–(e) that with the increase of penetration ratio of CAVs, the distribution of sampled resilience metrics demonstrates a rightward shift, which means that more CAVs lead to better resilience of the TN in the recovery scheduling. This trend can also be found in Figure 6.6(a)–(e): the final optimal resilience metrics of three methods all increase with the rise of penetration ratio of CAVs.



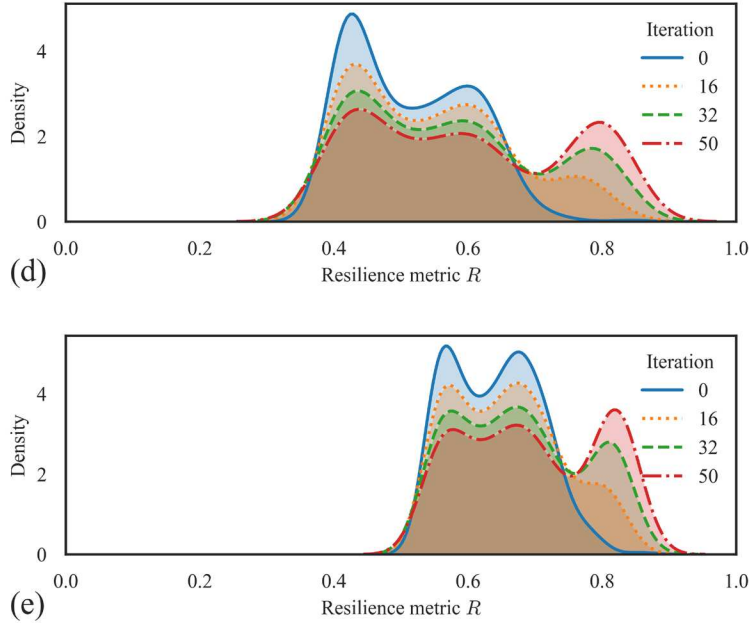


Figure 6.7 Evolution of distribution of sampled resilience metrics with optimization iteration using DEAEEO under different penetration ratios of CAVs ($n_{crews} = 5$): (a) $\rho = 0$; (b) $\rho = 0.25$; (c) $\rho = 0.50$; (d) $\rho = 0.75$; (e) $\rho = 1$

Figure 6.8 shows the recovery trajectories of final optimal schedules derived with three methods under different penetration ratios of CAVs. It can be seen that the optimal recovery trajectory from the DEAEEO nearly envelopes the recovery trajectories from the BFS and GA from the top in each scenario, implying a larger resilience metric. Moreover, the DEAEEO solution exhibits large functionality improvement in the early stage of the recovery horizon (i.e., the first 10 months). This can be desirable and critical in practice as the TN can be restored to a less degraded state in a timely manner, so not only can the economic loss of TN itself be reduced, but the recovery of other infrastructure dependent on TN's functionality can be accelerated at the same time. In contrast, the BFS solution gives the worst recovery trajectory, in which the functionality level of TN remains nearly the same as the disrupted one immediately after hazard without recovery until about 30 months; the GA's recovery trajectory lies in between DEAEEO's and BFS's trajectories.

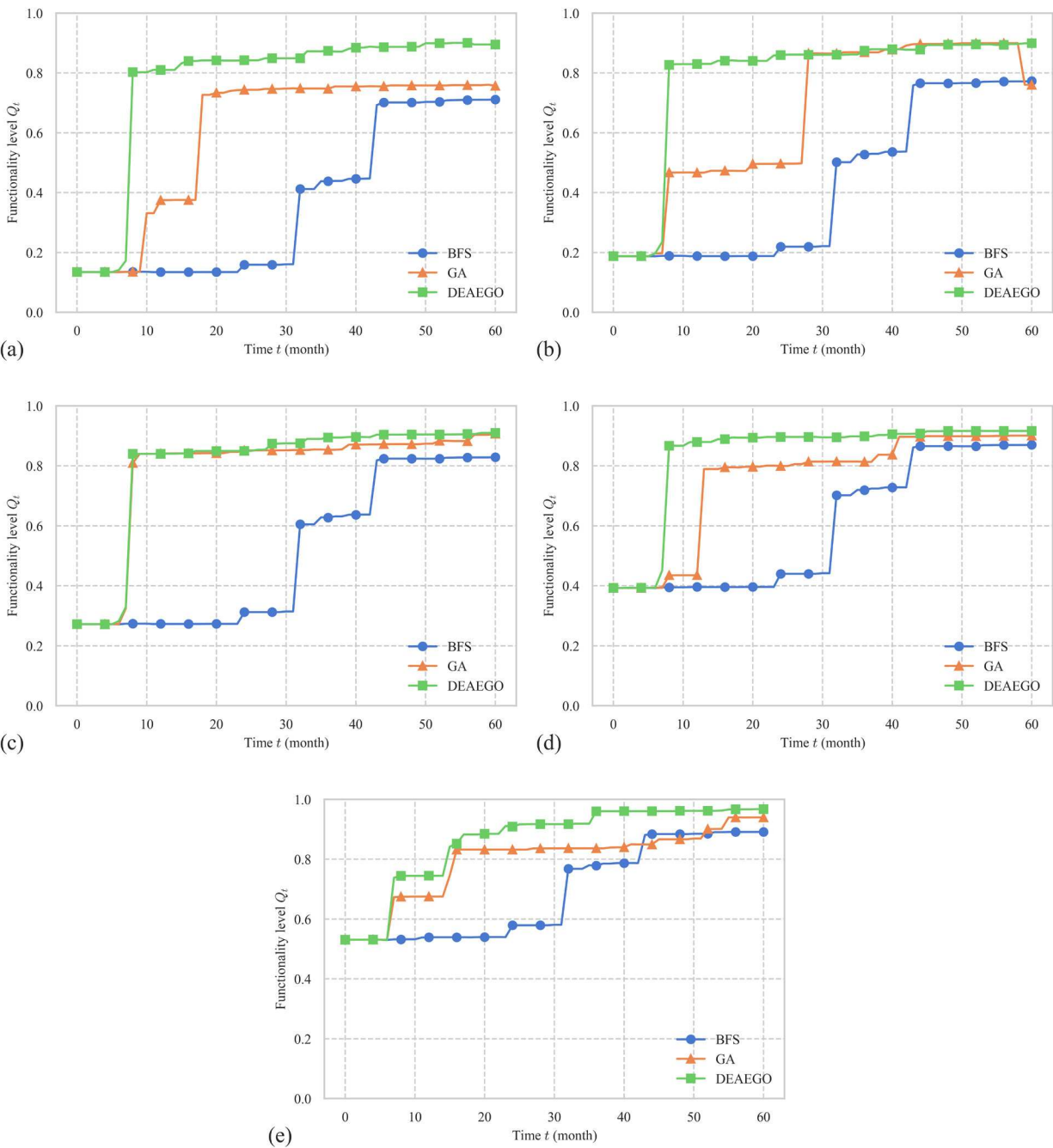
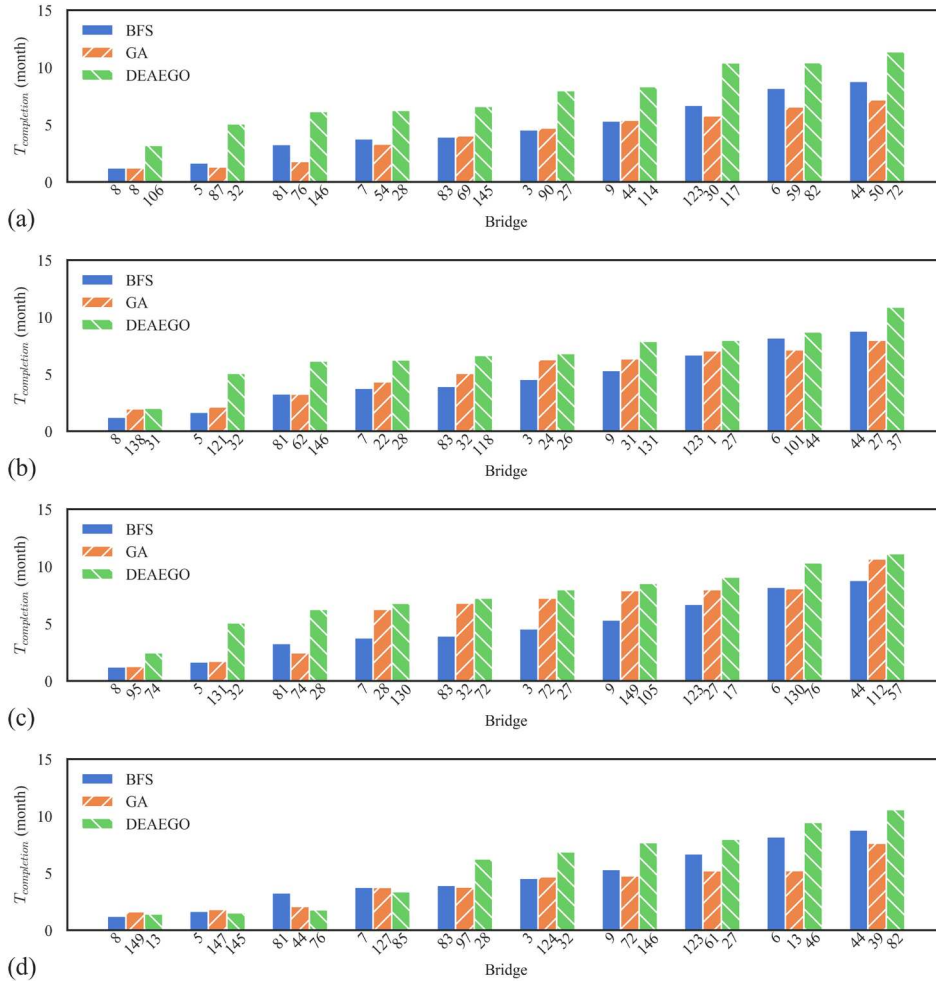


Figure 6.8 Optimal recovery trajectories of BFS, GA, and DEAEGO under different penetration ratios of CAVs ($n_{crews} = 5$): (a) $\rho = 0$; (b) $\rho = 0.25$; (c) $\rho = 0.50$; (d) $\rho = 0.75$; (e) $\rho = 1$

Figure 6.9 further compares the earliest 10 bridges being repaired from the three methods. It shows that different methods result in different priorities in bridge selection for repair schedule. Interestingly, the bridges selected from DEAEGO generally show longer repair completion time than those from BFS and

GA. Along with observations from Figure 6.8, it can be inferred that the DEAEGO optimizes the schedule by arranging important bridges in higher priority, which may require a little longer repair completion time at first due to the severer damage states, but can eventually lead to large functionality improvement of the overall TN in the early stage of the recovery horizon. In addition, Figure 6.9(a)–(e) also show that the optimal recovery schedule varies in the bridge repair sequence under different penetration ratios of CAVs, which indicates that the presence of CAVs improves the functionality of the TN and thus may affect the recovery planning.



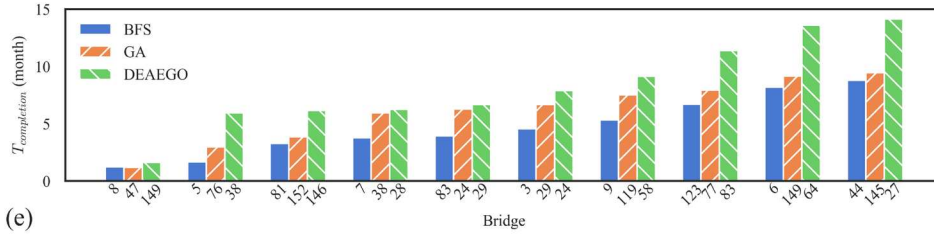


Figure 6.9 The earliest 10 bridges being repaired from BFS, GA, and DEAEGO under different penetration ratios of CAVs ($n_{crews} = 5$): (a) $\rho = 0$; (b) $\rho = 0.25$; (c) $\rho = 0.50$; (d) $\rho = 0.75$; (e) $\rho = 1$

The impact of the penetration ratio of CAVs on the resilience-based recovery scheduling optimization is further investigated and depicted in Figure 6.10. It can be observed that increasing the ratio of CAVs in the fixed total travel demand can monotonically drive up the optimal resilience metric achieved by the DEAEGO. Since the functionality index used to compute the resilience metric is a normalized one as in Eq. (6.22), it can be deduced that more CAVs in the mixed traffic are beneficial to the recovery of the overall TN after the disruption. Meanwhile, Figure 6.10 also shows that more available recovery sources, i.e., more repair crews here, can result in higher resilience objective in the recovery scheduling, which is as expected because more damaged bridges can be repaired simultaneously.

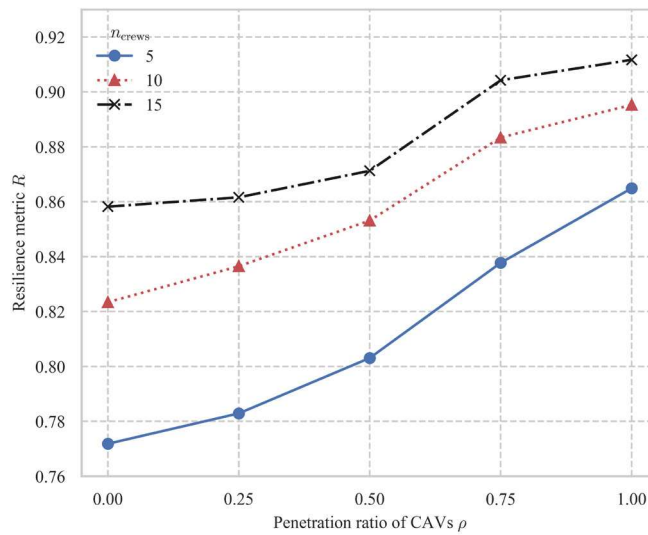


Figure 6.10 The variation of optimal resilience metric with the penetration ratio of CAVs under different number of repair crews

Results presented in Figure 6.6–Figure 6.10 demonstrate that even under relatively stringent computational budget (i.e., the total number of optimization iterations $K = 50$ and number of samples to be evaluated $n_{new} = 4$), the DEAEGO can still solve the recovery scheduling problem efficiently and effectively to find the optimal schedule enhancing the resilience of TN and outperform the BFS and GA.

6.4.2 Stochastic case

In the stochastic case, the repair durations of damaged bridges are regarded as the normal random variables, and the Monte Carlo simulation is used to generate $N = 20$ samples; therefore, the corresponding 20 deterministic resilience-based recovery scheduling optimization problems are constructed and solved by the DEAEGO separately. Then, the CS of each damaged bridge is obtained, and the recovery priority is established according to Eqs. (6.41) and (6.42).

Figure 6.11 illustrates the top 30 bridges based on the CS ranking on repair completion time under different penetration ratios of CAVs, and the locations of these bridges are marked in the map shown in Figure 6.12. Similar to the deterministic case, the expected resilience objective also increases with the growth of the CAV penetration ratio, and different CAV penetration ratios result in different rankings of CSs of the bridges, corresponding to different optimal schedules. Many of these bridges in high priority of repair scheduling under different CAV penetration ratios differ in their locations, as depicted in Figure 6.12. It is also noted that among these different CS rankings of bridges, there are some common bridge selections shared across scenarios with different penetration ratios of CAVs which are scheduled to be repaired in the early stage of the recovery horizon. The red bars in Figure 6.11(a)–(e) mark the common bridge selections of the earliest 10 bridges being repaired in the recovery scheduling under different CAV penetration ratios. Figure 6.12 further shows that these common bridges are mainly located in an eastern area of the TN with

the largest number of overlapped colored circles, which are marked with the dashed black box in the map.

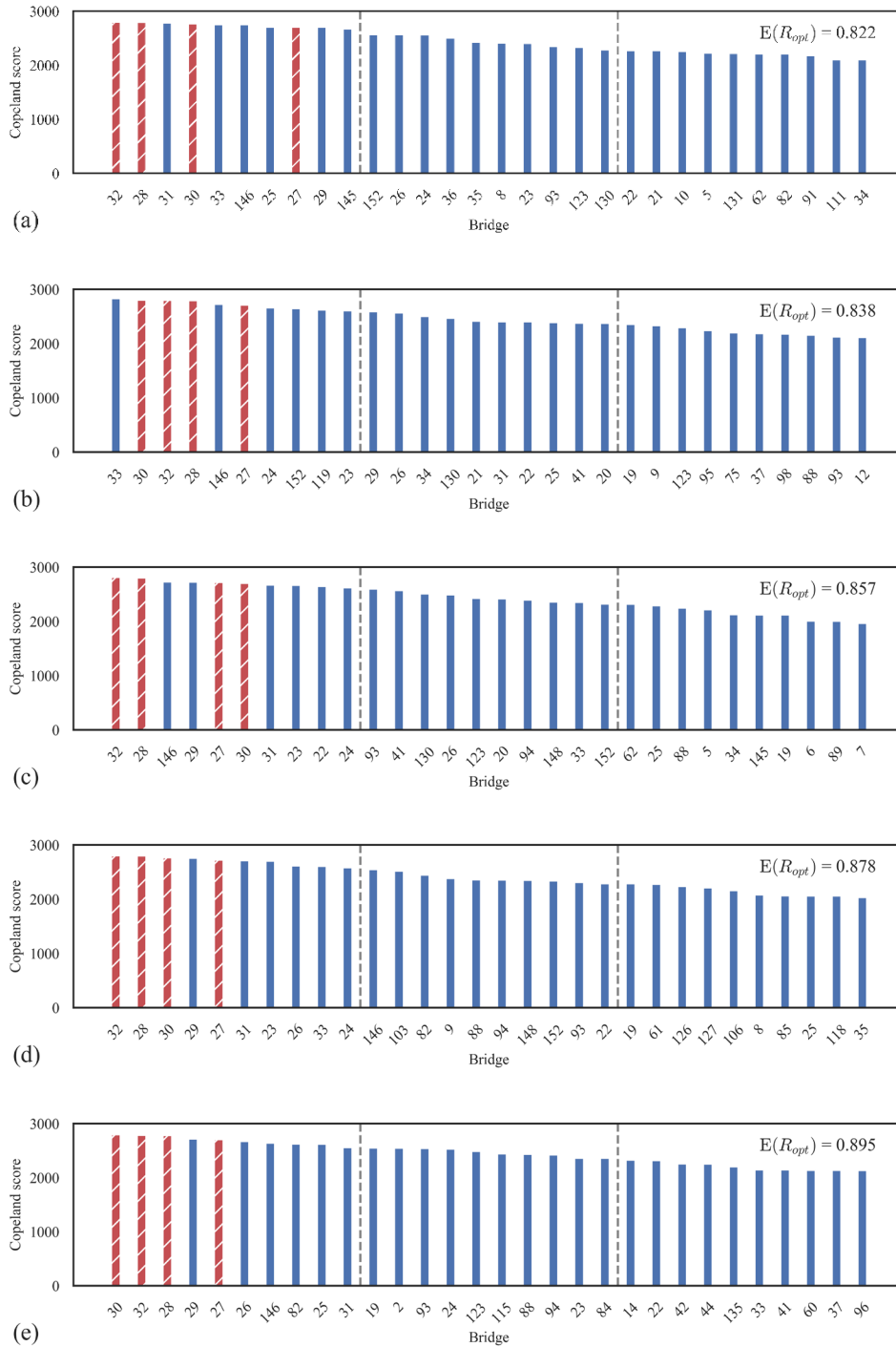


Figure 6.11 Top 30 bridges based on stochastic ranking on repair completion time under different penetration ratios of CAVs ($n_{crews} = 10$): (a) $\rho = 0$; (b) $\rho = 0.25$; (c) $\rho = 0.50$; (d) $\rho = 0.75$; (e) $\rho = 1$

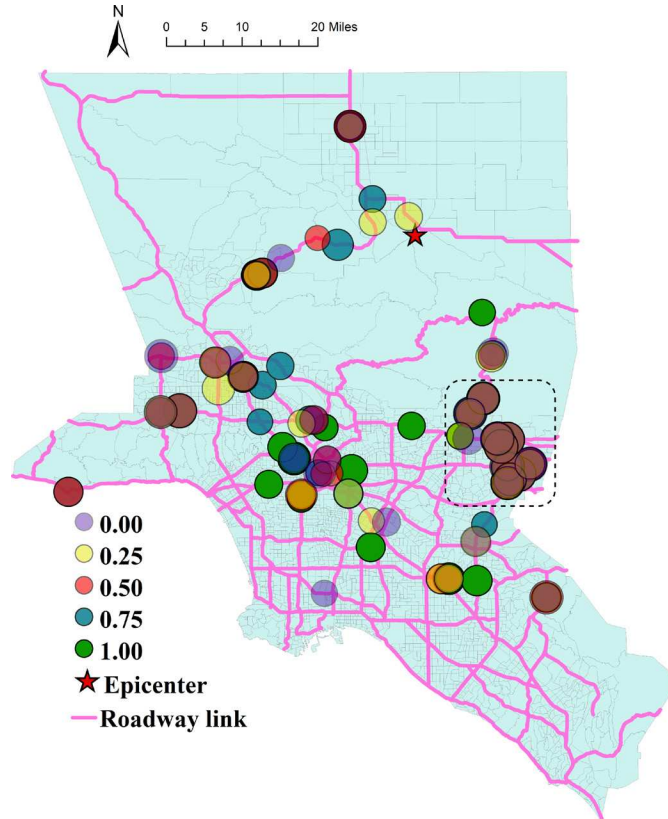


Figure 6.12 Locations of top 30 bridges based on stochastic ranking on repair completion time under different penetration ratios of CAVs ($n_{crews} = 10$)

To compare the ranking results of bridges based on the proposed DEAEGO algorithm with their betweenness values used in the BFS, the correlation coefficients (CRs) between the CSs and the betweenness values under different penetration ratios of CAVs are examined, as shown in Figure 6.13. It can be found that CRs in all scenarios are very low, i.e., less than 0.06, which means that the betweenness values have no obvious correlation with the CSs and therefore are not good indicators in guiding the resilience-based recovery scheduling.

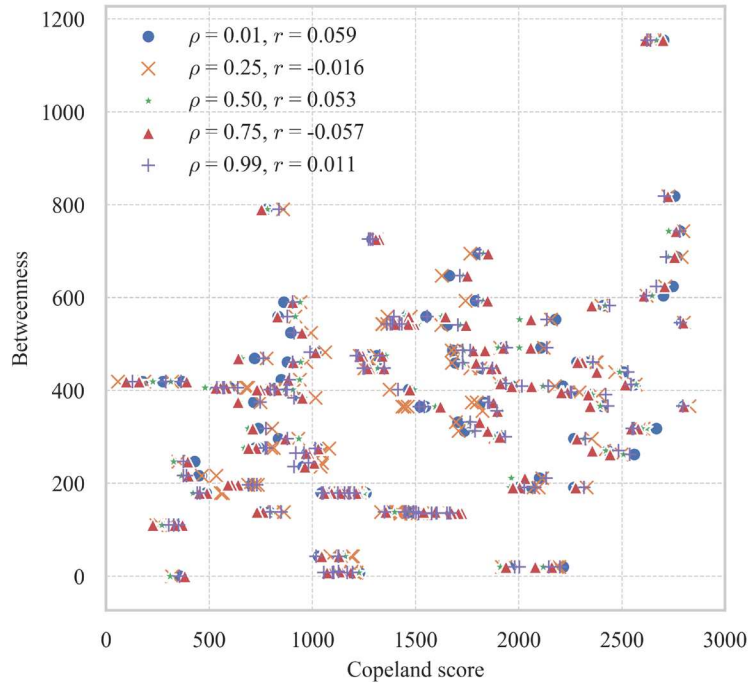


Figure 6.13 Scatterplot of the Copeland scores with the betweenness values of damaged bridges

6.4.3 Computational cost

All analyses in this study are coded using Python 3.7.4 and the deep CNN ensemble is realized using PyTorch 1.4.0. The computations are carried out on a desktop computer with an Intel core i7-6700 3.40 GHz CPU, a 16 GB RAM, and a 64-bit Windows 10 operating system. The running time of evaluating each schedule sample in the optimization (i.e., $f(\cdot)$ in Eq. (6.33)) is about 15 min due to the multiple invokes of iterative path-swapping procedure for the multiclass user traffic assignment model. The running time of training the deep ensemble in each iteration without GPU support is about 4 min. So for each combination of CAV penetration ratio and number of repair crews, it takes approximately 50 h to prepare the initial training set of the size of 200 for the DEAEEO and GA, and additional 64 h and 50 h to complete 50 optimization iterations of DEAEEO and GA, respectively. Although the GA takes shorter running time, the GA fails to improve the solutions from the randomly generated initial training set due to the very small number of samples to be generated and evaluated in this study. To make the GA work requires increased

number of samples to be evaluated using the expensive function $f(\cdot)$, which would significantly increase the computational cost to a prohibitive level. The efficiency of the DEAEEO can be further improved from the perspectives of the computational setting (e.g., training the deep ensemble on a GPU-enabled cluster) and algorithm (e.g., optimizing the convergence speed of the path-swapping algorithm).

6.5 Conclusions

This chapter presents a bi-level decision model for the resilience-based recovery scheduling of the TN in a mixed traffic environment in the presence of both CAVs and HDVs. The lower level quantifies the functionality of TN over time in the recovery process. Two types of users are considered with different levels of information perception and travel behavior: the CAV users are well-informed thanks to the advanced communication and automation technologies and the travel behavior is characterized using the UE model while the less-informed HDV users' behavior is described using the CNL model. The upper level presents the novel DEAEEO algorithm for solving the network recovery scheduling problem balancing optimization performance and computational cost. The deep CNN ensemble is fed with high dimensional schedule solutions as images and are trained to predict both mean and standard deviation of the resilience-based recovery metrics. This uncertainty quantification capability enables the deep ensemble not only to assist in exploring the large solution space sufficiently as a computationally cheap surrogate function, but also to be combined with the EGO algorithm to be sequentially updated in an active learning fashion and lead the optimization in the right direction to find improved recovery schedule solutions.

With the adoption of different travel behavior of CAV and HDV users and the adjustable CAV penetration ratio, the proposed framework can help decision makers better quantify the functionality of TN to support effective recovery scheduling of TN by preparing themselves for the transition from HDV-

dominant traffic to the future CAV-dominant traffic. The proposed DEAEGO algorithm can effectively and efficiently improve the recovery schedule in terms of the resilience improvement considering more complex and realistic low-level network functionality quantification with the potential to be extended to general large-scale network recovery scheduling optimization problems. The proposed methodology is demonstrated using a real-world traffic network in Southern California after an earthquake considering deterministic and stochastic repair durations.

The main findings of this study include: (1) the DEAEGO outperforms the BFS and GA and can find better recovery schedules efficiently resulting greater resilience of the TN; (2) different penetration ratios of CAVs lead to different optimal recovery schedules and more CAVs facilitate the recovery of the TN; (3) in the stochastic case, the recovery priority of each damaged bridge can be established based on the CS ranking and reflect the relative importance and contribution of each bridge in the resilience-based recovery of the whole TN.

7.1 Summary and conclusions

The contributions and findings of this dissertation are summarized in the following, which correspond to Chapter 2 to 6:

- (1) An agent-based crowd model to simulate passenger movements under normal conditions and evacuations under extreme conditions is established including people from both the subway trains and platform. Some detailed configurations of the station and pedestrians' different behavior are considered. Parametric studies including some main variables are conducted and the impacts of several major variables on the evacuation time are also discussed. Different from the previous studies focusing on some single aspects of the evacuation of people inside the subway station, this study provides a more comprehensive and holistic model for assessing the egress safety of a typical subway station for people in both trains and platforms under normal and extreme conditions. Some valuable insights are made from the demonstration and parametric study to understand the major causes of delay of evacuations and possible improvements of the subway system design in terms of emergency response. It is also found that more comprehensive studies based on specific emergency events are needed to provide more customized analysis, which can provide the site- and event-specific emergency response plan including optimal routes and potential design improvements for different emergency incidents.
- (2) A new methodology is proposed for crowd evacuation simulation under toxic gas incident considering the effects of emotion contagion and information transmission. The concentration of the toxic gas quantified by the gas dispersion model determines the casualty and the impairment of the pedestrian

mobility. The spread of the information about the incident and the exits is modeled by the information diffusion model. The emotion contagion model quantifies the emotion and panic. Then the social force model is modified to integrate these effects to govern the movements of people in the evacuation process. Two cases, i.e., room with one and two exits, were used to demonstrate the proposed simulation framework. The effects of number of agents, perception radius, and ratio of authority figures on the evacuation process are further examined. This study highlights the importance of human factors, i.e., emotion and perception, on the crowd evacuation simulation in emergency scenarios. The proposed model and findings can help implement more effective emergency evacuation planning strategy, including adopting some smart sensing and information sharing technology through artificial intelligence and incorporating more realistic modeling of pedestrians' behavior.

- (3) A holistic framework is proposed for the resilience assessment of an interdependent traffic-electric power system subject to hurricanes. Based on the graph theory, the traffic and electric power systems are represented by two directed graphs and three typical types of interdependencies are captured. A modeling procedure coupled with Monte Carlo simulation is presented to assess the resilience of both systems and to integrate different improvement strategies into corresponding stages of resilience. The traffic and electric power systems in Centerville considering three improvement strategies are studied to demonstrate the proposed framework. The results show that interdependencies can significantly affect the resilience of both systems, leading to different most effective strategies for each system. While hardening hurricane-vulnerable components and adopting a better repair schedule both improve resilience of the electric power system significantly, adopting a better repair schedule works best for the resilience of the traffic system. The equal repair mode can achieve the resilience improvement in a

balanced fashion. The results also highlight the importance of repair scheduling to the resilience improvement of these two interdependent systems when the available recovery resources are limited. Due to the interdependencies, the faster the functionality of traffic system can recover, the more efficiently the repair activities can be conducted and thus the greater resilience of both systems can be achieved.

- (4) A bi-level, stochastic, and simulation-based decision-making framework is proposed to prioritize mitigation and repair resources to maximize the expected resilience improvement of an interdependent traffic-electric power system under budgetary constraints. The upper level of this framework aims to find the optimal plan of allocating limited mitigation and repair resources to multiple disrupted components to estimate the maximum attainable functionality gain. At the lower level, the functionalities of the traffic and electric power systems are obtained based on network analysis methods. Three types of interdependencies have been considered. The problem is solved by the binary particle swarm optimization (BPSO) combined with the knapsack-based heuristic and mitigation and repair priorities of disrupted components are then established based on the solutions. Results show that:
- (a) the preference parameter in the framework can be set to different values to obtain corresponding mitigation and repair resource allocation plan according to the decision-maker's preference or needs;
 - (b) the established priority indices can reflect the importance and contribution of components to the resilience improvement of the coupled system in both mitigation and repair actions;
 - (c) the modified BPSO can produce better resource allocation plan than the knapsack-based heuristic to achieve greater resilience improvement.
- (5) A bi-level decision model is proposed for the resilience-based recovery scheduling of the TN in a

mixed traffic environment with connected and autonomous vehicles (CAVs) and human-driven vehicles (HDVs). The lower level quantifies the TN's functionality over time considering different travel behavior of CAV and HDV users arisen from their different levels of information perception. The upper level presents a novel deep-ensemble-assisted active learning approach to balance optimization performance and computational cost. This framework can help decision makers better quantify the TN's functionality to support effective recovery scheduling of TN with different mixed traffic scenarios ranging from HDV-only to future CAV-dominant traffic. The optimization approach bears the potential to be extended to solving general large-scale network recovery scheduling problems effectively and efficiently.

7.2 Directions for future research

Some possible improvements and extensions in future based on the current research are discussed in the following.

7.2.1 Walking mobility

The proposed crowd simulation models in Chapter 2 and Chapter 3 aim to investigate the egress behavior in complex subway station environment and characterize interplay among emotion contagion, information diffusion, decision-making process, and crowd dynamics, respectively.

Due to the scope limit, the proposed models are not free of limitation and some potential improvements or extensions may be of interest for future research.

First, further experimental and observation data can be used to calibrate some key parameters of the proposed agent-based model in Chapter 2 to achieve more realistic and site-specific simulation results. Hazardous scenarios (e.g., fire and toxic gas) can also be incorporated. And more comprehensive studies

based on specific emergency events are needed to provide more customized analysis, which can provide the site- and event-specific emergency response plan including optimal routes and potential design improvements for different emergency incidents.

Second, more complex indoor environment can be considered in the proposed model in Chapter 3. The current model carries out the simulation in a room with a simple layout. Realistic buildings can be much more complex (e.g., different layouts, multiple stories, furniture, many exits and routes), as the subway station in Chapter 2. More advanced computational fluid dynamics (CFD) -based gas dispersion model can be adopted to simulate the hazardous scenarios.

Third, the emotion contagion and information transmission models in Chapter 3 can be refined. Only the dimension “neuroticism” in the OCEAN personality model was used to establish the methodology. The effects of the other four dimensions of personality (i.e., “openness”, “conscientiousness”, “extroversion”, and “agreeableness”) on the emergency evacuation and information transmission have yet to be explored. Meanwhile, the information can have different levels of complexity and uncertainty and human can display heterogeneous behavior in their perception and reasoning process. Quantifying the diffusion of complex information and its effect on the crowd dynamics remains a challenging task.

Fourth, the parameters of human factors in the proposed model in Chapter 3 need to be further calibrated. It is recognized that validating a numerical evacuation model considering human factors against the real world scenario is usually challenging because human behavior is highly complex and the related dataset, especially for the true disaster scenarios, is often lacking (Choi et al. 2018; Liu et al. 2015). Therefore, existing efforts in this area still mainly center on the simulation technology to obtain a better understanding of emergency egress behavior. To the best knowledge of the authors, the data for the

described toxic gas incident is unfortunately not available to calibrate this model at this point. To generate such data, the most common method is conducting the post-event survey, which involves interviewing with survivors and analyzing surveillance video and incident reports. But in practice, related reliable records are usually scarce and incomplete (Zou et al. 2017). Another way usually comes from conducting experiments (e.g., evacuation drill). However, due to the safety and ethical issues, such experiments require careful preparations and many resources (e.g., environment setting, volunteer recruiting, survey design, and data collection). Moreover, it was found that since the drill scenario usually cannot be set as a true hazardous one, the participants may behave rationally and calmly, which cannot effectively replicate the panicking behavior of interest in the emergency scenarios (Liu et al. 2015). Other researchers also proposed using animals such as ants (Shiwakoti and Sarvi 2013) to perform emergency evacuation experiments, although debates still remain in terms of whether the behavior found from animals can be generalized to humans.

A promising solution to this problem may rely on the emerging virtual reality (VR) technology. The advantage of this technology is that it can conveniently create near real-life, low-risk, and highly controllable immersive virtual environments (Zou et al. 2017), which is especially desirable for the emergency evacuation behavior studies. Recent years have seen some exploratory studies that investigated the emotional responses in virtual evacuation tasks and tested the ecological validity of the VR-based results. Ergan et al. (2018) quantified the effect of architectural design features on human physiological, emotional, and cognitive statuses with the help of the VR and body sensor networks. Cao et al. (2019) examined the effect of spatial exploration mode on the wayfinding behavior during a virtual fire emergency.

Based on these emerging studies, the application of the VR technology for validation of the proposed model may include the following key points:

- (1) Creating the high-fidelity immersive virtual environment. The quality of the data collecting using the VR technology depends on the ecological validity, i.e., whether the findings in the virtual environment can be generalized to real-world scenarios. It was found that virtual environments with different levels of realism can arouse distinguishable emotional responses (Tucker et al. 2018; Zou et al. 2017). High details of visual and audio effects in the real-world setting should be replicated in the virtual environment with appropriate VR equipment.
- (2) Developing subjective and objective measures assessing the emotional states and information perception of evacuees. The subjective measures based on the self-report questionnaires can include the exit choice, the knowledge of the incident, the emotional contagion scale, which reflects the tendency to resonate with others' emotions, and the empathic concern scale of the interpersonal activity index, which represents the propensity of affective reactions to others' emotions (Neves et al. 2018). The objective measures refer to physiological indicators such as galvanic skin response and heart-rate variability which are strongly correlated with the emotional responses (Stephens et al. 2010). Zou et al. (2017) showed that these measures have the potential to be used to evaluate the emotional responses in the virtual evacuation environment. However, the scales of these measures differ from value ranges of parameters of the proposed model in Table 3.3. Therefore, it requires further research to establish appropriate mappings from the psychological and physiological metrics to the corresponding parameters.
- (3) Calibrating the parameters in the social force model with the evacuation data from the virtual evacuation environment. After introducing the effects of information transmission and emotion contagion, the values of the parameters being used the original social force model

may not be suitable to reflect the crowd dynamics obtained from the VR experiments. Lovreglio et al. (2015) used the maximum likelihood estimation to calibrate the parameters of the cellular automata model with the trajectory data from the VR experiments. Although the differential-equation-based social force model is different from the discrete, probabilistic cellular automata model, the calibration can still be done using other types of evacuation data. An optimization problem can be established with the goal of minimizing the difference between the outflow record of evacuees or the variation of crowd density obtained from the model and that from the VR experiments (Li et al. 2015).

7.2.2 Driving mobility

7.2.2.1 Resilience of interdependent traffic-electric power system subject to hurricanes

Chapter 4 and Chapter 5 present resilience modeling and decision-making frameworks for the interdependent traffic-electric power system subject to hurricanes, respectively. The proposed framework can be further refined, and the following potential improvements or extensions may be of interest for future research:

- (1) A more advanced hurricane hazard model can be incorporated. By collecting the time-dependent data of a real hurricane, including the wind speed, the center pressure, the landing time, the duration, the impacted area, and the moving path, a detailed time-varying wind field of the hurricane can be created based on real data. The detailed damage propagation process of the hurricane on the TN and EPN can be modeled, which can demonstrate how fast the functionality levels of the two systems drop off during the hazard.
- (2) More realistic O-D traffic demands before and after hurricane can be used. Forecasting the

uncertain post-hazard traffic demand is important because the authorities can make more timely and effective plans for evacuations, rescue, and recovery. However, it remains as a very challenging task since socio-economic and behavioral analyses are required and can introduce additional level of uncertainty. Future work may involve collecting available data to update the O-D demand matrix to reflect the evolution of the post-hazard traffic demand over time.

- (3) The locations for the depot nodes for the repair teams can be optimized as a preparedness strategy. Since the repair teams are all dispatched from the depot nodes after the systems are disrupted, the location of these depot nodes in the TN can impact the accessibility and the speed of the repair teams reaching the locations of damaged components. Strategically choosing locations of depot nodes before the disaster is expected to increase the dispatching efficiency and accelerate the whole recovery process. This problem bears a resemblance to the classical facility location problem (FLP) and vehicle routing problem (VRP), which are both NP-hard. It may require developing tailored solution methodology to exploit the problem structure. Moreover, due to the probabilistic nature of the hazard impact, the repair demand (i.e., where and how many the damage components are) after the hazard is uncertain. Determining the optimal locations of depot nodes considering the uncertainty of the hazard impact can be challenging and usually requires stochastic or robust optimization techniques. In addition, when multiple depot nodes exist, how the total repair resources can be optimally assigned to each depot node should also be taken into account.
- (4) The recovery process can be refined. These studies in Chapter 4 and Chapter 5 simplify the resource requirements for repairing the damaged components: it assumed that a set of generic

recovery resource units (or repair teams) is available and each damaged component only requires one unit of resource for recovery. In practice, the collaboration of multiple repair teams may exist, and the repair teams usually are not generic, rather only performing certain types of repair activity. For example, the repair teams for recovering EPN may not carry out the task of debris removal for restoring TN. Moreover, the repair teams can compete for other limited shared recovery resources such as machines, vehicles and materials. These factors can be integrated into current framework to better simulate the recovery process in detail. For example, a collaboration probability may be introduced to account for the multiple repair teams working on the same task.

- (5) The importance ranking method used to determine the repair schedule may result in a suboptimal solution, and more advanced discrete optimization algorithms can be applied to find a near-optimal repair schedule maximizing the resilience. The DEAEGO algorithm proposed in Chapter 6 can be used.
- (6) The realistic repair durations can be different from the pre-estimated ones, and the repair schedule should be dynamically adjusted during the process with the updates of actual schedule.

7.2.2.2 Resilience-based recovery scheduling of transportation networks

Chapter 6 presents a decision model for the resilience-based recovery scheduling of the TN considering multiclass users' travel behavior and proposes the DEAEGO to solve general large-scale network recovery problem efficiently. The proposed decision model can be further improved. First, as in Chapter 4 and Chapter 5, this study also assumes that the post-hazard traffic demand data is same as the pre-hazard one.

Since the traffic data affects the functionality quantification of the TN, more realistic post-hazard OD traffic demand data can be incorporated when such site-specific data is available. Second, the choice of the recovery scheduling optimization objectives depends on different recovery goals and decision maker's judgement; sometimes multiple objectives can exist and even compete with each other, the DEAEGO can be extended to the multi-objective recovery scheduling optimization. Third, in reality, the TN can be functionally and geographically interdependent with other infrastructure systems, and such interdependencies, if significant, may impact the recovery processes of these systems and should be included in the future studies of recovery scheduling. The interdependency modeling in Chapter 4 and Chapter 5 can be incorporated.

REFERENCES

- Abdelghany, A., Abdelghany, K., Mahmassani, H., and Alhalabi, W. (2014). "Modeling framework for optimal evacuation of large-scale crowded pedestrian facilities." *Eur. J. Oper. Res.*, 237(3), 1105–1118.
- Abedi, A., Gaudard, L., and Romerio, F. (2019). "Review of major approaches to analyze vulnerability in power system." *Reliab. Eng. Syst. Saf.*, 183, 153–172.
- Adjetej-Bahun, K., Birregah, B., Châtelet, E., and Planchet, J. L. (2016). "A model to quantify the resilience of mass railway transportation systems." *Reliab. Eng. Syst. Saf.*, 153, 1–14.
- Ahmed, S., Dey, K., and Fries, R. (2019). "Evaluation of transportation system resilience in the presence of connected and automated vehicles." *Transp. Res. Rec.*, 2673(9), 562–574.
- Alipour, A., Aly, A. M., Davis, B., Gutierrez Soto, M., Kijewski-Correa, T., Lenjani, A., Lichty, B., Miner, N., Roueche, D., Salman, A., Smith, D., Sutley, E., Mosalam, K., Prevatt, D., and Robertson, I. (2018). *StEER - Hurricane Michael: Preliminary virtual assessment team (P-VAT) report*.
- Alipour, A., and Shafei, B. (2016). "Seismic resilience of transportation networks with deteriorating components." *J. Struct. Eng.*, 142(8), C4015015.
- Almeida, J. E., Kokkinogenis, Z., and Rossetti, R. J. F. (2012). "NetLogo Implementation of an Evacuation Scenario." *2012 7th Iber. Conf. Inf. Syst. Technol. (CISTI 2012)*, Piscataway, NJ IEEE, Madrid, Spain, 1016–1019.
- Almoghathawi, Y., and Barker, K. (2019). "Component importance measures for interdependent infrastructure network resilience." *Comput. Ind. Eng.*, 133, 153–164.

- Almoghathawi, Y., Barker, K., and Albert, L. A. (2019). “Resilience-driven restoration model for interdependent infrastructure networks.” *Reliab. Eng. Syst. Saf.*, 185, 12–23.
- Arcidiacono, V., Cimellaro, G. P., Reinhorn, A. M., and Bruneau, M. (2012). “Community resilience evaluation including interdependencies.” *Proc. 15th World Conf. Earthq. Eng.*, Sociedade Portuguesa de Engenharia Sismica (SPES), Lisbon, Portugal, 24–28.
- ASCE. (2017). *2017 report card for America’s infrastructure*. Washington, DC.
- Bagloee, S. A., Sarvi, M., Patriksson, M., and Rajabifard, A. (2017). “A mixed user-equilibrium and system-optimal traffic flow for connected vehicles stated as a complementarity problem.” *Comput. Civ. Infrastruct. Eng.*, 32(7), 562–580.
- Bansal, P., and Kockelman, K. M. (2017). “Forecasting Americans’ long-term adoption of connected and autonomous vehicle technologies.” *Transp. Res. Part A Policy Pract.*, 95, 49–63.
- Barbosa, H., Barthelemy, M., Ghoshal, G., James, C. R., Lenormand, M., Louail, T., Menezes, R., Ramasco, J. J., Simini, F., and Tomasini, M. (2018). “Human mobility: Models and applications.” *Phys. Rep.*, 734, 1–74.
- Barker, K., Ramirez-Marquez, J. E., and Rocco, C. M. (2013). “Resilience-based network component importance measures.” *Reliab. Eng. Syst. Saf.*, 117, 89–97.
- Baroud, H., and Barker, K. (2018). “A Bayesian kernel approach to modeling resilience-based network component importance.” *Reliab. Eng. Syst. Saf.*, 170, 10–19.
- Barrett, A. M., and Adams, P. J. (2011). “Chlorine truck attack consequences and mitigation.” *Risk Anal.*, 31(8), 1243–1259.
- Beluch, W. H., Genewein, T., Nürnberger, A., and Köhler, J. M. (2018). “The power of ensembles for active

- learning in image classification.” *Proc. IEEE Comput. Soc. Conf. Comput. Vis. Pattern Recognit.*, IEEE, Salt Lake City, UT, USA, 9368–9377.
- Ben-Akiva, M. E., Gao, S., Wei, Z., and Wen, Y. (2012). “A dynamic traffic assignment model for highly congested urban networks.” *Transp. Res. Part C Emerg. Technol.*, 24, 62–82.
- Blake, E. S., and Zelinsky, D. A. (2018). *Hurricane Harvey. Natl. Hurric. Cent. Trop. Cyclone Rep.*
- Bocchini, P., and Frangopol, D. M. (2011). “A stochastic computational framework for the joint transportation network fragility analysis and traffic flow distribution under extreme events.” *Probabilistic Eng. Mech.*, 26, 182–193.
- Bocchini, P., and Frangopol, D. M. (2012). “Restoration of bridge networks after an earthquake: multicriteria intervention optimization.” *Earthq. Spectra*, 28(2), 427–455.
- Bocchini, P., and Frangopol, D. M. (2013). “Connectivity-based optimal scheduling for maintenance of bridge networks.” *J. Eng. Mech.*, 139(6), 760–769.
- Bonabeau, E. (2002). “Agent-based modeling: Methods and techniques for simulating human systems.” *Proc. Natl. Acad. Sci. U. S. A.*, 99(SUPPL. 3), 7280–7287.
- Bosse, T., Duell, R., Memon, Z. A., Treur, J., and van der Wal, C. N. (2009). “A multi-agent model for mutual absorption of emotions.” *Proc. 23rd Eur. Conf. Model. Simul. (ECMS 2009)*, J. Otamendi, A. Bargiela, J. L. Montes, and L. M. D. Pedrera, eds., Madrid, Spain, 212–218.
- Brown, T., Beyeler, W., and Barton, D. (2004). “Assessing infrastructure interdependencies: the challenge of risk analysis for complex adaptive systems.” *Int. J. Crit. Infrastructures*, 1(1), 108–117.
- Bruneau, M., Chang, S. E., Eguchi, R. T., Lee, G. C., O’Rourke, T. D., Reinhorn, A. M., Shinozuka, M., Tierney, K., Wallace, W. A., and Von Winterfeldt, D. (2003). “A framework to quantitatively assess

- and enhance the seismic resilience of communities.” *Earthq. Spectra*, 19(4), 733–752.
- Burstedde, C., Klauck, K., Schadschneider, A., and Zittartz, J. (2001). “Simulation of pedestrian dynamics using a two-dimensional cellular automaton.” *Phys. A Stat. Mech. its Appl.*, 295, 507–525.
- Calvert, S. C., and Snelder, M. (2018). “A methodology for road traffic resilience analysis and review of related concepts.” *Transp. A Transp. Sci.*, 14(1–2), 130–154.
- Campbell, K. W. (1997). “Empirical near-source attenuation relationships for horizontal and vertical components of peak ground acceleration, peak ground velocity, and pseudo-absolute acceleration response spectra.” *Seismol. Res. Lett.*, 68(1), 154–179.
- Cao, L., Lin, J., and Li, N. (2019). “A virtual reality based study of indoor fire evacuation after active or passive spatial exploration.” *Comput. Human Behav.*, 90, 37–45.
- Cao, M., Zhang, G., Wang, M., Lu, D., and Liu, H. (2017). “A method of emotion contagion for crowd evacuation.” *Phys. A Stat. Mech. its Appl.*, 483(1), 250–258.
- Cao, S., Song, W., Lv, W., and Fang, Z. (2015). “A multi-grid model for pedestrian evacuation in a room without visibility.” *Phys. A Stat. Mech. its Appl.*, 436, 45–61.
- Chang, L., Elnashai, A. S., and Spencer, B. F. (2012a). “Post-earthquake modelling of transportation networks.” *Struct. Infrastruct. Eng.*, 8(10), 893–911.
- Chang, L., Peng, F., Ouyang, Y., Elnashai, A. S., and Spencer Jr., B. F. (2012b). “Bridge seismic retrofit program planning to maximize postearthquake transportation network capacity.” *J. Infrastruct. Syst.*, 18(2), 75–88.
- Chang, S. E., Shinozuka, M., and Moore, J. E. (2000). “Probabilistic earthquake scenarios: extending risk analysis methodologies to spatially distributed systems.” *Earthq. Spectra*, 16(3), 557–572.

- Chen, C. K., Li, J., and Zhang, D. (2012). "Study on evacuation behaviors at a T-shaped intersection by a force-driving cellular automata model." *Phys. A Stat. Mech. its Appl.*, 391(7), 2408–2420.
- Chen, L., and Miller-Hooks, E. (2012). "Resilience: an indicator of recovery capability in intermodal freight transport." *Transp. Sci.*, 46(1), 109–123.
- Chen, X., Li, H., Miao, J., Jiang, S., and Jiang, X. (2017). "A multiagent-based model for pedestrian simulation in subway stations." *Simul. Model. Pract. Theory*, 71, 134–148.
- Chen, X., Meaker, J. W., and Zhan, F. B. (2006). "Agent-based modeling and analysis of hurricane evacuation procedures for the Florida Keys." *Nat. Hazards*, 38(3), 321–338.
- Chiu, C. C., Cheng, Y. T., and Chang, C. W. (2012). "Comparison of particle swarm optimization and genetic algorithm for the path loss reduction in an urban area." *J. Appl. Sci. Eng.*, 15(4), 371–380.
- Chiu, Y., Bottom, J., Mahut, M., Paz, A., Balakrishna, R., Waller, T., and Hicks, J. (2011). "Dynamic traffic assignment: A primer." *Transp. Res. Circ. E-C153*, paper #09–3721.
- Choi, M., Lee, S., Park, M., and Lee, H. (2018). "Effect of dynamic emergency cues on fire evacuation performance in public buildings." *J. Infrastruct. Syst.*, 24(4), 04018029.
- Cimellaro, G. P., Renschler, C., Reinhorn, A. M., and Arendt, L. (2016). "PEOPLES: a framework for evaluating resilience." *J. Struct. Eng.*, 142(10), 04016063.
- Cong, H., He, Y., Wang, X., and Jiang, C. (2018). "Robust optimization for improving resilience of integrated energy systems with electricity and natural gas infrastructures." *J. Mod. Power Syst. Clean Energy*, 6(5), 1066–1078.
- Daganzo, C. F., and Sheffi, Y. (1997). "On stochastic models of traffic assignment." *Transp. Sci.*, 11(3), 253–274.

- Darestani, Y. M., Shafieezadeh, A., and DesRoches, R. (2018). “Effects of adjacent spans and correlated failure events on system-level hurricane reliability of power distribution lines.” *IEEE Trans. Power Deliv.*, 33(5), 2305–2314.
- Davidich, M., Geiss, F., Mayer, H. G., Pfaffinger, A., and Royer, C. (2014). “Waiting zones for realistic modelling of pedestrian dynamics: A case study using two major German railway stations as examples.” *Transp. Res. Part C Emerg. Technol.*, 37, 210–222.
- DHS. (2009). *HAZUS-MH MR4 earthquake model user manual*. Department of Homeland Security, Federal Emergency Management Agency, Mitigation Division, Washington, DC.
- Dolan, R. J. (2002). “Emotion, cognition, and behavior.” *Science (80-.)*, 298(5596), 1191–1194.
- Dossetti, V., Bouzat, S., and Kuperman, M. N. (2017). “Behavioral effects in room evacuation models.” *Phys. A Stat. Mech. its Appl.*, 479, 193–202.
- Dueñas-osorio, L., and Vemuru, S. M. (2009). “Cascading failures in complex infrastructure systems.” *Struct. Saf.*, 31(2), 157–167.
- Durupinar, F. (2010). “From audiences to mobs: Crowd simulation with psychological factors.” Bilkent University.
- Edrissi, A., Nourinejad, M., and Roorda, M. J. (2015). “Transportation network reliability in emergency response.” *Transp. Res. Part E Logist. Transp. Rev.*, 80, 56–73.
- El-rashidy, R. A., and Grant-muller, S. M. (2014). “An assessment method for highway network vulnerability.” *J. Transp. Geogr.*, 34, 34–43.
- Elbeltagi, E., Hegazy, T., and Grierson, D. (2005). “Comparison among five evolutionary-based optimization algorithms.” *Adv. Eng. Informatics*, 19(1), 43–53.

- Ellingwood, B. R., Cutler, H., Gardoni, P., Peacock, W. G., Lindt, J. W. Van De, and Wang, N. (2016). “The Centerville Virtual Community: a fully integrated decision model of interacting physical and social infrastructure systems.” *Sustain. Resilient Infrastruct.*, 1(3–4), 95–107.
- Ergan, S., Radwan, A., Zou, Z., Tseng, H. A., and Han, X. (2019). “Quantifying Human Experience in Architectural Spaces with Integrated Virtual Reality and Body Sensor Networks.” *J. Comput. Civ. Eng.*, 33(2), 04018062.
- Fang, Y., Pedroni, N., and Zio, E. (2015). “Optimization of cascade-resilient electrical infrastructures and its validation by power flow modeling.” *Risk Anal.*, 35(4), 594–607.
- Fang, Y., Pedroni, N., and Zio, E. (2016). “Resilience-based component importance measures for critical infrastructure network systems.” *IEEE Trans. Reliab.*, 65(2), 502–512.
- Fang, Y., and Sansavini, G. (2017). “Optimizing power system investments and resilience against attacks.” *Reliab. Eng. Syst. Saf.*, 159, 161–173.
- Fang, Y., and Sansavini, G. (2019). “Optimum post-disruption restoration under uncertainty for enhancing critical infrastructure resilience.” *Reliab. Eng. Syst. Saf.*, 185, 1–11.
- Faturechi, R., and Miller-Hooks, E. (2014a). “Measuring the performance of transportation infrastructure systems in disasters: a comprehensive review.” *J. Infrastruct. Syst.*, 21(1), 04014025.
- Faturechi, R., and Miller-Hooks, E. (2014b). “Travel time resilience of roadway networks under disaster.” *Transp. Res. Part B Methodol.*, 70, 47–64.
- Feliciani, C., and Nishinari, K. (2016). “An improved Cellular Automata model to simulate the behavior of high density crowd and validation by experimental data.” *Phys. A Stat. Mech. its Appl.*, 451, 135–148.
- Feng, K., Hou, G., and Li, Q. (2017). “Evaluating the role of transportation system in community resilience

- assessment.” *Proc. 12th Int. Conf. Struct. Saf. Reliab.*, C. Bucher, B. R. Ellingwood, and D. M. Frangopol, eds., International Association for Structural Safety and Reliability (IASSAR), New York, Vienna, Austria, 6–10.
- Fotouhi, H., Moryadee, S., and Miller-Hooks, E. (2017). “Quantifying the resilience of an urban traffic-electric power coupled system.” *Reliab. Eng. Syst. Saf.*, 163, 79–94.
- Freiria, S., Ribeiro, B., and Tavares, A. O. (2015). “Understanding road network dynamics: Link-based topological patterns.” *J. Transp. Geogr.*, 46, 55–66.
- Fu, L., Song, W., and Lo, S. (2017). “A fuzzy-theory-based method for studying the effect of information transmission on nonlinear crowd dispersion dynamics.” *Commun. Nonlinear Sci. Numer. Simul.*, 42, 682–698.
- Fu, L., Song, W., Lv, W., and Lo, S. (2014). “Simulation of emotional contagion using modified SIR model: A cellular automaton approach.” *Phys. A Stat. Mech. its Appl.*, 405, 380–391.
- Gal, Y. (2016). “Uncertainty in deep learning.” University of Cambridge.
- Ghaffarpour, R., Reza, M., Oskuee, J., and Mohammad, A. (2018). “Resilience-oriented distribution network optimal planning to improve the continuity of power supply.” *Int. J. Ambient Energy*.
- Gong, J., Lee, E. E., Mitchell, J. E., and Wallace, W. A. (2009). “Logic-based multiobjective optimization for restoration planning.” *Optim. Logist. Challenges Enterp.*, 30, 305–324.
- Gong, J., Mitchell, J. E., Krishnamurthy, A., and Wallace, W. A. (2014). “An interdependent layered network model for a resilient supply chain.” *Omega*, 46, 104–116.
- González, A. D., Dueñas-Osorio, L., Sánchez-Silva, M., and Medaglia, A. L. (2016). “The interdependent network design problem for optimal infrastructure system restoration.” *Comput. Civ. Infrastruct. Eng.*,

31(5), 334–350.

Grundmann, O. (2014). “The current state of bioterrorist attack surveillance and preparedness in the US.”

Risk Manag. Healthc. Policy, 7, 177–187.

Guo, A., Liu, Z., Li, S., and Li, H. (2017). “Seismic performance assessment of highway bridge networks considering post-disaster traffic demand of a transportation system in emergency conditions.” *Struct. Infrastruct. Eng.*, 13(12), 1523–1537.

Struct. Infrastruct. Eng., 13(12), 1523–1537.

Guo, R. Y., and Huang, H. J. (2016). “A discrete dynamical system of formulating traffic assignment:

Revisiting Smith’s model.” *Transp. Res. Part C Emerg. Technol.*, 71, 122–142.

Gupta, A. K., and Yadav, P. K. (2004). “SAFE-R: A new model to study the evacuation profile of a building.”

Fire Saf. J., 39(7), 539–556.

Hackl, J., Adey, B. T., and Lethanh, N. (2018). “Determination of near-optimal restoration programs for transportation networks following natural hazard events using simulated annealing.” *Comput. Civ. Infrastruct. Eng.*, 33(8), 618–637.

Comput. Civ. Infrastruct. Eng., 33(8), 618–637.

Haimes, Y. Y. (2009). “On the definition of resilience in systems.” *Risk Anal.*, 29(4), 498–501.

Haimes, Y. Y., Horowitz, B. M., Lambert, J. H., Santos, J. R., Lian, C., and Crowther, K. G. (2005).

“Inoperability input-output model for interdependent infrastructure sectors. I: theory and methodology.” *J. Infrastruct. Syst.*, 11(2), 67–79.

Haimes, Y. Y., and Jiang, P. (2001). “Leontief-based model of risk in complex interconnected infrastructures.” *J. Infrastruct. Syst.*, 7(1), 1–12.

J. Infrastruct. Syst., 7(1), 1–12.

Hanna, S., Dharmavaram, S., Zhang, J., Sykes, I., Witlox, H., Khajehnajafi, S., and Koslan, K. (2008).

“Comparison of six widely-used dense gas dispersion models for three recent chlorine railcar

- accidents.” *Process Saf. Prog.*, 27(3), 248–259.
- Hasan, S., and Foliente, G. (2015). “Modeling infrastructure system interdependencies and socioeconomic impacts of failure in extreme events: emerging R&D challenges.” *Nat. Hazards*, 78(3), 2143–2168.
- Helbing, D. (1992). “A fluid-dynamic model for the movement of pedestrians.” *Complex Syst.*, 6, 391–415.
- Helbing, D., Buzna, L., Johansson, A., and Werner, T. (2005). “Self-organized pedestrian crowd dynamics: Experiments, simulations, and design solutions.” *Transp. Sci.*, 39(1), 1–24.
- Helbing, D., Farkas, I. J., Molnar, P., and Vicsek, T. (2002). “Simulation of pedestrian crowds in normal and evacuation situations.” *Pedestr. evacuation Dyn.*, M. Schreckenberg and S. Sharma, eds., Springer, Berlin, Germany, 21–58.
- Helbing, D., Farkas, I., and Vicsek, T. (2000). “Simulating dynamical features of escape panic.” *Nature*, 407, 487–490.
- Helbing, D., and Johansson, A. (2013). “Pedestrian, crowd, and evacuation dynamics.” *Encycl. Complex. Syst. Sci.*, 16(4), 6476–6495.
- Helbing, D., and Molnár, P. (1995). “Social force model for pedestrian dynamics.” *Phys. Rev. E*, 51(5), 5.
- Helbing, D., and Mukerji, P. (2012). “Crowd disasters as systemic failures: analysis of the Love Parade disaster.” *EPJ Data Sci.*, 1, 7.
- Henderson, D. A. (1999). “The looming threat of bioterrorism.” *Science (80-.)*, 283, 1279–1283.
- Henderson, L. F. (1971). “The statistics of crowd fluids.” *Nature*, 229(5284), 381–383.
- Henein, C. M., and White, T. (2010). “Microscopic information processing and communication in crowd dynamics.” *Phys. A Stat. Mech. its Appl.*, 389(21), 4636–4653.
- Heracleous, C., Kolios, P., Panayiotou, C. G., Ellinas, G., and Polycarpou, M. M. (2017). “Hybrid systems

- modeling for critical infrastructures interdependency analysis.” *Reliab. Eng. Syst. Saf.*, 165, 89–101.
- Hong, L., Gao, J., and Zhu, W. (2016). “Simulating emergency evacuation at metro stations: an approach based on thorough psychological analysis.” *Transp. Lett.*, 8(2), 113–120.
- Hosseini, S., Barker, K., and Ramirez-Marquez, J. E. (2016). “A review of definitions and measures of system resilience.” *Reliab. Eng. Syst. Saf.*, 145, 47–61.
- Hu, F., Yeung, C. H., Yang, S., Wang, W., and Zeng, A. (2016). “Recovery of infrastructure networks after localised attacks.” *Sci. Rep.*, 6(1), 24522.
- Hughes, R. L. (2002). “A continuum theory for the flow of pedestrians.” *Transp. Res. Part B Methodol.*, 36(6), 507–535.
- Ip, W. H., and Wang, D. (2011). “Resilience and friability of transportation networks: evaluation, analysis and optimization.” *IEEE Syst. J.*, 5(2), 189–198.
- Janet, J. P., Duan, C., Yang, T., Nandy, A., and Kulik, H. J. (2019). “A quantitative uncertainty metric controls error in neural network-driven chemical discovery.” *Chem. Sci.*, Royal Society of Chemistry, 10(34), 7913–7922.
- Jayakrishnan, R., Tsai, W. T., Prashker, J. N., and Rajadhyaksha, S. (1994). “A faster path-based algorithm for traffic assignment.” *Transp. Res. Rec.*, 1443, 75–83.
- Jeon, G. Y., Kim, J. Y., Hong, W. H., and Augenbroe, G. (2011). “Evacuation performance of individuals in different visibility conditions.” *Build. Environ.*, 46(5), 1094–1103.
- Johansson, F., Peterson, A., and Tapani, A. (2015). “Waiting pedestrians in the social force model.” *Phys. A Stat. Mech. its Appl.*, 419, 95–107.
- Johansson, J., and Hassel, H. (2010). “An approach for modelling interdependent infrastructures in the

- context of vulnerability analysis.” *Reliab. Eng. Syst. Saf.*, 95(12), 1335–1344.
- Jones, D. R., Schonlau, M., and Welch, W. J. (1998). “Efficient global optimization of expensive black-box functions.” *J. Glob. Optim.*, 13(4), 455–492.
- Kazama, M., and Noda, T. (2012). “Damage statistics (Summary of the 2011 off the Pacific Coast of Tohoku Earthquake damage).” *Soils Found.*, 52(5), 780–792.
- Kempe, D., Kleinberg, J., and Tardos, É. (2003). “Maximizing the spread of influence through a social network.” *Proc. ninth ACM SIGKDD Int. Conf. Knowl. Discov. data Min.*, Association for Computing Machinery (ACM), New York, 137–146.
- Kennedy, J., and Eberhart, R. C. (1997). “A discrete binary version of the particle swarm algorithm.” *1997 IEEE Int. Conf. Syst. Man, Cybern. Comput. Cybern. Simul.*, 5, 4104–4108.
- Khademi, N., Balaei, B., Shahri, M., Mirzaei, M., Sarrafi, B., Zahabiun, M., and Mohaymany, A. S. (2015). “Transportation network vulnerability analysis for the case of a catastrophic earthquake.” *Int. J. Disaster Risk Reduct.*, 12, 234–254.
- Kilanitis, I., and Sextos, A. (2019). “Integrated seismic risk and resilience assessment of roadway networks in earthquake prone areas.” *Bull. Earthq. Eng.*, 17, 181–210.
- Kirchner, A., and Schadschneider, A. (2002). “Simulation of evacuation processes using a bionics-inspired cellular automaton model for pedestrian dynamics.” *Phys. A Stat. Mech. its Appl.*, 312, 260–276.
- Koks, E. E., Rozenberg, J., Zorn, C., Tariverdi, M., Vousdoukas, M., Fraser, S. A., Hall, J. W., and Hallegatte, S. (2019). “A global multi-hazard risk analysis of road and railway infrastructure assets.” *Nat. Commun.*, 10, 2677.
- Korhonen, T. (2016). *Fire dynamics simulator with evacuation: FDS+Evac - Technical reference and user’s*

- guide (FDS 6.5.2, Evac 2.5.2, Draft)*. VTT, Espoo, Finland.
- Krizhevsky, A., Sutskever, I., and Hinton, G. E. (2012). "ImageNet classification with deep convolutional neural networks." *Proc. 25th Int. Conf. Neural Inf. Process. Syst.*, F. Pereira, C. J. C. Burges, L. Bottou, and K. Q. Weinberger, eds., Curran Associates Inc., Lake Tahoe, NV, USA, 1097–1105.
- Lakshminarayanan, B., Pritzel, A., and Blundell, C. (2017). "Simple and scalable predictive uncertainty estimation using deep ensembles." *Proc. 31st Int. Conf. Neural Inf. Process. Syst.*, U. V. Luxburg, I. Guyon, S. Bengio, H. Wallach, and R. Fergus, eds., Curran Associates Inc., Long Beach, CA, USA, 6405–6416.
- Lecun, Y., Bengio, Y., and Hinton, G. (2015). "Deep learning." *Nature*, 521(7553), 436–444.
- Lee, E. E., Mitchell, J. E., and Wallace, W. A. (2007). "Restoration of services in interdependent infrastructure systems: A network flows approach." *IEEE Trans. Syst. Man, Cybern. - Part C Appl. Rev.*, 37(6), 1303–1317.
- Lee, S., Soak, S., Oh, S., Pedrycz, W., and Jeon, M. (2008). "Modified binary particle swarm optimization." *Prog. Nat. Sci.*, 18(9), 1161–1166.
- Lee, Y., Song, J., Gardoni, P., and Lim, H. (2011). "Post-hazard flow capacity of bridge transportation network considering structural deterioration of bridges." *Struct. Infrastruct. Eng.*, 7(7–8), 509–521.
- Lei, W., Li, A., Gao, R., Hao, X., and Deng, B. (2012). "Simulation of pedestrian crowds' evacuation in a huge transit terminal subway station." *Phys. A Stat. Mech. its Appl.*, 391(22), 5355–5365.
- Leibig, C., Allken, V., Ayhan, M. S., Berens, P., and Wahl, S. (2017). "Leveraging uncertainty information from deep neural networks for disease detection." *Sci. Rep.*, 7(1), 1–14.
- Levin, M. W., and Boyles, S. D. (2015). "Effects of autonomous vehicle ownership on trip, mode, and route

- choice.” *Transp. Res. Rec.*, 2493(1), 29–38.
- Levin, M. W., and Boyles, S. D. (2016). “A multiclass cell transmission model for shared human and autonomous vehicle roads.” *Transp. Res. Part C Emerg. Technol.*, 62, 103–116.
- Li, M., Zhao, Y., He, L., Chen, W., and Xu, X. (2015). “The parameter calibration and optimization of social force model for the real-life 2013 Ya’an earthquake evacuation in China.” *Saf. Sci.*, 79, 243–253.
- Li, W., Gong, J., Yu, P., Shen, S., Li, R., and Duan, Q. (2014). “Simulation and analysis of individual trampling risk during escalator transfers.” *Phys. A Stat. Mech. its Appl.*, 408, 119–133.
- Li, Z., Jin, C., Hu, P., and Wang, C. (2019a). “Resilience-based transportation network recovery strategy during emergency recovery phase under uncertainty.” *Reliab. Eng. Syst. Saf.*, 188, 503–514.
- Li, Z., Wu, Q., Yu, H., Chen, C., Zhang, G., Tian, Z. Z., and Prevedouros, P. D. (2019b). “Temporal-spatial dimension extension-based intersection control formulation for connected and autonomous vehicle systems.” *Transp. Res. Part C Emerg. Technol.*, 104, 234–248.
- Liao, T. Y., Hu, T. Y., and Ko, Y. N. (2018). “A resilience optimization model for transportation networks under disasters.” *Nat. Hazards*, 93(1), 469–489.
- Liu, H. X., He, X., and He, B. (2009). “Method of successive weighted averages (MSWA) and self-regulated averaging schemes for solving stochastic user equilibrium problem.” *Networks Spat. Econ.*, 9(4), 485–503.
- Liu, M., and Frangopol, D. M. (2005). “Balancing connectivity of deteriorating bridge networks and long-term maintenance cost through optimization.” *J. Bridg. Eng.*, 10, 468–481.
- Liu, T. T., Liu, Z., Ma, M., Xuan, R., Chen, T., Lu, T., and Yu, L. (2017). “An information perception-based emotion contagion model for fire evacuation.” *3D Res.*, 8(1), 10.

- Liu, Y. C., McNeil, S., Hackl, J., and Adey, B. T. (2020). "Prioritizing transportation network recovery using a resilience measure." *Sustain. Resilient Infrastruct.*
- Liu, Z., Jacques, C. C., Szyniszewski, S., Guest, J. K., Schafer, B. W., Igusa, T., and Mitrani-Reiser, J. (2015). "Agent-based simulation of building evacuation after an earthquake: coupling human behavior with structural response." *Nat. Hazards Rev.*, 17(1), 04015019.
- Lizotte, D. J. (2008). "Practical bayesian optimization." University of Alberta, Edmonton, Alberta, Canada,.
- Loggins, R. A., and Wallace, W. A. (2015). "Rapid assessment of hurricane damage and disruption to interdependent civil infrastructures systems." *J. Infrastruct. Syst.*, 21(4), 04015005.
- Lovreglio, R., Fonzone, A., Dell'Olio, L., and Borri, D. (2016). "A study of herding behaviour in exit choice during emergencies based on random utility theory." *Saf. Sci.*, 82, 421–431.
- Lovreglio, R., Ronchi, E., and Nilsson, D. (2015). "Calibrating floor field cellular automaton models for pedestrian dynamics by using likelihood function optimization." *Phys. A Stat. Mech. its Appl.*, 438, 308–320.
- Lu, C. C., Mahmassani, H. S., and Zhou, X. (2009). "Equivalent gap function-based reformulation and solution algorithm for the dynamic user equilibrium problem." *Transp. Res. Part B Methodol.*, 43(3), 345–364.
- Ma, Y., Yuen, R. K. K., and Lee, E. W. M. (2016). "Effective leadership for crowd evacuation." *Phys. A Stat. Mech. its Appl.*, 450, 333–341.
- Manley, M., Kim, Y. S., Christensen, K., and Chen, A. (2016). "Airport emergency evacuation planning: an agent-based simulation study of dirty bomb scenarios." *IEEE Trans. Syst. Man, Cybern. Syst.*, 46(10), 1390–1403.

- Manoochery, S., and Rasouli, H. R. (2017). "Recurrent human tragedy during Hajj." *Int. J. Travel Med. Glob. Heal.*, 5(1), 36–37.
- Markolf, S. A., Hoehne, C., Fraser, A., Chester, M. V., and Underwood, B. S. (2019). "Transportation resilience to climate change and extreme weather events – Beyond risk and robustness." *Transp. Policy*, 74, 174–186.
- Marshall, N. L. (2018). "Forecasting the impossible: The status quo of estimating traffic flows with static traffic assignment and the future of dynamic traffic assignment." *Res. Transp. Bus. Manag.*
- Mattsson, L.-G., and Jenelius, E. (2015). "Vulnerability and resilience of transport systems - A discussion of recent research." *Transp. Res. Part A Policy Pract.*, 81, 16–34.
- Mazloumi, E., Moridpour, S., and Mohsenian, H. (2010). "Delay function for signalized intersections in traffic assignment models." *J. Urban Plan. Dev.*, 136(1), 67–74.
- Mckenzie, B. (2015). *Who Drives to Work? Commuting by Automobile in the United States: 2013*. USA.
- Medury, A., and Madanat, S. (2013). "Incorporating network considerations into pavement management systems: A case for approximate dynamic programming." *Transp. Res. Part C Emerg. Technol.*, 33, 134–150.
- Mensah, A. F., and Dueñas-osorio, L. (2016). "Efficient resilience assessment framework for electric power systems affected by hurricane events." *J. Struct. Eng.*, 142(8), C4015013.
- Miller-Hooks, E., Zhang, X., and Faturechi, R. (2012). "Measuring and maximizing resilience of freight transportation networks." *Comput. Oper. Res.*, 39(7), 1633–1643.
- Mostafizi, A., Dong, S., and Wang, H. (2017). "Percolation phenomenon in connected vehicle network through a multi-agent approach: Mobility benefits and market penetration." *Transp. Res. Part C*

- Emerg. Technol.*, 85, 312–333.
- Murata, T., Ishibuchi, H., and Tanaka, H. (1996). “Genetic algorithms for flowshop scheduling problems.” *Comput. Ind. Eng.*, 30(4), 1061–1071.
- Nan, C., and Sansavini, G. (2017). “A quantitative method for assessing resilience of interdependent infrastructures.” *Reliab. Eng. Syst. Saf.*, 157, 35–53.
- National Fire Protection Association. (2019). *Fire loss in the United States during 2018*. Quincy, MA, USA.
- NBI. (2016). “National Bridge Inventory.” <<https://www.fhwa.dot.gov/bridge/nbi/2016/CA16.txt>> (Oct. 10, 2019).
- Neto, A. B. F., Pelachaud, C., and Musse, S. R. (2015). “Emotion contagion model for crowds.” *SBC J. Interact. Syst.*, 6(2), 37–44.
- Neves, L., Cordeiro, C., Scott, S. K., Castro, S. L., and Lima, C. F. (2018). “High emotional contagion and empathy are associated with enhanced detection of emotional authenticity in laughter.” *Q. J. Exp. Psychol.*, 71(11), 2355–2363.
- Nguyen, V. T., Longin, D., Ho, T. V., and Gaudou, B. (2014). “Integration of emotion in evacuation simulation.” *Int. Conf. Inf. Syst. Cris. Response Manag. Mediterr. Ctries. (ISCRAM-med 2014)*, C. Hanachi, F. Bénaben, and F. Charoy, eds., Toulouse, France, 192–205.
- Nicolas, A., Bouzat, S., and Kuperman, M. N. (2016). “Statistical fluctuations in pedestrian evacuation times and the effect of social contagion.” *Phys. Rev. E*, 94(2), 1–12.
- Nie, Y., Zhang, H. M., and Lee, D.-H. (2004). “Models and algorithms for the traffic assignment problem with link capacity constraints.” *Transp. Res. Part B Methodol.*, 38(4), 285–312.
- Nikoo, N., Babaei, M., and Mohaymany, A. S. (2018). “Emergency transportation network design problem:

- Identification and evaluation of disaster response routes.” *Int. J. Disaster Risk Reduct.*, 27, 7–20.
- Nogal, M., and Honfi, D. (2019). “Assessment of road traffic resilience assuming stochastic user behaviour.” *Reliab. Eng. Syst. Saf.*, 185, 72–83.
- Nozhati, S., Ellingwood, B. R., and Chong, E. K. P. (2020). “Stochastic optimal control methodologies in risk-informed community resilience planning.” *Struct. Saf.*, 84, 101920.
- Nozhati, S., Sarkale, Y., Ellingwood, B., K.P. Chong, E., and Mahmoud, H. (2019). “Near-optimal planning using approximate dynamic programming to enhance post-hazard community resilience management.” *Reliab. Eng. Syst. Saf.*, 181, 116–126.
- NRC. (2006). *Facing hazards and disasters: Understanding human dimensions*. Tech. rep., National Research Council, The National Academies Press, Washington, D.C., USA.
- Osman, O. A., and Ishak, S. (2016). “Genetic algorithm-based approach for optimal deployment of roadside units in connected and automated vehicle environments.” *Transp. Res. Rec.*, 2595, 139–147.
- Ouyang, M. (2014). “Review on modeling and simulation of interdependent critical infrastructure systems.” *Reliab. Eng. Syst. Saf.*, 121, 43–60.
- Ouyang, M., and Dueñas-osorio, L. (2014). “Multi-dimensional hurricane resilience assessment of electric power systems.” *Struct. Saf.*, 48, 15–24.
- Ouyang, M., Dueñas-osorio, L., and Min, X. (2012). “A three-stage resilience analysis framework for urban infrastructure systems.” *Struct. Saf.*, 36–37, 23–31.
- Ouyang, M., Liu, C., and Xu, M. (2019). “Value of resilience-based solutions on critical infrastructure protection: Comparing with robustness-based solutions.” *Reliab. Eng. Syst. Saf.*, 190, 106506.
- Ouyang, M., and Wang, Z. (2015). “Resilience assessment of interdependent infrastructure systems: with a

- focus on joint restoration modeling and analysis.” *Reliab. Eng. Syst. Saf.*, 141, 74–82.
- Ouyang, M., Xu, M., Zhang, C., and Huang, S. (2017). “Mitigating electric power system vulnerability to worst-case spatially localized attacks.” *Reliab. Eng. Syst. Saf.*, 165, 144–154.
- Ouyang, M., Zhao, L., Pan, Z., and Hong, L. (2014). “Comparisons of complex network based models and direct current power flow model to analyze power grid vulnerability under intentional attacks.” *Phys. A Stat. Mech. its Appl.*, 403, 45–53.
- Özdamar, L., Tüzün Aksu, D., and Ergüneş, B. (2014). “Coordinating debris cleanup operations in post disaster road networks.” *Socioecon. Plann. Sci.*, 48(4), 249–262.
- Panda, S., and Padhy, N. P. (2008). “Comparison of particle swarm optimization and genetic algorithm for FACTS-based controller design.” *Appl. Soft Comput. J.*, 8(4), 1418–1427.
- Panteli, M., Pickering, C., Wilkinson, S., Dawson, R., and Mancarella, P. (2017). “Power system resilience to extreme weather: fragility modelling, probabilistic impact assessment, and adaptation measures.” *IEEE Trans. Power Syst.*, 32(5), 3747–3757.
- Peeta, S., and Yang, T. (2003). “Stability issues for dynamic traffic assignment.” *Automatica*, 39(1), 21–34.
- Pines, J. M. (2018). “Freestanding emergency department visits and disasters: The case of Hurricane Harvey.” *Am. J. Emerg. Med.*, 36(8), 1513–1515.
- Prashker, J. N., and Bekhor, S. (1999). “Stochastic user-equilibrium formulations for extended-logit assignment models.” *Transp. Res. Rec.*, (1676), 145–152.
- Prashker, J. N., and Bekhor, S. (2004). “Route choice models used in the stochastic user equilibrium problem: A review.” *Transp. Rev.*, 24(4), 437–463.
- Pumpuni-Lenss, G., Blackburn, T., and Garstenauer, A. (2017). “Resilience in complex systems: an agent-

- based approach.” *Syst. Eng.*, 20(2), 158–172.
- Qu, Y., and Dan, Y. (2014). “Modeling the evacuation behavior considering the effect of dangerous source.” *Procedia - Soc. Behav. Sci.*, 138, 800–810.
- Qu, Y., Gao, Z., Xiao, Y., and Li, X. (2014). “Modeling the pedestrian’s movement and simulating evacuation dynamics on stairs.” *Saf. Sci.*, 70, 189–201.
- Reed, D., Wang, S., Kapur, K., and Zheng, C. (2016). “Systems-based approach to interdependent electric power delivery and telecommunications infrastructure resilience subject to weather-related hazards.” *J. Struct. Eng.*, 142(8), C4015011.
- Reggiani, A., Nijkamp, P., and Lanzi, D. (2015). “Transport resilience and vulnerability: The role of connectivity.” *Transp. Res. Part A Policy Pract.*, 81, 4–15.
- Rinaldi, S. M., Peerenboom, J. P., and Kelly, T. K. (2001). “Identifying, understanding, and analyzing critical infrastructure interdependencies.” *IEEE Control Syst. Mag.*, 21(6), 11–25.
- Roh, J. S., Ryou, H. S., Park, W. H., and Jang, Y. J. (2009). “CFD simulation and assessment of life safety in a subway train fire.” *Tunn. Undergr. Sp. Technol.*, 24(4), 447–453.
- Romero, N., Nozick, L. K., Dobson, I., and Xu, N. (2015). “Seismic retrofit for electric power systems.” *Earthq. Spectra*, 31(2), 1157–1176.
- Salman, A. M. (2016). “Risk-based assessment and strengthening of electric power systems subjected to natural hazards.” Michigan Technological University, Houghton, Michigan, USA.
- Salman, A. M., and Li, Y. (2015). “Age-dependent fragility and life-cycle cost analysis of wood and steel power distribution poles subjected to hurricanes.” *Struct. Infrastruct. Eng.*, 12(8), 890–903.
- Salman, A. M., Li, Y., and Stewart, M. G. (2015). “Evaluating system reliability and targeted hardening

- strategies of power distribution systems subjected to hurricanes.” *Reliab. Eng. Syst. Saf.*, 144, 319–333.
- Santos, J. R., and Haimés, Y. Y. (2004). “Modeling the demand reduction input-output (I-O) inoperability due to terrorism of interconnected infrastructures.” *Risk Anal.*, 24(6), 1437–1451.
- Satuntira, G., and Dueñas-Osorio, L. (2010). “Synthesis of modeling and simulation methods on critical infrastructure interdependencies research.” *Sustain. Resilient Crit. Infrastruct. Syst.*, G. K. and P. S., eds., Springer, Berlin, Heidelberg, 1–51.
- Sbayti, H., Lu, C.-C., and Mahmassani, H. (2007). “Efficient implementation of method of successive averages in simulation-based dynamic traffic assignment models for large-scale network applications.” *Transp. Res. Rec. J. Transp. Res. Board*, 2029, 22–30.
- SCAG. (2016). *SCAG regional travel demand model and 2012 model validation*.
- Sener, O., and Savarese, S. (2018). “Active learning for convolutional neural networks: A core-set approach.” *6th Int. Conf. Learn. Represent. - Conf. Track Proc.*
- Seriani, S., and Fernandez, R. (2015). “Pedestrian traffic management of boarding and alighting in metro stations.” *Transp. Res. Part C Emerg. Technol.*, 53, 76–92.
- Shahriari, B., Swersky, K., Wang, Z., Adams, R. P., and Freitas, N. de. (2016). “Taking the human out of the loop: a review of Bayesian optimization.” *Proc. IEEE*, 104(1), 148–175.
- Sheffi, Y. (1985). *Urban transportation networks: equilibrium analysis with mathematical programming methods*. Prentice-Hall, Inc., Englewood Cliffs, New Jersey.
- Shi, C., Zhong, M., Nong, X., He, L., Shi, J., and Feng, G. (2012). “Modeling and safety strategy of passenger evacuation in a metro station in China.” *Saf. Sci.*, 50(5), 1319–1332.

- Shi, J., Ren, A., and Chen, C. (2009). "Agent-based evacuation model of large public buildings under fire conditions." *Autom. Constr.*, 18(3), 338–347.
- Shields, T. J., and Boyce, K. E. (2000). "Study of evacuation from large retail stores." *Fire Saf. J.*, 35, 25–49.
- Shin, Y., Kim, S., and Moon, I. (2019). "Integrated optimal scheduling of repair crew and relief vehicle after disaster." *Comput. Oper. Res.*, 105, 237–247.
- Shiwakoti, N., and Sarvi, M. (2013). "Enhancing the panic escape of crowd through architectural design." *Transp. Res. Part C Emerg. Technol.*, 37, 260–267.
- Smith, B. L., Qin, L., and Venkatanarayana, R. (2003). "Characterization of freeway capacity reduction resulting from traffic accidents." *J. Transp. Eng.*, 129(4), 362–368.
- Song, Y., Gong, J., Li, Y., Cui, T., Fang, L., and Cao, W. (2013). "Crowd evacuation simulation for bioterrorism in micro-spatial environments based on virtual geographic environments." *Saf. Sci.*, 53, 105–113.
- Stapelberg, R. F. (2008). "Infrastructure systems interdependencies and risk informed decision making (RIDM): Impact scenario analysis of infrastructure risks induced by natural, technological and intentional hazards." *J. Syst. Cybern. Informatics*, 6(5), 21–27.
- Statistics, B. of T. (2018). "March 2018 North American Freight Numbers." <<https://www.bts.gov/newsroom/march-2018-north-american-freight-numbers>> (Nov. 18, 2019).
- Stephens, C. L., Christie, I. C., and Friedman, B. H. (2010). "Autonomic specificity of basic emotions: Evidence from pattern classification and cluster analysis." *Biol. Psychol.*, 84(3), 463–473.
- Szegedy, C., Liu, W., Jia, Y., Sermanet, P., Reed, S., Anguelov, D., Erhan, D., Vanhoucke, V., and

- Rabinovich, A. (2015). "Going deeper with convolutions." *Proc. IEEE Comput. Soc. Conf. Comput. Vis. Pattern Recognit.*, IEEE, Boston, MA, USA, 1–9.
- Tan, L., Hu, M., and Lin, H. (2015). "Agent-based simulation of building evacuation: Combining human behavior with predictable spatial accessibility in a fire emergency." *Inf. Sci. (Ny)*, 295, 53–66.
- Tong, C. O., and Wong, S. C. (2000). "A predictive dynamic traffic assignment model in congested capacity-constrained road networks." *Transp. Res. Part B Methodol.*, 34(8), 625–644.
- Transportation Research Board (TRB). (2000). *Highway capacity manual (HCM)*. *Transp. Res. Rec. 209*, Transportation Research Board, Washington, D.C.
- Tsai, J., Bowring, E., Marsella, S., and Tambe, M. (2013). "Empirical evaluation of computational fear contagion models in crowd dispersions." *Auton. Agent. Multi. Agent. Syst.*, 27(2), 200–217.
- Tsai, J., Fridman, N., Bowring, E., Brown, M., Epstein, S., Kaminka, G., Marsella, S., Ogden, A., Rika, I., Sheel, A., Taylor, M. E., Wang, X., Zilka, A., and Tambe, M. (2011). "ESCAPES - evacuation simulation with children, authorities, parents, emotions, and social comparison." *Proc. Tenth Int. Conf. Auton. Agents Multiagent Syst. (AAMAS 2011)*, K. Tume, P. Yolum, L. Sonenberg, and P. Stone, eds., International Foundation for Autonomous Agents and Multiagent Systems (IFAAMAS), Taipei, Taiwan, 457–464.
- Tucker, A., Marsh, K. L., Gifford, T., Lu, X., Luh, P. B., and Astur, R. S. (2018). "The effects of information and hazard on evacuee behavior in virtual reality." *Fire Saf. J.*, 99, 1–11.
- Tuzun Aksu, D., and Ozdamar, L. (2014). "A mathematical model for post-disaster road restoration: Enabling accessibility and evacuation." *Transp. Res. Part E Logist. Transp. Rev.*, 61, 56–67.
- Ulusan, A., and Ergun, O. (2018). "Restoration of services in disrupted infrastructure systems: A network

- science approach.” *PLoS One*, 13(2), 1–28.
- Unnikrishnan, V. U., and van de Lindt, J. W. (2016). “Probabilistic framework for performance assessment of electrical power networks to tornadoes.” *Sustain. Resilient Infrastruct.*, 1(3–4), 137–152.
- Vodák, R., Bíl, M., and Křivánková, Z. (2018). “A modified ant colony optimization algorithm to increase the speed of the road network recovery process after disasters.” *Int. J. Disaster Risk Reduct.*, 31, 1092–1106.
- Vorst, H. C. M. (2010). “Evacuation models and disaster psychology.” *Procedia Eng.*, 3, 15–21.
- Vugrin, E. D., Turnquist, M. A., and Brown, N. J. K. (2014). “Optimal recovery sequencing for enhanced resilience and service restoration in transportation networks.” *Int. J. Crit. Infrastructures*, 10(3/4), 218–246.
- Wallace, W., Wojtowicz, J., Torrey, D., Renna, N., and Tan, J. (2009). *Guidelines for traffic signal energy back-up systems*. New York, USA.
- Wan, J., Sui, J., and Yu, H. (2014). “Research on evacuation in the subway station in China based on the Combined Social Force Model.” *Phys. A Stat. Mech. its Appl.*, 394, 33–46.
- Wang, H., Mostafizi, A., Cramer, L. A., Cox, D., and Park, H. (2016). “An agent-based model of a multimodal near-field tsunami evacuation: Decision-making and life safety.” *Transp. Res. Part C Emerg. Technol.*, 64, 86–100.
- Wang, J., Peeta, S., and He, X. (2019). “Multiclass traffic assignment model for mixed traffic flow of human-driven vehicles and connected and autonomous vehicles.” *Transp. Res. Part B Methodol.*, 126, 139–168.
- Wang, J., Zhang, L., Shi, Q., Yang, P., and Hu, X. (2015). “Modeling and simulating for congestion

- pedestrian evacuation with panic.” *Phys. A Stat. Mech. its Appl.*, 428, 396–409.
- Wang, L., Zhang, Q., Cai, Y., Zhang, J., and Ma, Q. (2013). “Simulation study of pedestrian flow in a station hall during the Spring Festival travel rush.” *Phys. A Stat. Mech. its Appl.*, 392(10), 2470–2478.
- Wang, Q., and Taylor, J. E. (2016). “Patterns and limitations of urban human mobility resilience under the influence of multiple types of natural disaster.” *PLoS One*, 11(1), 1–14.
- Wiggins, J. S. (1996). *The five-factor model of personality: Theoretical perspectives*. Guilford Press, New York.
- Xu, Z., Ramirez-Marquez, J. E., Liu, Y., and Xiahou, T. (2020). “A new resilience-based component importance measure for multi-state networks.” *Reliab. Eng. Syst. Saf.*, 193, 106591.
- Yan, Y., Hong, L., He, X., Ouyang, M., Peeta, S., and Chen, X. (2017). “Pre-disaster investment decisions for strengthening the Chinese railway system under earthquakes.” *Transp. Res. Part E Logist. Transp. Rev.*, 105, 39–59.
- Ye, L., and Yamamoto, T. (2018). “Modeling connected and autonomous vehicles in heterogeneous traffic flow.” *Phys. A Stat. Mech. its Appl.*, 490, 269–277.
- Yonca, N., Duzgun, H. S., Rudolf, H., and Wenzel, F. (2018). “Framework for improving the resilience and recovery of transportation networks under geohazard risks.” *Int. J. Disaster Risk Reduct.*, 31, 832–843.
- Yuen, J. K. K., and Lee, E. W. M. (2012). “The effect of overtaking behavior on unidirectional pedestrian flow.” *Saf. Sci.*, 50(8), 1704–1714.
- Zhang, J., Song, B., Zhang, Z., and Liu, H. (2014a). “An approach for modeling vulnerability of the network of networks.” *Phys. A Stat. Mech. its Appl.*, 412, 127–136.

- Zhang, L., Liu, M., Wu, X., and AbouRizk, S. M. (2016). "Simulation-based route planning for pedestrian evacuation in metro stations: A case study." *Autom. Constr.*, 71, 430–442.
- Zhang, Q., Han, B., and Li, D. (2008). "Modeling and simulation of passenger alighting and boarding movement in Beijing metro stations." *Transp. Res. Part C Emerg. Technol.*, 16(5), 635–649.
- Zhang, S., Wu, Y., Liu, H., Huang, R., Un, P., Zhou, Y., Fu, L., and Hao, J. (2014b). "Real-world fuel consumption and CO₂ (carbon dioxide) emissions by driving conditions for light-duty passenger vehicles in China." *Energy*, 69, 247–257.
- Zhang, W., and Wang, N. (2016). "Resilience-based risk mitigation for road networks." *Struct. Saf.*, 62, 57–65.
- Zhang, W., and Wang, N. (2017). "Bridge network maintenance prioritization under budget constraint." *Struct. Saf.*, 67, 96–104.
- Zhang, W., Wang, N., and Nicholson, C. (2017). "Resilience-based post-disaster recovery strategies for road-bridge networks." *Struct. Infrastruct. Eng.*, 2479, 1–10.
- Zhang, X., and Miller-Hooks, E. (2015). "Scheduling short-term recovery activities to maximize transportation network resilience." *J. Comput. Civ. Eng.*, 29(6), 04014087.
- Zhang, X., Miller-Hooks, E., and Denny, K. (2015). "Assessing the role of network topology in transportation network resilience." *J. Transp. Geogr.*, 46, 35–45.
- Zhao, X., Wang, Z., Xu, Z., Wang, Y., Li, X., and Qu, X. (2020). "Field experiments on longitudinal characteristics of human driver behavior following an autonomous vehicle." *Transp. Res. Part C Emerg. Technol.*, 114, 205–224.
- Zhao, Y., Li, M., Lu, X., Tian, L., Yu, Z., Huang, K., Wang, Y., and Li, T. (2017). "Optimal layout design

- of obstacles for panic evacuation using differential evolution.” *Phys. A Stat. Mech. its Appl.*, 465, 175–194.
- Zheng, L., Peng, X., Wang, L., and Sun, D. (2019). “Simulation of pedestrian evacuation considering emergency spread and pedestrian panic.” *Physica A*, 522, 167–181.
- Zheng, X., and Cheng, Y. (2011). “Conflict game in evacuation process: A study combining Cellular Automata model.” *Phys. A Stat. Mech. its Appl.*, 390(6), 1042–1050.
- Zheng, Y., Jia, B., Li, X. G., and Jiang, R. (2017). “Evacuation dynamics considering pedestrians’ movement behavior change with fire and smoke spreading.” *Saf. Sci.*, 92, 180–189.
- Zhong, H., Li, W., Burris, M. W., Talebpour, A., and Sinha, K. C. (2020). “Will autonomous vehicles change auto commuters’ value of travel time?” *Transp. Res. Part D Transp. Environ.*, 83, 102303.
- Zhou, X., and Taylor, J. (2014). “DTALite: A queue based mesoscopic traffic simulator for fast model evaluation and calibration.” *Cogent Eng.*, 1, 961345.
- Zhou, Y., Wang, J., and Yang, H. (2019). “Resilience of transportation systems: concepts and comprehensive review.” *IEEE Trans. Intell. Transp. Syst.*, 20(12), 4262–4276.
- Zou, H., Li, N., and Cao, L. (2017). “Emotional response-based approach for assessing the sense of presence of subjects in virtual building evacuation studies.” *J. Comput. Civ. Eng.*, 31(5), 04017028.
- Zou, Q., and Chen, S. (2019). “Enhancing resilience of interdependent traffic-electric power system.” *Reliab. Eng. Syst. Saf.*, 191, 106557.
- Zou, Q., and Chen, S. (2020a). “Resilience modeling of interdependent traffic-electric power system subject to hurricanes.” *J. Infrastruct. Syst.*, 26(1), 04019034.
- Zou, Q., and Chen, S. (2020b). “Simulation of crowd evacuation under toxic gas incident considering

emotion contagion and information transmission.” *J. Comput. Civ. Eng.*, 34(3), 04020007.

Zou, Q., and Chen, S. (2020c). “Resilience-based recovery scheduling of transportation network in mixed traffic environment: a deep-ensemble-assisted active learning approach.” *Reliab. Eng. Syst. Saf.*, Under Review.

Zou, Q., Fernandes, D. S., and Chen, S. (2019). “Agent-based evacuation simulation from subway train and platform.” *J. Transp. Saf. Secur.*

CURRICULUM VITAE

Qiling Zou

Education

- Ph.D.** Civil Engineering, 2016-2020
Colorado State University, Fort Collins, CO, USA
Dissertation title: Modeling and improving urban human mobility in disaster scenarios
Advisor: Professor Suren Chen
- M.S.** Civil Engineering, 2013-2016
Hunan University, Changsha, Hunan, China
Thesis title: Certainty and uncertainty analysis of vehicle-bridge interaction model
Advisor: Professor Lu Deng, Professor Tieding Guo
- B.Eng.** Civil Engineering, 2009-2013
Hunan University, Changsha, Hunan, China

Publications

- Zou, Q. L., and Chen, S. R. (2020a). "Resilience modeling of interdependent traffic-electric power system subject to hurricanes". *Journal of Infrastructure Systems, ASCE*, 26(1), 04019034.
- Zou, Q. L., and Chen, S. R. (2020b). "Simulation of crowd evacuation under toxic gas incident considering emotion contagion and information transmission". *Journal of Computing in Civil Engineering, ASCE*, 34(3), 04020007.
- Zou, Q. L., and Chen, S. R. (2020c). "Resilience-based recovery scheduling of transportation network in mixed traffic environment: a deep-ensemble-assisted active learning approach". *Reliability Engineering and System Safety*, Under Review.
- Zou, Q. L., Pool, K., and Chen, S. R. (2019). "Performance of suspension bridge hangers exposed to hazardous material fires considering wind effects". *Advances in Bridge Engineering*, 1, 2.
- Zou, Q. L., and Chen, S. R. (2019). "Enhancing resilience of interdependent traffic-electric power system". *Reliability Engineering and System Safety*, 191, 106557.
- Zou, Q. L., Fernandes, D. S., and Chen, S. R. (2019). "Agent-based evacuation simulation from subway train and platform". *Journal of Transportation Safety and Security*.
- Zou, Q. L., Deng, L., and Jiang, C. (2016). "Predicting the bounds of vehicle-induced bridge responses using the interval analysis method". *Journal of Bridge Engineering, ASCE*, 21(9), 04016046.

- Zou, Q. L., Deng, L., Guo, T. D., and Yin, X. F. (2016). " Comparative study of different numerical models for vehicle-bridge interaction analysis". *International Journal of Structural Stability and Dynamics*, 16(9), 1550057.
- Deng, L., Yu, Y., and Zou, Q. L. (2015). "State-of-the-art review of dynamic impact factors of highway bridges". *Journal of Bridge Engineering, ASCE*, 20(5), 04014080.